LEAKAGE AND ROTORDYNAMIC EFFECTS OF POCKET DAMPER SEALS AND SEE-THROUGH LABYRINTH SEALS

A Dissertation

by

AHMED MOHAMED GAMAL ELDIN

Submitted to the Office of Graduate Studies of
Texas A&M University
in partial fulfillment of the requirements for the degree of

DOCTOR OF PHILOSOPHY

December 2007

Major Subject: Mechanical Engineering

LEAKAGE AND ROTORDYNAMIC EFFECTS OF POCKET DAMPER SEALS AND SEE-THROUGH LABYRINTH SEALS

A Dissertation

by

AHMED MOHAMED GAMAL ELDIN

Submitted to the Office of Graduate Studies of
Texas A&M University
in partial fulfillment of the requirements for the degree of

DOCTOR OF PHILOSOPHY

Approved by:

Chair of Committee,	John M. Vance
Committee Members,	Dara W. Childs
	Gerald L. Morrison
	Robert E. Randall
Head of Department,	Dennis L. O'Neal

December 2007

Major Subject: Mechanical Engineering

ABSTRACT

Leakage and Rotordynamic Effects of Pocket Damper Seals and See-Through Labyrinth Seals. (December 2007)
Ahmed Mohamed Gamal Eldin, B.Sc., The American University in Cairo;
M.S., Texas A&M University
Chair of Advisory Committee: Dr. John M. Vance

This dissertation discusses research on the leakage and rotordynamic characteristics of pocket damper seals (PDS) and see-through labyrinth seals, presents and evaluates models for labyrinth seal and PDS leakage and PDS force coefficients, and compares these seals to other annular gas seals. Low-pressure experimental results are used alongside previously-published high-pressure labyrinth and PDS data to evaluate the models. Effects of major seal design parameters; blade thickness, blade spacing, blade profile, and cavity depth; on seal leakage, as well as the effect of operating a seal in an off-center position, are examined through a series of non-rotating tests. Two reconfigurable seal designs were used, which enabled testing labyrinth seals and PDS with two to six blades.

Leakage and pressure measurements were made with air as the working fluid on twenty-two seal configurations. Increasing seal blade thickness reduced leakage by the largest amount. Blade profile results were more equivocal, indicating that both profile and thickness affected leakage, but that the influence of one factor partially negated the influence of the other. Seal leakage increased with increased eccentricity at lower supply pressures, but that this effect was attenuated for higher pressure drops. While cavity depth effects were minor, reducing depths reduced leakage up to a point beyond which leakage increased, indicating that an optimum cavity depth existed. Changing blade spacing produced results almost as significant as those for blade thickness, showing that reducing spacing can detrimentally affect leakage to the point of negating

the benefit of inserting additional blades. Tests to determine the effect of PDS partition walls showed that they reduce axial leakage. The pressure drop was found to be highest across the first blade of a seal for low pressure drops, but the pressure drop distribution became parabolic for high pressure drops with the largest drop across the last blade. Thirteen leakage equations made up of a base equations, a flow factor, and a kinetic energy carryover factor were examined. The importance of the carryover coefficient was made evident and a modified carryover coefficient is suggested. Existing fully-partitioned PDS models were expanded to accommodate seals of various geometries.

DEDICATION

To my mother, for her love,

my father, for his support,

my brothers, for their friendship,

and my grandmother, for her faith

To my little brother, Karim, who changed my life with his love, support, friendship, faith, humor, and generosity, I miss you.

"O soul that art at peace, return to your Lord, content and well-pleasing. Enter then among My worshipers, and enter into My Heaven."

- The Holy Quran, Al-Fajr (The Dawn), 27-30

ACKNOWLEDGEMENTS

I would like to express my gratitude and appreciation to Dr. John M. Vance for his guidance and support. Dr. Vance's understanding and kind advice have served as sources of inspiration that have aided me in completing this dissertation. Sincere thanks are due to Dr. Dara W. Childs for the many recommendations and references he provided and to Dr. Gerald L. Morrison for the input he offered regarding the experimental setup. I would also like to thank Dr. Robert E. Randall for serving on my committee.

While so many of my coworkers have been of great help to me, I am especially grateful to Mr. Kiran Toram for his help in machining test components, to Mr. Rahul Kar for assistance with the testing, to Dr. Mohsin Jafri for his analytical input, and to Dr. Bugra Ertas for making his experimental data and theoretical models readily available. A great deal of thanks goes to Mr. Eddie Denk at the Turbomachinery Laboratory for his guidance on almost every practical issue that was encountered.

I would like to acknowledge the friendship and support of my coworkers at the Turbo Lab and my friends in College Station; particularly Ms. Tyann Blessington, Dr. Arun Suryanarayanan, and Mr. Joe Fermelia, without whom the past few years would have been considerably less interesting. Finally, I will always be indebted to my parents and my brothers, who have been unwavering in their love and support.

TABLE OF CONTENTS

Page

CHAPTER Page

CHAPTER Page

LIST OF FIGURES

Page

Page

Page

Page

Page

LIST OF TABLES

Page

Page

CHAPTER I

ANNULAR GAS SEALS: AN INTRODUCTION

In response to constantly increasing demand for higher levels of productivity, turbomachines are being designed to run at higher speeds, last longer, and operate more efficiently. This has resulted in a need to reach an optimum balance between a turbomachine's leakage characteristics and its rotordynamic performance, while dealing with ever-tightening rotor-to-stator clearances. Research on one particular component used in such machines, the annular gas seal, has been instrumental in achieving the operating speeds and efficiency levels that are regularly attained today.

Annular gas seals, which include labyrinth seals, pocket damper seals, and hole-pattern seals, limit fluid flow across regions of unequal pressure. These seals have proven invaluable in this respect due to their desirable leakage prevention characteristics and their non-contacting nature, which allows rotor speeds to be increased significantly. While labyrinth seals are the most widely used and simplest of these seals, they have certain undesirable rotordynamic characteristics related to instability. In addition, labyrinth seals offer only limited damping of rotor vibrations, leaving the bearing locations as the only feasible locations to add significant damping.

The pocket damper seal (PDS), developed in 1991 at Texas A&M University, does not exhibit the labyrinth seal's instability problems, and at the same time allows the application of a considerable amount of damping at the seal location. The PDS (known commercially as the TAMSEAL™) has since shown in both lab tests and field applications that it can significantly lower rotor vibration amplitudes. These seals can, for example, be used in place of the labyrinth seals currently employed in high-pressure compressors.

Labyrinth seals, such as the one shown in Figure 1.1, are made up of a series of blades and cavities. The ratio of the radial clearance to the journal diameter is usually on

---

This dissertation follows the style of the ASME Journal of Turbomachinery.

the order of 1:100 for such annular gas seals (as compared to 1:1000 for fluid-film bearings). The annular constrictions formed by the seal blades cause the working fluid to throttle and then expand repeatedly, thereby reducing the total pressure of the fluid from one cavity to the next, and limiting the overall axial leakage rate.

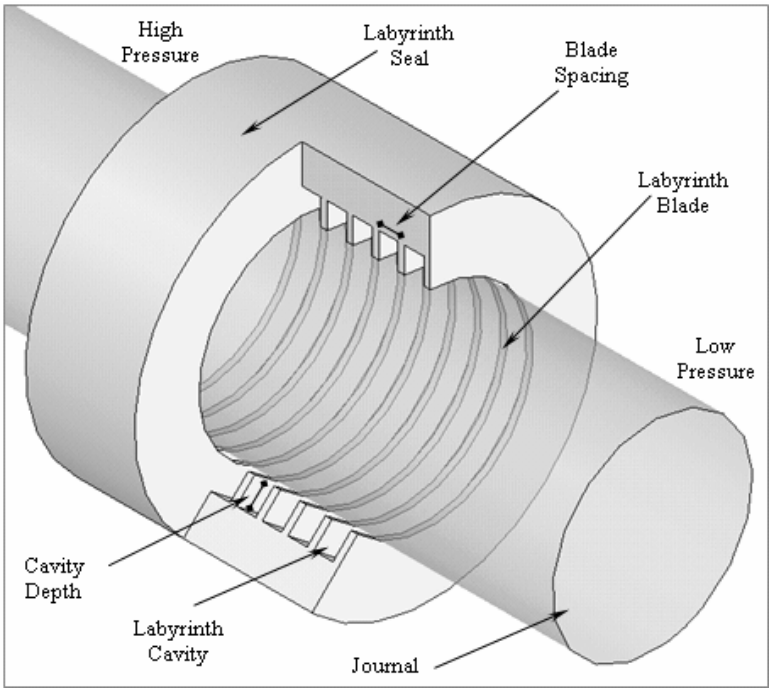

Figure 1.1 Ten-bladed see-through labyrinth seal

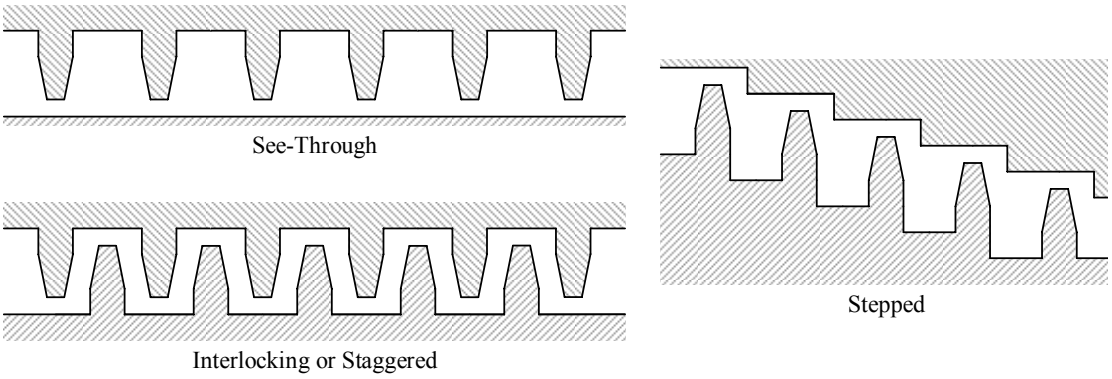

Figure 1.2 Labyrinth seal configurations

There are several different configurations of labyrinth seals, the simplest of which is to be examined in this dissertation. Labyrinth seals can be first categorized as see-through or interlocking as shown in Figure 1.2, and see-through seals can in turn be categorized as either tooth-on-rotor (TOR) or tooth-on-stator (TOS) seals. Labyrinth seals can also be stepped as shown in Figure 1.2.

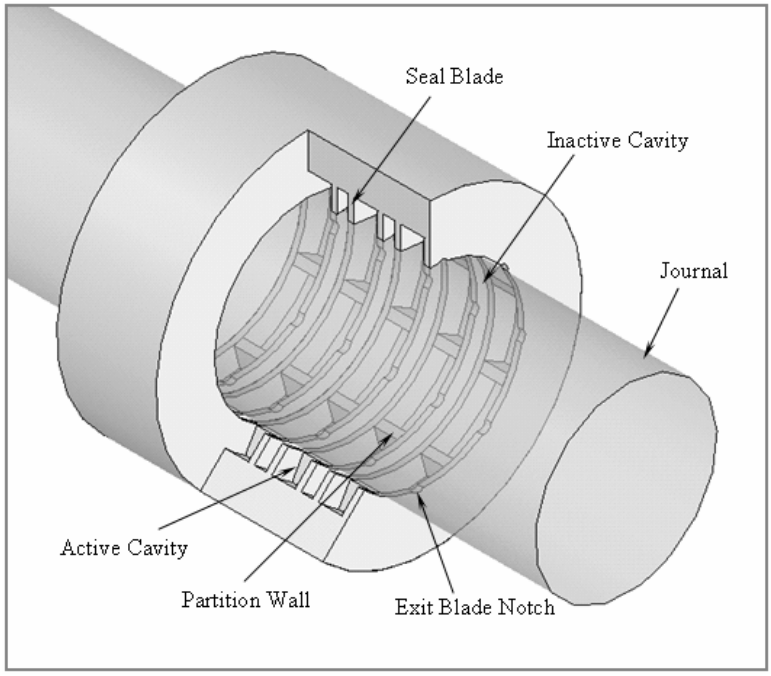

Figure 1.3 Ten-bladed conventional pocket damper seal

The original pocket damper seal design (shown in Figure 1.3) is made up of a series of blades dividing the seal into active and inactive cavities and a series of circumferential partition walls, which divide the active cavities into pockets. This design will henceforth be referred to as the *conventional* pocket damper seal. The active cavities normally have a longer pitch length and are diverging (the blade-to-journal clearance area at the cavity inlet is smaller than that at the exit), while the inactive plenums are usually converging. Comparisons of flow-rates through these seals with those through other annular gas seals, including honeycomb, hole-pattern (shown in Figure 1.4) and labyrinth seals, have shown that PDSs have comparable (and in some instances,

especially for short seal lengths, lower) leakage. At the same time, the damping and stability characteristics of PDSs are superior to those of labyrinth seals and are comparable (and in some cases superior) to those of other damper seals. A PDS is therefore usually a more attractive choice than a labyrinth seal from a rotordynamic point of view, but may also have better leakage reduction characteristics, especially for short seal lengths.

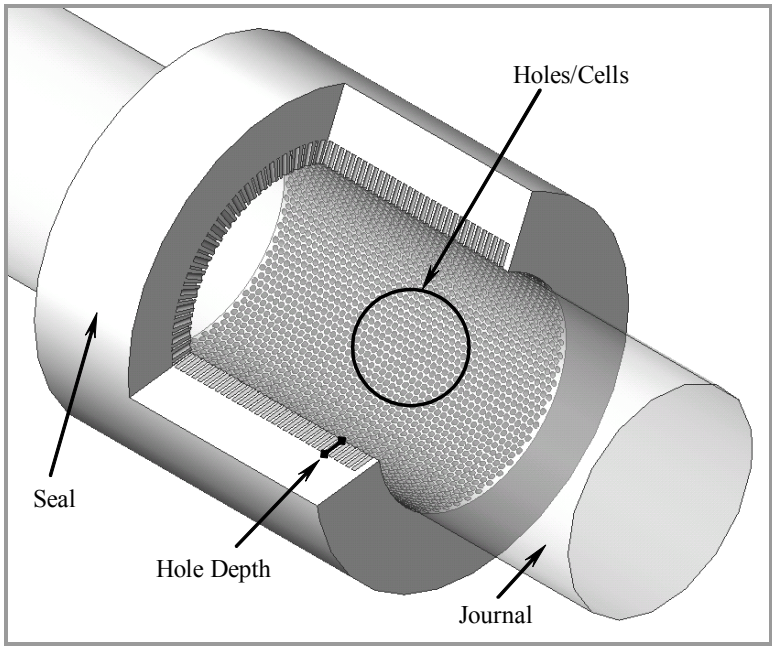

Figure 1.4 Hole-pattern damper seal

A more recent PDS design, known as the *fully-partitioned* pocket damper seal, features partition walls that extend along the entire length of the seal. This seal's cavities are all, therefore, partitioned into circumferential pockets and are referred to as primary and secondary rather than active and inactive. These newer seals (shown in Figure 1.5) can be designed with diverging clearances (or notched exit blades) as is done with the conventional seals, or can be used as straight-through (1:1 clearance ratio) configurations, which still offer significant damping.

While the rotordynamic characteristics of pocket damper seals can affect the reliability of a turbomachine, and are therefore worthy of study, leakage reduction

remains an important purpose of these seals. Conversely, while leakage reduction is the intended purpose of labyrinth seals, the potentially undesirable rotordynamic characteristics of these seals makes their effects on machinery vibration and stability an important topic. Developing an accurate model for the prediction of the flow-rate through such seals and understanding the interrelationship between seal leakage and seal rotordynamic force coefficients are therefore essential first steps in their design.

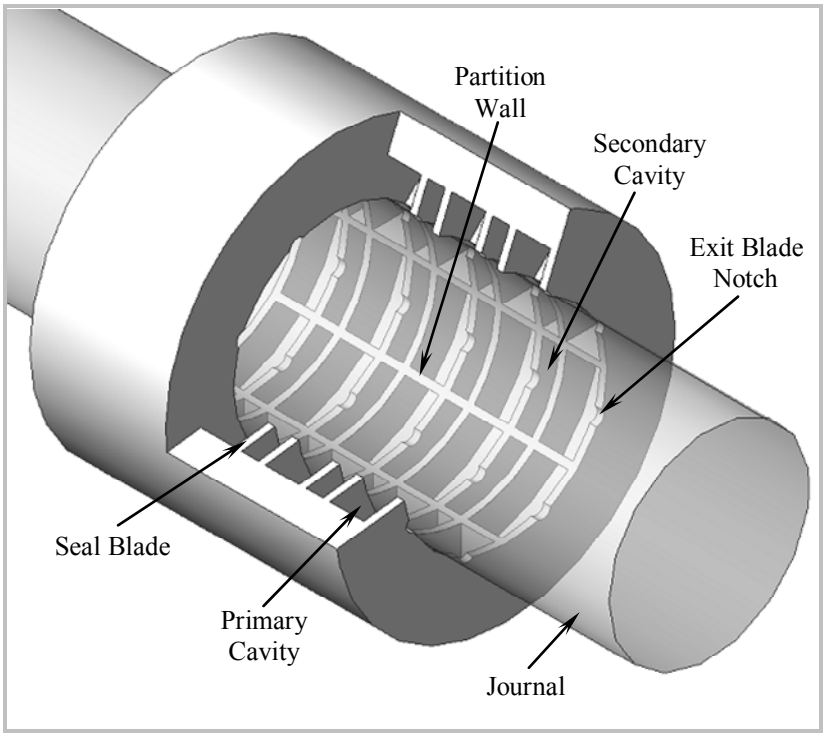

Figure 1.5 Ten-bladed fully-partitioned pocket damper seal

CHAPTER II

LITERATURE REVIEW

This review of background literature is divided into two sections. The first section, following the preliminary remarks below, constitutes a review of relevant work on the rotordynamic properties of labyrinth and pocket damper seals. The second section is a review of those works specifically examining the leakage of these two seal types and the effects of operating conditions and geometric parameters on seal leakage.

A review of experimental and theoretical research on both liquid and gas annular seals for turbomachinery applications was recently presented by Tiwari, Manikandan, and Dwivedy [1]. This review of the literature provided details on the types, geometries, and operating conditions of smooth, labyrinth, hole-pattern, honeycomb, pocket damper, and hybrid brush seal tests and analyses. Another extensive, but more qualitative, description of turbomachinery sealing elements was presented by Hendricks, Tam, and Muszynska [2]. The description of the literature presented below overlaps somewhat with the reviews presented in these two references, but concentrates on work more directly related to the objectives of this dissertation.

One of the earliest references to labyrinth seals in the literature was made in a paper by Martin [3] in 1908, in which the first use of "labyrinth packings" was attributed to Charles A. Parsons, who used these seals to limit leakage in his steam turbine. In that same paper, Martin provided the first equation that could be used to calculate the leakage through a labyrinth seal. Various forms of his equation still form the basis for prediction and analysis tolls in use today.

ROTORDYNAMIC ANALYSIS AND TESTING

A 1997 paper by Childs and Vance [4] reviewed the working theories of labyrinth, plain annular (smooth), honeycomb, and pocket damper seals and described the major analyses and tests that had been carried out on annular gas seals. The two subsections

below describe some of the major developments in the analytical and experimental study of the rotordynamic effects of labyrinth seals and pocket dampers seals.

Labyrinth Seal Analyses and Tests

An analysis of annular seals was published by Alford [5] in 1965 in which a method for predicting the direct damping coefficients of labyrinth seals was presented. This analysis was limited to two-bladed seals with choked flow. Alford postulated that the time-varying pressure distribution around a seal would oppose vibratory velocity in the case of a diverging clearance along the direction of fluid flow and drive the vibratory velocity in the case of a converging clearance. In other words, a diverging clearance would result in positive damping while a converging clearance would result in negative damping. A fundamental flaw in Alford's analysis was the assumption that the gas pressure could vary around the continuous annular groove in a labyrinth seal without circumferential flow of the gas, and without equalization of the pressure differences at acoustic velocities. While the analysis was limited in its practicality due to this assumption of unidirectional flow, it was the precursor to, and was cited by, most of the work pertaining to seal rotordynamics discussed below.

While Alford's paper was concerned with damping, two other seal rotordynamic coefficients of interest, the direct and the cross-coupled stiffness coefficients were measured by Benckert and Wachter [6] for different labyrinth geometries. In these experiments the rotor was displaced and the resulting reaction forces, both inline with and normal to the rotor displacement, were measured. The conclusion was that while the direct stiffness was negligible, the cross-coupled stiffness was not, and that it was caused by the circumferential flow of the fluid around the annular cavities of the seals. Benckert and Wachter also employed swirl-brakes to reduce this circumferential flow and attenuate the potentially destabilizing tangential (to the whirl orbit) force arising from the cross-coupled stiffness.

Childs and Scharrer [7,[8] and Pelletti [9] presented results of low-pressure tests on labyrinth seals. Childs and Scharrer tested seals at pressures between 44 and 120 psi-a

(3.08 and 8.22 bar-a) while Pelletti's tests were conducted at pressures between 115 and 265 psi-a (7.9 and 18.3 bar-a). Higher pressure labyrinth seal tests were carried out by Wyssmann et al. [10] (2000 psi-a or 140 bar-a) and Wagner and Steff [11] (1000 psi-a or 70 bar-a). Picardo and Childs [12] presented experimental data for a tooth-on-stator labyrinth seal with supply pressures of up to approximately 1000 psi (70 bar) and rotor speeds of up to 20,200 rpm. The results consisted of direct and cross-coupled stiffness and damping measurements as well as leakage measurements.

The bulk-flow model developed by Hirs [13], in which a Blasius friction factor formulation is used to model shear stresses, forms the basis for most of the analytical analyses for labyrinth seals. Iwatsubo [14] developed a one control volume model for labyrinth seal rotordynamic coefficients. Childs [15] presents a thorough description of tests carried out on various labyrinth seal configurations (including some of the tests described above) and also describes these models. Wyssmann et al. [10] used a box-in-box control volume model and compared teeth-on-stator and teeth-on-rotor seals. They predicted that TOS seals would have higher direct damping, but also higher cross-coupled stiffness, than TOR or interlocking seals. Their model also predicts that the rotordynamic coefficients are heavily influenced by tooth height. Nelson [16] presented an analysis of the leakage and rotordynamic coefficients of tapered annular gas seals based on the theory developed by Hirs. Childs and Scharrer [17] modified the continuity and circumferential momentum equations in Iwatsubo's model to include the angular area derivatives. Scharrer [18] developed a two-control-volume model, which accounted for vortex flow in the seal cavities.

Computational Fluid Dynamics (CFD) techniques were first used to estimate labyrinth seal leakage and rotordynamic coefficients by Nordmann and Weiser [19] in 1988. The results of this code were compared with the experimental results obtained by Benckert and Wachter [6] and were found to over-predict the direct stiffness and under-predict the cross-coupled stiffness. CFD methods have also been used for rotordynamic analysis and force calculations by Rhode [20], Moore [21] and Kirk [22].

Pocket Damper Seal Analyses and Tests

Building on Alford's work, Murphy and Vance [23] expanded the labyrinth seal damping model for to account for subsonic flow and for seals with more than two blades. Their analysis contained the same conceptual error as Alford's and misleadingly showed that a diverging-clearance ten-bladed labyrinth seal with a 10:1 pressure ratio would generate about 500 lb-s/in (87.6 KN-s/m) of damping, far more than has ever been obtained from such a labyrinth seal. According to Childs and Vance [4], the cross-coupled stiffness, which was not considered in Alford's theory, becomes the dominant factor in labyrinth seals, and decreases the effective damping. Friction between the fluid and the rotor results in circumferential fluid flow that in turn creates a "follower force" that is tangential to the whirl orbit and that further drives this orbit. Were a pressure differential to be artificially created around the seal, a pressure wave traveling at the speed of sound would equalize the pressures around the seal annulus. The failure to recognize the importance of these factors in both the analysis by Alford and in that by Murphy and Vance stems from the assumption of axial one-dimensional flow in the cavity of a labyrinth seal.

In 1974, Lund [24] published a paper in which he cited the potential beneficial effects of installing a damping mechanism, which he modeled with a damper bearing, at the mid-span location of a rotor. Lund also stated, however, that "in practice it would be very difficult to provide a damper bearing at this location". Vance and Shultz [25] realized that Lund's difficulty could be overcome if the damping were to be supplied by a seal rather than a bearing and in 1991 they developed the Pocket Damper Seal (PDS), or TAMSEAL®. The pocket damper seal allowed virtually no circumferential flow due to the incorporation of circumferentially placed partition walls that allowed for radial pressure differentials around the seal and at the same time greatly reduce any circumferential flow, unlike the labyrinth seal. This feature of the pocket damper seal meant that its flow could effectively be considered one-dimensional and that the earlier models proposed by Alford [5] and by Murphy and Vance [23], along with the high direct damping coefficients those models had predicted, were more representative of the

rotordynamic effects of this new seal than they were of labyrinth seals. An analysis based on unconnected circumferential control volumes, which had been developed by Sundararajan and Vance [26] for a bearing damper, also produced relatively accurate predictions for pocket damper seals. The analysis was based on the pressure differentials across the seal resulting from changes in the fluid density.

Following the preliminary research described above, the pocket damper seal was tested extensively to both demonstrate its utility and to examine the effects of design factors and operating conditions on its performance. Shultz [27] demonstrated through static tests that a two-bladed PDS produced more damping than a labyrinth seal with comparable geometry. Dynamic tests were conducted by Li and Vance [28] to study the effect of clearance ratio on seal performance. Vance and Li [29] published results showing how a PDS could virtually eliminate a system's response to imbalance. Richards, Vance, and Zeidan [30] cited the use of PDSs in industrial compressors to suppress sub-synchronous vibration. The stiffness and damping coefficients of a short PDS were determined experimentally by Ransom, Li, San Andres, and Vance [31]. Laos [32] compared two four-bladed PDS configurations (one with four and one with eight pockets) with a six-bladed labyrinth seal. The damping of the labyrinth seal was found to be lower than that of either PDS. Moreover, the labyrinth seal became violently unstable at pressures above 3 bar (44 Psi). The eight-pocket PDS was found to have higher damping than the four-pocket PDS. Li, Kushner, and De Choudhury [33] presented results for rotating tests on a "slotted" (now referred to as "fully-partitioned") PDS, which featured partition walls in all cavities, at pressures up to 14.5 bar, or about 210 Psi.

Armstrong and Perricone [34] showed that honeycomb seals, another type of damper seal, could be used in place of labyrinth seals to eliminate instabilities in steam turbines. Childs and Vance [4] stated that the honeycomb seal has superior leakage characteristics except for small seal lengths for which the two seals have similar leakage characteristics. The same paper presented empirical data showing that decreasing the blade-to-journal clearances in a PDS increased the damping and reduced the leakage and

that reducing the number of blades increased the damping, but it also increased the leakage.

Vance, Sharma, and Jaykar [35] presented a dimensionless group analysis of pocket damper seals and demonstrated the effect of PDS damping on the synchronous imbalance response of a rotor as shown in Figure 2.1 for a 70 psi (4.8 bar) pressure drop across the seal. Li et al. [36] examined the bulk-flow theory of pocket damper seals. More recent developments in PDS research include the investigation by Sharma [37] of the effects of high frequency excitation, Bhamidipati's [38] tests on hybrid metal mesh pocket damper seals, and Kannan's [39] study the effect of notching the exit blades of a PDS as opposed to employing actual diverging clearances.

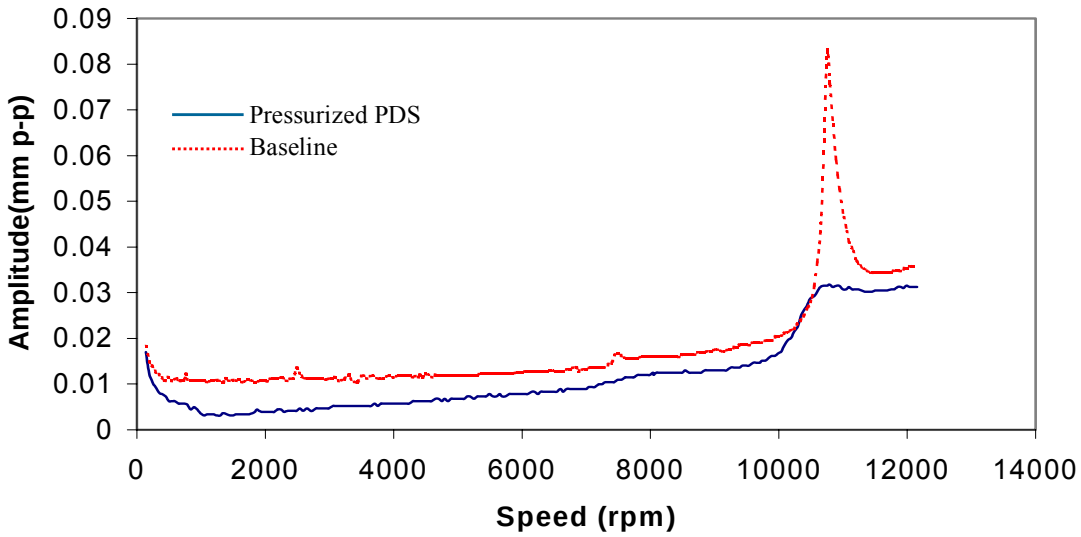

Figure 2.1 Effect of PDS on synchronous imbalance response

Experimental and analytical results of shaker tests on pocket damper seals at pressures of slightly over 1000 psi (68.9 bar) were presented by Gamal [40] and Ertas [41]. Results for six-bladed, eight-bladed, and twelve-bladed pocket damper seals showed high positive direct damping frequencies over a wide range of frequencies, with the maximum damping at lower frequencies. The results also showed negative direct stiffness values and small same-sign (therefore not destabilizing) cross-coupled stiffness coefficients for the test seals. This latter result confirmed that destabilizing cross-

coupled stiffness, a major factor in labyrinth seal instability, was not a concern in pocket damper seals even at elevated supply pressures and rotor speeds under either static conditions (Gamal) or over a 0 Hz to 300 Hz range of excitation frequencies (Ertas). Gamal [40] also developed a design and analysis code for conventional pocket damper seals, which he used to study the effect of clearances, clearance ratios, number of blades, pocket depth, pressure drop, pressure ratio, and excitation frequency on PDS direct stiffness coefficients. The validity of his code was demonstrated through comparisons with experimental results.

LEAKAGE ANALYSIS AND TESTING

As was mentioned above, the first equation for labyrinth seal leakage was presented by Martin [3]. This equation assumed a linear pressure drop across the seal and assumed that the kinetic energy of the fluid entering a cavity was completely dissipated through turbulence in the cavity. The simplicity of the equation and the fact that it provides, at the very least, a rough estimate of seal leakage have contributed to the fact it that continues to be used and cited in research to this day.

In his 1927 book on steam and gas turbines, Stodola [42] discussed labyrinth seals with clearances that can be made as small as 0.008 in (0.2 mm). Stodola presents two equations for labyrinth seal leakage; one for subsonic flow and one for choked flow. He also shows that for a large number of teeth, the weight flow-rate is inversely proportional to the square root of the number of teeth. Stodola presented experimental results on interlocking seals with *axial* clearances (redrawn in Figure 2.2 with only three of ten teeth) ranging from 5.5 mils to 15 mils (0.14 to 0.38 mm) and for pressures ranging from 43 to 143 psi (0.9 to 9.8 bar). Leakage values predicted using his equations matched the experimental results with an error of less than 10% for all but one test case. Stodola carried out his tests with a non-rotating shaft and argued that shaft rotation would have "but little effect" on the axial rate of flow.

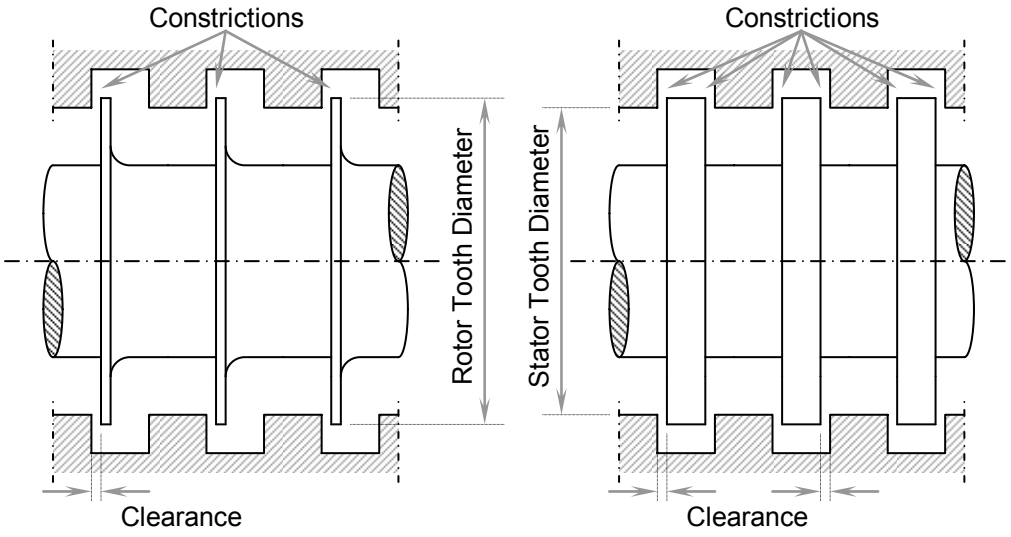

Figure 2.2 Stodola's seals with single and double constrictions per tooth

In 1935, Egli [43] presented a paper on the leakage of steam through labyrinth seals in which he examined both staggered and see-through labyrinth configurations analytically and experimentally. The clearances (between 15 and 40 mils) and pressure ratios studied, while relevant to axial turbine applications of the time, were considerably larger and lower, respectively, than those of interest in modern compressor applications. Egli based his analysis on Martin's Equation (Spurk [44]), but took into consideration, in his area calculation, the contraction undergone by a fluid jet as it passes through an orifice He also defined a "carry-over" factor, which he determined experimentally and used to represent the portion of kinetic energy transferred from one cavity to the next. He reasoned that since the jet emerging from the constriction increases with increasing axial distance, the percentage of kinetic energy carried over from one throttling to the next would decrease with increasing spacing between the blades or with decreasing clearance. Egli verified this theory through experimental results, which showed that the carryover effect depends on the clearance-to-spacing ratio, but also pointed out that work carried out by Friedrich [45], who used seals with tighter radial clearances of 6 to 10 mils, did not show a strong dependence on blade pitch. The equations developed by Egli

and Martin were cited as the starting points of almost all papers on labyrinth seal leakage that were reviewed for this dissertation.

In 1937 Keller [46] used fine sawdust sprinkled into the water entering his liquid labyrinth seal test rig to qualitatively examine the effects on seal leakage of various rub conditions. He also presented experimental results for an air labyrinth seal rig investigating similar effects. These results, summarized in Figure 2.3, showed how seals with interlocking blade configurations are more effective in reducing leakage than analogous see-through seals. Keller's tests were performed on a non-rotating test-rig with rectangular, not circular, blades, resulting in clearances in the form of long rectangular strips rather than thin annuli.

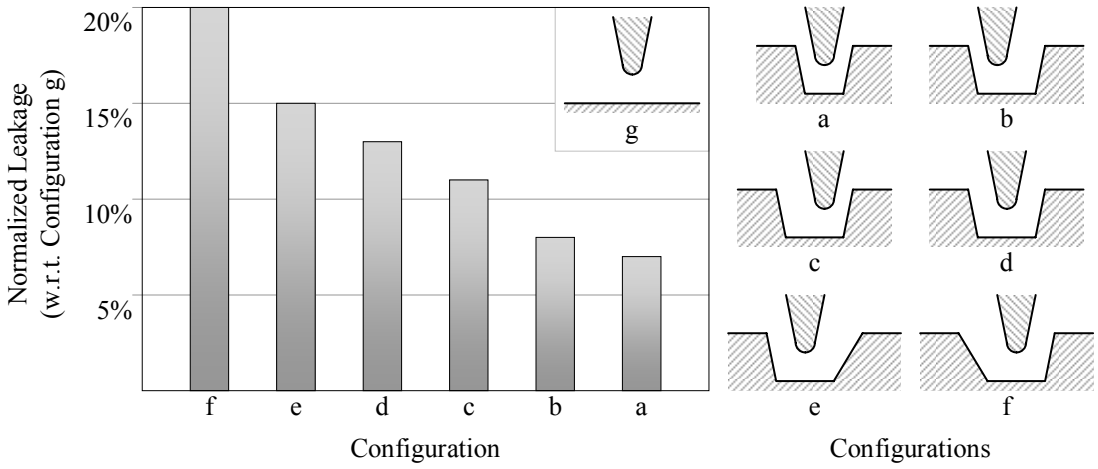

Figure 2.3 Keller's blade configurations and leakage results

Building on the Egli's work, Hodkinson [47] pointed out that the leakage equation that had been in customary use (Martin's equation) took into account neither the effect of the carry-over of kinetic energy from one cavity to the next nor the fact that there is a critical value of the back pressure beyond which flow rates will not increase with decreasing back pressure. Whereas Egli had used empirically obtained coefficients, Hodkinson derived an equation for the carry-over factor that he based on the assumption that the jet-stream expands conically at a small angle from the tip of the upstream blade

(he ignores the vena contracta) and that a portion of it carries on undisturbed into the next cavity.

Hodkinson also discussed the effects of eccentricity and rotational speed on labyrinth seal leakage. He stated that the effect of eccentricity is far more pronounced in the case of laminar flow than in the case of turbulent flow and found that, for laminar flow, fully eccentric mounting of his test seals resulted in flow that was up to 2.5 higher than the flow through the centered seals. Regarding the effect of shaft rotational speed on the axial flow-rate, Hodkinson observed that there would be little difference between using a rotating or non-rotating test-rig, a result which he based on experiments with oil flowing between stationary and rotating surfaces.

Bell and Bergelin [48] presented experimental data for flow through annular orifices and claimed that their data would also apply to the case of flow through the constrictions of labyrinth seals. They explained that at low Reynolds numbers, the main mechanism of energy loss is viscous shear in the fluid, while kinetic effects are only significant at the entrance to the orifice. At higher *Re* values, kinetic effects become predominant as relates to fluid acceleration, contraction, expansion, and turbulent friction. An equation is given for predicting the effects of eccentricity for low *Re* flow. Bell and Bergelin showed that in the case of turbulent flow through a thick orifice, there is also a partial recovery of kinetic energy as pressure as the fluid expands from the vena contracta. They also showed that there are wall friction losses as the fluid passes through the thicker orifice and that if the orifice is not sharp, there will be little or no contraction of the stream. An expression is given that can be used to examine the effect of thickness for straight and round orifices.

Bell and Bergelin found that at higher Reynolds numbers, the increasing orifice thickness increases frictional losses but also increases pressure recovery. Pressure recovery begins at thickness-to-clearance ratios of 1.0 and increases up to a value of 6.0 after which frictional effects become predominant and the flow-rate begins to drop. For ratios between 10 and 100, the flow-rate is comparable to that for a sharp-tipped orifice,

and for higher ratios the flow-rate is lower. At lower *Re* values, pressure recovery is not a factor and flow-rate decreases with increasing thickness for all values of thickness.

Zimmerman and Wolff [49] examined the flow through see-through labyrinth seals and presented an improved calculation method for leakage, treating the first constriction separately. This paper stated that since the carry-over effect is not present in the case of the first constriction, it is more effective at reducing the flow than at least some (but not all) of the downstream constrictions. They state that this holds true even though, generally, the "effectiveness" of each constriction increases in the downstream direction.

Zimmerman and Wolff also present and discuss a seemingly anomalous result showing that the pressure in the second cavity of a labyrinth seal can in some instances exceed that in the first cavity. They attributed this to the idea that in the case of a large clearance, the vena contracta (the narrowest point of the carry-over jet) in a cavity can occur well into the downstream cavity, causing a re-diffusion effect in this second cavity and raising its pressure.

The authors applied their equation to the first labyrinth constriction, but used Martin's equation [3], modified by a carry-over factor, which they developed and which is similar, but not identical to, that developed by Hodkinson [47], for all downstream blades. The theoretical predictions presented by Zimmerman and Wolff matched their experimental measurements reasonably well, and provided higher prediction accuracy to the equations found in all but one of their references (the exception being the equations developed by Wittig et al. [50]).

Wittig et al. used prediction codes to estimate discharge coefficients in labyrinth seals and verified the accuracy of their predictions through comparisons with test results. The authors cited sources stating that the effect of rotation on leakage is only significant in the case of a low Reynolds Number and a high Taylor Number. Their analysis neglected side wall effects because the ratio of the channel width to the depth of a cavity was large (more than 100). In the case of a staggered seal, a pressure difference was observed between the upper (stator side) and lower (rotor side) portions of a cavity. This was found in both the experiments and the calculated predictions and was attributed to

the existence of a stagnation point location at the bottom of each cavity. In the case of a see-through seal, higher discharge coefficients are observed because of the carry-over effect of the kinetic energy of the fluid from the preceding (upstream) chamber. The dependence of the discharge coefficients on clearance was found to be far higher in the case of see-through seals, but this dependence decreased with increasing number of blades. The discharge coefficients were generally found to increase with increasing clearance, but this trend became less pronounced, and was eventually reversed, when the number of blades was greatly reduced (the reversal occurred for the case of one blade).

Recent work such as that by Morrison and Rhode [51] has concentrating on using experimental techniques or CFD analysis to evaluate the effects of geometric factors on labyrinth seal performance. Gamal, Ertas, and Vance [52], in the only paper to date concentrating exclusively on PDS leakage, presented experimental evidence that such geometric considerations also have a significant effect on the leakage through pocket damper seals.

Other leakage formulae, including those developed by Vermes [53] and Neumann (Childs [15]), have been used as alternatives to the older equations mentioned above. These equations are presented and addressed in more detail in the *Leakage Model Theory* chapter of this dissertation.

CHAPTER III

RESEARCH JUSTIFICATION AND OBJECTIVES

Genuine engineering concerns justify the need for the research presented in this dissertation and the objectives this research aims to achieve. The close connection between the leakage rates and the rotordynamic coefficients of annular gas seals form the basis for the issues addressed.

RESEARCH JUSTIFICATION

Empirical results as well as theoretical analyses have shown that several factors affect the flow-rate through labyrinth and pocket damper seals. The pressure drop across a seal, the blade-to-journal clearances, the blade angle, the cavity depth, the blade shape, and the blade thickness are among the factors that may impact a seal's leakage. Results of past experiments suggest that these design parameters do indeed affect the leakage through the seal. Certain surprising results arising from comparisons of experimental data obtained from different seals can be linked to differences in the geometries of the seals being compared. While blade profile, blade spacing, blade thickness, and cavity depth may seem to be of secondary importance to such parameters as clearances and the number of blades, the former factors seem to have contributed to the unexpected results and can explain results which the latter factors cannot explain. The relation between the force coefficients and the leakage rates of annular gas seals implies that not only the efficiency, but also the rotordynamic performance and stability of turbomachinery would be affected by such considerations. A study of the effects of these factors and of potentially beneficial seal design modifications is therefore essential to developing more complete seal models.

Leakage Questions

Much of the research performed on labyrinth seals today is still based on Martin's original equation. There has not been a significant need to investigate the actual nature of fluid flow and to try to improve on this equation. Part of the reason for this is that seal leakage, which is essentially axial flow, has a large influence on the direct coefficients of seals, which affect the damping and stiffness of the seal, but it is the circumferential flow that affects the cross-coupled coefficients. In the case of labyrinth seals, which are the most commonly used non-contacting seals in turbomachinery, the direct damping is often so small that it is un-measurable (or at least insignificant), but the cross-coupled stiffness is significant and is the primary cause of instabilities originating in labyrinth seals. The issue was succinctly summarized by Whalen, Alvarez, and Palliser [54], who stated that when the initial leakage equations were developed, the influence of labyrinth seal leakage on overall machine efficiency was considered negligible. As seal clearances were made tighter, and as efficiencies improved this was no longer the case, but after the recognition of the influences labyrinth seals could have on rotating machinery stability, "further work on labyrinth seals then started to concentrate on their impact on rotordynamics; leakage flow concern became secondary once again. Oddly enough, most of the modern day computer codes that are used to calculate rotordynamic coefficients of labyrinth seals use a version of Martin's equation to estimate the axial flow through the seal. This is because axial flow impact on the coefficients is trivial; it is the circumferential flow that creates the destabilizing forces". While the last sentence quoted may hold true for most labyrinth seals, it is certainly untrue for pocket damper seals, in which the cross-coupled coefficients are of practically no significance, but the direct stiffness and damping, which are highly dependent on the axial flow-rates, are highly important. An accurate axial flow prediction model is therefore essential for pocket damper seals.

Beyond this point, certain assumptions have generally been made in the analysis and design of these seals that no longer hold true. Egli [43] states that "in a labyrinth, the friction in the short passage through the throttling gap plays a minor role only", and

Stodola [42] states that labyrinth constrictions are "so short that the friction loss can always be neglected". While this may be true for seals with knife-edge teeth, the developments made in such areas as tolerance control and materials technology, (including polymeric seals) allow thicker teeth to be employed if desired.

With regard to pocket damper seals, the fundamental leakage equation that has been used to analyze seal leakage has been the St. Venant orifice discharge equation. This equation, as derived by Spurk [44], is Torricelli's formula written for incompressible flow, even though pocket damper seals can only function with a compressible working fluid. This justifies reexamining the validity of the assumptions made in the use of this equation and the utility of the equation or others like it. It also justifies an investigation of the possibility of using an alternative equation which does not make such assumptions.

Unexpected experimental results obtained on labyrinth and pocket damper seals have also led to questions. Laos [32] tested a six-bladed labyrinth seal which leaked more than a four-bladed pocket damper seal and Gamal, Ertas, and Vance [52] tested a twelve-bladed PDS which leaked more than an eight-bladed PDS. Both these cases may be explained by taking into account geometric differences that are ignored in many leakage models.

Rotordynamic Questions

While the leakage-related issues to be discussed in this dissertation are concerned with both labyrinth and pocket damper seals, the rotordynamic issues to be addressed are mostly, although not completely, limited to pocket damper seals. Comparisons of PDS performance with labyrinth seal and other damper seal performance, as well as an investigation of the effects of certain design factors on the rotordynamic behavior of labyrinth seals, is also to be included.

The limited tests that have been carried out on fully-partitioned pocket damper seals have had promising results and show that these newer seals may eventually replace conventional pocket damper seals. Indications are that fully-partitioned PDSs would

have higher damping, lower circumferential flow, and do not necessarily have the high negative stiffness associated with the conventional seals. The number of factors affecting the coefficients of these seals means that design codes, similar to those developed for conventional seals, would be needed to fully analyze and design such seals. The nature of these seals allows them to be more easily "fine-tuned" in the design process so as to provide desirable combinations of stiffness, damping, and leakage. Additionally, there are indications that the rotordynamic performance of a fully-partitioned PDS is considerably less sensitive to changes in clearance ratio than that of a conventional PDS. This means that rotor-stator rubs that commonly occur during machine operation would have a far less detrimental effect on the newer seal design.

Pocket damper seals also offer an easy way to induce stiffness asymmetry into a rotating machine. Considering the large amount of damping that can be provided by such seals, it remains to be seen whether such additional orthotropy would be of any use, but it is worth investigating as an additional source of rotor stability, especially in cases where due to geometric constraints, the seal cannot be optimized for damping.

Simulations have shown that most of the damping of a pocket damper seal comes from the downstream cavities (particularly the last two cavities). Since this damping is proportional to the pocket volume, it is worth investigating the possibility of creating non-uniform seals that will have more upstream blades to limit leakage and fewer downstream blades to create larger cavities.

RESEARCH OBJECTIVES

The research to be presented aims to present an improved understanding of the leakage through labyrinth and pocket damper seals and of the rotordynamic effects of these seals. This is to be achieved through and examination of the effects of design parameters on the leakage and the direct rotordynamic coefficients of labyrinth seals and pocket damper seals. The following is a list of the main objectives of the research presented in this dissertation.

- Present a summary of the simulation and experimental data leading to questions about the effect of certain secondary design parameters on the leakage through these seals.
- Examine the differences in leakage rates through conventional and fully-partitioned pocket damper seal designs.
- Experimentally investigate the effects of blade thickness, cavity depth, blade profile, seal eccentricity, and blade spacing on seal leakage.
- Evaluate the numerous equations used in the literature in order to determine which best predicts the axial leakage through the tested and simulated seals. This is to be achieved through comparisons with the newly-obtained results of low-pressure experiments, with the high-pressure labyrinth seal data obtained by Picardo [55], with the high-pressure pocket damper seal data obtained by Gamal [40].
- Develop a model for the design and analysis of fully-partitioned pocket damper seals.
- Incorporate corrected area calculations in the pocket damper seal code.
- Investigate the possibility of developing pocket damper seals with non-uniform pitch so as to optimize damping versus leakage performance.
- Examine the possibility of using pocket damper seals to induce stiffness orthotropy and the potential stabilizing effects of such a design.
- Describe, through analytical simulations, the effects of various design parameters on the direct damping of pocket damper seals. Examine the effects of partition wall thickness and number of pockets on the leakage and rotordynamic coefficients of pocket damper seals.

CHAPTER IV

LEAKAGE MODELS

The leakage models examined in this dissertation are each built on one of three basic leakage formulae: the St. Venant Equation, Martin's Equation, and Neumann's Equation. The leakage models described in this chapter are combinations of one of these equations combined with different kinetic energy carry-over coefficients and flow-coefficients (both defined below). Each of the leakage models to be evaluated is described in a separate section below.

LEAKAGE MODEL DESCRIPTIONS

The nomenclature used in the descriptions of the eleven models presented in this section is explained by Figure 4.1. Of these eleven equations, eight are evaluated through a comparison to experimental results in the *Evaluation of Leakage Models* chapter of this dissertation. Five additional equations, made up of modified forms of the original eight equations or of combinations of the elements of those equations, are also described and evaluated in that chapter.

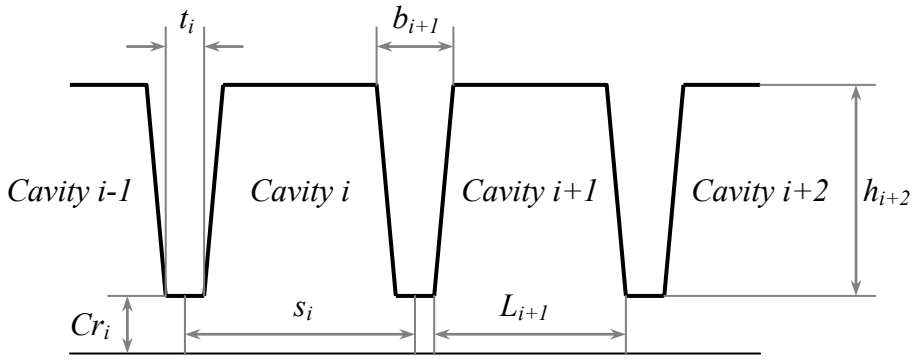

Figure 4.1 Seal geometry nomenclature

The St. Venant Equation

Vennard and Street [56] carried out an energy balance on a one dimensional flow element such as that shown in Figure 4.2 and obtained the Euler Equation of Equation (4.1). Neglecting the changes in height the term $g \cdot dz$ can be eliminated. Applying the isentropic relation of Equation (4.2) and integrating the Euler Equation results in the velocity expression of Equation (4.3).

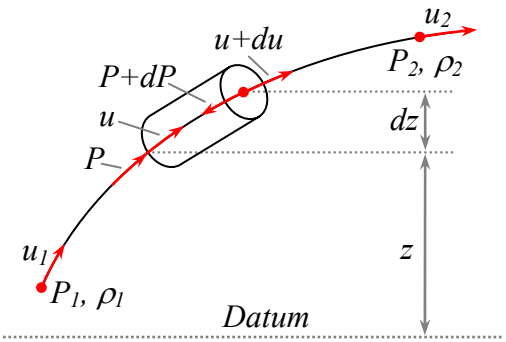

Figure 4.2 Energy balance on differential fluid element along a streamline

$$\frac{dP}{\rho} + u \cdot du + g \cdot dz = 0 \tag{4.1}$$

$$\frac{P_i}{\rho_i^{\gamma}} = \frac{P_{i+1}}{\rho_{i+1}^{\gamma}} \tag{4.2}$$

$$\frac{u_i^2 - u_{cav}^2}{2} = \int_{P_{i+1}}^{P_i} \frac{dP}{\rho} = \frac{P_i}{\rho_i} \cdot \frac{\gamma}{\gamma - 1} \cdot \left[1 - \left(\frac{P_{i+1}}{P_i} \right)^{\gamma - 1 / \gamma} \right] \tag{4.3}$$

$$u_i = \sqrt{\frac{2 \cdot \gamma}{\gamma - 1} \cdot \frac{P_i}{\rho_i} \cdot \left[1 - \left(\frac{P_{i+1}}{P_i} \right)^{\gamma - 1 / \gamma} \right]} \tag{4.4}$$

$$\dot{m}_i = \rho_i \cdot A_i \cdot u_i \tag{4.5}$$

$$\dot{m}_i = \frac{P_i \cdot A_i}{\sqrt{R \cdot T_i}} \cdot \sqrt{\frac{2 \cdot \gamma}{\gamma - 1} \cdot \left[1 - \left(\frac{P_{i+1}}{P_i} \right)^{\gamma - 1 / \gamma} \right]} \tag{4.6}$$

$$\dot{m}_i = \frac{P_i \cdot A_i}{\sqrt{\gamma \cdot R \cdot T_i}} \cdot \sqrt{\frac{2 \cdot \gamma^2}{\gamma - 1} \cdot \left[\left(\frac{P_{i+1}}{P_i} \right)^{2 / \gamma} - \left(\frac{P_{i+1}}{P_i} \right)^{\gamma + 1 / \gamma} \right]} \tag{4.7}$$

For flow through a seal constriction, the flow velocity in the cavity upstream of the constriction can be neglected relative to the velocity of the flow through the constriction. This yields the St. Venant-Wantzel discharge formula, which Spurk [44] defines using Equation (4.4). Defining the mass flow-rate (or weight rate of flow in the case of U.S. Customary Units) according to Equation (4.5), rearranging terms, and reapplying Equation (4.2) yields the St. Venant leakage equation (Equation (4.7)) first used by Schultz [27] to calculate pocket damper seal flow-rates.

Martin's Equation

Martin [3] presented the first leakage equation specifically intended for labyrinth seals. His formula, which assumes incompressible ideal gas behavior, is shown in Equation (4.8). Martin's Equation is derived based on the approach of determining the number of blades required to achieve a given pressure drop, then relating that number to the work done in dropping the pressure. The work done is then related to the flow-rate through the kinetic energy of the fluid.

$$\dot{m} = \frac{A \cdot P_{in}}{\sqrt{R \cdot T}} \cdot \sqrt{\frac{1 - \left(\frac{P_{out}}{P_{in}} \right)^2}{n - \ln\left(\frac{P_{out}}{P_{in}} \right)}} \tag{4.8}$$

Whereas the St. Venant Equation applied to a single constriction and therefore required an iterative algorithm to calculate the leakage through multiple blades, Martin's Equation offers a single-step procedure to determine the flow-rate. This means that intermediate pressures in the seal's cavities are not implicitly calculated by this equation.

Egli's Equation

Egli [43] used Martin's Equation as a starting point and suggested the use of a flow correction factor and a kinetic energy carry-over coefficient, which he determined empirically. Without the empirical coefficients, Egli's Equation is identical to Martin's Equation and will therefore not be analyzed separately.

$$\dot{m} = \mu_i^{emperical} \cdot \frac{A \cdot P_{in}}{\sqrt{R \cdot T}} \cdot \sqrt{\frac{1 - \left(\frac{P_{out}}{P_{in}}\right)^2}{n - \ln\left(\frac{P_{out}}{P_{in}}\right)}} \qquad \textbf{(4.9)}$$

Egli's flow coefficient is based on the fact that flow area in his equation, however is not the clearance area of the seal and not the area at the vena contracta, but the area of the jet of fluid at some point after it passes through the constriction. The use of the jet area comes from the assumption that at some point along the jet, shortly after the constriction, the pressure in the jet is equal to the cavity pressure in the downstream cavity (the cavity being entered).

The need for a kinetic energy carry-over coefficient is evident from Egli's description of the flow through the constrictions of a labyrinth seal: "as the steam flows through the labyrinth, a pressure drop occurs across each throttling. After each throttling, a small part of the kinetic energy of the steam jet will be reconverted into pressure energy, a second part will be destroyed and transferred into heat, and the remaining kinetic energy will enter the following throttling." The carry-over coefficient therefore represents the portion of kinetic energy carried over from one cavity to the

next. Egli reasons that since the jet emerging from the constriction increases with increasing axial distance, the percentage of kinetic energy carried over from one throttling to the next must decrease with increasing spacing between the blades or with decreasing clearance. Using Egli's method, the flow through a labyrinth seal can be shown to follow the proportionality of Equation (4.10) and this proportionality can be approximated to $n^{0.5}$.

$$\dot{m} \propto \frac{1}{\sqrt{n - \ln\left(\frac{P_{out}}{P_{in}}\right)}} \qquad \textbf{(4.10)}$$

Hodkinson's Equation

Hodkinson's Equation is a modification of Egli's Equation, but whereas Egli used an empirical coefficient to account for kinetic energy carry-over, Hodkinson [47] developed a semi-empirical expression for this coefficient based on an assumption regarding the gas jet's geometry. He assumed that the fluid jet expands conically at a small angle from the tip of the upstream blade and that a portion of it carries on undisturbed into the next cavity.

Hodkinson makes several references to Egli's experimental data, but also points out that Egli does not take into consideration the higher velocity through the final constriction. The former then derives a carry-over factor based on a linear increase in pressure drop with each constriction, which is based on a liquid labyrinth seal. This factor also incorporates the idea of a conically shaped (linearly increasing) stream and does not take into account vena contracta effects. Hodkinson provides two methods for coming up with his result; one based on pressure drops and one based on energy losses. The test data presented shows that a conical stream angle with a tangent of 0.02 best fit the data.

$$\dot{m}_i = \mu_i \cdot \frac{A \cdot P_{in}}{\sqrt{R \cdot T}} \cdot \sqrt{\frac{1-\left(\frac{P_{out}}{P_{in}}\right)^2}{n-\ln\left(\frac{P_{out}}{P_{in}}\right)}} \qquad \textbf{(4.11)}$$

$$\mu_i = \sqrt{\frac{1}{1-\left(\frac{n-1}{n}\right)\cdot\left(\frac{Cr_i/L_i}{(Cr_i/L_i)+0.02}\right)}}$$

The carry-over coefficient cannot increase indefinitely, but has a numerical limit which is defined in the paper since if clearances continue to increase, the fluid will blow straight through and the seal will act like one with a single constriction.

Hodkinson points out that with a very large pressure drop, the carry-over factor becomes unnecessary since at the acoustic velocity, seal leakage is more or less determined by the clearance of the final blade. At pressures further from the critical ratio or with a liquid in place of a gas, the carry-over effects become significant.

Vermes' Equation

Vermes [53] developed his own kinetic energy carry-over factor expression and combined this factor with Martin's leakage equation. Vermes' carry-over factor, represented by the expression of Equation (4.13) was developed from boundary layer theory.

$$\dot{m}_i = \mu_i \cdot \frac{A \cdot P_{in}}{\sqrt{R \cdot T}} \cdot \sqrt{\frac{1-\left(\frac{P_{out}}{P_{in}}\right)^2}{n-\ln\left(\frac{P_{out}}{P_{in}}\right)}} \qquad \textbf{(4.12)}$$

$$\mu_i = \sqrt{\frac{1}{(1-\alpha_i)}} \qquad \text{where} \qquad \alpha_i = \frac{8.52}{\frac{s_i - t_i}{Cr_i} + 7.23} \qquad \textbf{(4.13)}$$

Neumann's Equation

Neumann developed the empirical leakage expression of Equation (4.14) (Childs [15]). This equation contains a semi-empirical flow coefficient *Cf* and a kinetic energy carry-over coefficient μ. The former is a coefficient that accounts for the further contraction of flow after it has passed through the plane of the physical constriction and is calculated using Chaplygin's formula, shown in Equation (4.15), as defined by Gurevich [57].

$$\dot{m}_i = Cf_i \cdot \mu_i \cdot A_i \cdot \sqrt{\frac{P_i^2 - P_{i+1}^2}{R \cdot T}} \qquad \textbf{(4.14)}$$

$$Cf_i = \frac{\pi}{\pi + 2 - 5\beta_i + 2\beta_i^2} \quad \text{where} \quad \beta_i = \left(\frac{P_i}{P_{i+1}}\right)^{\gamma-1/\gamma} - 1 \qquad \textbf{(4.15)}$$

$$\mu_i = \sqrt{\frac{n}{n \cdot (1-\alpha_i) + \alpha_i}} \quad \text{where} \quad \alpha_i = 1 - \frac{1}{\left(1 + 16.6 \cdot Cr_i/s_i\right)^2}$$

Method of Zimmerman and Wolf

Zimmerman and Wolf [49] examined the flow through straight-through labyrinth seals and presented a calculation method for leakage, which treated the first constriction separately. They also presented experimental results that supported their analysis.

The paper states that, since the carry-over effect is not present in the case of the first constriction, it is more effective at reducing the flow than at least some (but not all) of the downstream constrictions. It is stated that this holds true even though, generally, the "effectiveness" of each constriction increases in the downstream direction.

The method developed by Zimmerman and Wolf is given by Equation (4.16), which applies the St. Venant Equation to the first constriction, then applies Martin's Equation, with a carry-over coefficient, to the remainder of the seal (the latter part of the method is identical to applying Hodkinson's Equation).

$$\dot{m}_i = \begin{cases} \dfrac{P_i \cdot A_i}{\sqrt{\gamma \cdot R \cdot T_i}} \cdot \sqrt{\dfrac{2 \cdot \gamma^2}{\gamma - 1} \cdot \left[\left(\dfrac{P_{i+1}}{P_i} \right)^{2/\gamma} - \left(\dfrac{P_{i+1}}{P_i} \right)^{\gamma+1/\gamma} \right]} & \text{For i} = 1 \\ \mu_i \cdot \dfrac{A \cdot P_{in}}{\sqrt{R \cdot T}} \cdot \sqrt{\dfrac{1 - \left(\dfrac{P_{out}}{P_{in}} \right)^2}{n - \ln\left(\dfrac{P_{out}}{P_{in}} \right)}} & \text{For i} > 1 \end{cases} \quad \textbf{(4.16)}$$

Scharrer's Equation

As was mentioned above, in the development of their one control volume model, Childs and Scharrer [8] used a form of Neumann's Equation. However, when Scharrer [18] developed his two control volume model, he used the non-constant kinetic energy carry-over coefficient developed by Vermes. This combination of the equations developed by Neumann and Vermes is referred to as Scharrer's Equation in this dissertation (this equation was also used by Dereli and Esser [58], who (while they reference Scharrer's work) refer to the equation as the Neumann Modified Method).

$$\dot{m}_i = Cf_i \cdot \mu_i \cdot A_i \cdot \sqrt{\frac{P_i^2 - P_{i+1}^2}{R \cdot T}} \quad \textbf{(4.17)}$$

$$Cf_i = \frac{\pi}{\pi + 2 - 5\beta_i + 2\beta_i^2} \quad \text{where} \quad \beta_i = \left(\frac{P_i}{P_{i+1}} \right)^{\gamma-1/\gamma} - 1 \quad \textbf{(4.18)}$$

$$\mu_i = \sqrt{\frac{1}{(1 - \alpha_i)}} \quad \text{where} \quad \alpha_i = \frac{8.52}{\dfrac{s_i - t_i}{Cr_i} + 7.23} \quad \textbf{(4.19)}$$

Equation of Esser and Kazakia

Esser and Kazakia [59] also used Neumann's Equation as a base equation, but use a constant flow coefficient instead of using Chaplygin's formula. They carried out a computational fluid dynamics analysis of the behavior of a fluid jet through planar constriction (a rectangular strip rather than an annular orifice) and concluded that a constant value (Equation (4.20)) for the flow coefficient would be more accurate than Chaplygin's formula.

$$\dot{m}_i = Cf_i \cdot \mu_i \cdot A_i \cdot \sqrt{\frac{P_i^2 - P_{i+1}^2}{R \cdot T}} \quad \text{where} \quad Cf_i = 0.716 \tag{4.20}$$

$$\mu_i = \sqrt{\frac{n}{n \cdot (1 - \alpha_i) + \alpha_i}} \quad \text{where} \quad \alpha_i = 1 - \frac{1}{\left(1 + 16.6 \cdot {Cr_i}/{s_i}\right)^2} \tag{4.21}$$

Equation of Kurohashi et al.

Kurohashi's [60] analysis focused on calculating the circumferential pressures developed in a seal when the journal is displaced, but also presented a method for calculating axial leakage. This equation was based on Neumann's Equation, but used a newly derived kinetic energy carry-over coefficient, which is given by Equation (4.17). The flow coefficient is calculated based on Reynolds Number using graphical data. The fact that the flow coefficient appears in the equation for the kinetic energy carry-over coefficient means that both the multipliers for this equation depend on empirical values.

$$\dot{m}_i = Cf_i \cdot \mu_i \cdot A_i \cdot \sqrt{\frac{P_i^2 - P_{i+1}^2}{R \cdot T}} \tag{4.22}$$

$$\mu_i = \begin{cases} \sqrt{\dfrac{1}{1-\alpha_i+\alpha_i^2}} & \text{For i} = 1 \\ \sqrt{\dfrac{1}{1-2\cdot\alpha_i+\alpha_i^2}} & \text{For i} > 1 \end{cases} \qquad \textbf{(4.23)}$$

$$\alpha_i = \frac{(Cr_i/s_i)}{(Cr_i/s_i)\cdot Cf_i + \tan\theta} \quad \text{where} \quad \theta = 6^{\circ}$$

Equation of Sriti et al.

Sriti et al. [61] began their analysis with Neumann's Equation as described by Childs [15], but developed an equation, also based on Neumann's Equation, which better matched their results. This equation used a single multiplier coefficient, given by Equation (4.24) to account for both flow contraction and kinetic energy carry-over effects. Sriti et al. use a time dependent area to account for eccentricity variations in their perturbation (dynamic) analysis to obtain rotordynamic coefficients. For the leakage (static) analysis of a centered seal, this eccentricity variable simplifies to the flow area of Equation (4.24). For a centered journal, the expression for H_i reduces to the radial clearance. The multiplier λ depends on the Reynolds Number of the flow through the seal as given by Equation (4.25).

$$\dot{m}_i = \lambda\cdot\left(1.57\cdot\frac{Cr_i}{L_i}+1\right)\cdot A_i\cdot\sqrt{\frac{P_i^2-P_{i+1}^2}{R\cdot T}} \qquad \textbf{(4.24)}$$

$$\lambda = \begin{cases} 0.8\cdot \mathrm{Re}^{-0.014} & \text{for Re} \le 1250 \\ 3.65\cdot \mathrm{Re}^{-0.22} & \text{for Re} > 1250 \end{cases} \qquad \textbf{(4.25)}$$

CHAPTER DISCUSSION

A summary of the leakage models presented in this chapter and of the main components on which they are built is presented in

Table 4.1. Of the eleven equations listed, ten are examined in the *Evaluation of Leakage Models* chapter of this dissertation through a comparison to new and previously published experimental data.

Table 4.1 Summary of leakage models

Model	Fundemental Equation	K.E. Coefficient	Flow Coefficient
St. Venant	St. Venant	None	None
Martin	Martin	None	Constant
Egli	Martin	Emperical	Emperical
Hodkinson	Martin	Hodkinson	Emperical
Vermes	Martin	Vermes	Emperical
Neumann	Neumann	Neumann	Chaplygin
Zimmerman & Wolf	St. Venant & Martin	Emperical	Emperical
Scharrer	Neumann	Vermes	Chaplygin
Esser & Kazakia	Neumann	Esser & Kazakia	Constant
Kurohashi et al.	Neumann	Kurohashi et al.	Emperical
Sirti et al.	Neumann	Sirti et al.*	Sirti et al.*

** For Sirti et al., K.E. & flow coefficients not evaluated separately (only one multiplier used)*

Previous Comparisons

Benvenuti, Ruggeri, and Tomasini [62] presented a paper in 1979 in which they compared several leakage models to their experimental results. They found that the models that did not take into account kinetic energy carry-over effects matched their results more closely. However, their data are presented in purely dimensionless form and provide no information regarding either the seal geometry or the supply pressures used during testing.

Table 4.2 Comparison of Neumann's Equ. and the St. Venant Equ. (Kearton and Keh)

Pressure Ratio	"Error" due to use of Neumann's Equation
0.95	-1.00%
0.90	-1.84%
0.85	-2.60%
0.80	-3.52%

Kearton and Keh [63] derived an equation identical to Neumann's (without the two coefficients) in 1950, 14 years before Neumann's paper was published. This derivation

was for a single constriction and was compared to the St. Venant Equation, which the authors considered to an equation that was more theoretically accurate, but also more difficult to implement. The prediction error of Neumann's Equation compared to the St. Venant Equation is shown in Table 4.2 for different pressure ratios. Since all the literature surveyed refers to this equation as Neumann's Equation, it is referred to in this same way in this dissertation.

As mentioned earlier, Esser and Kazakia [59] found that multiplying their leakage equation by a constant flow coefficient of 0.716 matched their CFD predictions more accurately than using Chaplygin's formula. Their analysis was limited in two ways; the pressure drop across the clearance area was relatively small, and the simulated geometry did not match that of a real seal. In reference to the first point, the pressure downstream of the constriction was maintained at 101 KPa (14.47 psi) while the upstream pressure was varied from 102 to 109 KPa (from 14.61 to 15.61 psi), meaning that the pressure ratio was never lower than approximately 0.93. In reference to the second point, Esser and Kazakia simulated the flow over a flat rectangular plate (the geometry for which Chaplygin's formula had been derived) to determine the contraction coefficient, rather than the flow through an annular clearance.

Iterative vs. Single-Application Equations

The leakage equations can be classified as either iterative equations or as single-application equations. For instance, the St. Venant Equation requires an iterative technique to solve for the leakage through a seal, whereas Martin's equation can be applied to an entire seal at once. The iterative equations provide predictions for intermediate seal cavity pressures, whereas the single-application equations do not. In order to obtain these pressures, the single-application equation can be applied to each blade individually after flow-rate has been calculated. This method allows prediction of the pressure in each cavity using the pressure in the preceding cavity and assuming a one-bladed seal. In this way, the final pressure should match the prescribed seal back-

pressure (since the previously calculated flow-rate is used for each cavity pressure calculation).

Pressure Recovery

Zimmerman and Wolf [49] show how a seemingly anomalous result can be obtained when the pressure in the second cavity exceeds that in the first. This is explained by the idea that in the case of a large clearance, the vena contracta (the narrowest point of the carry-over jet) in a cavity can occur well into the cavity, causing a re-diffusion effect in the second cavity, which raises the pressure of the second cavity. Zimmerman and Wolf experimental data that demonstrates this phenomenon in the form of cavity pressure measurements showing a pressure in the second cavity of a seal that is higher than the pressure in the seal's first cavity.

CHAPTER V

POCKET DAMPER SEAL THEORY AND MODELING

The basic theory of operation of pocket damper seals and the modeling of the forces generated within a seal are the subject of this chapter. The theoretical models for the determination of the rotordynamic coefficients of pocket damper seals differ depending on whether the seal under investigation is of the conventional or the full-partitioned configuration. As a result, the rotordynamic models developed for each configuration are discussed separately. Whereas the force coefficient theory (dynamic model) of the seals is different, the same leakage theory (static model) is used for each seal. Furthermore, the techniques by which force coefficients are experimentally extracted (seal force theory) are the same for both seals.

The expressions for the stiffness and damping of a two-bladed conventional pocket damper seal were derived by Shultz [27], were restated by Gamal [40], and are summarized below. The first stage of the derivation assumes no journal vibration (not necessarily zero rotational speed) and provides an expression for the overall mass flow-rate through a seal and the steady-state pressures in the pockets using a selected leakage model. The second stage of the derivation; the perturbation analysis; uses the calculated flow-rate as an input and obtains expressions for the seal's direct rotordynamic coefficients.

STATIC MODEL

Shultz's [27] two-bladed seal model is shown in Figure 5.1. For the static case $x(t)=0$, the following steady-state condition for the flow-rates across each seal blade applies:

$$\dot{m}_1 = \dot{m}_2 = \dot{m}_3 = \ldots = \dot{m}_n = \dot{m} \qquad \textbf{(5.1)}$$

Where n is the number of blades in the seal, $\dot{m}_1$ is the flow-rate through area A_1, and $\dot{m}_n$ is the flow-rate through area A_n. If the working fluid is assumed to be a perfect gas and the process is assumed to be isentropic, the mass flow-rate for the subsonic flow is given by the St. Venant Equation of Equation (5.2) or by any of the leakage models discussed in the *Leakage Model Descriptions* chapter of this dissertation. For choked flow, the flow-rate becomes independent of the downstream pressure and is given by Equation (5.3). With assumed cavity pressures, the mass flow-rates ($\dot{m}_1$, $\dot{m}_2$, …, $\dot{m}_n$) can be calculated, and the solution can be iterated until Equation (5.1)) is satisfied.

$$\dot{m}_i = \frac{P_i \cdot A_i}{\sqrt{\gamma \cdot R \cdot T_i}} \cdot \sqrt{\frac{2 \cdot \gamma^2}{\gamma - 1} \cdot \left[\left(\frac{P_{i+1}}{P_i} \right)^{2/\gamma} - \left(\frac{P_{i+1}}{P_i} \right)^{\gamma+1/\gamma} \right]} \qquad \textbf{(5.2)}$$

$$\dot{m}_i = \beta \cdot P_i \cdot A_i \Big/ \sqrt{R \cdot T_i} \qquad (\beta = 0.5283 \text{ for air}) \qquad \textbf{(5.3)}$$

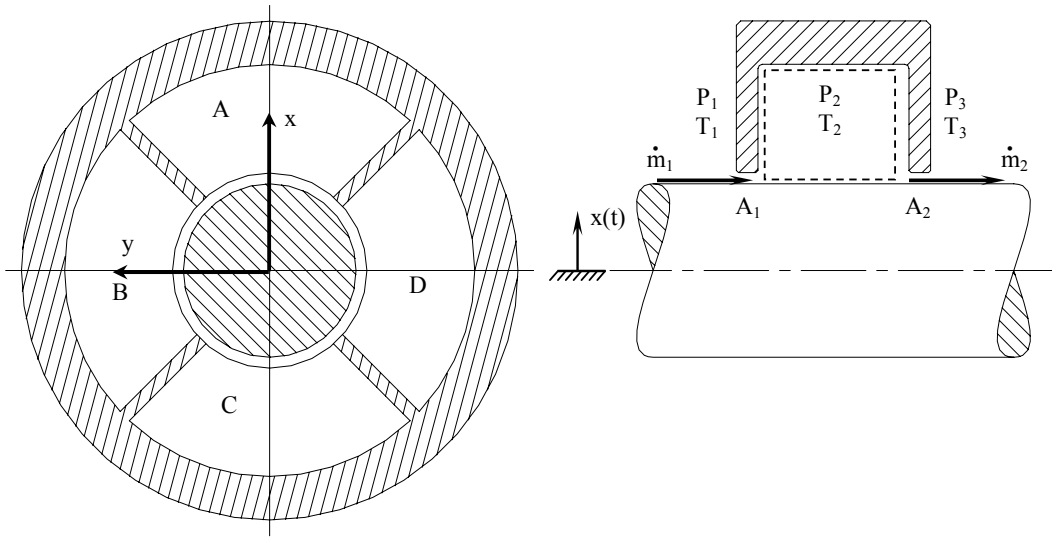

Figure 5.1 2-bladed seal model

DYNAMIC MODEL: CONVENTIONAL SEALS

A detailed derivation of the direct force coefficients of conventional pocket damper seals was presented by Gamal [40]. This section highlights the main points in that derivation. For a journal oscillating with a frequency of vibration ω, the journal motion is assumed to be sinusoidal and given by

$$x(t) = X \cdot \sin(\omega \cdot t) \tag{5.4}$$

In this case, there will be a variation with time in the pressures within the cavities. Writing the conservation of mass equation:

$$\dot{m}_i = \dot{m}_{i+1} + \frac{\partial}{\partial t}\left(\rho_{i+1} \cdot V_{i+1}\right) \tag{5.5}$$

The latter part of the right side of this equation is an expression for the rate of change of mass in the pocket due to time variations of the density and volume. Applying the ideal gas law to this expression yields Equation (5.6), which when substituted into Equation (5.5) gives Equation (5.7).

$$\frac{\partial}{\partial t}\left(\rho_i \cdot V_i\right) = V_i \cdot \frac{\partial \rho_i}{\partial t} + \rho_i \cdot \frac{\partial V_i}{\partial t}$$

$$\therefore \frac{\partial}{\partial t}\left(\rho_i \cdot V_i\right) = V_i \cdot \frac{\partial \rho_i}{\partial P_i} \cdot \frac{\partial P_i}{\partial t} + \rho_i \cdot \frac{\partial V_i}{\partial t}$$

$$\frac{1}{P} - \frac{\gamma}{\rho} \cdot \frac{\partial \rho}{\partial P} = 0 \qquad \therefore \frac{\partial \rho}{\partial P} = \frac{\rho}{P \cdot \gamma}$$

$$\frac{\partial \rho}{\partial P} = \frac{1}{\gamma \cdot R \cdot T} = \frac{1}{(\text{speed of sound})^2}$$

$$\frac{\partial}{\partial t}(\rho_i \cdot V_i) = \frac{V_i}{\gamma \cdot R \cdot T_i} \cdot \frac{\partial P_i}{\partial t} + \frac{P_i}{R \cdot T_i} \cdot \frac{\partial V_i}{\partial t} \qquad \textbf{(5.6)}$$

$$\dot{m}_i - \dot{m}_{i+1} = \left(\frac{V_{i+1}}{\gamma \cdot R \cdot T_{i+1}}\right) \cdot \frac{\partial P_{i+1}}{\partial t} + \left(\frac{P_{i+1}}{R \cdot T_{i+1}}\right) \cdot \frac{\partial V_{i+1}}{\partial t} \qquad \textbf{(5.7)}$$

It should be noted that these equations, as initially developed by Shultz, implicitly assume that the rate of change of temperature with time is zero. This assumption is inconsistent with the assumption of isentropic flow, but the alanysis is presented here as it was derived by Shultz. In this form, the difference in the mass flow-rates across two consecutive blades is a function of two time-dependent parameters; the pressure $P_{i+1}(t)$ in the i^{th} cavity and the pocket volume $V(t)$ (which is a function of the journal displacement $x(t)$).

$$\dot{m}_i - \dot{m}_{i+1} = f(P_{i+1}(t), x(t)) \qquad \textbf{(5.8)}$$

Expanding Equation (5.8) in the form of a Taylor Series up to first order derivatives yields:

$$\dot{m}_i - \dot{m}_{i+1} = \left.\frac{\partial \dot{m}_i}{\partial P_{i+1}}\right|_{P_{i+1}} \cdot P_{i+1}(t) + \left.\frac{\partial \dot{m}_i}{\partial x}\right|_{x} \cdot x(t) - \left.\frac{\partial \dot{m}_{i+1}}{\partial P_{i+1}}\right|_{P_{i+1}} \cdot P_{i+1}(t) + \left.\frac{\partial \dot{m}_{i+1}}{\partial x}\right|_{x} \cdot x(t)$$

Substituting the result into Equation (5.7) yields:

$$\left.\frac{\partial \dot{m}_i}{\partial P_{i+1}}\right|_{P_{i+1}} \cdot P_{i+1}(t) + \left.\frac{\partial \dot{m}_i}{\partial x}\right|_{x} \cdot x(t) - \left.\frac{\partial \dot{m}_{i+1}}{\partial P_{i+1}}\right|_{P_{i+1}} \cdot P_{i+1}(t) - \left.\frac{\partial \dot{m}_{i+1}}{\partial x}\right|_{x} \cdot x(t)$$

$$= \left(\frac{V_{i+1}}{\gamma \cdot R \cdot T_{i+1}}\right) \cdot \frac{\partial P_{i+1}}{\partial t} + \left(\frac{P_{i+1}}{R \cdot T_{i+1}}\right) \cdot \frac{\partial V_{i+1}}{\partial t}$$

This can be rewritten as:

$$\left(\frac{\partial \dot{m}_i}{\partial P_{i+1}} - \frac{\partial \dot{m}_{i+1}}{\partial P_{i+1}}\right) \cdot P_{i+1} + \left(\frac{\partial \dot{m}_i}{\partial x} - \frac{\partial \dot{m}_{i+1}}{\partial x}\right) \cdot x$$

$$= \left(\frac{V_{i+1}}{\gamma \cdot R \cdot T_{i+1}}\right) \cdot \frac{\partial P_{i+1}}{\partial t} + \left(\frac{P_{i+1}}{R \cdot T_{i+1}}\right) \cdot \frac{\partial V_{i+1}}{\partial t} \qquad \textbf{(5.9)}$$

The partial derivatives with respect to pressure of Equation (5.9) were defined by Gamal [40] as:

$$\frac{\partial \dot{m}_i}{\partial P_{i+1}} = \frac{1}{2} \cdot \frac{P_i \cdot A_i}{\sqrt{\gamma \cdot R \cdot T_i}} \cdot \left[\frac{\dfrac{4 \cdot \gamma}{(\gamma - 1) \cdot P_i} \cdot \left(\dfrac{P_{i+1}}{P_i}\right)^{(2-\gamma)/\gamma} + \dfrac{2 \cdot \gamma \cdot (\gamma + 1)}{(k-1)} \cdot \left(\dfrac{P_{i+1}}{P_i}\right)^{1/\gamma}}{\sqrt{\dfrac{2 \cdot \gamma^2}{\gamma - 1} \cdot \left[\left(\dfrac{P_{i+1}}{P_i}\right)^{2/\gamma} + \left(\dfrac{P_{i+1}}{P_i}\right)^{(\gamma+1)/\gamma}\right]}} \right] \qquad \textbf{(5.10)}$$

The journal orbit can be represented by the superposition of two displacements, *x(t)* and *y(t)*, along orthogonal axes. In Shultz's [27] model, the orthogonal axes were drawn so that they bisected each of the four pockets, as shown in Figure 5.1. Displacing the

journal a distance *x* along one axis results in a reduction in the clearance between the journal and the seal blades over the arc length of the pocket towards which the journal was displaced. Due to the curvatures of the blades and the journal, the reduction in clearance will be greatest at the midpoint of the arc. Shultz, however, made the assumption that the reduction in clearance is equal to the journal displacement *x* over the entire arc length (see section titled *Modulation of Clearance Geometry* below). Shultz's predictions using this approximated model accurately matched his experimental results. The derivatives of the mass flow-rates with respect to the journal displacement can therefore be expanded as follows:

$$\frac{\partial \dot{m}_i}{\partial x} = \frac{\pi \cdot d \cdot P_i}{N \cdot \sqrt{\gamma \cdot R \cdot T_i}} \cdot \sqrt{\frac{2 \cdot \gamma^2}{\gamma - 1} \cdot \left[\left(\frac{P_{i+1}}{P_i} \right)^{2/\gamma} - \left(\frac{P_{i+1}}{P_i} \right)^{\gamma+1/\gamma} \right]}$$

$$\frac{\partial \dot{m}_{i+1}}{\partial x} = \frac{\pi \cdot d \cdot P_{i+1}}{N \cdot \sqrt{\gamma \cdot R \cdot T_{i+1}}} \cdot \sqrt{\frac{2 \cdot \gamma^2}{\gamma - 1} \cdot \left[\left(\frac{P_{i+2}}{P_{i+1}} \right)^{2/\gamma} - \left(\frac{P_{i+2}}{P_{i+1}} \right)^{\gamma+1/\gamma} \right]} \qquad \textbf{(5.11)}$$

This can be rewritten as:

$$\frac{\partial \dot{m}_i}{\partial x} = \frac{\pi \cdot d}{N \cdot A_i} \cdot \dot{m}_i \quad \text{and} \quad \frac{\partial \dot{m}_{i+1}}{\partial x} = \frac{\pi \cdot d}{N \cdot A_{i+1}} \cdot \dot{m}_{i+1} \qquad \textbf{(5.12)}$$

To obtain a more compact form of the equations for seal stiffness and damping, the following variables were used:

$$a_i = \frac{V_i}{\gamma \cdot R \cdot T_{i+1}} \quad \text{and} \quad b_i = \left(\frac{\partial \dot{m}_i}{\partial P_{i+1}} - \frac{\partial \dot{m}_{i+1}}{\partial P_{i+1}} \right) \qquad \textbf{(5.13)}$$

$$d_i = \left(\frac{\partial \dot{m}_i}{\partial x} - \frac{\partial \dot{m}_{i+1}}{\partial x} \right) \quad \text{and} \quad e_i = \frac{-P_{i+1} \cdot W_i \cdot d}{N \cdot R \cdot T_{i+1}}$$

These four variables simplify Equation (5.9) into the following form:

$$a_i \cdot \frac{P_{i+1}(t)}{\partial t} + b_i \cdot P_{i+1}(t) + d_i \cdot x(t) + e_i \cdot \frac{\partial x(t)}{\partial t} = 0 \qquad \textbf{(5.14)}$$

Differentiating the assumed sinusoidal displacement of the rotor results in an expression for the time-varying journal velocity.

$$\dot{x}(t) = \frac{dx(t)}{dt} = \omega \cdot X \cdot \cos(\omega \cdot t) \qquad \textbf{(5.15)}$$

The force developed in the seal is proportional to the time dependent displacement and velocity of the journal and the seal can be modeled using the spring-mass-damper system. As a result of the assumed motion of the journal, the seal force will be of a similar form and can be represented by:

$$F(t) = K \cdot x(t) + C \cdot \dot{x}(t) = F_c \cdot \cos(\omega \cdot t) + F_s \cdot \sin(\omega \cdot t) \qquad \textbf{(5.16)}$$

Since this force is developed due to the pressures in the cavities, it can be assumed that the dynamic pressure is given by:

$$P_d(t) = P_c \cdot \cos(\omega \cdot t) + P_s \cdot \sin(\omega \cdot t) \qquad \textbf{(5.17)}$$

The pressure in a given cavity at any instant in time is the summation of this dynamic pressure and the static pressure. The expressions for the cavity pressure and its time derivative are given by:

$$P_i(t) = \underbrace{\overline{P_i}}_{\text{Static Pressure}} + \underbrace{P_{ci}(t)\cdot\cos(\omega\cdot t) + P_{si}(t)\cdot\sin(\omega\cdot t)}_{\text{Dynamic Pressure}}$$

$$\therefore \frac{\partial P_i}{\partial t} = \omega\cdot P_{si}(t)\cdot\cos(\omega\cdot t) - \omega\cdot P_{ci}(t)\cdot\sin(\omega\cdot t) \qquad \textbf{(5.18)}$$

Substituting the sinusoidal pressure expression of in Equation (5.18) and the journal displacement and velocity expressions into Equation (5.14) and separating sine and cosine terms yields two expressions in the two pressure coefficients P_{si} and P_{ci} unknowns (Equation (5.19)). These equations can be solved for the pressure coefficients of Equation (5.20).

$$\begin{aligned} a_i\cdot\omega\cdot P_{si} + b_i\cdot P_{ci} + e_i\cdot\omega\cdot X = 0 \\ -a_i\cdot\omega\cdot P_{ci} + b_i\cdot P_{si} + d_i\cdot X = 0 \end{aligned} \qquad \textbf{(5.19)}$$

$$P_{si} = \frac{-\left(b_i\cdot d_i + a_i\cdot e_i\cdot\omega^2\right)}{b_i^{\,2} + a_i^{\,2}\cdot\omega^2}\cdot X \quad \text{and} \quad P_{ci} = \frac{\left(a_i\cdot d_i - b_i\cdot e_i\right)\cdot\omega}{b_i^{\,2} + a_i^{\,2}\cdot\omega^2}\cdot X \qquad \textbf{(5.20)}$$

Assuming that the pressure in cavity i acts on an area A_{Pi}, the direct rotordynamic coefficients of the seal can be obtained from Equations (5.16) and (5.20) as:

$$K_i = \frac{-\left(b_i\cdot d_i + a_i\cdot e_i\cdot\omega^2\right)}{b_i^{\,2} + a_i^{\,2}\cdot\omega^2}\cdot A_{Pi} \qquad \textbf{(5.21)}$$

$$C_i = \frac{\left(a_i \cdot d_i - b_i \cdot e_i\right)}{b_i^{\,2} + a_i^{\,2} \cdot \omega^2} \cdot A_{Pi}$$

These coefficients are highly dependent on the frequency of vibration of the journal. They are, however, independent of the amplitude of that vibration, due to the first-order expansion (linearization) of Equation (5.8). The results of this derivation are the mass flow-rate through the seal and the direct stiffness and direct damping generated in each seal cavity.

DYNAMIC MODEL: FULLY-PARTITIONED SEALS

The static model is identical for both the conventional and the fully-partitioned configurations of the pocket damper seal, but the dynamic model from which the rotordynamic coefficients are determined differs for each of the two seal types. Equation (5.8) represents the first point in the derivation at which the dynamic model for a fully-partitioned seal differs from that for a conventional seal.

For a fully-partitioned pocket damper seal, there are no cavities in which the pocket pressures are not modulated by the displacement of the journal; that is, all pocket pressures vary with time. Equation (5.8) must therefore be rewritten in the form of Equation (5.22) to reflect the time-varying nature of all the pocket pressures. This expression is applicable for all cavities except the first and last cavities for which the pressures P_i and P_{i+1} respectively do not vary with time.

$$\dot{m}_i - \dot{m}_{i+1} = f\left(P_i(t), P_{i+1}(t), x(t)\right) \qquad \textbf{(5.22)}$$

Expanding Equation (5.22) in the form of a Taylor Series up to first order derivatives yields:

$$\dot{m}_i - \dot{m}_{i+1} = \left.\frac{\partial \dot{m}_i}{\partial P_i}\right|_{P_i} \cdot P_i(t) + \left.\frac{\partial \dot{m}_i}{\partial P_{i+1}}\right|_{P_{i+1}} \cdot P_{i+1}(t) + \left.\frac{\partial \dot{m}_i}{\partial x}\right|_{x} \cdot x(t)$$
$$- \left.\frac{\partial \dot{m}_{i+1}}{\partial P_{i+1}}\right|_{P_{i+1}} \cdot P_{i+1}(t) - \left.\frac{\partial \dot{m}_{i+1}}{\partial P_{i+2}}\right|_{P_{i+2}} \cdot P_{i+2}(t) - \left.\frac{\partial \dot{m}_{i+1}}{\partial x}\right|_{x} \cdot x(t)$$

Substituting the result into Equation (5.7) yields:

$$\left.\frac{\partial \dot{m}_i}{\partial P_i}\right|_{P_i} \cdot P_i(t) + \left.\frac{\partial \dot{m}_i}{\partial P_{i+1}}\right|_{P_{i+1}} \cdot P_{i+1}(t) + \left.\frac{\partial \dot{m}_i}{\partial x}\right|_{x} \cdot x(t) - \left.\frac{\partial \dot{m}_{i+1}}{\partial P_{i+1}}\right|_{P_{i+1}} \cdot P_{i+1}(t)$$
$$- \left.\frac{\partial \dot{m}_{i+1}}{\partial P_{i+2}}\right|_{P_{i+2}} \cdot P_{i+2}(t) - \left.\frac{\partial \dot{m}_{i+1}}{\partial x}\right|_{x} \cdot x(t)$$
$$= \left(\frac{V_{i+1}}{\gamma \cdot R \cdot T_{i+1}}\right) \cdot \frac{\partial P_{i+1}}{\partial t} + \left(\frac{P_{i+1}}{R \cdot T_{i+1}}\right) \cdot \frac{\partial V_{i+1}}{\partial t}$$

This can be rewritten as:

$$\left(\frac{\partial \dot{m}_i}{\partial P_i}\right) \cdot P_i + \left(\frac{\partial \dot{m}_i}{\partial P_{i+1}} - \frac{\partial \dot{m}_{i+1}}{\partial P_{i+1}}\right) \cdot P_{i+1} - \left(\frac{\partial \dot{m}_{i+1}}{\partial P_{i+2}}\right) \cdot P_{i+2}$$
$$+ \left(\frac{\partial \dot{m}_i}{\partial x} - \frac{\partial \dot{m}_{i+1}}{\partial x}\right) \cdot x = \left(\frac{V_{i+1}}{\gamma \cdot R \cdot T_{i+1}}\right) \cdot \frac{\partial P_{i+1}}{\partial t} + \left(\frac{P_{i+1}}{R \cdot T_{i+1}}\right) \cdot \frac{\partial V_{i+1}}{\partial t} \qquad \textbf{(5.23)}$$

In Equation (5.23), the partial derivatives $\partial \dot{m}_i / \partial P_{i+1}$ and $\partial \dot{m}_{i+1} / \partial P_{i+2}$ can be obtained using Equations (5.10), as was done for the conventional pocket damper seal, and the partial derivative $\partial \dot{m}_i / \partial P_i$ can be obtained using Equation (5.24). The

derivatives of the mass flow-rates with respect to the journal displacement are unchanged, and are still given by (5.11).

$$\frac{\partial \dot{m}_i}{\partial P_i} = \frac{P_{i+1} \cdot A_i}{2P_i \cdot \sqrt{\gamma \cdot R \cdot T_i}} \cdot \left[\frac{\frac{4 \cdot \gamma}{(\gamma - 1)} \cdot \left(\frac{P_{i+1}}{P_i} \right)^{(2-\gamma)/\gamma} + \frac{2 \cdot \gamma \cdot (\gamma + 1)}{(\gamma - 1)} \cdot \left(\frac{P_{i+1}}{P_i} \right)^{1/\gamma}}{\sqrt{\frac{2 \cdot \gamma^2}{\gamma - 1} \cdot \left[\left(\frac{P_{i+1}}{P_i} \right)^{2/\gamma} + \left(\frac{P_{i+1}}{P_i} \right)^{(\gamma+1)/\gamma} \right]}} \right] \quad \textbf{(5.24)}$$

Whereas Equation (5.9) results in a system of uncoupled equations for flow through the constrictions of a conventional seal, Equation (5.23) will result in a system of coupled equations. This is due to the dependence of the dynamic pocket pressure in an FP-PDS on the pressures of the upstream and downstream pockets (pressures which are also modulated by the displacement of the journal). The dynamic pocket pressure equations cannot, therefore, be solved independently of each other and must be solved in matrix form (this procedure was first used by Ertas [41] for his six-bladed seal case). Dummy variables can be used to simplify the analysis, as was done for the conventional pocket damper seal. These variables are defined in Equations (5.25) through (5.28). To reiterate the terminology being used; $\dot{m}_i$ is the flow rate through the i^{th} constriction and entering the $(i+1)^{th}$ cavity in which the pressure, temperature and volume are given by P_{i+1}, T_{i+1}, and V_{i+1} respectively.

$$a_i' = \left(\frac{V_{i+1}}{\gamma \cdot R \cdot T_{i+1}} \right) \quad \textbf{(5.25)}$$

$$b_i' = \frac{\partial \dot{m}_i}{\partial P_{i+1}} \quad \text{if } i \text{ is odd} \qquad \text{and} \qquad b_i' = \frac{\partial \dot{m}_i}{\partial P_i} \quad \text{if } i \text{ is even} \quad \textbf{(5.26)}$$

$$d_i^{'} = \frac{\partial \dot{m}_i}{\partial x} - \frac{\partial \dot{m}_{i+1}}{\partial x} \qquad \textbf{(5.27)}$$

$$e_i^{'} = \left(\frac{P_{i+1}}{R \cdot T_{i+1}} \right) \qquad \textbf{(5.28)}$$

Using these dummy variables, the dynamic pressure equations can be rewritten in matrix form of Equation (5.29). These equations are equivalent to Equations (5.18) procedure is analogous to that followed for conventional seals in the form of (5.20), which resolved the dynamic pressures into components in-line with and 90^o degrees out of phase with to the journal displacement. The coefficient matrix M can be written using the sub-matrix defined in Equation (5.30). The terms marked *Diagonal* in Equation (5.30) are centered on the diagonal and the remaining terms are inserted into the matrix relative to these diagonal terms. The subscript *i* refers to the matrix column number. For example, the coefficient matrix for a four-bladed seal would be given by Equation (5.31).

$$\overline{M} \cdot \overline{\Pi} = \overline{\Gamma} \qquad \text{or} \qquad \overline{\Pi} = \overline{M}^{-1} \cdot \overline{\Gamma} \qquad \textbf{(5.29)}$$

$$\overline{M}_{sub} = \begin{bmatrix} -b_i' & 0 \\ 0 & -b_{i-1}' \\ \underbrace{b_i' - b_{i+1}'}_{Diagonal} & -\omega \cdot a_{i/2}' \\ -\omega \cdot a_i' & \underbrace{b_{i-1}' - b_i'}_{Diagonal} \\ b_{i+1}' & 0 \\ 0 & b_i' \end{bmatrix} \quad \text{where } i \text{ is the column number} \qquad \textbf{(5.30)}$$

$$\overline{M}_4 = \begin{bmatrix} b_1' - b_2' & -\omega \cdot a_1' & -b_3' & 0 & 0 & 0 \\ \omega \cdot a_1' & b_1' - b_2' & 0 & -b_3' & 0 & 0 \\ b_2' & 0 & b_3' - b_4' & -\omega \cdot a_2' & -b_5' & 0 \\ 0 & b_2' & \omega \cdot a_2' & b_3' - b_4' & 0 & -b_5' \\ 0 & 0 & b_4' & 0 & b_5' - b_6' & -\omega \cdot a_3' \\ 0 & 0 & 0 & b_4' & \omega \cdot a_3' & b_5' - b_6' \end{bmatrix} \qquad \textbf{(5.31)}$$

The right-hand vector Γ can be written using the two-element sub-vector given by Equation (5.32). The subscript *i* refers to the vector row number. For example, the right-hand vector for a four-bladed seal would be given by Equation (5.33).

$$\overline{\Gamma}_{sub} = \begin{Bmatrix} -\omega \cdot X \cdot e_i' \\ X \cdot d_{i-1}' \end{Bmatrix} \quad \text{where } i \text{ is the row number} \qquad \textbf{(5.32)}$$

$$\overline{\Gamma}_4 = \begin{Bmatrix} -\omega \cdot X \cdot e_1' \\ X \cdot d_1' \\ -\omega \cdot X \cdot e_2' \\ X \cdot d_2' \\ -\omega \cdot X \cdot e_3' \\ X \cdot d_3' \end{Bmatrix} \qquad \textbf{(5.33)}$$

Using these definitions, the dynamic pressures (contained in the matrix Π) can be determined using Equation (5.29). The vector Π now consists of components that are in phase and 90^o degrees out of phase with the displacement of the journal in accordance with the sine and cosine terms of Equation (5.18) (this accounts for the Π having *2n-2* elements for a seal with *n* blades). To calculate the individual pocket contributions the overall reaction force applied to the journal, the dynamic pocket pressures are multiplied by the area of the journal on which the pressure acts. The stiffness force component is then divided by the journal displacement amplitude to give the pocket stiffness and the damping force component is divided by the journal velocity amplitude to give the pocket damping.

$$C_i = \frac{\overline{\Pi}(2 \cdot i - 1) \cdot Ap_i}{\omega \cdot X} \qquad \text{and} \qquad K_i = \frac{\overline{\Pi}(2 \cdot i) \cdot Ap_i}{X} \qquad \textbf{(5.34)}$$

The implementation of these equations in the form of a computer algorithm is discussed in the *Leakage and Rotordynamic Model Implementation* chapter of this dissertation.

MODULATION OF CLEARANCE GEOMETRY

A preliminary step in determining the dynamic pressures in the pockets of a PDS, is the determination of the changes in the annular clearance areas between the seal blades and the journal. When the journal vibrates, the area of the annular clearance sector

between two adjacent partition walls is modulated by the displacement of the journal. Referring to Figure 5.2, displacing the journal an arbitrary distance δ at an arbitrary angle α from an original center point O_1 to a new rotor center O_2 changes this clearance area from A_{c1} to A_{c2}.

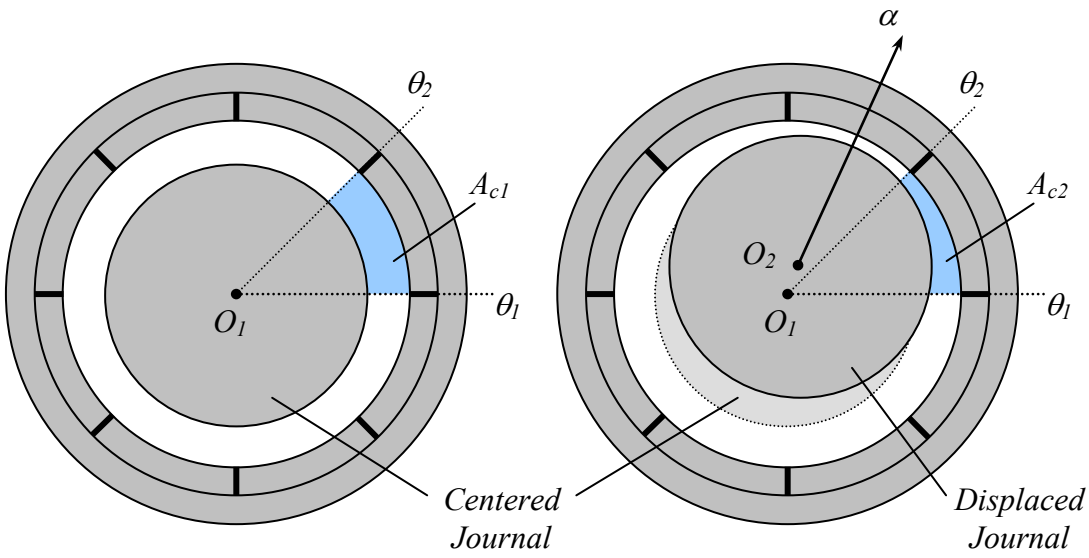

Figure 5.2 Clearance areas with centered and displaced journals

Both the initial PDS model developed by Shultz [27] and the more comprehensive model developed by Gamal [40] assumed that the motion of the journal resulted in a uniform change in clearance across the annular sector in question and the change in clearance area was calculated as in Equation (5.35). However, such a displacement of the journal results in a non-uniform change in clearance across a seal pocket sector. In the model for fully-partitioned pocket damper seals, these calculations have been updated to accurately calculate the dynamic clearance area changes. These changes affect the dynamic clearance flow areas as well as the dynamic pocket volumes, both of which are factors which affect the dynamic pressures in the pockets and therefore the direct rotordynamic force coefficients of the seal.

$$\Delta A_c^* = \delta \cdot R \cdot (\theta_2 - \theta_1) \tag{5.35}$$

The sector areas of the seal and the centered journal between the two angles are given by Equations (5.36) and (5.37) respectively. Using the center of the seal as the origin of a polar coordinate system, the vector equation of the curve representing the seal's inner surface is given by Equation (5.38). Likewise, the initial and final (after displacement) vector equations of the curves representing the rotor's surface are given by Equations (5.39) and (5.40) respectively. The vector representing the displaced rotor surface is shown in Figure 5.3 and its magnitude is given by Equation (5.41).

$$A_s = \tfrac{1}{2} \cdot d_s \cdot \left(\frac{\theta_2 - \theta_1}{2\pi} \right) \tag{5.36}$$

$$A_{r1} = R \cdot \left(\frac{\theta_2 - \theta_1}{2\pi} \right) \tag{5.37}$$

$$\vec{r_s} = \tfrac{1}{2} \cdot d_s \cdot e^{i\theta} \tag{5.38}$$

$$\overrightarrow{r_{r1}} = R \cdot e^{i\theta} \tag{5.39}$$

$$\overrightarrow{r_{r2}} = R \cdot e^{i\theta} + \delta \cdot e^{i\alpha} \tag{5.40}$$

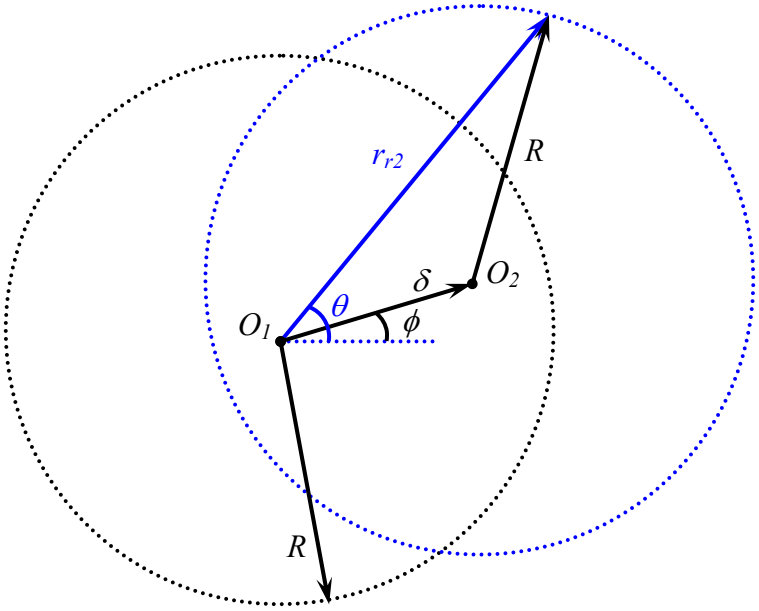

Figure 5.3 Journal displacement vector diagram

$$r_{r2} = \sqrt{R^2 - \delta^2 \cdot \sin^2(\theta - \alpha)} + \delta^2 \cdot \cos^2(\theta - \alpha) \tag{5.41}$$

$$A_{r2} = \tfrac{1}{2} \cdot \int_{\theta_1}^{\theta_2} r_{r2}^2 \cdot d\theta \tag{5.42}$$

$$A_{r2} = \tfrac{1}{2} \cdot \int_{\theta_1}^{\theta_2} \left[\sqrt{R^2 - \delta^2 \cdot \sin^2(\theta - \alpha)} + \delta^2 \cdot \cos^2(\theta - \alpha) \right]^2 \cdot d\theta \tag{5.43}$$

$$\begin{aligned} A_{r2} = {} & \tfrac{1}{4} \cdot \delta^2 \cdot \left[\sin(2\theta_2 - 2\alpha) - \sin(2\theta_1 - 2\alpha) \right] + \tfrac{1}{2} \cdot R^2 \cdot \left[\theta_2 - \theta_1 \right] \\ & + \delta \cdot R \cdot \left[\sin(\theta_2 - \alpha) - \sin(\theta_1 - \alpha) \right] - \tfrac{1}{2} \cdot \delta^2 \cdot \left[\sin^2(\theta_2 - \alpha) - \sin^2(\theta_1 - \alpha) \right] \end{aligned} \tag{5.44}$$

The original clearance area A_{c1} (with the rotor in the centered position) can be calculated by subtracting the centered rotor sector area (Equation (5.37)) from the seal sector area (Equation (5.36)). Likewise, the new clearance area A_{c2} (with the rotor in the displaced position) can be calculated by subtracting the displaced rotor sector area (Equation (5.44)) from the seal sector area (Equation (5.36)). Once the two clearance areas are known, the change in clearance area is given by Equation (5.45).

$$A_{c1} = A_s - A_{r1}$$
$$A_{c2} = A_s - A_{r2}$$
$$\Delta A_c = A_{c2} - A_{c1} \quad \textbf{(5.45)}$$

Both the change in clearance area and the rate of change in clearance area impact the dynamic pressures of the seal pockets and therefore affect the force coefficients of the seal. Unless the pocket depth of a given seal is so small as to be comparable with the magnitude of journal displacement, the mean change in pocket volume will be negligible. However, the rate of change of the pocket volumes affects the dynamic pressures in the pockets and must be considered.

CHAPTER DISCUSSION

Since all pocket pressures are time-varying quantities in a fully-portioned PDS, all cavities will contribute to the overall damping and stiffness of the seal. The terms *active* and *inactive*, used to describe the cavities of a conventional PDS are therefore no longer applicable and the analogous terms *primary* and *secondary* are used instead.

Dynamic Pressure Calculations

The dynamic pressures vary not only from cavity to cavity along the length of the seal, but also from pocket to pocket around the seal's circumference. Ertas' [41] analysis of his eight-bladed seal with eight pockets calculated coefficients by setting the number of pockets to four. This limited the variation of dynamic pressures to either zero (in the two pockets orthogonal to displacement) or non-zero quantities (in the two pockets in-line with displacement) as shown in Figure 5.4. This effectively calculates the stiffness and damping of an analogous seal with four pockets.

The current model makes no assumptions regarding the number of pockets of a seal. The code through which the model is implemented, however, does limit the number of pockets to multiples of four for reasons described in the *Fully-Partitioned PDS Model Implementation* chapter of this dissertation. Figure 5.4 shows that for the current model,

a displacement of the journal towards the center of the seal's first quadrant is initially assumed and the modulation of the clearance sector area for each pocket within that quadrant (two pockets for a seal with eight pockets or three pockets for a seal with twelve pockets) is calculated separately.

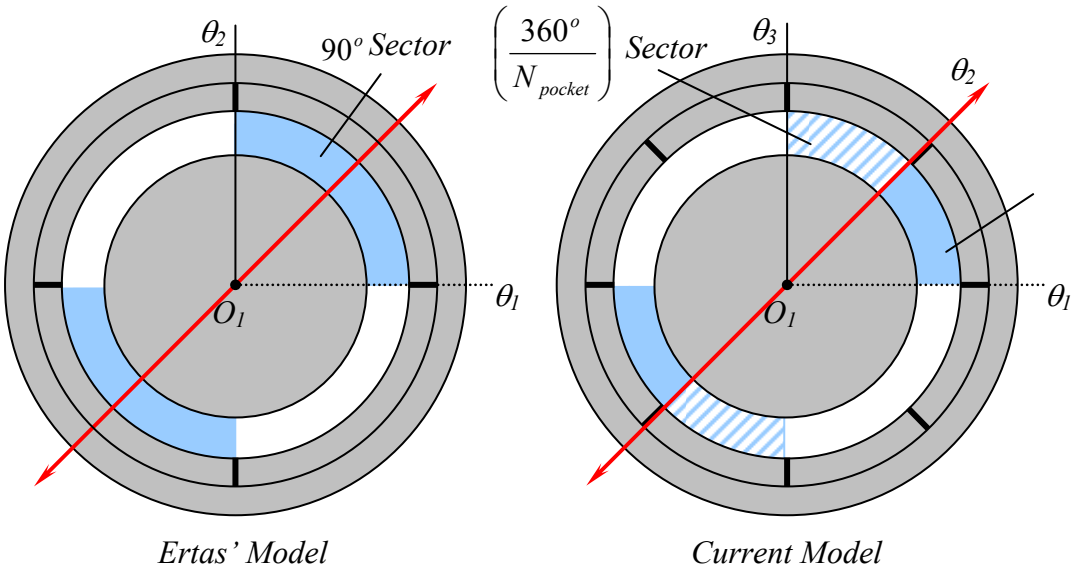

Figure 5.4 Individual pocket contributions of Ertas' model and the current model

Cross-Coupled Forces

If cross-coupled force coefficients exist, they would be caused by pressure differences between the pockets on the side (pockets *B* and *D* along the *y* axis of Figure 5.1). However, the *x*-direction motion of the journal produces only a small change in the clearance areas on the sides. Furthermore, these changes are equal and simultaneous (that is, in phase), and so the dynamic pressures are in phase.

Sonic Flow Conditions

For cases in which the flow through the last blade (or several blades) is choked, the pressure downstream of the final blade calculated using the maximum allowable pressure ratio is not the same as the prescribed back pressure. The pressure immediately downstream of a constriction through which flow is choked is given by this calculated

value and not by the prescribed back pressure (Vennard and Street [56]) and, as a result, it is this pressure that is used in calculating the rotordynamic coefficients of the seal.

CHAPTER VI

FULLY-PARTITIONED PDS MODEL IMPLEMENTATION

This chapter describes the implementation of the leakage and rotordynamic models, discussed in the two preceding chapters, in the form of a design and analysis code for fully-partitioned pocket damper seals. A description of main features of this FP-PDS code is also included.

LEAKAGE MODEL IMPLEMENTATION

The basic assumption on which the damper seal code's leakage calculation is based is that the steady-state mass flow-rate through each constriction created by the seal's blades and the journal is the same. Based on this, a logical starting point is to assume a constant value for the mass flow-rate and to then employ a corrective iterative algorithm to obtain the actual value of the flow-rate. The required input parameters to the code are the inlet and exit pressures, the seal geometry, and the properties of the fluid. These variables are related to each other and to the flow-rate by the selected leakage equation.

The three main variables involved in the algorithm are the pressure in a given cavity, the pressure directly upstream of that cavity, and the mass flow-rate through the constriction at the inlet to that cavity.

Since the mass flow-rate is initially assumed, its value and the value of the inlet pressure are known quantities. The only unkown is thus the pressure downstream of the first constriction. This pressure can be calculated from selected leakage equation and is used as the upstream pressure to calculate the pressure downstream of the second constriction. In this way, all the pressures can be calculated until a value of the pressure downstream of the last constriction (the back pressure) is obtained. This method is analagous to Holzer's method, which Vance [64] employs for torsional vibration calculations.

This final obtained pressure will match the prescribed exit pressure when the guess for the mass flow-rate is correct. A calculated final pressure that is higher than the specified exit pressure indicates that not enough fluid is leaking through the seal and that the guess for the flow-rate needs to be raised. If the final pressure is lower than the exit pressure, then the guess for the flow-rate is too high and needs to be lowered.

The code can be divided into sections responsible for input, initial estimation of the flow-rate, calculation of the pressures, correction of the flow-rate, final checks on obtained values, and output.

Calculation of Pressures

Input parameters such as fluid properties, seal geometry, and inlet and exit pressures are read and modified as needed. The input values are converted to the appropriate unit system. These data are used to calculate other needed parameters such as constriction areas and pressure drops as well as constants for use in later equations.

The iterative algorithm used to sequentially calculate each cavity pressure is based on solving the selected leakage equation in the slightly modified form of Equation (6.1) (shown for the St. Venant Equation).

$$f\left(\dot{m}, P_n, P_{n+1}\right) = \dot{m}_n^2 - \left[\frac{P_n^2 \cdot A_n^2}{\gamma \cdot R \cdot T_n} \cdot \frac{2 \cdot \gamma^2}{\gamma - 1} \cdot \left[\left(\frac{P_{n+1}}{P_n}\right)^{2/\gamma} - \left(\frac{P_{n+1}}{P_n}\right)^{\gamma+1/\gamma}\right]\right] = 0 \qquad \textbf{(6.1)}$$

The terms of the equation are squared to avoid problems with negative numbers under the square root during iteration. In this form, the solution of the equation is the point of intersection of the curve representing the function *f* with the pressure axis. Figure 6.1 is a sample plot of this function with inlet and exit pressures of 900 psi (62 bar) and 500 psi (34 bar) respectively (represented by the two vertical lines).

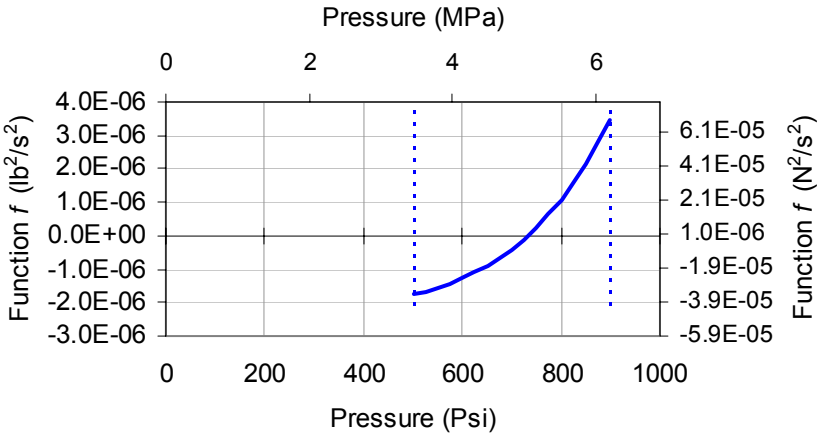

Figure 6.1 Sample cavity pressure calculation plot

If $f < 0$, the pressure estimate for a given cavity is too low and needs to be increased. If $f > 0$, then the estimate is too high. A change in the sign of f indicates that the correct value of the pressure is between the current and the last values of the pressure. The incremental change in pressure is then halved and the process continues until the difference between the results of two consequtive iterations is less than an acceptably small predetermined percentage of the newly obtained pressure.

Calculation of Flow-Rate

Before the pressures can be calculated as described above, an initial estimate of the flow-rate must be provided. An estimate that is too high will lead to the function f not intersecting the pressure axis and no solution will be found.

The code first assumes a linear pressure distribution in the seal cavities and calculates the flow-rate across each constriction. The minimum flow-rate value is used as an initial estimate. This value is then checked to see whether or not the function f has a negative value for pressures close to the exit pressure. If this is not the case, then the estimate is too high and is lowered by 25%. The two pressures used in the equation to calculate f are taken as P_{exit} and 110% of P_{exit}.

As mentioned above, if the final pressure is lower than the exit pressure, the flow-rate must be reduced, and if the final pressure is higher than the exit pressure, the flow-

rate is too low. As was the case with the incremental change in pressure, the incremental change in flow-rate with each iteration is halved every time the status of the flow-rate changes from being too high to too low and vice versa. Several constants are incorporated into the algorithm to speed up convergence.

Two main checks are carried out as part of the solution. These checks allow the code to run in two special cases: if the flow through any of the constrictions is choked or if the inlet and exit pressure values are close to each other. The algorithm, in a sense, automatically takes care of the first check. When the flow through a given cavity is choked, the code will not be able to find a cavity pressure that satisfies the selected leakage equation. If this is the case, the code exits the mass flow-rate correction loop and calculates the pressures in the downstream cavities of the constriction through which the flow-rate has been identified as being choked using the modified equation for choked flow.

When the inlet and exit pressure values are close to each other (for example 1000 Psi (68.9 bar) and 998 Psi (68.1 bar)), the stopping criteria for the iterative process may be too large. If this is the case, the cavity pressures returned by the code may be lower than the exit pressure or higher than the inlet pressure. The ratio of the pressure drop to the inlet pressure is checked and the stopping criterion is modified accordingly so as to avoid this.

Finally, the code presents the output of the algorithm. This output is in the form of the cavity pressures, the pressure ratios across each constriction, the mass flow-rate, and an indication of which cavities, if any, are downstream of constrictions through which flow is choked. This output is then used to calculate the stiffness and damping of the seal based on the equations presented in this chapter.

ROTORDYNAMIC MODEL IMPLEMENTATION

As was discussed in the *Pocket Damper Seal Theory and Modeling* chapter of this dissertation, the dynamic pressures of each cavity are coupled. This necessitated the use of a matrix solution of the equations to obtain the individual cavity stiffness and

damping contributions. In order to solve the coupled system of equations, a set of coefficient matrix variables were used (listed once more in Equations (6.2) to (6.5)).

$$a_i^{'} = \left(\frac{V_{i+1}}{\gamma \cdot R \cdot T_{i+1}} \right) \tag{6.2}$$

$$b_i^{'} = \frac{\partial \dot{m}_i}{\partial P_{i+1}} \quad \text{if } i \text{ is odd} \qquad \text{and} \qquad b_i^{'} = \frac{\partial \dot{m}_i}{\partial P_i} \quad \text{if } i \text{ is even} \tag{6.3}$$

$$d_i^{'} = \frac{\partial \dot{m}_i}{\partial x} - \frac{\partial \dot{m}_{i+1}}{\partial x} \tag{6.4}$$

$$e_i^{'} = \left(\frac{P_{i+1}}{R \cdot T_{i+1}} \right) \tag{6.5}$$

In a typical pocket damper seal, a blade's clearance with the journal will depend on whether it is the inlet or the exit blade of a primary cavity (the exit blade of a primary cavity is the inlet blade of the next secondary cavity). This serves to create a diverging clearance that, at least in the case of conventional pocket damper seals, is required to obtain significant positive damping. The clearance between the centered rotor and the seal blades varies from cavity to cavity, but does not vary from pocket to pocket. In other words, the annular sector defined by the rotor surface, the blade tip surface, and the two partition walls of a pocket varies only along the length of the seal and not around its circumference. Once the rotor is displaced, however, the clearance area in not the same in either the axial or circumferential directions. The net change in clearance area will be the same along the length of the seal, but will change from pocket to pocket, depending on the direction in which the journal was displaced.

The dependence of these three variables on the cavity and pocket number results in similar dependencies of the four coefficient matrix variables (Equations (6.2) to (6.5)) on the same factors as summarized in Table 6.1. When the coefficient matrix and right-hand vector are written for a seal, these variations are taken into account. The variables are therefore defined as vectors and matrices themselves; meaning that the dynamic pressure coefficient matrix becomes a matrix of matrices and the right-hand vector becomes a vector of vectors. Storing the variables in this format is necessary in transitioning from a model for a single seal design to one applicable to seals with variable numbers of blades and pockets.

Table 6.1 Variation of variables along seal length and circumference

Variable	Description	Varies from Cavity to Cavity	Varies from Pocket to Pocket
A_{C1}	Original clearance area	Yes	No
A_{C2}	Displaced clearance area	Yes	Yes
ΔA_C	Change in clearance area	No	Yes
a'	Coefficient matrix variable	Yes	No
b'	Coefficient matrix variable	Yes	No
d'	Coefficient matrix variable	Yes	Yes
e'	Coefficient matrix variable	Yes	Yes

For a seal with N blades, the dimensions of the coefficient matrix variable vectors, the right-hand vector, and the coefficient matrix itself are listed in Table 6.2. Also listed, are the dimensions for three different seal configurations. Each of these vectors and matrices would normally have to be evaluated for each pocket, meaning that for a seal with eight pockets, there would be eight Π matrices. In order to simplify the calculations, however, calculations are only performed for the first quadrant of the seal. As can be seen from in Figure 5.4 (in the preceding chapter), the modulation of the clearance area of the third seal quadrant is equal in magnitude to, but 180^o out of phase with, the modulation of the clearance area of the first quadrant. The modulation of the clearance areas of the second and fourth quadrants is negligible in comparison and is therefore ignored. The overall effect of the seal, as discussed in the previous chapter, is

therefore twice the effect (in terms of stiffness and damping) of a single quadrant. Since the code through which the model is implemented (but not the model itself) requires the seal to be segmented into quadrants, the code is only capable of analyzing and designing seals for which the number of pockets is a multiple of four. The number of times each vector or matrix is evaluated for a seal with N_{pocket} pockets and the overall number of terms evaluated per vector or matrix are listed in Table 6.3.

Table 6.2 Dimensions of single-pocket matrices for dynamic pressure calculation

Matrix or Vector	Dimensions	No. of Elements for 8 Blades	No. of Elements for 12 Blades
a'	(N - 1) x 1	7	11
b'	(2N - 2) x 1	14	22
d'	(N - 1) x 1	7	11
e'	(N - 1) x 1	7	11
Γ	(2N - 2) x 1	14	22
Π	(2N - 2) x (2N - 2)	196	484

Table 6.3 No. of elements evaluated for multi-pocket dynamic pressure calculation

Matrix or Vector	Number of Times Evaluated	Total No. of Elements Evaluated for Seal with:		
		8 Blades 8 Pockets	12 Blades 8 Pockets	12 Blades 12 Pockets
a'	1	7	11	11
b'	1	14	22	22
d'	¼ x N_{pocket}	14	22	33
e'	¼ x N_{pocket}	14	22	33
Γ	¼ x N_{pocket}	28	44	66
Π	¼ x N_{pocket}	392	968	1452

FP-PDS CODE DESCRIPTION

The design and analysis code developed for fully-partitioned pocket damper seals was written in the form of Visual Basic macros with a Microsoft Excel user interface. The code is divided into five worksheets that can be used separately to analyze different aspects of a PDS or together in an iterative seal design process. The *Massflow*

worksheet is the primary input and output worksheet for the code. It is on this sheet that the seal's geometry, the gas properties, and the operating conditions are first defined. This sheet implements the leakage and rotordynamic models and supplies output in the form of individual cavity and overall seal damping and stiffness as well as leakage through the seal. The *Clearances* worksheet allows a user to vary clearances, clearance ratios, and pitch ratios (ratio of primary to secondary cavity lengths). The *Blades* worksheet compares seal designs with different numbers of blades and determines the optimum pocket depth (required to maximize damping) for each seal. Both the *Clearances* and *Blades* worksheets use the seal geometry originally defined on the *Massflow* worksheet. These three worksheets can be used to iteratively design a seal or can be used to examine the effect of various design parameters on seal behavior. The *Pockets* worksheet allows a user to change the number of pockets and the partition wall thickness in a seal and to examine the resulting effect on seal behavior. Finally, the *Frequencies* worksheet plots seal damping and stiffness against frequency. This allows a user to examine a seal's behavior over a user-defined range of operation. The rotordynamic coefficients can be calculated based on an input pocket depth (for analysis) or on an optimum pocket depth calculated for each excitation frequency (for design).

CHAPTER VII

TEST EQUIPMENT AND METHODOLOGY

The test results presented in this dissertation were obtained from a reconfigurable labyrinth seal, which was tested on a non-rotating test-rig at the Turbomachinery Lab. The components of the test facility, consisting of the non-rotating test-rig, air supply system, test labyrinth seal, and required instrumentation, are described in this section.

The test apparatus and equipment described herein were used for both leakage measurements and rotordynamic coefficient evaluation of pocket damper seals and labyrinth seals. The equipment used and the methodology employed by Picardo [55], Ertas [41], and Gamal [40] to obtain the High Pressure Experimental Data (HPED) are explained in the chapters describing those experimental results. In the following sections, the test-rig, air-supply system, labyrinth test seals, pocket damper test seals, instrumentation, and testing methodologies are described in that order.

TEST-RIG AND AIR SUPPLY SYSTEM

The test-rig, shown in Figure 7.1 with a six-bladed labyrinth seal installed, was first used by Shultz [27] to test a two-bladed pocket damper seal and has been used since to test wire mesh dampers and labyrinth seals. Pressurized air enters the chamber at the bottom and exhausts to atmosphere through the clearance between the test seal's blades and the journal, which is mounted on a cantilevered shaft. The seal rests on the upper surface of the test stand (an O-ring seals the interface) and is held in place by four adjustable toggle clamps. The seal is clamped down, not bolted, onto the housing so as to allow for lateral movement during the centering process. The test-rig is supplied with pressurized air (up to 275 Psi) from an Atlas Copco GR 1520 Compressor. The inlet pressure to the seal was remotely controlled using a Masoneilan valve. The test seals and remaining instrumentation are described in the following sections.

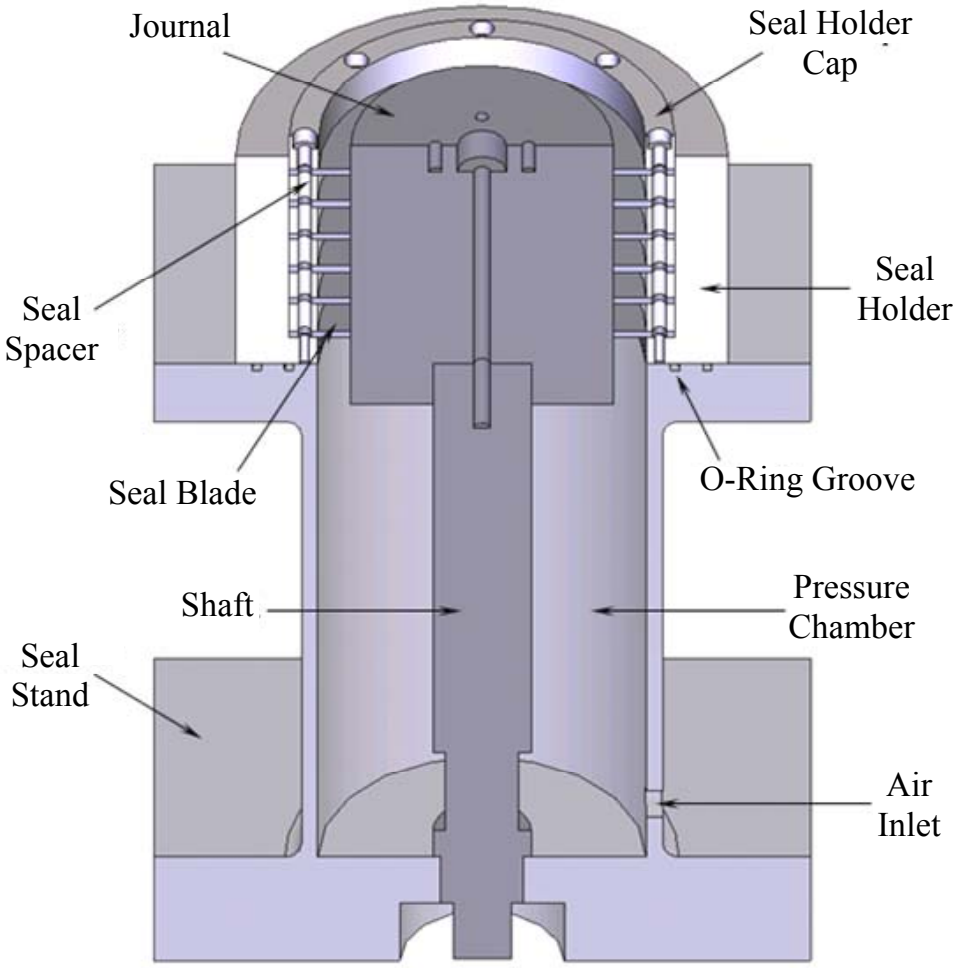

Figure 7.1 Non-rotating seal test-rig

LABYRINTH SEALS

Carrying out the tests on two reconfigurable seals allowed the number of blades, blade spacing (pitch), cavity depth, and blade thickness to be varied while using the same sets of blades. This had the dual advantage of not requiring a large number of different test seals and of eliminating the difficulty involved in ensuring that the blade tip clearances were kept constant for all tests cases.

Two separate sets of seal hardware (described below) were used. The older set of seals was used only for blade profile tests and is referred to below as Seal Set A. The newer hardware was used to examine the effect of blade thickness and eccentricity, as

well as to reexamine the effect of blade profile, and is referred to below as Seal Set B. A table detailing the tested seal configurations can be found in the appendix of this dissertation.

Seal Set A

Due to extended delays in the delivery of the labyrinth seals that were originally designed for the purpose of this research, this older set of seal hardware was created out of retrofitted seals. Three air-buffer seals, which had been used on another test-rig at the Turbomachinery Laboratory, were modified to create a reconfigurable labyrinth seal.

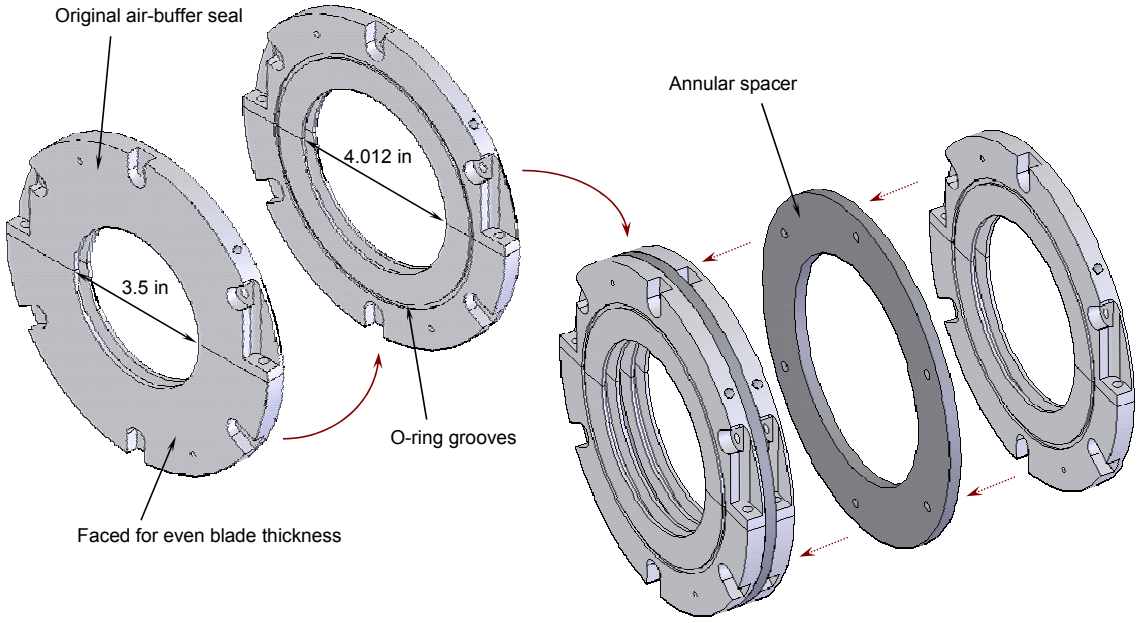

Figure 7.2 Seal set A: manufacturing and assembly

The following modifications were made to the original air-buffer seals:

- The seals were faced to ensure that their surfaces were flat and that all the blades had the same thickness.
- The inner diameter of the seals was increased from 3.5 in to 4.012 in.
- O-ring grooves were machined into the surfaces of two of the air-buffer seals.

- Two spacers were manufactured in order to create cavities between the second and third labyrinth blades and between the fourth and fifth labyrinth blades.

Table 7.1 Test seal geometry (seal set A)

Design Parameter	Configurations Tested
No. of Blades	2, 4, 6
Cavity Depth	0.4 in (10.16 mm)
Blade Spacing	0.245 in (6.223 mm)
Inner Diameter	4.012 in (101.9 mm)
Radial Clearance	6 mils (152.4 mm)
Blade Thickness	0.075 in (1.905 mm)

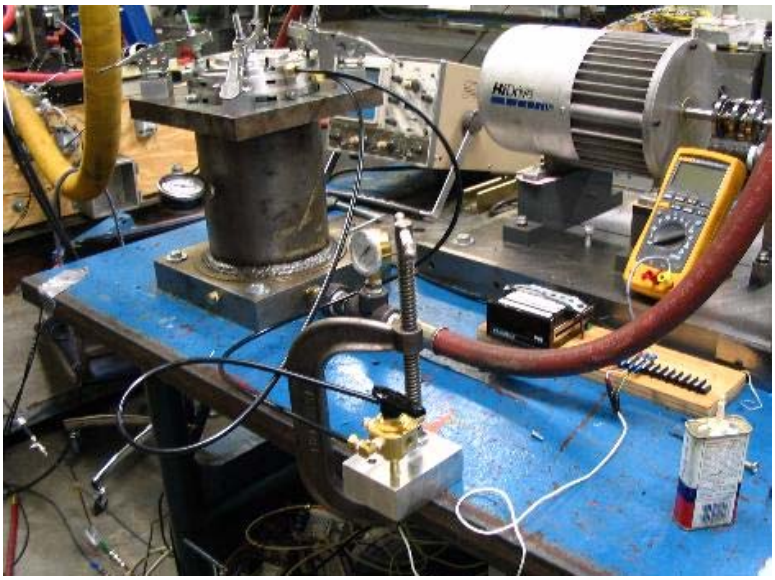

Figure 7.3 Test set-up with six-bladed seal of seal set A installed

With these modifications, the two-bladed seal base units could be assembled, along with the annular spacers to construct two-, four-, or six-bladed labyrinth seals as shown in Figure 7.2. The main geometric features of these test seals are detailed in Table 7.1. Leakage and pressure tests were carried out on two-, four-, and six-bladed seals (shown mounted onto the test-rig in Figure 7.3) of this type with flat-tipped blades. Once the tests were completed, bevels were machined into the same blades and the seal was tested

with upstream-beveled blades, then flipped over and tested with downstream-beveled blades. Seal Set A was made up of a total of nine test configurations.

Seal Set B

This seal design consists of a seal holder, a set of blades, three sets of spacers, a set of cavity inserts, and a seal holder cap (components shown in Figure 7.4). The main geometric features of the test seals (made up of either four or six blades) are detailed in Table 7.2.

Figure 7.4 New reconfigurable seal components (Seal Set B)

The initial blade thickness was 1/8-in (3.2-mm), but the blades could be arranged in the holder in pairs to create blades which were 1/4-in (6.4-mm) thick (Figure 7.5). The depths of the cavities could be modified from the original 0.5-in (12.8-mm) to 0.1-in (2.5-mm) by inserting a series of 0.4-in (10.2 mm) thick annular inserts between the blades resulting in a reduction of 80% as shown in Figure 7.6. Leakage and pressure tests were carried out on 6 four-bladed and 5 six-bladed seals with flat-tipped blades and 2 four-bladed and 1 six-bladed seals with beveled blades for a total of 14 seals tested.

Table 7.2 Test seal geometry (seal set B)

Design Parameter	Configurations Tested
No. of Blades	4, 6
Cavity Depth	0.1 in, 0.5 in (2.5 mm, 12.7 mm)
Blade Spacing	1/8 in, 1/4 in, 1/2 in (3.2mm, 6.4 mm, 12.7 mm)
Inner Diameter	4.008 in (101.8 mm)
Radial Clearance	4 mils (101.6 mm)
Blade Thickness	1/8-in, 1/4-in, (3.2 mm, 6.4 mm)

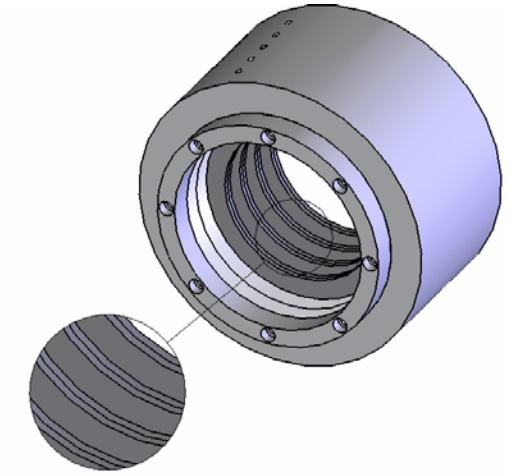

Figure 7.5 Four-bladed labyrinth seal with double blade thickness

Figure 7.6 Six-bladed labyrinth seals with shallow (left) and deep (right) cavities

POCKET DAMPER SEALS

The test-rig described above was also used to study the effects of design factors on the leakage and rotordynamics of pocket damper seals. Both conventional and fully partitioned pocket damper seal configurations were to be tested, thereby demonstrating the effects of such factors while at the same time allowing a comparison of the characteristics of the two seal types. Furthermore, non-uniform pocket damper seals were tested to examine the effect of non-uniform spacing and the effect of non-uniform pocket depth around the seal circumference. Some of the spacers used to create reconfigurable pocket damper seals are shown in Figure 7.7.

Figure 7.7 Pocket damper seal spacers

INSTRUMENTATION

The mass-flow rate through the seal was measured using an Omega FTB-938 turbine flow meter. The volumetric flow-rate was read in actual cubic feet per minute (acfm), which were converted first into standard cubic feet per minute, and subsequently into weight rate of flow units of lb/s. The conversion and calibration information for the flow meter, and for the other instrumentation used, can be found in the appendix of this dissertation.

The pressure at the location of the flow meter (which is required to obtain the mass flow-rate) and the seal's inlet pressure were measured with Bourdon pressure gauges that were calibrated for accuracy prior to the tests. The cavity pressures were measured using a Kulite XT-190M strain gauge type pressure transducer. The transducer was connected using Nylon tubing to radial holes in the seal via a multidirectional valve so that readings could be taken in multiple cavities with one transducer.

To ensure that the seal remained in the centered position throughout testing, two orthogonally mounted proximity probes were used to display and monitor the journal position with respect to the seal on an oscilloscope. Figure 7.8 is a photograph of the test-stand with the toggle clamps raised and the seal removed to reveal the journal.

Figure 7.8 Non-rotating test-rig (seal not installed)

TESTING PROCEDURE

During assembly, a tight fit (0.5 mils or 12.7 μm radial) between the outer diameter of the blades and the inner diameter of the seal holder served to ensure that the blades of Seal Set B would be aligned when they were installed around the journal. The seal holder therefore doubled as an "external mandrel" for the assembly purposes. The seal sections and spacers of Seal Set A were assembled on a separate internal mandrel with a 0.5 mil (12.7 μm) radial clearance with the blades. To eliminate any radial leakage at the interfaces between the seal blades and the spacers, the interface surfaces were machined closely and treated with a sealing compound. After several checks it was determined that the sealant was unnecessary for the newer set of blades. Shims were used to center the seal around the journal before it was clamped into place. The seals' inlet pressures were varied using the supply valve and flow-rate, and cavity pressure readings were recorded. Several of the seal configurations were also tested in an off-center position to determine the effect of eccentricity. This position was achieved by releasing the toggle clamps following a centered test and pushing the seal over until the blades came into contact with the journal and repeating the test.

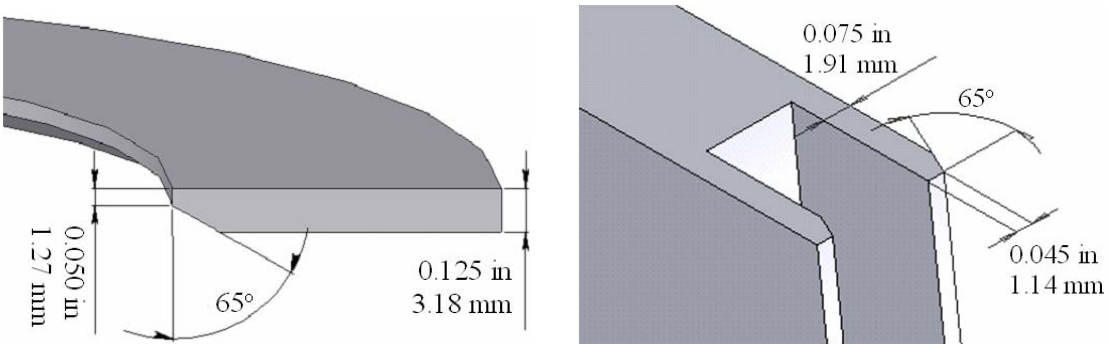

Figure 7.9 Beveled blades for new (left) and old (right) seals

After the required configurations were tested, the seals were retested with bevels (chamfers) machined into the downstream and upstream sides of the blades. Short segments of land area were left on the blades to ensure that clearances were not altered by the beveling process. The remaining portions of the blade tips were beveled at an angle from the seal's axis as shown in Figure 7.9.

Concurrent with the leakage tests, cavity pressure measurements were made in the four- and six-bladed seals of Set A and all the seals of Set B. Due to geometric restrictions in the seals of Set A, pressure measurements could not be made in the first upstream two-bladed seal section or in the cavities formed by the spacers. As a result, cavity pressure data was taken in the third cavity of the four-bladed seal and in the third and fifth cavities of the six-bladed seal. Cavity pressure measurements were made in all cavities of the seals of Set B except for the seals with short pitch lengths.

EARLIER HIGH PRESSURE TESTS

The facility used to test the seals at high pressures was initially built to test hydrostatic bearings at the Turbomachinery Laboratory at Texas A&M University and has since been modified to test annular gas seals. A high pressure pipeline from a wind-tunnel provides air at pressures of up to 2500 Psi (17.3 MPa). A schematic of the test facility is shown in Figure 7.10 and more detailed descriptions of the test-rig are given by Childs and Hale [65], Picardo [55], and Gamal [40]. In addition to the leakage and

static pressure tests that are the subject of this paper, the test-rig and test seals described here were used to determine the rotordynamic coefficients of pocket damper seals at high pressures as described by Gamal [40] and Ertas [41].

The rig consists of a rotor connected by a coupling to a gearbox with the test seals mounted in a stator assembly around the rotor. The rotor was spun at speeds of 10,200 RPM, 15,200 RPM, and 20,200 RPM. The stator is connected to two Zonic® shakers. The rotor possesses a fundamental natural frequency that is significantly higher than the test frequency range and is mounted on hydrostatic bearings that have high stiffness. Two air-buffer seals utilizing shop air at 110 Psi (0.76 MPa) prevent leakage of the bearing water.

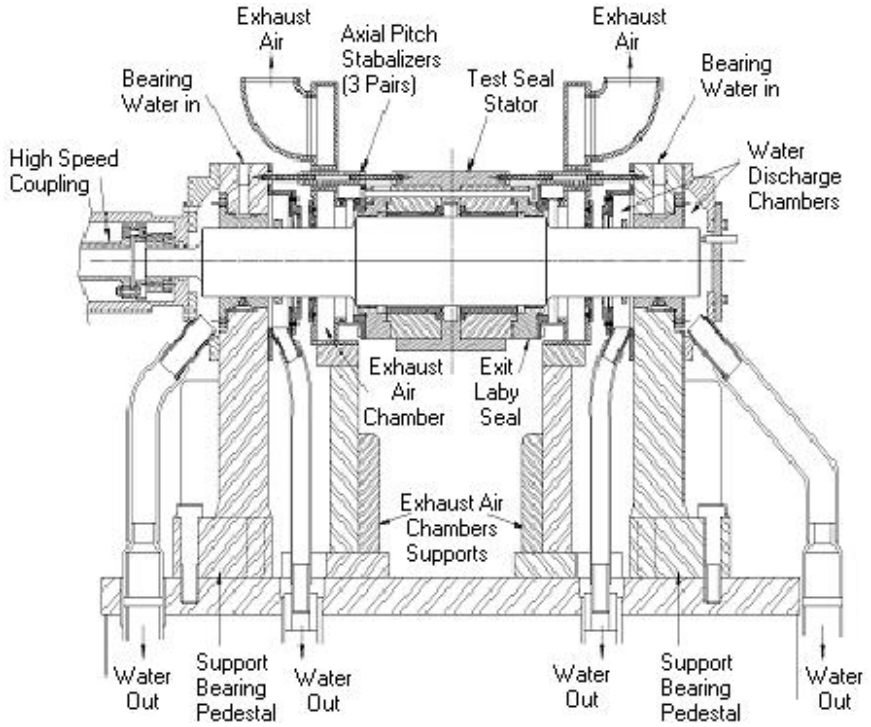

Figure 7.10 High-pressure annular gas seal test-rig schematic

Air enters the assembly through the center of the stator and moves axially outwards through two sets of identical seals. The pressure drop across the seals can be controlled by varying the inlet pressure and by opening or closing a back-pressure valve, which

modifies the seal's exit pressure. The same test-rig is also used to test hole-pattern and labyrinth seals. A photograph of the test-rig with the stator assembly installed is shown in Figure 7.11.

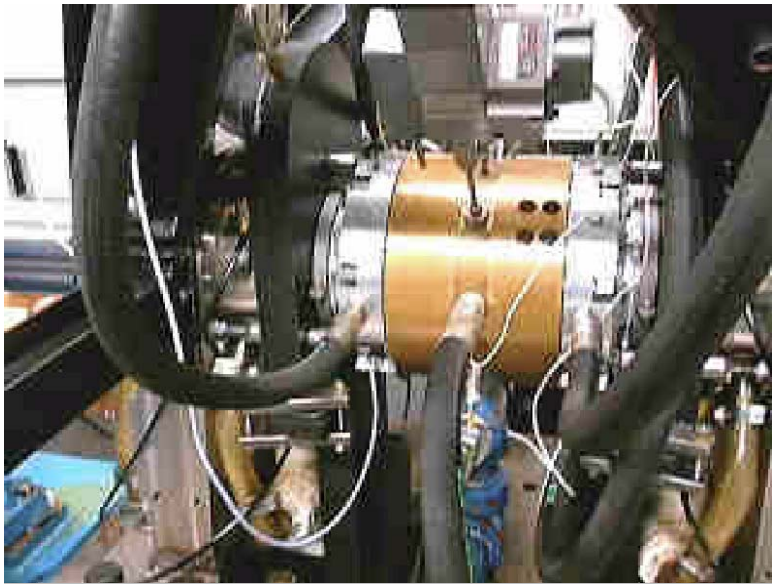

Figure 7.11 Assembled high-pressure test-rig

The stator assembly consists of five components: a brass stator, two steel pocket damper seals, and two aluminum labyrinth seals. The stator holds the seals in place and provides a method of connection to the shakers and the pressure, temperature, and vibration sensors. The labyrinth seals at either end of the stator control the pressure drop across the test seals by regulating the back-pressure. With the back-pressure valve fully open, there should be almost no flow across the labyrinth seals, and the PDS exit pressure will be on the order of 150 Psi (1.03 MPa) for an inlet pressure of 1000 Psi (6.92 MPa). With the valve fully closed, the back-pressure is maintained by the labyrinth seals.

Pocket Damper Seals

Initially, two seal types were tested; a twelve-bladed seal and an eight-bladed seal (Figure 7.12). Both seals were first tested with a 1:1 clearance ratio and then had their

exit blades notched to provide an effective 1:2 clearance ratio for the twelve-bladed seal and an effective 1:1.5 clearance ratio for the eight-bladed seal. These notches serve to provide the desired overall positive direct damping by creating an effective diverging clearance in the active cavities (as in hole-pattern and honeycomb seals, a diverging clearance in a PDS also generally results in positive damping). For each test, two of the same types of seals are placed back-to-back in the stator to minimize the resulting axial thrust.

Figure 7.12 12- and 8-bladed high-pressure pocket damper seals

The static cavity pressure measurements were made in the second and third active cavities of both configurations of the eight-bladed seal using Kulite™ XT-190M pressure transducers. The pressure probe holes can be seen on the eight-bladed seal of Figure 7.12.

For the twelve-bladed seal, the inlet blades for each active cavity are beveled on the upstream side and the exit blades for each active cavity are beveled on the downstream side. The major dimensions of the diverging configurations of the three seals are listed in Table 7.3. Solid models of the diverging configurations of the test seals (including the six-bladed seal that was tested later) are shown in Figure 7.13.

Table 7.3 Major dimensions of high-pressure pocket damper seals

Parameter	12-Bladed Seal		8-Bladed Seal		6-Bladed Seal	
	(in)	(mm)	(in)	(mm)	(in)	(mm)
Length	3.375	85.73	3.375	85.63	3.375	85.73
Inner Dia.	4.51	114.55	4.51	114.55	4.51	114.55
Radial Inlet Clearance	0.005	0.13	0.005	0.13	0.005	0.13
Radial Exit Clearance	0.010	0.25	0.0075	0.19	0.010	0.25
Pocket Depth	1.40	35.56	1.00	25.40	0.56	14.22
Number of Pockets	8		8		8	
Wall Thickness	0.15	3.81	0.20	5.08	0.20	5.08
Blade Thickness	0.125	3.18	0.125	3.18	0.125	3.18
Active Cavity Length	0.208	5.29	0.500	12.70	0.742	18.85
Inactive Cavity Length	0.125	3.18	0.125	3.18	0.200	5.08

Once the test seals were installed in the stator assembly and assembled onto the test rig described above, the procedure followed during testing and the method employed for data acquisition were identical to those used by Marquette, Childs, and San Andres [66]. The leakage through the seals was measured as described by Picardo [55].

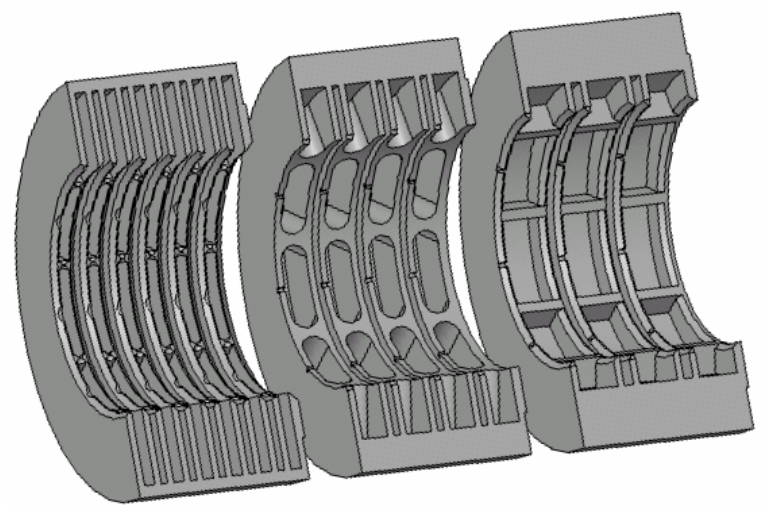

Figure 7.13 Sectioned models of diverging 12-, 8-, and 6-bladed seals

Labyrinth Seals

Picardo [55] used the same high-pressure test-rig to measure the leakage through and the rotordynamic force coefficients of an 18-bladed labyrinth seal (Figure 7.14). The same seal was tested with two shafts of different diameters to create two different

radial clearances (4 mils and 8 mils or 1 mm and 2 mm). The seal was also tested for three pre-swirl ratios, two supply pressures, three pressure ratios, and three shaft speeds for a total of 108 test cases.

Figure 7.14 High-pressure labyrinth test seal

CHAPTER VIII

LEAKAGE TESTS: EFFECTS OF SEAL DESIGN PARAMETERS

This chapter presents the results of low pressure tests carried out on labyrinth and pocket damper seals. This data includes flow-rate and cavity pressure measurements. Before the experimental data is presented, a review of the test results which led to questions concerning the effects of design parameters on leakage is included. These design parameters include the effects of eccentricity, blade profile, blade spacing, cavity depth, and blade thickness.

REVIEW OF EARLIER TESTS

An analytical examination of the impact of different blade profiles on the flow-rate through labyrinth seals was included in a 1972 study by Fasheh [67] of effects of various geometric factors on leakage. This study compared, among other configurations, a labyrinth seal with a flat blade profile with one with a tapered blade profile (Figure 8.1). The results of the analysis showed that the seal with the tapered blades had lower leakage values than the flat-bladed seal.

Experimental research on pocket damper seals also indicates that blade profile can significantly affect the leakage rates. Laos [32] conducted leakage tests on two four-bladed pocket damper seals (one with four pockets and one with eight pockets) and a six-bladed labyrinth seal. The results showed that the labyrinth seal, although it had a higher number of blades, leaked more than either pocket damper seal configuration. Laos attributed the discrepancy to the reduction in circumferential flow in the pocket damper seal due to the seal's partition walls. Aside from this characteristic of the pocket damper seal, however, there are other significant differences between the two seals, as can be seen from Figure 8.2 (note that for the seals shown in the figure, the flow enters through the center plenum and exits axially outwards). Both the cavity depth and the pitch length of the labyrinth seal are significantly smaller than those of the pocket

damper seal, and (more directly relevant to the topic of this report) the labyrinth seal blades are beveled in the downstream direction whereas the pocket damper seal blades are flat-tipped.

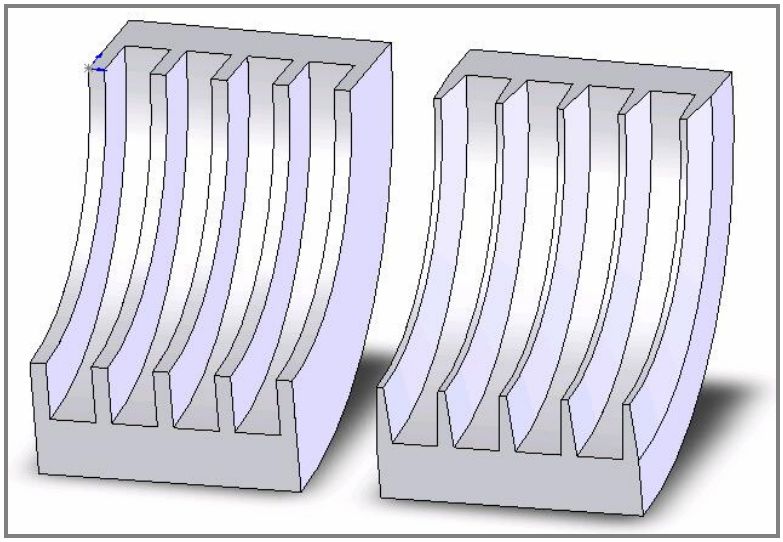

Figure 8.1 Labyrinth seal sectors with flat and tapered blade profiles

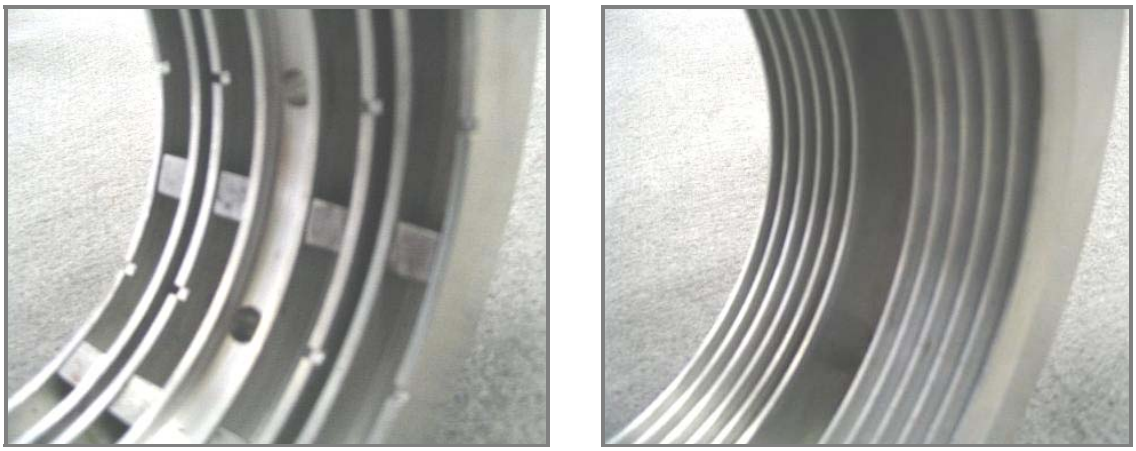

Figure 8.2 Laos's four-bladed PDS (left) and six-bladed labyrinth seal (right)

It is likely that a combination of these factors led to the higher leakage rates of the labyrinth seal. If blade profile was indeed a factor, then the predictions made by Fasheh [67] would seem to be contradicted by these results.

Laos's conclusion was backed up by the results of leakage tests conducted by Gamal [40] on eight-bladed and twelve-bladed pocket damper seals. These tests were conducted with pressure drops across the seals of up to 900 psi (62 bar) on diverging and straight-through seal configurations. The blades of the eight-bladed seal had a flat profile, whereas the twelve bladed seal had alternately downstream-beveled and upstream-beveled blades (Figure 8.3). The measurements showed that the twelve-bladed seal consistently leaked more than the eight-bladed seal for different test pressures, rotor speeds, and clearance ratios. This result was so surprising that the test was repeated, with confirmation.

Gamal suggested that the unexpectedly high leakage in the case of the twelve-bladed seal resulted from the beveled blade profile and from the short cavity pitch of that seal. Although the inlet clearances of the eight-bladed and twelve-bladed seals were identical, the clearance ratio (the ratio of an active cavity's exit clearance to its inlet clearance) of the diverging configuration of the twelve-bladed seal was higher than that of the diverging configuration of the eight-bladed seal. Additionally, the shapes of the exit blade notches were not the same for the two seals.

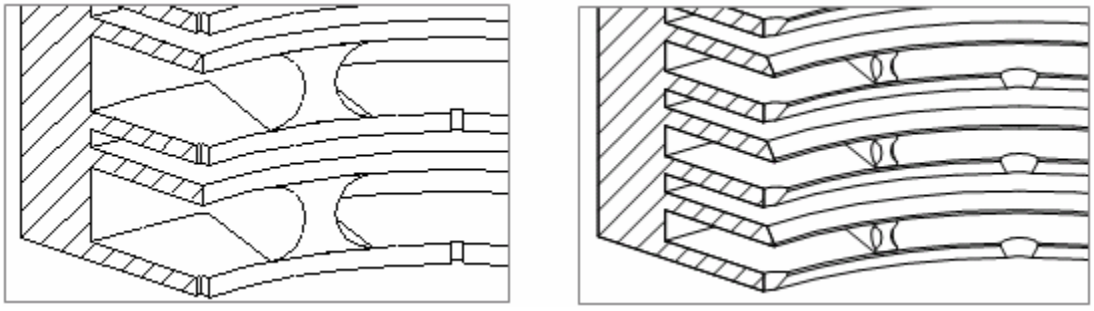

Figure 8.3 Blade profiles of Gamal's 8-bladed (left) and 12-bladed (right) PDSs

To eliminate such discrepancies, Ertas [41] tested two six-bladed pocket damper seals with a flat blade profile at similarly high pressures. These seals were then machined and re-tested with beveled blade profiles. (Figure 8.4). The tip of the blade was purposely left with a small flat land area to ensure that beveling the blade did not alter the blade-to-journal clearance. With all other geometric parameters and external

conditions kept constant, Ertas showed that the beveled pocket damper seal leaked more than the seal with flat-tipped blades, thereby supporting the results obtained by Gamal [40].

Figure 8.4 Ertas's 6-bladed pocket damper seal with beveled blades

The results obtained by Laos [32], Gamal [40], and Ertas [41] indicate that beveling the blades of a labyrinth-type seal, in either the downstream or upstream directions, reduces the seal's ability to limit leakage. While the cases being compared are not exactly identical, this does seem to contradict Fasheh's [67] findings that tapering a labyrinth seal's blades improves its leakage limiting performance.

Investigation of the effects of eccentricity, cavity depth, and blade thickness was suggested to provide further understanding of the impact of seal geometry on leakage. Since the above blade-profile tests involved comparisons to pocket damper seals, this paper presents experimental data comparing labyrinth seals with different blade profiles and blade thicknesses to each other. In addition, since such seals normally operate in an off-center position, the effect of eccentricity is examined to see if this too was a contributing factor to the results of the previous experiments.

A somewhat normalized comparison for the different test cases can be obtained, by examining the discharge coefficients calculated by Shultz [27], Gamal [40], and Ertas

[41] for their seals. These coefficients, summarized in Table 8.1, were computed using prediction codes based on a modified form of the St. Venant Equation shown below. Since this equation was derived for flow through an orifice of round cross-section, it is to be expected that the predicted flow-rate would not match the flow through the annular section formed by the blades and the journal. This discrepancy gives rise to the need for discharge coefficients as correcting factors. For pocket damper seals, the numerical value of the discharge coefficient *Cf* differs based on whether the equation is being written for the inlet blade or the exit blade of an active cavity. A discharge coefficient value greater than one indicates that the orifice equation under-predicts the leakage across the seal blades whereas a value less than one indicates that the leakage is being over-predicted.

Table 8.1 Discharge coefficients of pocket damper seals

Seal (Blade Profile)	Inlet Cf	Exit Cf
Diverging 6-blades (flat)	0.710	0.780
Diverging 6-blades (downstream bevel)	0.965	1.200
Diverging 8-blades (flat)	0.866	1.118
Diverging 12-blades (double bevel)	1.517	1.658

$$\dot{m}_i = Cf_i \cdot \frac{P_i \cdot A_i}{\sqrt{\gamma \cdot R \cdot T_i}} \cdot \sqrt{\frac{2 \cdot \gamma^2}{\gamma - 1} \cdot \left[\left(\frac{P_{i+1}}{P_i} \right)^{2/\gamma} - \left(\frac{P_{i+1}}{P_i} \right)^{\gamma+1/\gamma} \right]} \qquad \textbf{(8.1)}$$

Gamal [40] also found that while changing the magnitude of the discharge coefficients affected the predicted leakage through the seal, changing only the ratio of these coefficients had an impact on the predictions of the cavity pressures. Keeping the ratio of the inlet to the exit discharge coefficient as small as possible, while still obtaining an accurate prediction of the leakage, led to an improved prediction of the cavity pressures.

INTRODUCTION TO LATER TESTS

To further clarify the effect of the design factors mentioned above on the leakage through the seal, non-rotating tests were carried out on two-, three-, four-, five-, and six-bladed labyrinth seals and on four-, and six-bladed conventional and fully-partitioned pocket damper seals. The seals used for the low pressure tests were described in the previous chapter and were divided into Seal Set A and Seal Set B depending on the geometry of the blades used (all the pocket damper seals used the blades of set B). For labyrinth seals, leakage and mean cavity pressure measurements were made to examine blade thickness effects using two-, four-, and six-bladed seals of Set A, and to examine blade thickness, blade profile, cavity depth, blade spacing and eccentricity effects using three-, four-, five, and six-bladed seals of Set B. The blades of set B were also used to test four-bladed conventional PDSs to examine blade profile effects and four- and six-bladed conventional and fully-partitioned PDSs to examine blade spacing effects. The seals of set B were tested using spacers of long (0.5 in or 12.7 mm), intermediate (0.25 in or 6.35 mm), and short (0.125 in or 3.175 mm) lengths. In all cases of the initial round of tests, the exit pressure from the seal was atmospheric and the inlet pressure was varied up to 100 psi-a (6.89 bar-a). The test conditions were kept as close to constant as possible for each seal. Measurements on the newer hardware were made at seal inlet pressures of 15, 20, 25, 30, 35, 40, 45, 60, and 85 psi-g (1.03, 1.38, 1.72, 2.07, 2.41, 2.76, 3.10, 4.13, and 5.86 bar-g). These pressures correspond to the absolute pressure ratios shown in the figures below. After these initial tests were completed, a second round of tests was conducted with four-bladed labyrinth and pocket damper seals with elevated (non-atmospheric) seal exit pressure back pressure. Several seal configurations were retested in this way so as to raise the supply pressure while maintaining a pressure ratio of about 0.5.

Table 8.2 Quantitative interpretation of qualitative terms

Qualitative Term	Quantitative Interpretation
Long pitch	0.5 in (12.7 mm) pitch length
Intermediate pitch	0.25 in (6.35 mm) pitch length
Short pitch	0.125 in (3.175 mm) pitch length
Thin (regular) blades	0.125 in (3.175 mm) blade thickness
Thick blades	0.25 in (6.35 mm) blade thickness
Shallow cavities	0.1 in (2.54 mm) cavity depth
Deep cavities	0.5 in (12.7 mm) cavity depth

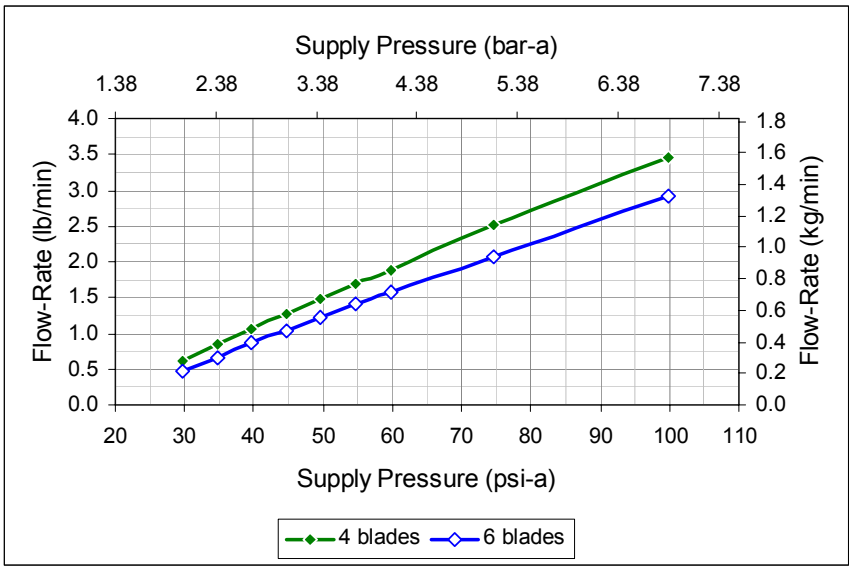

Figure 8.5 Seal leakage (4 and 6 blades, long pitch, deep cavity)

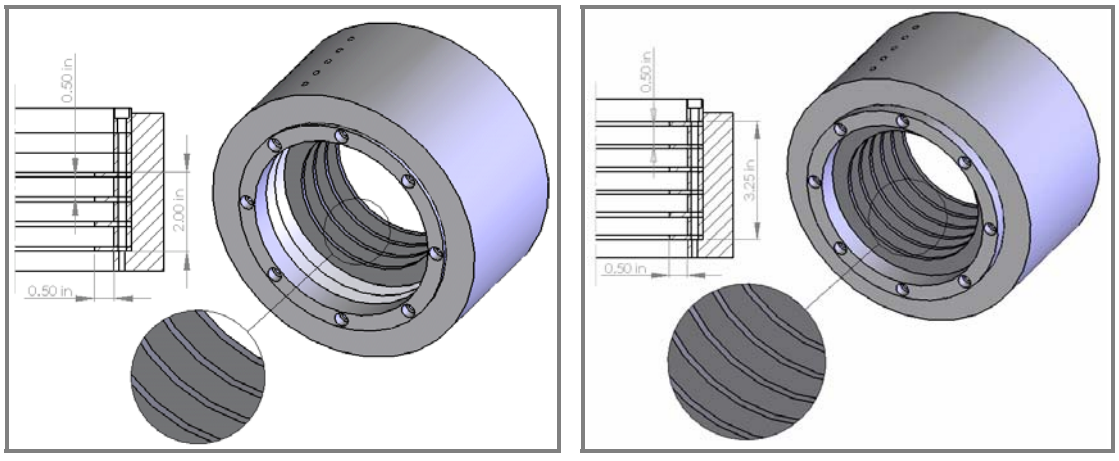

Figure 8.6 Four- and six-bladed seals with long pitch and deep cavities

For the sake of brevity, certain qualitative terms have been attributed to the seal configurations. These are summarized in Table 8.2 and are used throughout this chapter. A preliminary indication that the leakage measurements obtained from the tests were reasonable was provided by a comparison of the leakage through the four- and six-bladed seals of *Set B*. Figure 8.5 compares leakage through two seals (shown in Figure 8.6) with the same blade thickness, cavity depth, and blade spacing, but with different number of blades. Similar results were obtained from tests on seals with short (leakage shown in Figure 8.7) and intermediate pitch lengths and on the modified air-buffer labyrinth seals of *Set A*.

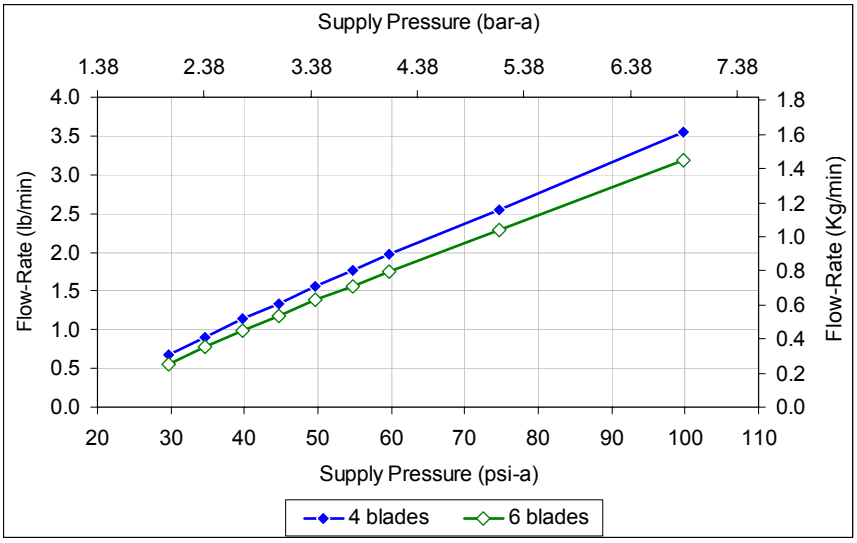

Figure 8.7 Seal leakage (4 and 6 blades, short pitch, deep cavity)

BLADE THICKNESS EFFECTS

Varying the thickness of the blades was found to have a significant impact on the leakage through the test seals of *Set B*. The blade thickness tests were carried out on four-bladed seals (see Figure 8.8) with eight blades arranged in pairs so as to create seal constrictions with double the original thickness (an increase from 0.125 in to 0.25 in or from 3.175 mm to 6.35 mm).

Four labyrinth configurations (listed in Table 8.3) were tested for this part of the experimentation; long pitch and intermediate pitch length seals each with single and double thickness blades. Figure 8.9 and Figure 8.10 compare the leakage rates through four-bladed seals with different blade thicknesses. The percent reduction in leakage resulting from replacing the original 0.125 in (3.175 mm) thick blades with the 0.25 in (6.35 mm) thick blades in two different four-bladed seals can be seen in Figure 8.11. A reduction in leakage of up to 20% was observed at low supply pressures and a reduction of roughly 10% to 15% is observed at higher pressures.

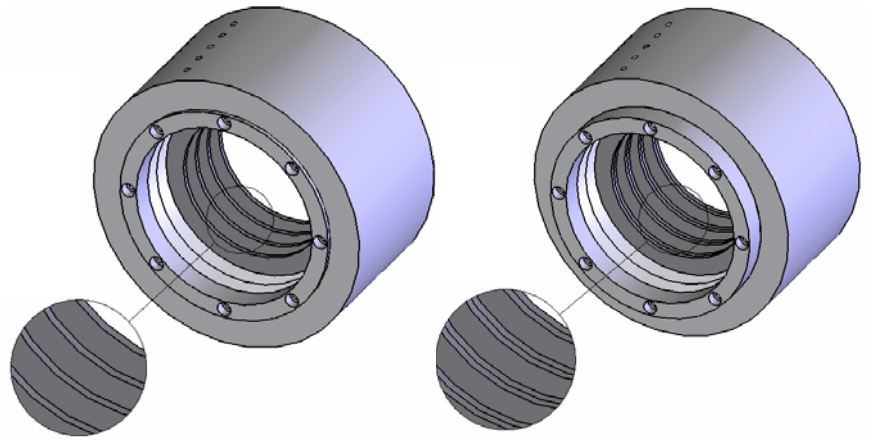

Figure 8.8 Single- and double- thickness 4-bladed seals w/ equal blade spacing

Table 8.3 Seals used for blade thickness effect tests

No. of Blades	Cavity Depth		Blade Pitch		Blade Thickness	
	(mils)	(mm)	(in)	(mm)	(in)	(mm)
4	500	12.7	0.5	12.7	0.125	3.175
4	500	12.7	0.5	12.7	0.25	6.35
4	500	12.7	0.25	6.35	0.125	3.175
4	500	12.7	0.25	6.35	0.25	6.35

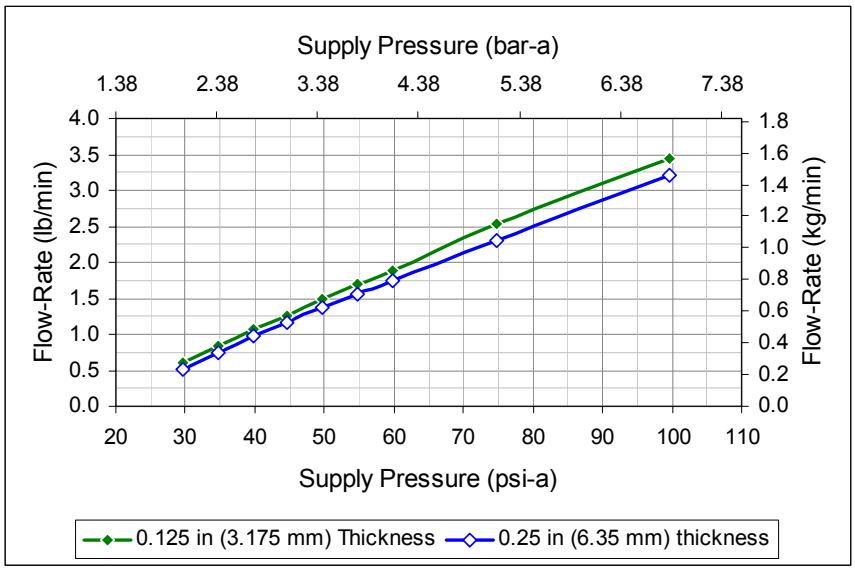

Figure 8.9 Blade thickness effect (4 blades, long pitch)

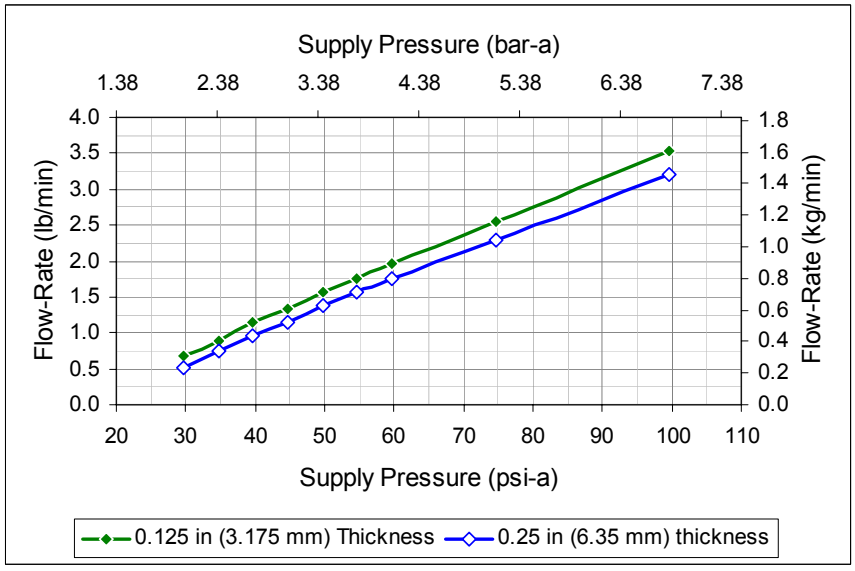

Figure 8.10 Blade thickness effect (4 blades, short pitch)

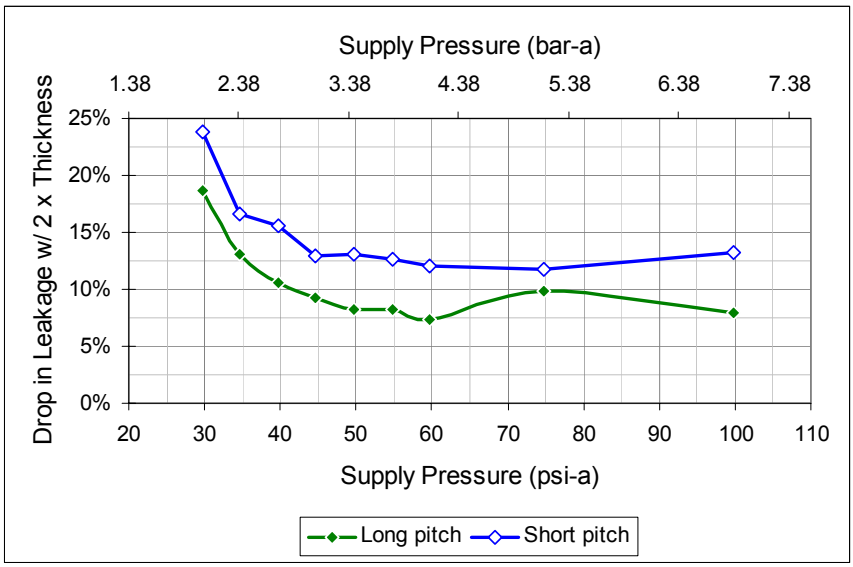

Figure 8.11 Effect of doubling blade thickness on leakage

BLADE PROFILE EFFECTS

Tests were carried out on two separate sets of seal hardware to investigate the effect of blade profile on labyrinth seal leakage. The results of the two sets of tests, presented below, were found to contradict each other. A possible explanation of this contradiction, which is related to blade thickness effects, is presented in the *Chapter Discussion* section of this chapter.

Labyrinth Seal Set A

The flow-rates for the two-bladed seal for all three blade profiles are shown in Figure 8.12. The effect of beveling the blades is insignificant at low pressures. At higher pressures, the different blade profiles still result in close leakage values (see table in appendix), but a trend begins to emerge, showing that the seals with the beveled blade profiles leak less than the flat profile seal. The flat-tipped seal was found to leak slightly more than the upstream beveled seal, which in turn leaked more than the downstream beveled seal. At pressures of approximately 60 psi-a (4.13 bar-a, PR=0.25), the downstream-beveled seal leaked up to 7.5% less than the flat-tipped seal.

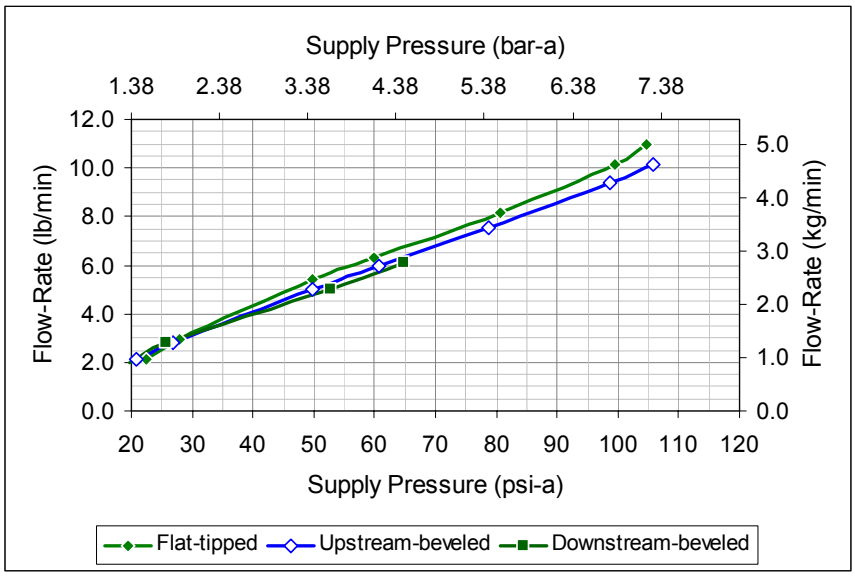

Figure 8.12 Effect of blade profile on leakage (2 blades)

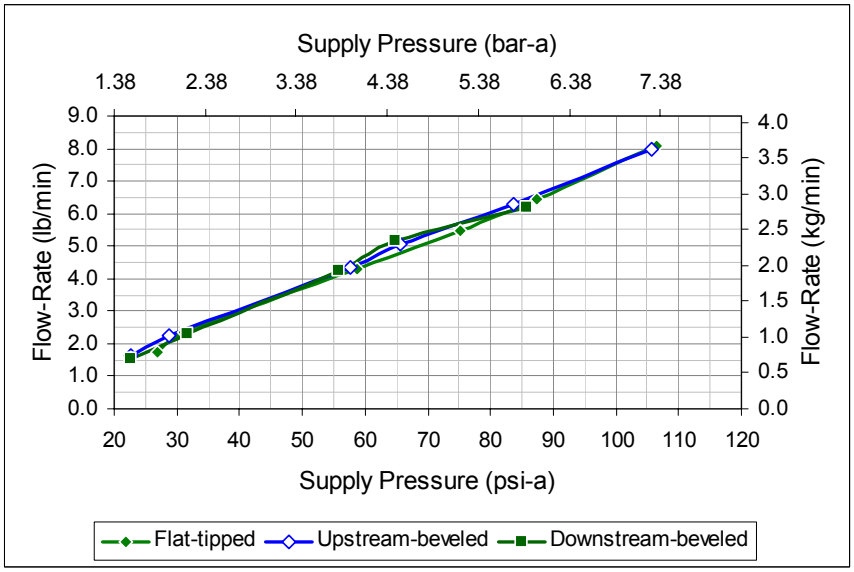

Figure 8.13 Effect of blade profile on leakage (4 blades)

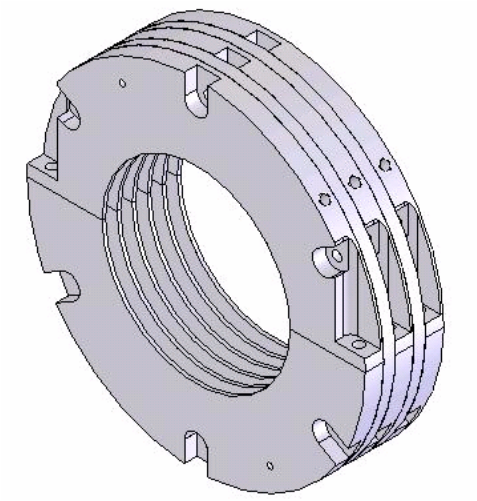

Figure 8.14 Six-bladed seal of seal set A

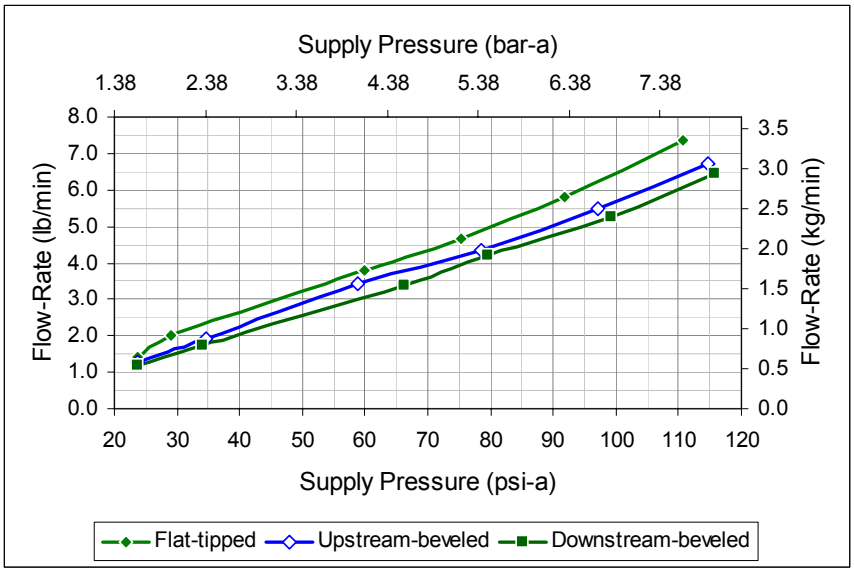

Figure 8.15 Effect of blade profile on leakage (6 blades)

The results of tests on the four-bladed seal configurations (Figure 8.13) show that beveling the blades has practically no effect on the leakage. The six-bladed seal (shown in Figure 8.14) displayed the highest dependency on blade profile (Figure 8.15). As in the case of the two-bladed seal, the upstream-beveled configuration leaked less than the flat-tipped profile and the downstream beveled seal leaked less than either of the other

configurations. Beveling the seal blades in the downstream direction reduced the leakage by 10% to 15% over the range of test pressures.

Concurrent with the leakage tests, cavity pressure measurements were made in the four-bladed and six-bladed seals. Due to geometric restrictions, pressure measurements could not be made in the lowermost two-bladed seal section or in the cavities formed by the spacers. As a result, cavity pressure data was taken in the third cavity of the four-bladed seal and the third and fifth cavities of the six-bladed seal

Figure 8.16 shows the variation of pressure in the third cavity of the four-bladed seal for the three blade profiles. Pressure readings from the beveled seals, particularly the downstream-beveled configuration, are clearly lower than those from the flat-tipped configuration. While the leakage results for the configurations of the four-bladed seal were especially close, the pressure data in the third cavity indicate that the first three blades of the beveled seals were more successful in dropping the gas pressure. This indicates that the beveled seals would be more effective in reducing the leakage through the seal.

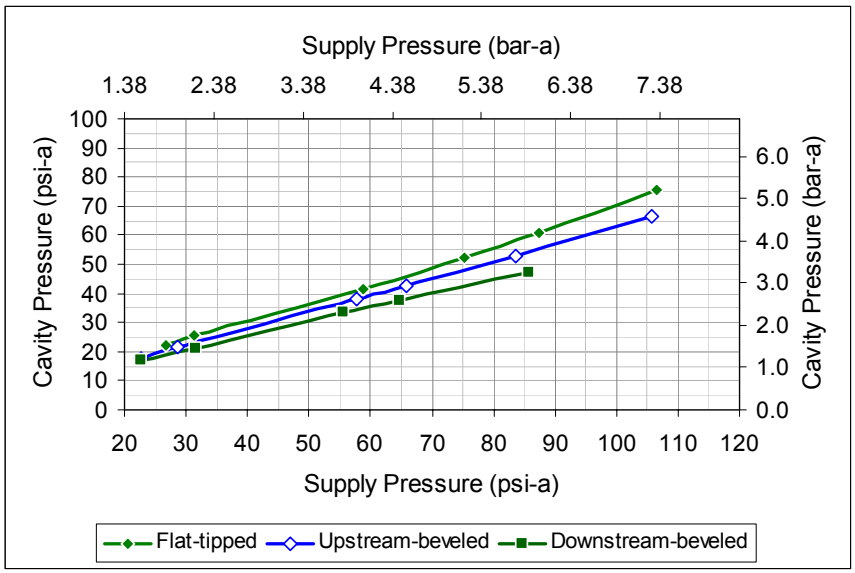

Figure 8.16 Pressure in third cavity of four-bladed seal

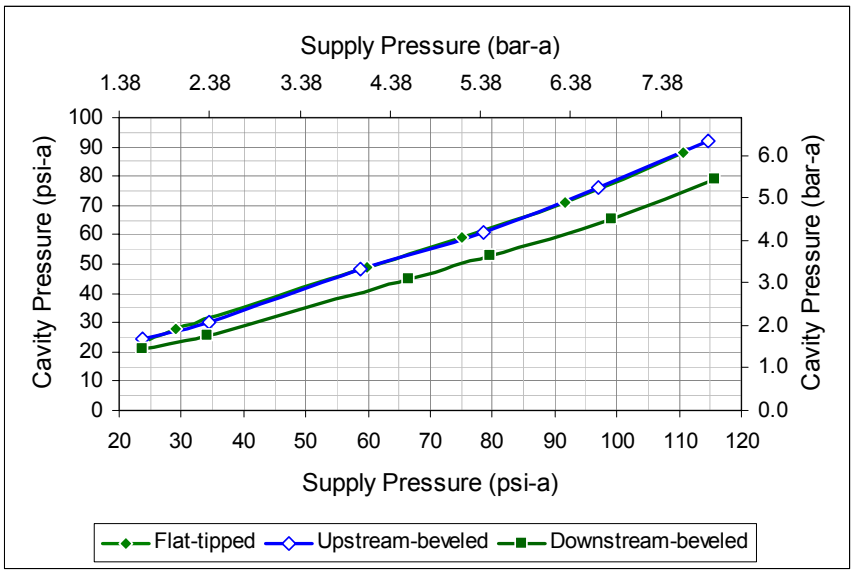

Figure 8.17 Pressure in third cavity of six-bladed seal

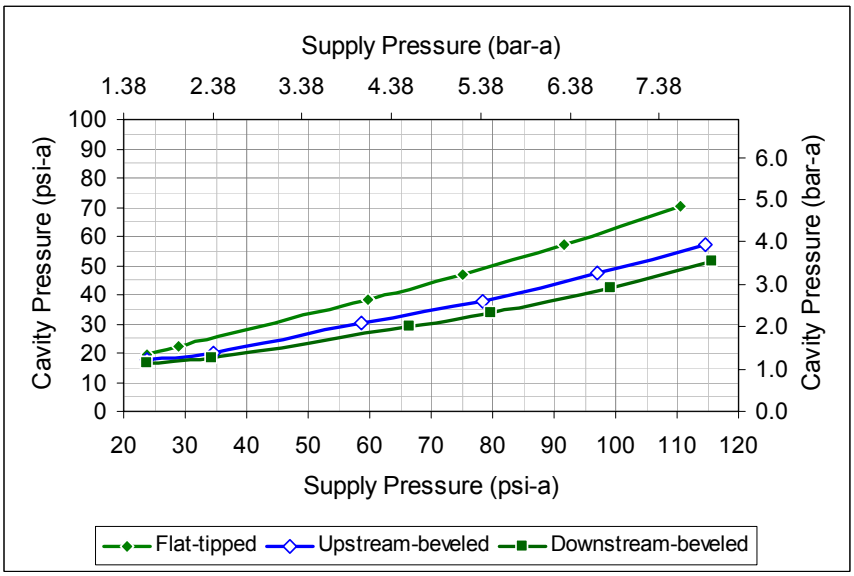

Figure 8.18 Pressure in fifth cavity of six-bladed seal

The cavity pressures in the third and fifth cavities of the six-bladed seal are represented in Figure 8.17 and Figure 8.18 respectively. Both these figures support the results of the cavity pressure measurements in the four-bladed seal and the leakage results presented above.

Labyrinth Seal Set B

The leakage results for four-bladed seals are shown in Figure 8.19 for long pitch and in Figure 8.20 for short pitch. Each of these plots compares the leakage through seals with 1/8 in (3.175 mm) thick flat-tipped blades, 1/4 in (6.35 mm) thick flat-tipped blades, and 1/4 in (6.35 mm) thick beveled blades. Two of the seals used for these comparisons are shown in Figure 8.21.

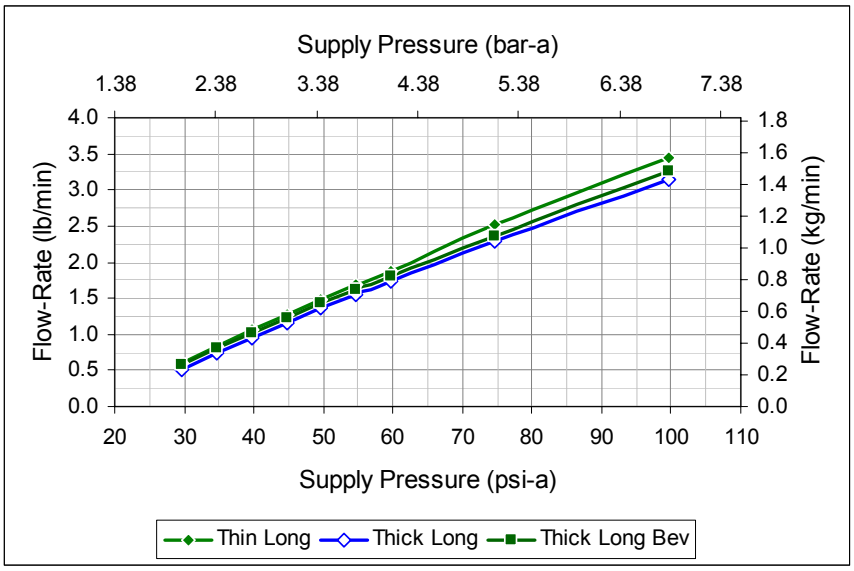

Figure 8.19 Effect of blade profile on leakage (4 blades, long pitch)

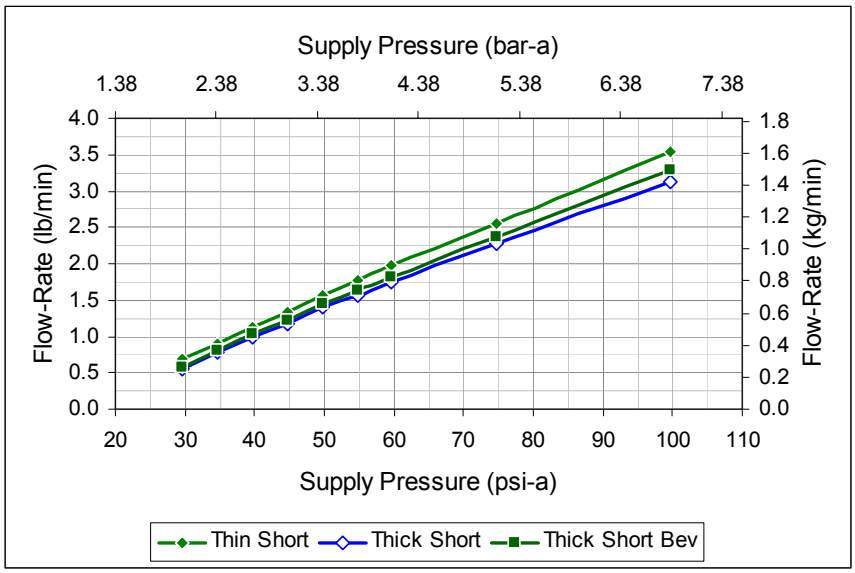

Figure 8.20 Effect of blade profile on leakage (4 blades, short pitch)

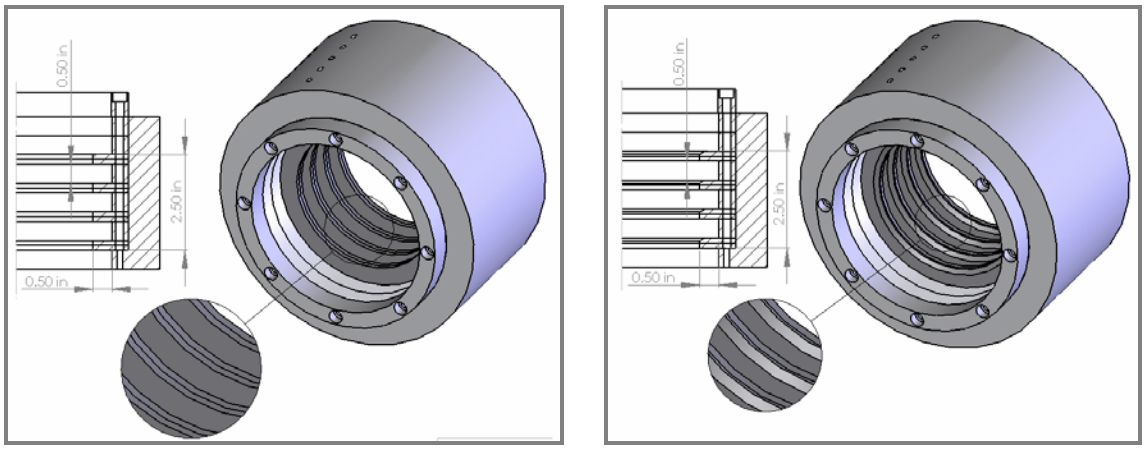

Figure 8.21 Four-bladed seals w/ flat-tipped and beveled double-thickness blades

Comparing the curves (or the data in the appendix) for thick flat-tipped and thick beveled blades shows that beveling the blades in the downstream direction increased the leakage through the seal. These results contradict the results obtained from the earlier set of blade profile tests. Furthermore, it appears from the graphs that for these seals, blade thickness was more of a factor than blade profile. This can be concluded from the fact that the thicker the tip of the blade, the lower the leakage regardless of blade profile.

Pocket Damper Seals

Conventional pocket damper seals were also tested with flat-tipped and beveled blades, but the latter set of blades were assembled in a double-beveled configuration. This was done primarily to avoid creating a gap between a chamfered edge of a blade and the partition wall downstream of it (Figure 8.22), but also resulted in a configuration similar to that tested for the high pressure pocket damper seal tested by Gamal [40]. Three configurations of a four-bladed conventional PDS were used for this comparison as shown in Table 8.4. The same trends were observed for pocket damper seals as for labyrinth seals. The seals double-beveled blades were found to leak more than the flat-tipped blades. This supports the partial explanation put forward earlier for effect of blade profile on leakage through the high pressure twelve-bladed (double-beveled) seal and eight-bladed (flat-tipped) seal.

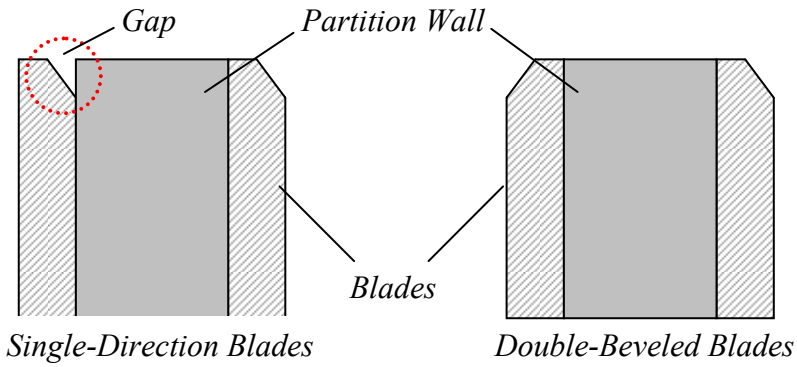

Figure 8.22 Double-beveled PDS test configuration

Table 8.4 Conventional PDSs used for blade profile tests

Blade Pitch		Blade Thickness		Blade Tip Thickness		Blade Profile
(in)	(mm)	(in)	(mm)	(in)	(mm)	
0.5	12.7	0.125	3.175	0.125	3.175	Flat
0.5	12.7	0.250	6.350	0.250	6.350	Flat
0.5	12.7	0.250	6.350	0.175	4.445	Double-Beveled

All seals had 4 blades and 500 mils (12.7 mm) depth

BLADE SPACING EFFECTS

In order to examine the effect of blade profile and blade thickness for as many seal configurations as possible, seals with different pitch lengths were tested. As expected, the spacing of the blades was found to affect the leakage through the seal. These tests made it apparent that the spacing of the blades has a significant effect on seal leakage. In fact, these preliminary results indicated that the effect of cavity pitch was almost as significant as that of blade thickness and was considerably more significant that either the effect of cavity depth or blade profile.

Labyrinth Seals

Table 8.5 describes the seals used to examine the effect of blade spacing. The most dramatic measured changes in leakage can be seen in Figure 8.23, which shows the percentage reduction in leakage resulting from increasing the blade spacing of two six-bladed seals from 0.125 in and 0.25 in to 0.5 in (from 3.175 mm and 6.35 mm to 12.7 mm). At lower supply pressures (and therefore lower pressure drops across the seal), the reduction in leakage is up to 16% for the seal in which the pitch was quadrupled and 12% for the seal in which the pitch was doubled. For higher pressure drops, the leakage rates were reduced by 5% to 10%.

Table 8.5 Seals used for blade pitch effect tests

No. of Blades	Blade Pitch (in)	Cavity Depth (mils)	Seal Length (in)
3	1/4	500	0.875
4	1/2	500	2.000
4	1/4	500	1.250
4	1/8	500	0.875
6	1/2	500	3.250
6	1/4	500	2.000
6	1/8	500	1.375

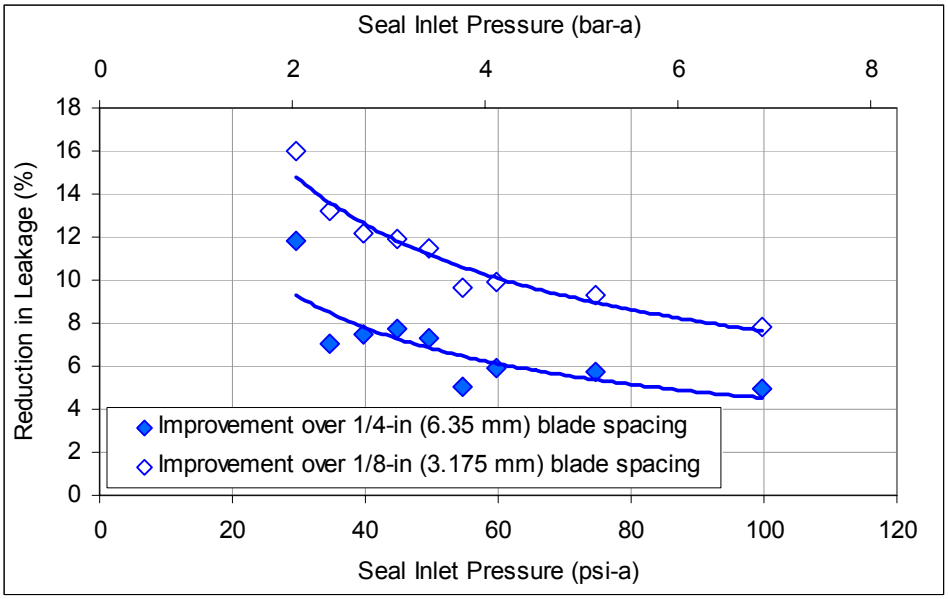

Figure 8.23 Reduction in leakage due to increased blade pitch (6-bladed seals)

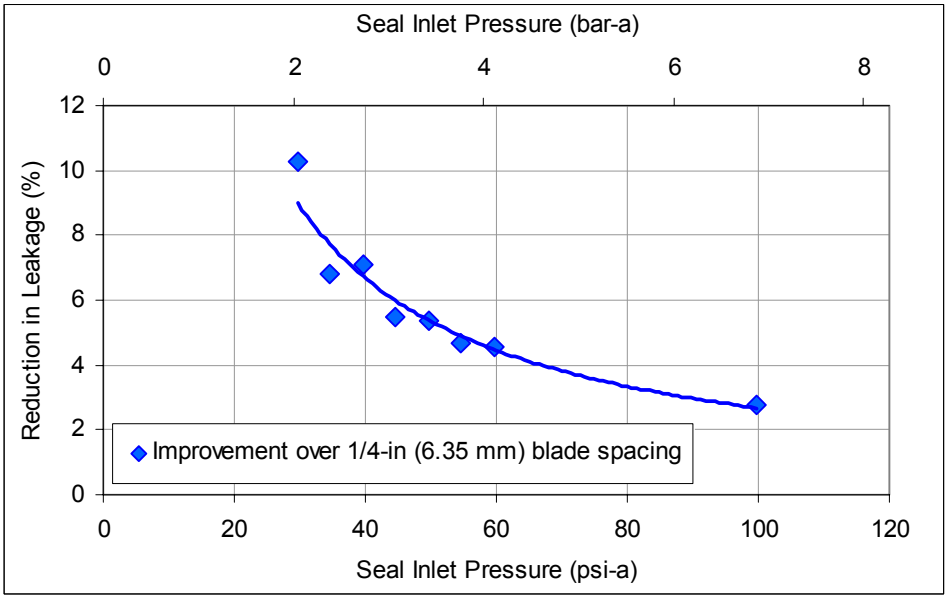

Figure 8.24 Reduction in leakage due to increased blade pitch (4-bladed seals)

Similar results were obtained from a comparison of two four-bladed seals (Figure 8.24). Increasing the blade spacing of this seal from 0.25 in to 0.5 in (from 6.35 mm to 12.7 mm) resulted in a drop in leakage of 5% to 10% over the range of test pressures.

These results indicate that there is a drop in carry-over kinetic energy with increasing pitch as well as with decreasing pressure drop.

As can be seen from Table 8.5, these changes in pitch led to an increase in overall lengths of the two initial six-bladed seals from 1.375 in and 2 in to 3.25 in (from 34.9 mm and 50.8 mm to 82.6 mm) and a doubling of the length of the initial four-bladed seal from 1.25 in to 2.5 in (from 31.75 mm to 63.5 mm). While reductions in leakage such as those observed during the tests may be desirable, such increases in seal lengths may not be possible because of space constraints in actual turbomachines. A comparison was therefore conducted on a pair of seals in which the pitch length was varied, but the overall length was kept constant by changing the number of blades. Figure 8.25 shows the leakage through a three-bladed labyrinth seal with 0.25 in (6.35 mm) blade pitch and an overall length of 0.875 in (22.23 mm) and a four-bladed labyrinth seal with 0.125 in (3.175 mm) blade pitch and the same overall length. While the three-bladed seal appears to leak slightly more than the four-bladed seal, the difference is practically negligible and the flow-rates through the two seals are practically indistinguishable for higher pressure drops.

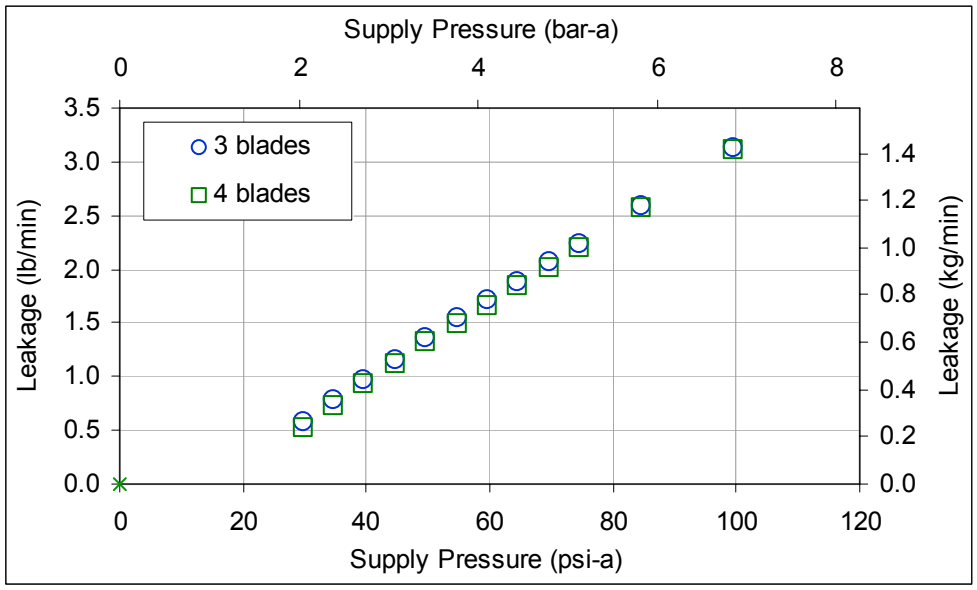

Figure 8.25 Leakage through seals with different pitch but same overall length

Increasing pitch is essentially an attempt to decrease the amount of carryover and to increase the percentage of the jet that experiences turbulence. For a given seal length, there will therefore be a trade off between the number of throttling points to be incorporated and the spacing between the blades which can be used to increase the turbulence undergone by the fluid.

Pocket Damper Seals

Similar trends were observed from the results of tests on pocket damper seals. For the PDS tests, two pitch lengths (primary and secondary for a fully-partitioned seal or active and inactive for a conventional seal) could be varied. Figure 8.26 shows comparative data for two pairs of conventional pocket damper seals. The upper curve in the figure represents the drop in leakage resulting from changing pitch lengths of a PDS from intermediate (active) and short (inactive) to intermediate (active) and intermediate (inactive). The lower curve in the figure represents the drop in leakage resulting from changing the pitch lengths from long (active) and short (inactive) to long (active) and intermediate (inactive). Figure 8.27 shows the drop in leakage resulting from changing pitch lengths of a *fully-partitioned* PDS from long (primary) and short (secondary) to long (primary) and intermediate (secondary). Both figures demonstrate that reducing the spacing between the blades of a pocket damper seal, as was shown for labyrinth seals, increases the leakage through the seal.

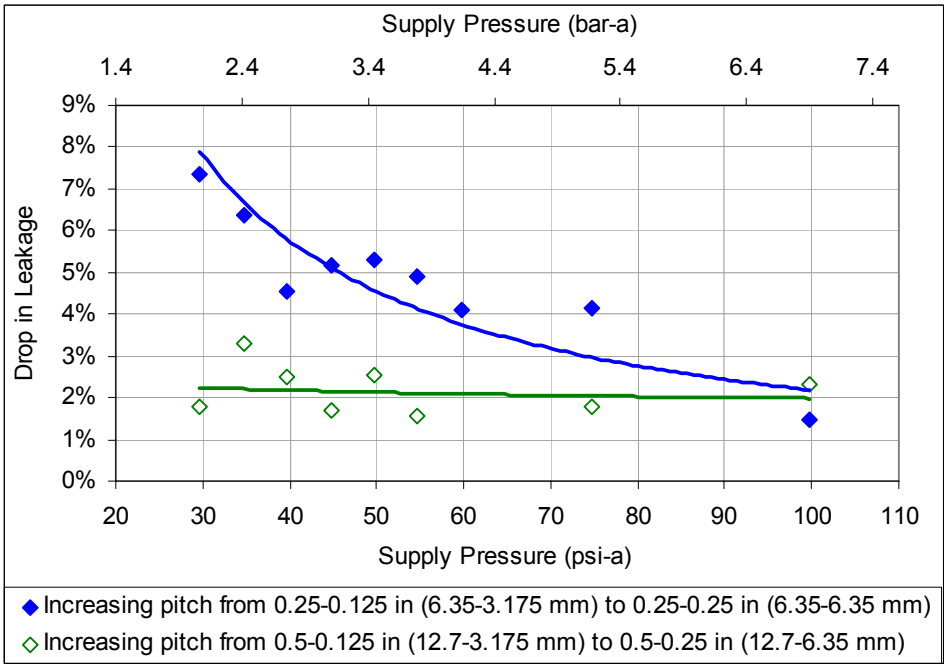

Figure 8.26 Drop in leakage resulting from increasing C-PDS blade spacing

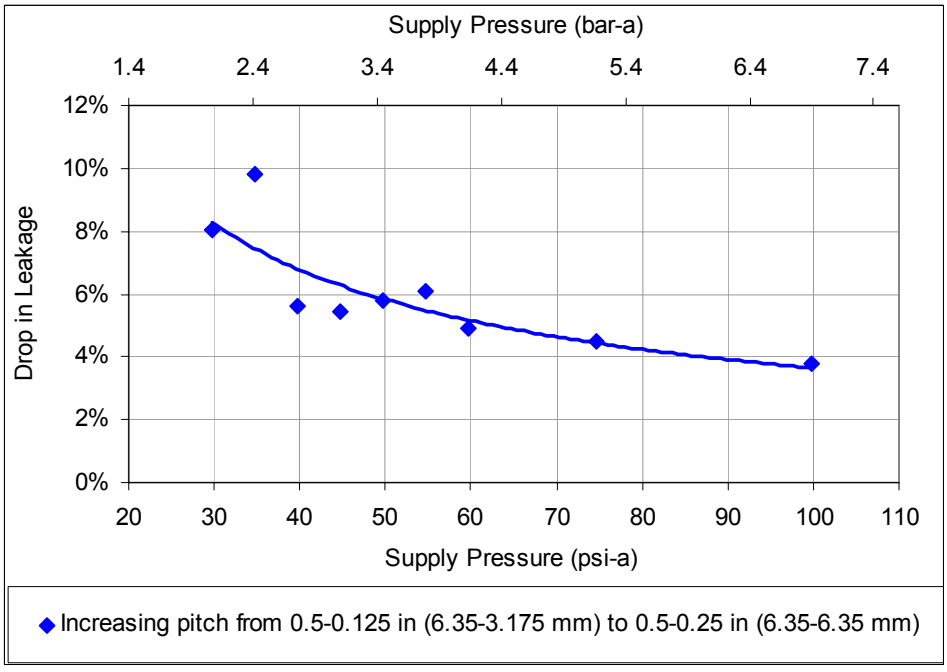

Figure 8.27 Drop in leakage resulting from increasing FP-PDS blade spacing

CAVITY DEPTH EFFECTS

Four six-bladed seals and two four-bladed seals (all with flat-tipped blades) were initially used to examine the effect of cavity depth. These seal configurations are listed in Table 8.6 and the shallow-cavity seals are shown in Figure 8.28. The cavity depth was changed by placing an annular insert between the blades; decreasing the cavity depth from 0.5-in to 0.1-in (from 12.7 mm to 2.54 mm).

Table 8.6 Seals used for initial cavity depth effect tests

No. of Blades	Cavity Depth (mils)	Cavity Depth (mm)	Blade Pitch (in)	Blade Pitch (mm)
6	500	12.7	0.5	12.7
6	100	2.54	0.5	12.7
6	500	12.7	0.25	6.35
6	100	2.54	0.25	6.35
4	500	12.7	0.125	3.175
4	100	2.54	0.125	3.175

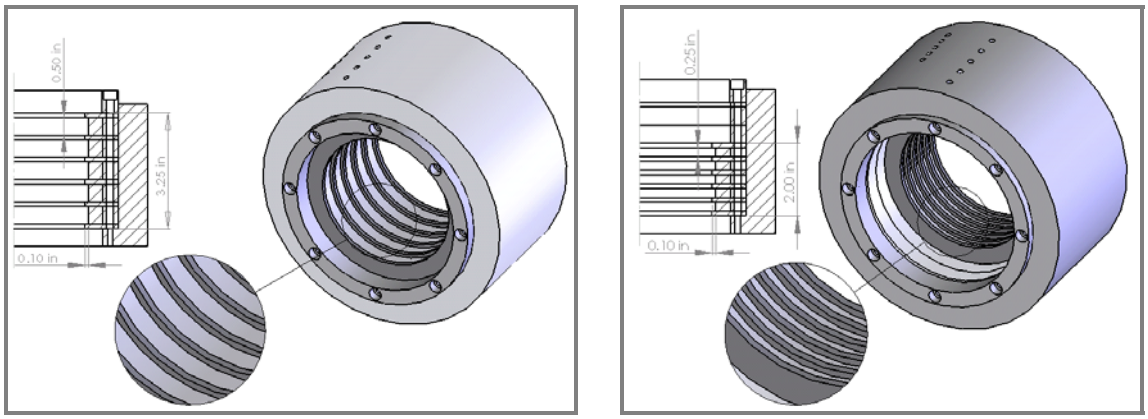

Figure 8.28 Six-bladed seals with shallow cavities

Figure 8.29 shows the effect of cavity depth on the leakage through six-bladed seals with 0.5-in (12.7 mm) blade spacing, and indicates that an 80% reduction in cavity depth has almost no impact on the leakage. The same result is observed from tests on the six-bladed seals with 0.25-in blade spacing, as show in Figure 8.30.

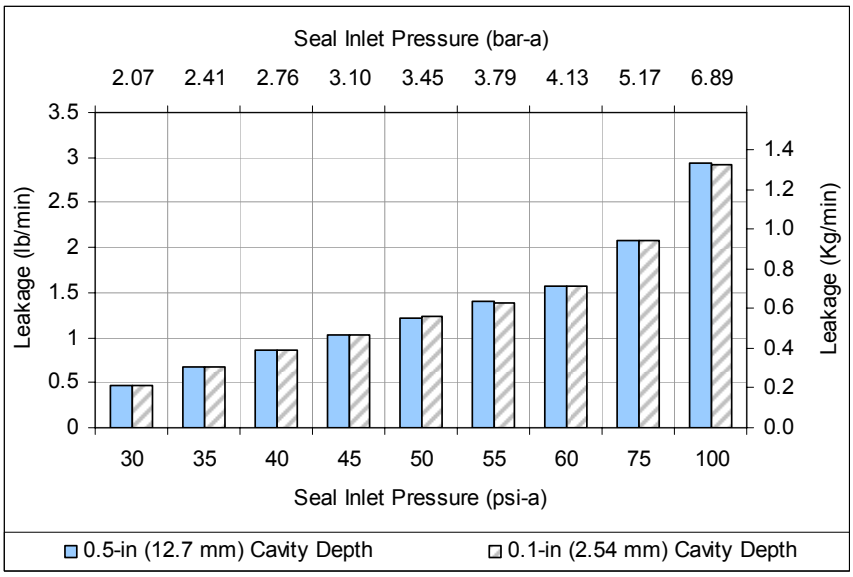

Figure 8.29 Effect of cavity depth on 6-bladed seal leakage with long pitch

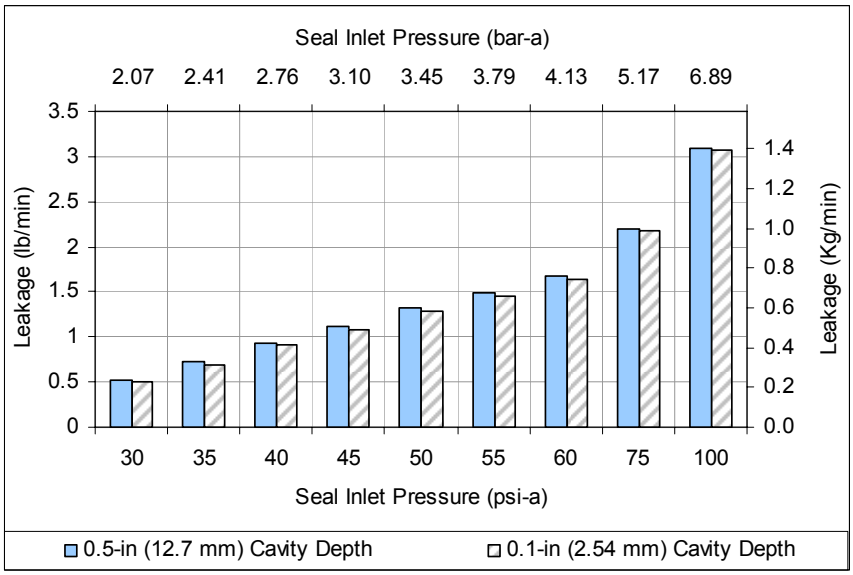

Figure 8.30 Effect of cavity depth on 6-bladed seal leakage with intermediate pitch

It is difficult to infer a trend from either of these plots, which show slightly higher leakage rates through the deep-cavity seal at some pressures and higher rates through the shallow-cavity seal at other pressures. The repeatability errors associated with the cavity

pressure measurements were found to be lower than those associated with the flow-rate measurements, and so in a case such as this in which the leakage data is difficult to interpret, the cavity pressure information can be used to clarify any trends that may exist. The cavity pressure in the third cavity of the six-bladed seal with long pitch is shown in Figure 8.31.

This cavity pressure plot confirms that the effect of cavity depth is small, but also shows a somewhat clearer trend than that suggested by the leakage data. The pressures in the cavities of the seal with deep cavities are lower than those in the seal with shallow cavities for almost all values of supply pressure. This is an indication that the seals with deep cavities are more effective at lowering the pressure along the length of the seal and that the seal with deeper cavities is slightly more effective at reducing leakage. Attempting to read a similar trend into the cavity pressure data for the six-bladed seal with intermediate pitch length is considerably more difficult as can be seen from the plot in Figure 8.32.

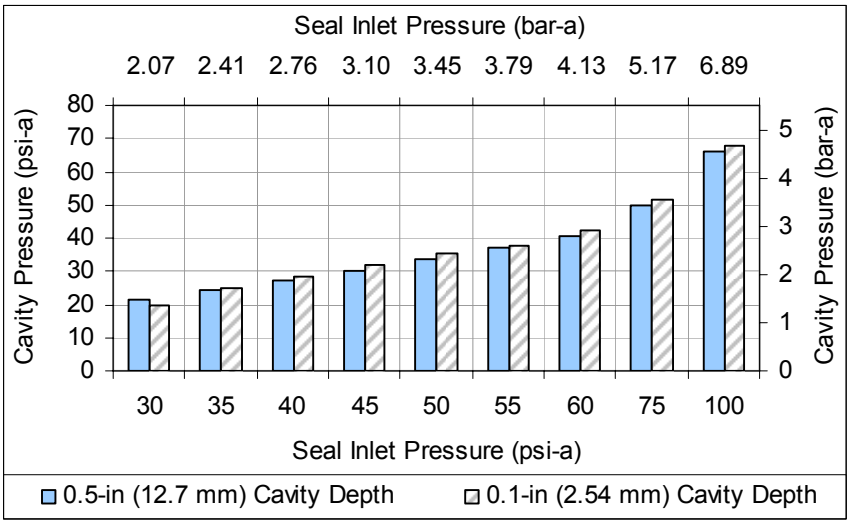

Figure 8.31 Effect of cavity depth on 6-bladed seal pressures with long pitch

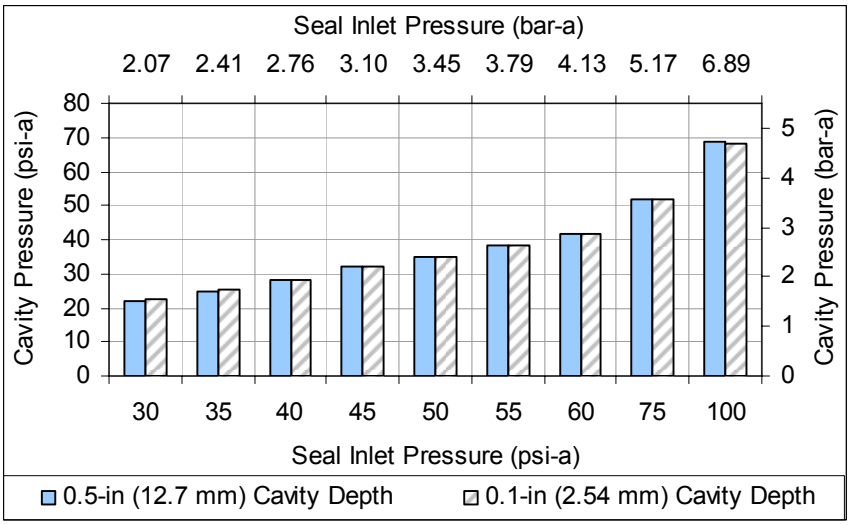

Figure 8.32 Effect of cavity depth on 6-bladed seal pressures with intermediate pitch

The leakage and pressure data from the two four-bladed seals with long pitch length (0.5-in or 12.7 mm) were used to generate the plots in Figure 8.33 and Figure 8.34 (pressure in the second cavity). As was the case with the results for the six-bladed seal with long pitch length, the leakage through the four-bladed seal seams to be virtually unaffected by cavity depth, but the cavity pressure data shows a trend indicating a small improvement in leakage reduction performance in the case of the seal with the deeper cavities.

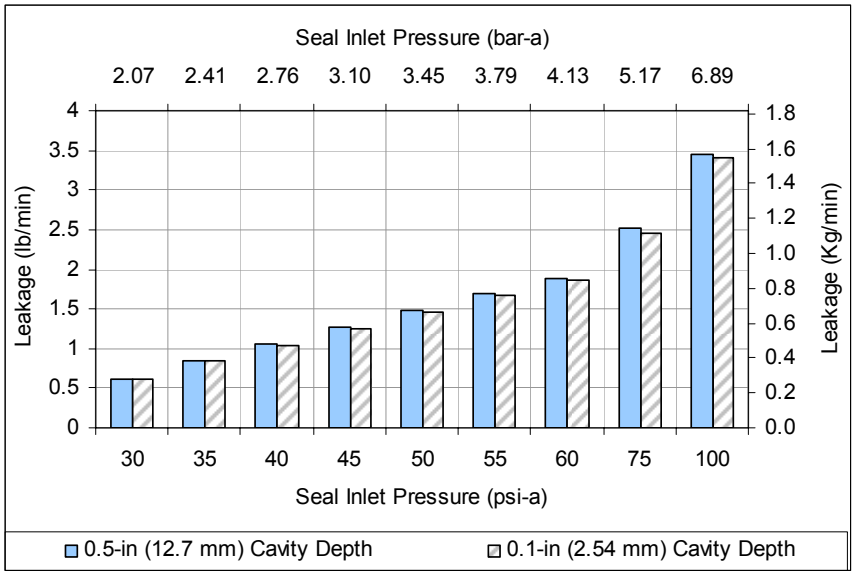

Figure 8.33 Effect of cavity depth on 4-bladed seal leakage with long pitch

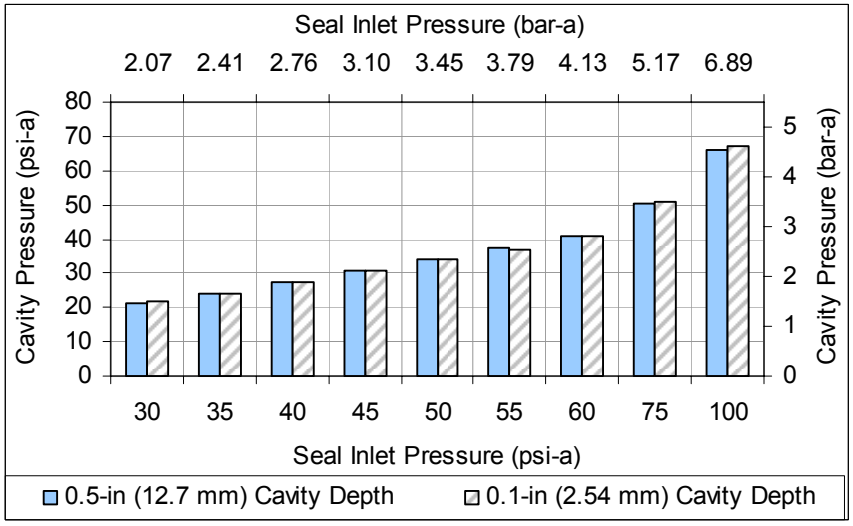

Figure 8.34 Effect of cavity depth on 4-bladed seal pressures with long pitch

Even though the cavity pressure data shows a minor trend, the absolute changes in leakage due to making changes to the cavity depths of the seals are small. These changes are under 5% for the test seals at low supply pressures and are under 1% for most other test conditions. Comparison plots of the variation of cavity pressure with

supply pressure for the remaining cavities of the six seal configurations discussed in this section show similar trends. These cavity pressures are listed in the *Appendix* of this dissertation.

Table 8.7 shows the ratio of leakage through the six-bladed seal with shallow cavities to that through a six-bladed seal with deep cavities, clearly indicating that an 80% reduction in cavity depth had virtually no impact on leakage. Similar results were obtained from tests on four-bladed seals with long and intermediate pitch lengths and a six-bladed seal with intermediate pitch length. Since no clear trends were discernable from the data obtained from the initial tests (Table 8.7), a second round of tests was conducted with shallower cavity depths. In these tests, leakage through four-bladed and six-bladed seals with cavity depths of 500 mils was measured. The same seals were then fitted with annular inserts between the blades which reduced the cavity depths to 100 mils (2.54 mm); an 80% reduction in depth. Figure 8.35 shows one of the seals used for these tests.

Table 8.7 Effect of reducing cavity depth by 80%

Seal Inlet Pressure		Leakage Ratio
(psi-a)	(bar-a)	
30	2.05	0.995
35	2.39	1.000
40	2.74	1.001
45	3.08	1.000
50	3.42	1.008
55	3.77	0.984
60	4.11	1.002
75	5.15	1.005
100	6.87	0.995

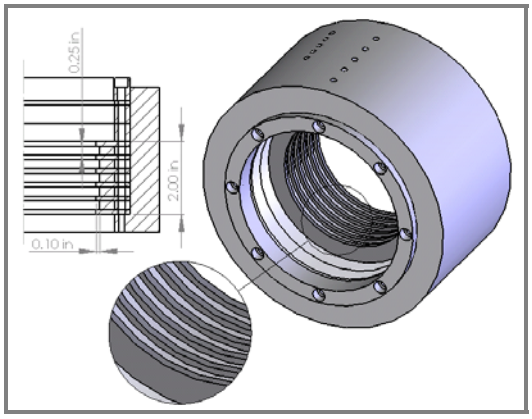

Figure 8.35 Use of annular inserts to reduce cavity depth

The geometries of the seal configurations used for the second round tests are described in Table 8.8. Once again, the cavity depth was changed by placing annular inserts between the blades.

Figure 8.36 shows the reduction in leakage through a four-bladed labyrinth seal with 500 mils (12.7 mm) cavity depth and 0.25 in (6.35 mm) pitch when the cavity depth is reduce to first 50 mils (6.35 mm) then 20 mils (6.35 mm). In both cases there is a drop in leakage associated with making the cavities shallower and the drop is higher for the seal with the shallowest cavities. This effect is more pronounced at higher supply pressures (about 7% for the 20 mils or 0.508 mm cavity depth)

Table 8.8 Seals used for second round of cavity depth effect tests

No. of Blades	Cavity Depth (mils)	Cavity Depth (mm)	Seal Length (in)	Seal Length (mm)
4	500	12.7	1.25	31.75
4	50	1.27	1.25	31.75
4	20	0.508	1.25	31.75
5	500	12.7	1.625	41.275
5	50	1.27	1.625	41.275
5	20	0.508	1.625	41.275

0.25 in (6.35 mm) blade spacing for all seals

Similar tests on five-bladed seals showed somewhat different results. Figure 8.37 shows that in the case of a five-bladed seal, decreasing the cavity depth to 50 mils (1.27

mm) reduced the leakage by up to 3%, but further decreasing the cavity depth increased the leakage by 2% to 4%. This could be an indication that there is an optimum cavity depth with respect to leakage reduction, but it should also be noted that the percentage drop in leakage associated with the 50 mils (1.27 mm) curve in Figure 8.37 is too small to be useful in making any general statements regarding the effect of cavity depth.

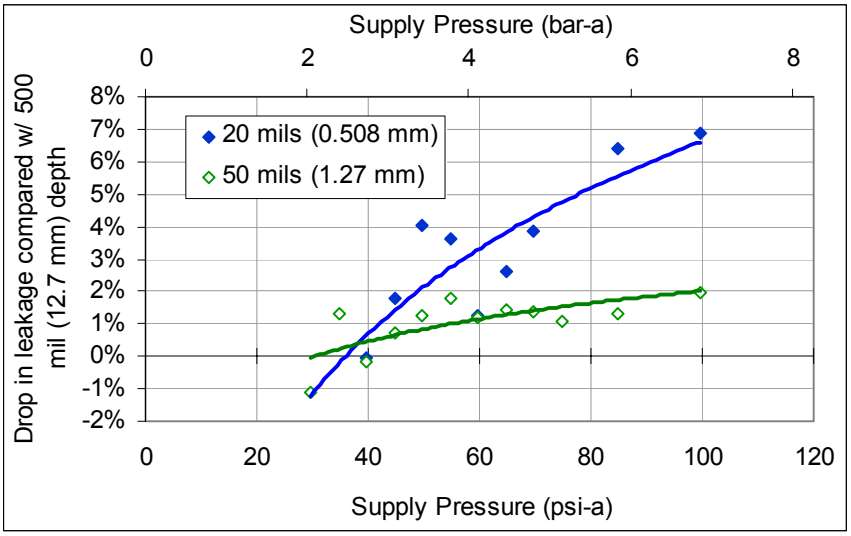

Figure 8.36 Effect of cavity depth on four-bladed seals (0.25-in pitch)

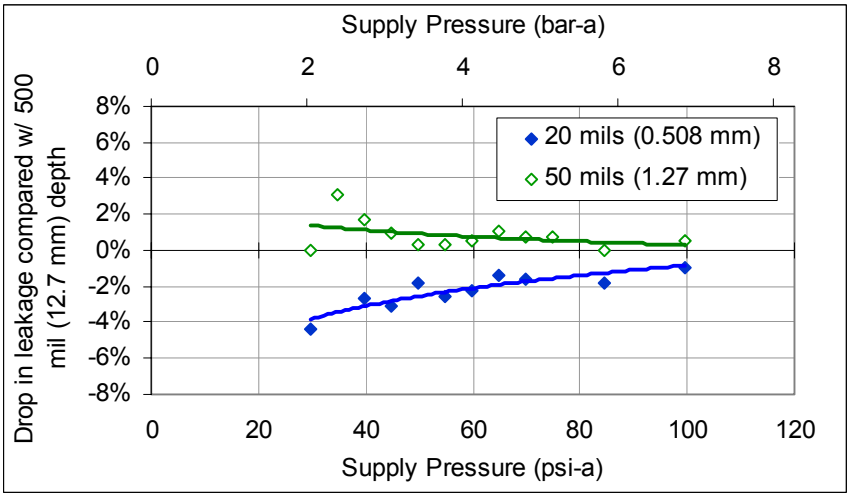

Figure 8.37 Effect of cavity depth on five-bladed seals (0.25-in pitch)

ECCENTRICITY AND PARTITION WALL EFFECTS

Immediately following several of the leakage tests, the seals of set B were moved to a fully eccentric position and retested to examine the effect of eccentricity on the leakage. As was expected, the seal leakage increased in the off-center position. These tests were initially proposed as an attempt to explain the contradiction between the effect of blade profile on labyrinth seal leakage and that on pocket damper seal leakage. The experimental results presented earlier and discussed in the next section suggest another reason for this contradiction, but the eccentricity results are presented here nonetheless. Figure 8.38 shows that increased eccentricity significantly increases leakage through the test seals at low supply pressures. The same leakage data is shown plotted against pressure ratio in Figure 8.39. Comparisons between leakage rates for centered and fully-eccentric pocket damper seals indicated the presence of partition walls reduced the effect of eccentricity at lower supply pressures. At higher supply pressures, the effect was on the same scale as that measured for labyrinth seals, meaning that over the range of test pressures, the effect of making the seal fully eccentric was under approximately 3%.

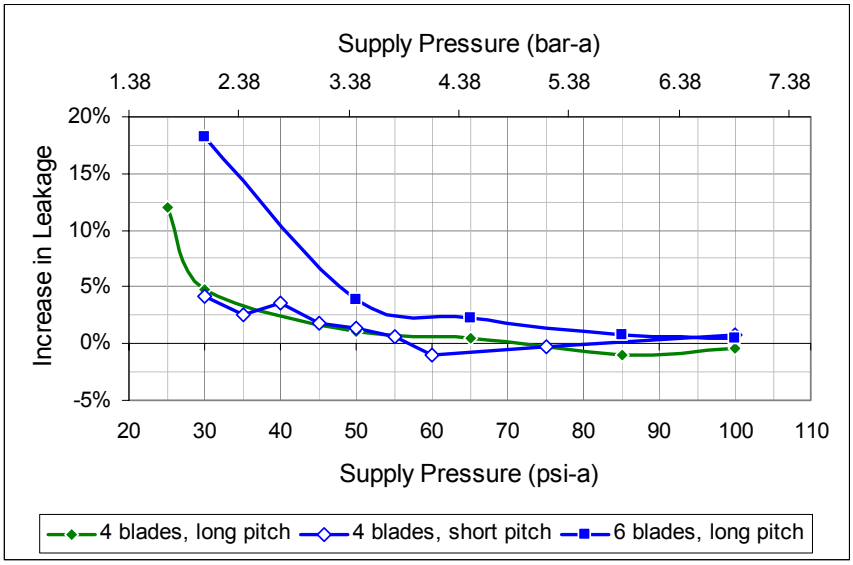

Figure 8.38 Increased leakage due to eccentricity

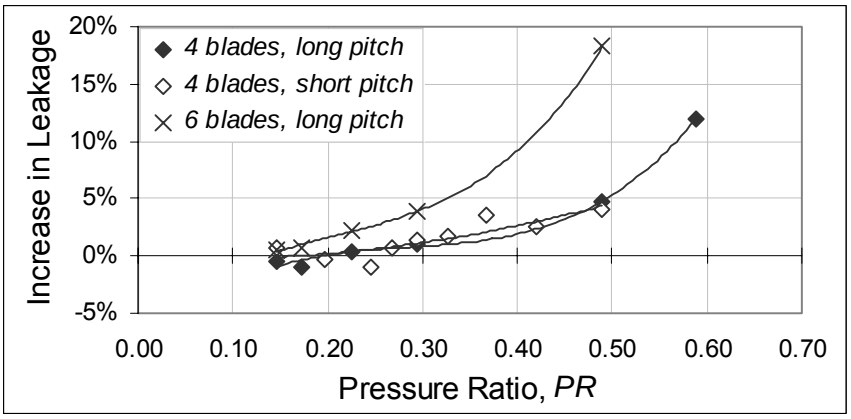

Figure 8.39 Increased leakage due to eccentricity (versus PR)

As discussed earlier, Laos' [32] experimental comparison of the leakage through a four-bladed pocket damper seal and a six-bladed labyrinth seal led to questions about the shape and spacing of the blades. This comparison, which showed lower leakage through the PDS, also led to questions about the differences between PDS flow and labyrinth seal flow and the influence of partition walls on axial leakage rates. Figure 8.40 compares leakage through two six-bladed seals; a conventional PDS and a fully-partitioned PDS with 0.25 in (6.35 mm) primary pitch and 0.125 in (3.175 mm) secondary pitch and deep cavities. This figure shows that the addition of partition walls in the two secondary cavities of the fully-partitioned seal reduces leakage.

Figure 8.41 compares the leakage through a six-bladed labyrinth seal and a six-bladed conventional PDS with 0.25 in (6.35 mm) pitch (for a fair comparison, the active and inactive pitch lengths of the PDS were made to match the single pitch length of the labyrinth seal.). The leakage through the PDS is clearly lower than that through the labyrinth seal, indicating that partition walls play a role in limiting leakage, even with the seal in the centered position. It should be noted that the conventional PDS of Figure 8.40 leaks more than the conventional PDS of Figure 8.41. Since the inactive pitch length of the former is shorter than that of the latter, this is in accordance with earlier results that showed the effect of blade spacing.

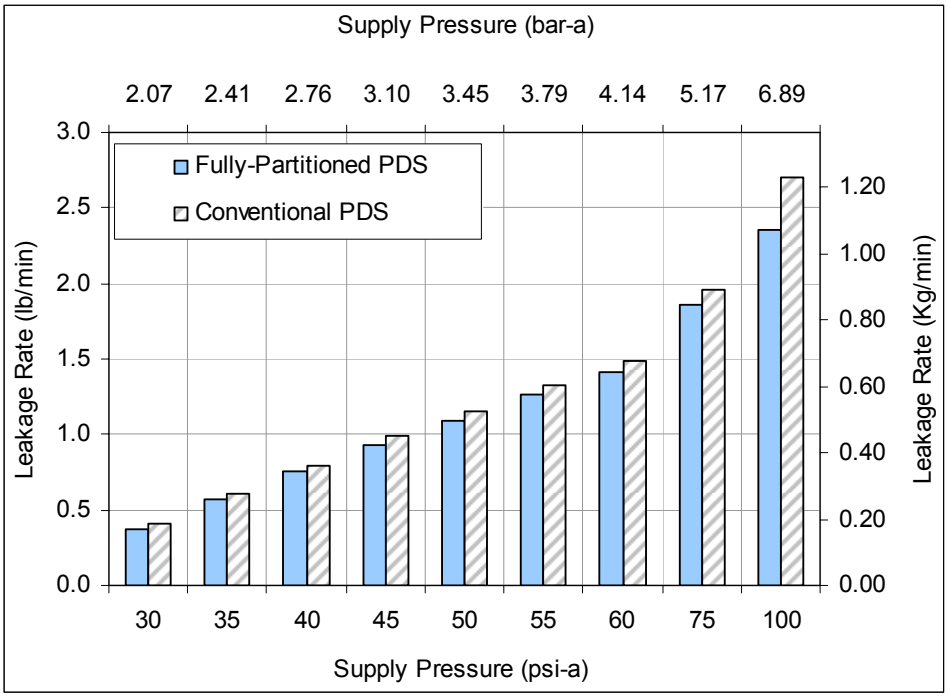

Figure 8.40 Leakage through conventional and FP 6-bladed PDS

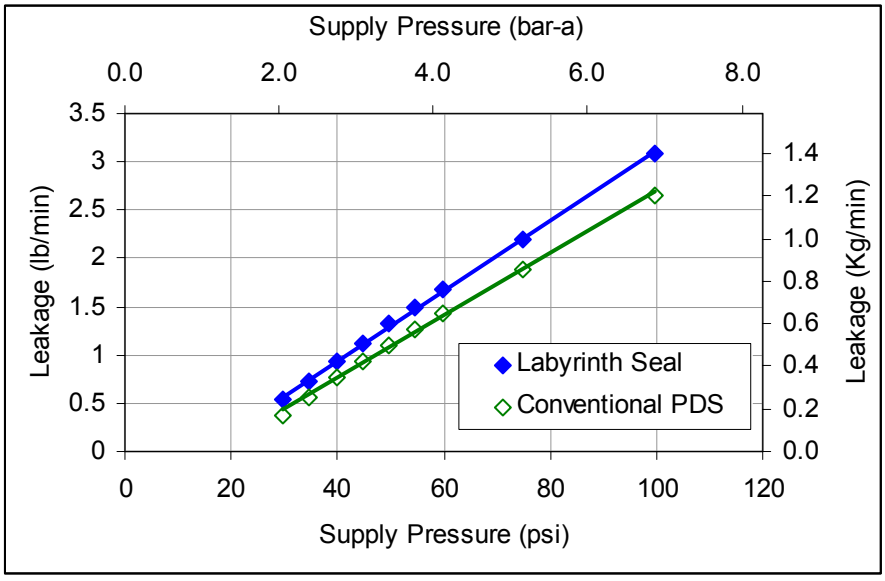

Figure 8.41 Leakage through 6-bladed labyrinth seal and FP-PDS (inter. pitch)

CAVITY PRESSURE RESULTS

Cavity pressures measurements were initially made to help clarify the effects of various design parameters (such as cavity depth) on seal leakage. However, the pressure drops across the seal blades were found to offer insight into the behavior of the flow through the seal. The cavity pressure data from the current round of tests has confirmed that this is the case as can be seen from Figure 8.42 for a six-bladed seal with long pitch and from Figure 8.43 for a six-bladed seal with intermediate pitch.

Plotting the first of these two figures with a log scale on the ordinate axis displays the trends at lower pressures more clearly (Figure 8.44). These figures also show that the drop in pressure across the first blade of the seal is large relative to pressure drops across the interior blades of the seal. The fraction of the overall pressure that is dropped across the first blade is highest at low supply pressures and decreases at higher pressures. Conversely, the amount by which the pressure dropped across the last blade is greater than that dropped across the interior blades increases with increasing supply pressure. A three-dimensional plot (Figure 8.45) of the pressures in each cavity for varying supply pressures provides a simple way to view the pressure distribution in the seal.

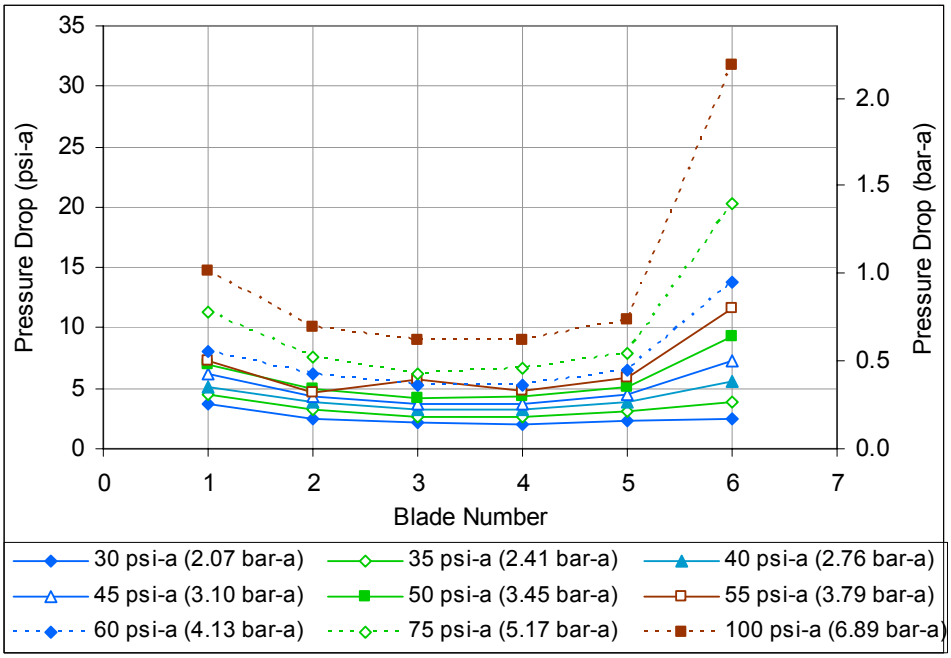

Figure 8.42 Blade ΔP for 6-bladed seal w/ flat blades, long pitch, deep cavities

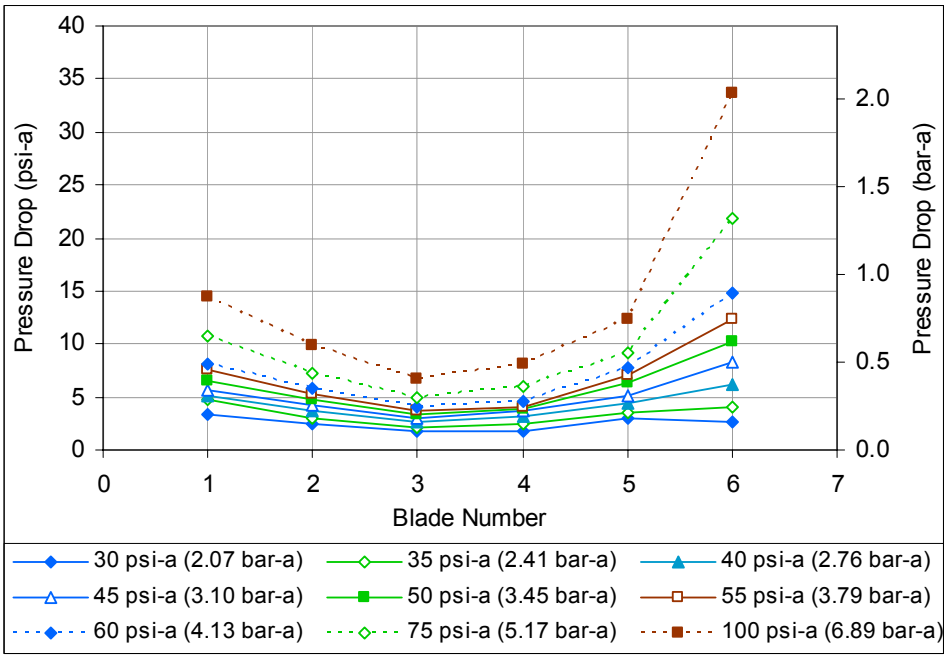

Figure 8.43 Blade ΔP for 6-bladed seal w/ flat blades, inter. pitch, deep cavities

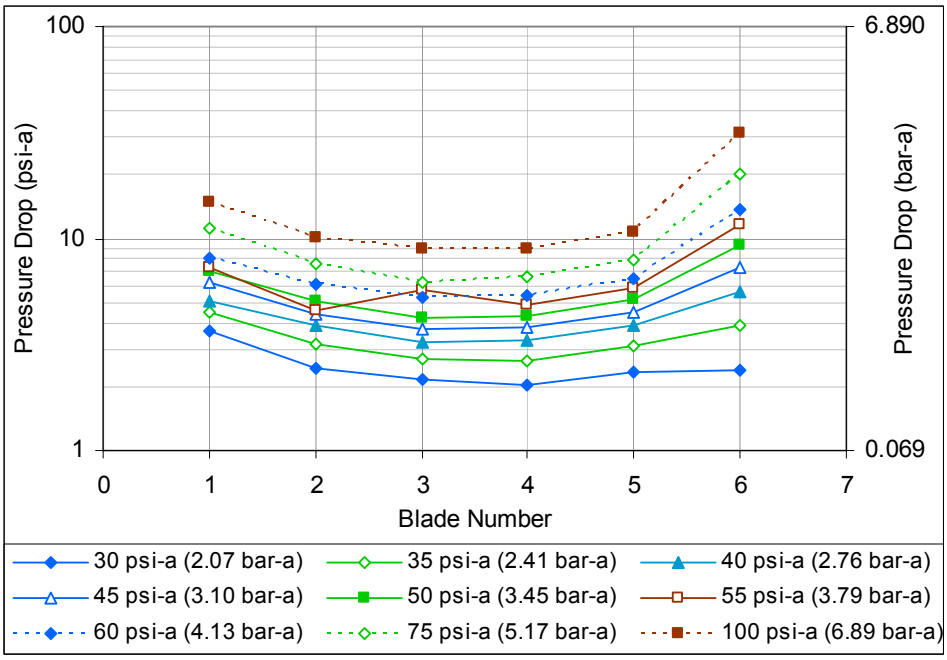

Figure 8.44 Blade ΔP for 6-bladed seal w/ flat blades, long pitch, deep cavities (log)

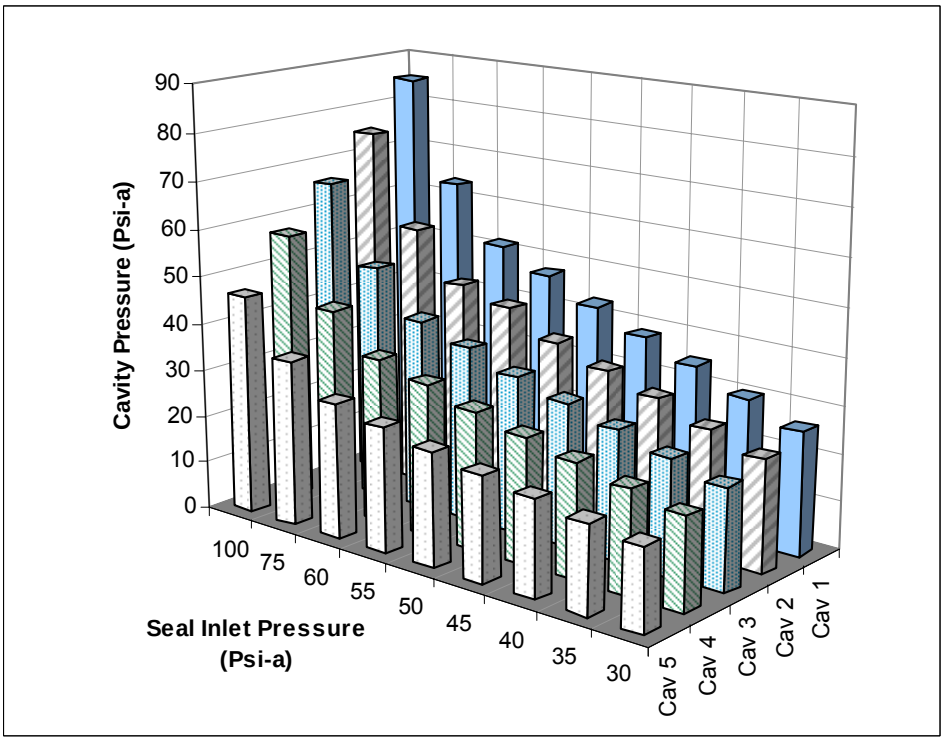

Figure 8.45 Pressure map for 6-bladed seal w/ flat blades, long pitch, deep cavities

Similar results were obtained from tests on conventional pocket damper seals. Figure 8.46 presents cavity pressure data in terms of the drop in pressure across each cavity, which is an important factor in determining the stiffness and damping of a conventional PDS cavity. The pressure drop is initially highest across the first cavity, but as the supply pressure is increased, the pressure distribution becomes parabolic and eventually, the highest pressure drop is across the last blade. For the seal shown in Figure 8.46, the flow through the last constriction is choked for the last two supply pressures shown. However, the parabolic trend and the increasing pressure drop across the last cavity are clear for subsonic conditions as well.

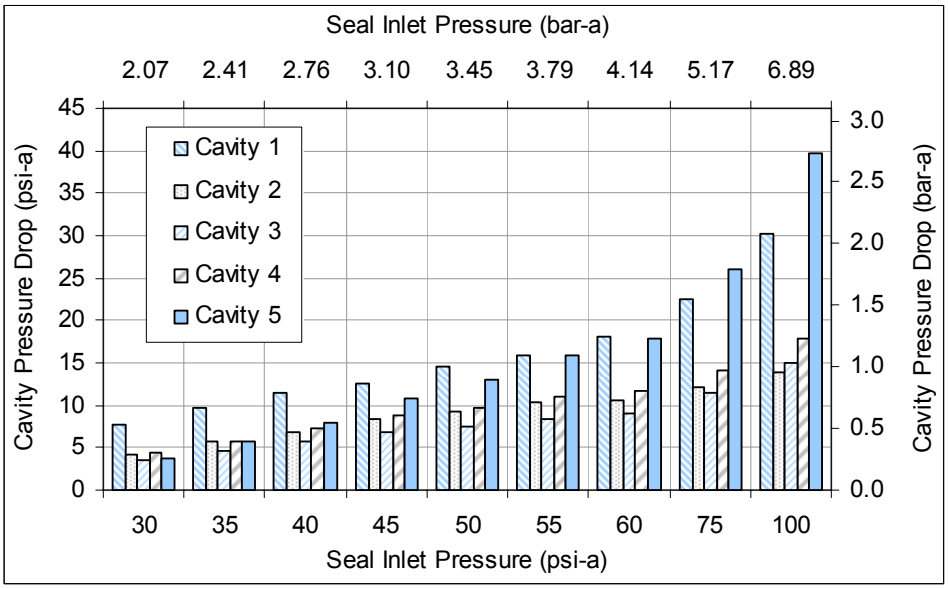

Figure 8.46 Pressure drop across six-bladed conventional PDS seal cavities

ELEVATED BACK-PRESSURE RESULTS

Five seals of the seal configurations discussed earlier were retested with non-atmospheric back pressure. This allowed the supply pressure to be raised without the reaching sonic flow conditions at the last seal constriction. It also allowed testing the seal at pressure ratios that are closer to those encountered in industrial applications

(approximately 0.5). The seals discussed in this section were first tested with a supply pressure of 125 psi (8.61 bar) and each seal was tested with three back pressures. One three-bladed seal, two four-bladed seals, and two five-bladed seals were used to examine blade spacing effects, blade thickness, and eccentricity effects. Figure 8.47 compares the leakage through a four-bladed seal and three-bladed seal. Figure 8.48 shows that for the elevated supply pressure, the reduction in thickness caused by increasing the blade pitch is almost constant for different pressure ratios. This supports the earlier conclusion that at higher pressure drops, the effect of blade thickness asymptotes to a constant value. This value, however, is higher than the value which the reduction in leakage for the seals tested earlier approached. At the elevated supply pressures, changes in measured leakage between seals in centered positions and in a fully-eccentric position were negligible near pressure ratios of 0.5. It should be noted that for the seals described in this section, a new set of blades was used.

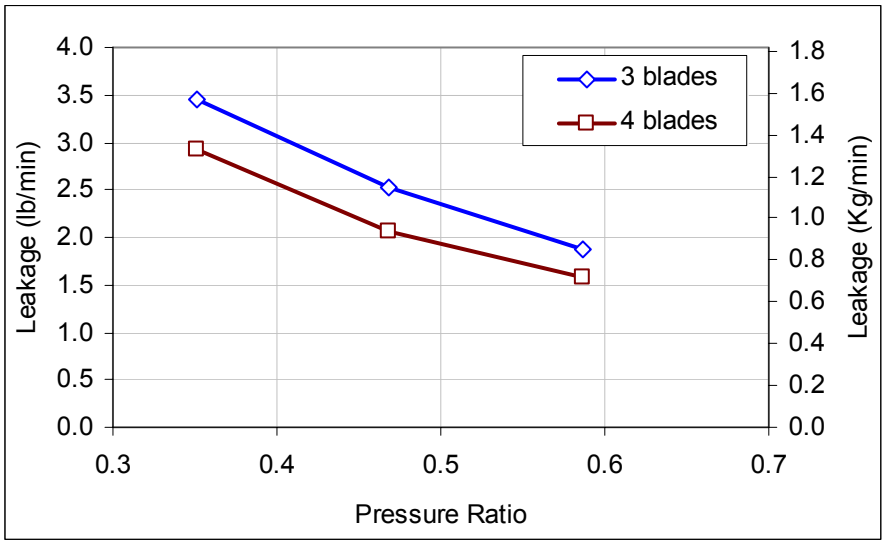

Figure 8.47 Leakage through 3- and 4-bladed seals with elevated back pressures

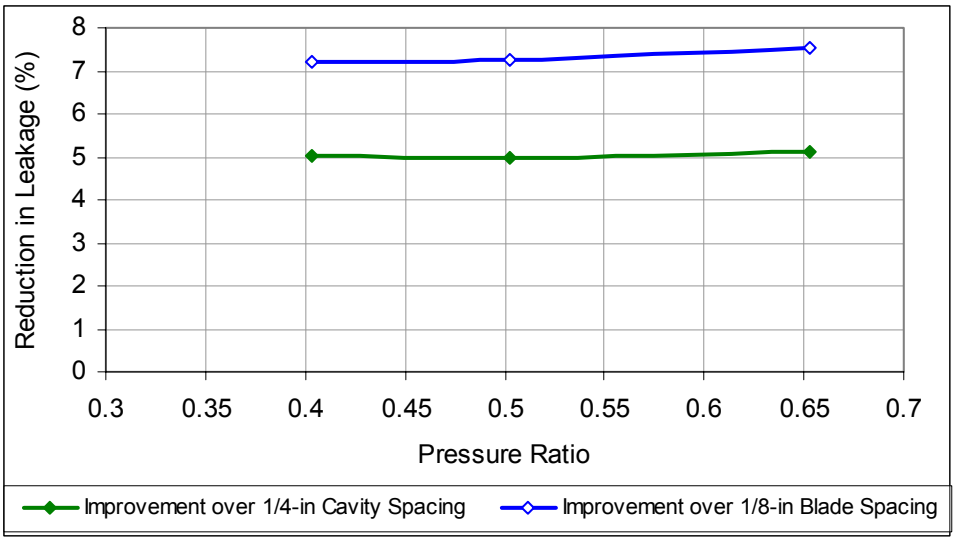

Figure 8.48 Increasing pitch to 0.5 in (12.7 mm), 4 blades, P_{in}=125 psi (8.61 bar)

The seals were also tested (after minor rig modifications) at supply pressures of 170 psi (11.7 bar) to provide further data at pressure ratios relevant to compressor applications. Figure 8.49 and Figure 8.50 show the leakage through four and six blades seals with long and short pitch. Figure 8.51 and Figure 8.52 show the pressure drops across each cavity of the same seals.

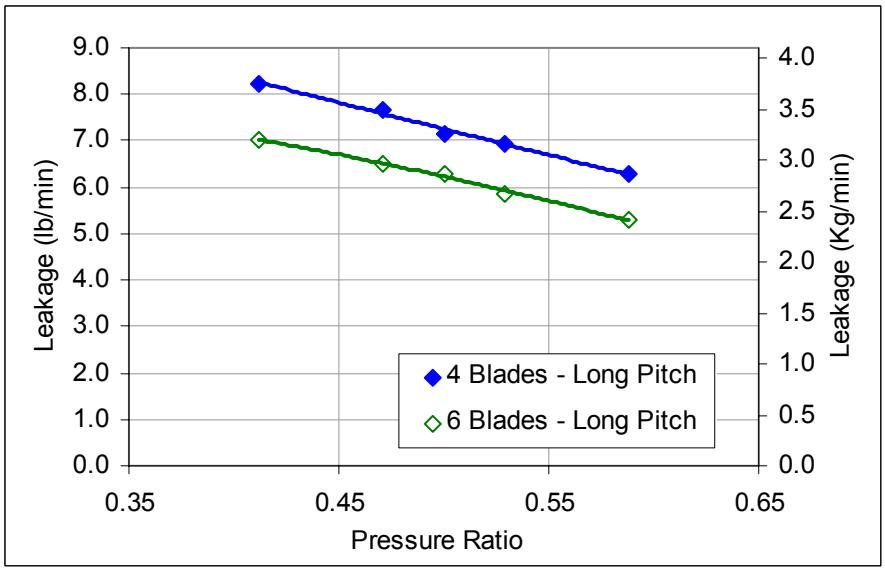

Figure 8.49 Leakage through seals with long pitch w/ 170 psi (11.7 bar) P_{in}

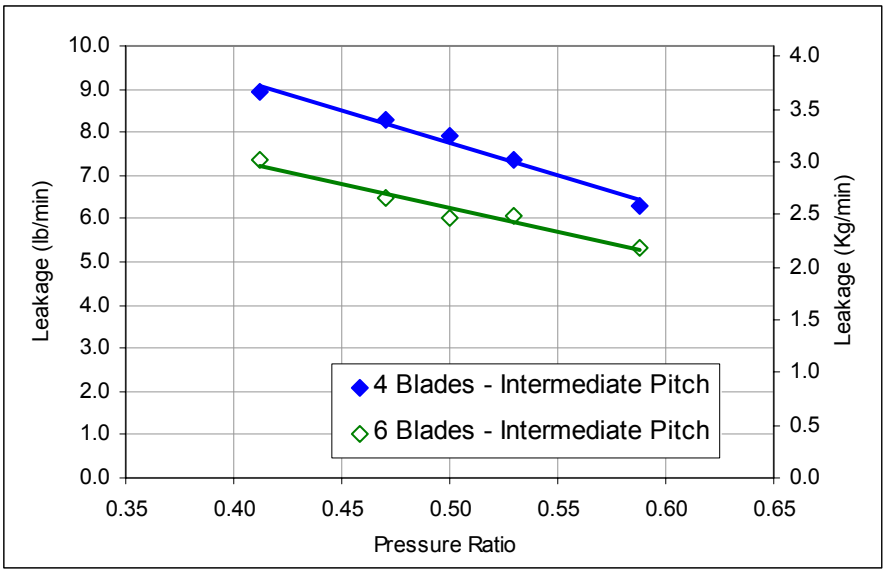

Figure 8.50 Leakage through seals with short pitch w/ 170 psi (11.7 bar) P_{in}

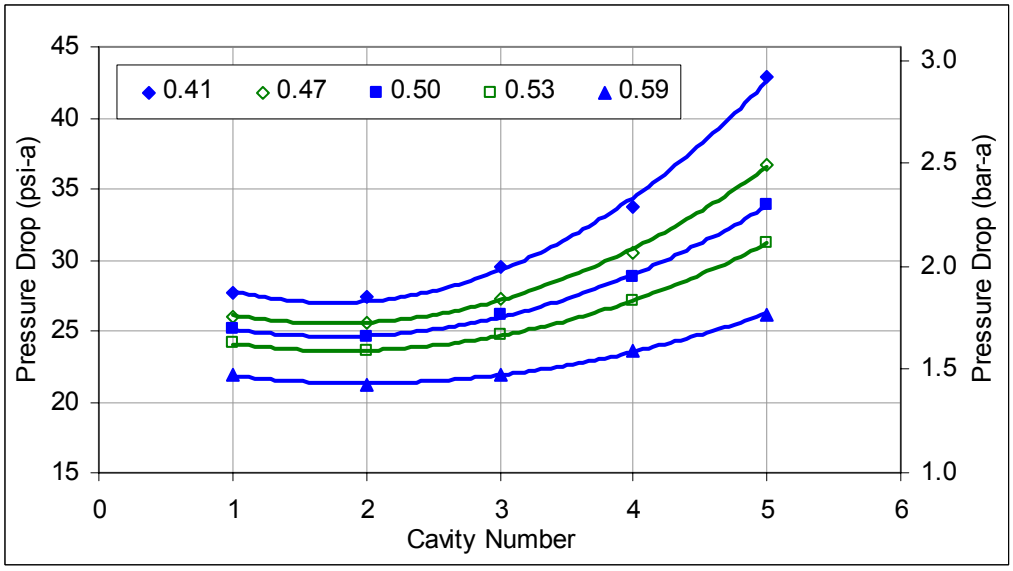

Figure 8.51 ΔP across 6-bladed seal cavities with 170 psi (11.7 bar) supply pressure

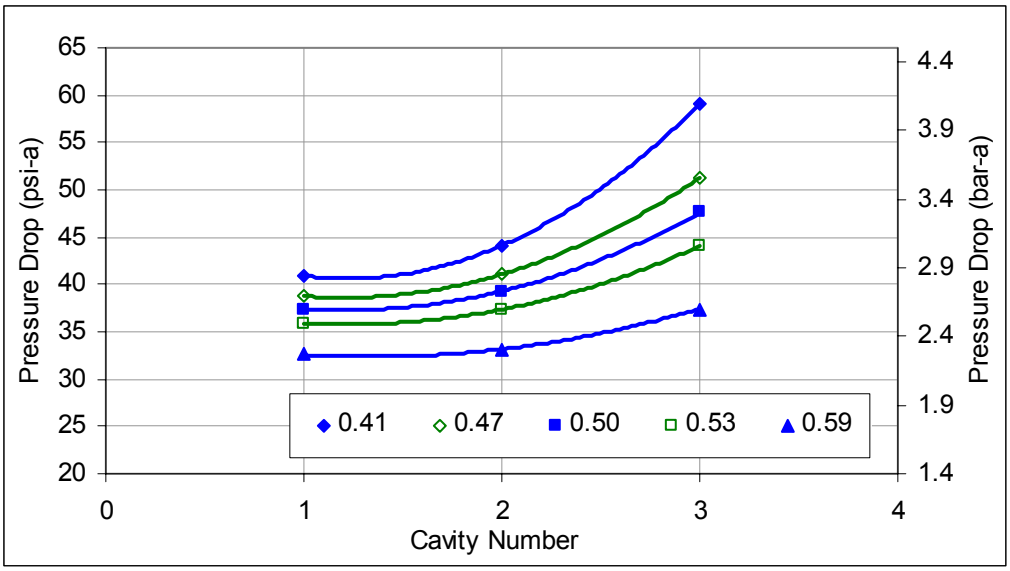

Figure 8.52 ΔP across 4-bladed seal cavities with 170 psi (11.7 bar) supply pressure

CHAPTER DISCUSSION

The results of the leakage and cavity pressure tests are most easily interpreted with respect to the effect of blade thickness and blade spacing. The effect of cavity depth is somewhat less clear and is also considerably less significant for the test conditions. The effect of blade profile is also significant, but the results of two sets of tests contradict each other. In the cases where the leakage data is somewhat ambiguous, as in the case of the cavity depth tests, the cavity pressure data was examined in an attempt to clarify the trends in question.

Interest in the effects of the geometric parameters under examination in this dissertation was partially initiated by the surprising results obtained by Gamal [40]. These results showed that a twelve-bladed pocket damper seal leaked considerably more than an eight-bladed pocket damper seal. The two seals had different blade profiles, cavity depths, and blade thicknesses, and blade pitches.

Discharge Coefficients

The current discussion of both labyrinth seals and pocket damper seals offers an opportunity to clarify a discrepancy in the terminology used in the literature pertaining to each of these two seal types. The term discharge coefficient as it has been used in the literature pertaining to pocket damper seals is not synonymous with that used in the literature pertaining to labyrinth seals. With regard to the latter, the discharge coefficient relates the leakage through a seal to the leakage through an analogous ideal labyrinth as described by Egli [43]. Such an ideal labyrinth is one in which the kinetic energy of the fluid jet passing through a constriction is completely depleted once it enters a downstream cavity.

With regard to pocket damper seals, however, the discharge coefficient is a factor that accounts for the difference between the calculated flow-rates and the experimentally measured leakage. The discharge coefficients described in the literature on pocket damper seals should more correctly be referred to as *empirical correction factors* that can be used to asses the degree to which a leakage model under-predicts or over-predicts the leakage through a seal.

Assembly Process

In order to ensure that the seal assembly process did not significantly impact the results, each seal configuration was assembled and tested several times (four times for most configurations and three times for some configurations). The data presented in this report are the averages of the multiple tests on each seal configuration. The standard deviation in the leakage and pressure measurements was plotted at each point and was found to be under 2% of the corresponding mean value for all data points in all test cases with the exception of some of the low pressure data points, which had standard deviations under 5%. In fact, the majority of data points had a standard deviation under 1%. As an example Table 8.9 lists the flow-rate data for a six-bladed seal with 1/8-in (3.175 mm) thick blades, 1/2-in (12.7 mm) long pitch, and 500 mil (12.7 mm) deep cavities.

Table 8.9 Sample test repeatability analysis

Supply Pressure		Average Leakage		Standard Deviation		
(psi-a)	(bar-a)	(lb/s)	(kg/s)	(lb/s)	(kg/s)	Percentage
30	2.07	0.467	0.212	0.003	0.001	0.68%
35	2.41	0.670	0.305	0.011	0.005	1.68%
40	2.76	0.868	0.395	0.007	0.003	0.83%
45	3.10	1.036	0.471	0.008	0.004	0.79%
50	3.45	1.221	0.555	0.017	0.008	1.41%
55	3.79	1.413	0.642	0.016	0.007	1.14%
60	4.13	1.571	0.714	0.01	0.005	0.63%
75	5.17	2.070	0.941	0.014	0.006	0.69%
100	6.89	2.929	1.331	0.026	0.012	0.89%

Another factor taken into account during the assemble process was the clearance of each individual blade. Blade diameter readings are listed in Table 8.10 for each blade of seal set B. While all blades were manufactured within the 0.5 mil (12.7 μm) tolerance, failing to assemble the blades in the same order for each test or using a blade with a tighter clearance while testing a six-bladed seal and removing that blade to test a seal with fewer blades could have affected the results. As a result, each of these seal blades were measured, numbered, and assigned to seal assemblies so that the addition of a blade did not tighten the tip clearances.

Table 8.10 Seal set B blade measurements

Blade	Inner Diameter	
	mils over 4 in	μm over 101.6 mm
1	7.60	193.04
2	7.90	200.66
3	8.23	209.13
4	7.53	191.35
5	7.90	200.66
6	8.23	209.13
7	7.97	202.35
8	7.93	201.51
Average	7.91	200.98

Blade Thickness Effects

Increasing the blade thickness resulted in a 10%-20% drop in leakage for all the configurations tested at all supply pressures. This was possibly the result of increased frictional losses in the longer constrictions of the thick-bladed seals. The blades initially had a thickness of 1/8 in (3.175 mm) and were thicker than the 0.070 in (1.778 mm) thick blades of the seals of Set A. Another possible explanation is provided by Bell and Bergelin [48], who state that there is a partial recovery of pressure after the fluid passes through a thin annular constriction and enters the subsequent cavity, but also state that this phenomenon is lessened when the orifice thickness is increased. A comparison with the leakage prediction code based on the modified St. Venant Equation described earlier showed that the newer seals leaked considerably less than predicted whereas the leakage through the older seals was predicted considerably more closely. While discharge coefficients are needed for this equation to accurately predict the leakage through a seal, the amount by which the code over-predicted the leakage (using discharge coefficients of 1) indicated that an additional factor was responsible for keeping the leakage levels low. It was assumed that this factor was the increased blade thickness and this hypothesis was supported by the results, which indicate a strong dependency on blade thickness.

As is discussed below, beveling the blades of the test seals increased their leakage rates. This contradicted the results of the tests on the older labyrinth seals and is another indication that the newer seals had a heightened sensitivity to blade thickness. It was further theorized that it was the tighter clearances of the newer seals that were responsible for this sensitivity.

Blade Profile Effects

The findings summarized by Fasheh [67], which state that a beveled blade profile would lead to lower leakage rates than a flat blade profile, were supported by the results obtained from the tests on the seals of *seal set A*. The tests conducted by Gamal [40] and

Ertas [41] n pocket damper seals show the opposite results, indicating that the mass flow-rate through a seal increases when the seal blades are beveled.

It was initially assumed that the main difference that could explain these conflicting results was the type of seal used. The seemingly contradictory results were attributed to differences in the flow regime through the two different seal types, but differences in the geometries of the pocket damper seals and the labyrinth seals were also considered as possible causes. The partition walls of the pocket damper seals tested by both Gamal and Ertas considerably reduced the flow of air in the circumferential direction and the effect of this on the overall leakage through the seal is not completely understood.

The seal inlet pressures for the pocket damper seal tests were one order of magnitude higher than the current sets of tests, indicating that the effect of blade profile may also be pressure dependent. The cavity depths, clearance ratio, number of blades, and pitch length of Gamal's seals were different, giving rise to several possible causes for the leakage results other than the blade profile. However, all of these factors were kept constant in the tests conducted by Ertas, leaving the effects of the partition walls and the higher pressures as the possible causes for the disagreement with the results.

It was thought that the effect of beveling the blades of a pocket damper seal might be different from the effect of beveling the blades of a labyrinth seal. This is clearly not the case however, since the labyrinth seal test results from seal set B presented here show that beveling the blades increased the leakage as was the case with the pocket damper seal tests.

A possible explanation for the contradictions described above is provided by simultaneous examination of the effects of blade thickness and blade profile. When the seals tested by Ertas [41] were beveled, only a short land pitch was left, reducing the blade tip thickness by 77%. The blade-tip thicknesses of seals of seal set A and seal set B were reduced by 40% and 60% respectively when their tips were beveled. These tip thickness changes are summarized in Table 8.11. The seal tests that indicated a detrimental effect of beveling the blades are also the tests in which more than half the blade-tip land pitch was removed in the beveling process.

Table 8.11 Blade-tip geometries before and after beveling

Seal	Initial Tip Thickness		Final Tip Thickness		Precent Reduction
	(in)	(mm)	(in)	(mm)	
Pocket Damper Seal	0.13	3.302	0.03	0.762	77%
Labyrinth Seal Set A	0.075	1.905	0.045	1.143	40%
Labyrinth Seal Set B	0.125	3.175	0.05	1.27	60%

These results can be explained if it assumed that both increasing blade thickness and beveling the blades can reduce the leakage. However, these trends work against one another to some extent in that beveling the blades will remove some of the blade-tip land area and therefore reduce the thickness. If the seal is more sensitive to thickness effects, as is the case with the current test seals, beveling the blades will increase the leakage. On the other hand if the seal is less sensitive to changes in blade thickness, beveling the blades will reduce the leakage as was the case with the seals of seal set A. These results are not intended to imply that a reduction in blade tip clearance through chamfering more than 50% of the tip thickness will increase the leakage and that a reduction of less than 50% will decrease the leakage. The results simply illustrate there are two factors with opposite effects on leakage that come into play when the blades are beveled.

The sensitivity of the leakage rates through a seal to the thickness of the blades seems to be linked to the seal clearances. The radial clearances for the pocket damper seals tested by Ertas were 5 mils (127 μm) and 7.5 mils (191 μm) for the inlet and exit of each blade pair respectively. For the current group of test seals, the radial clearances were 6 mils (152 μm) for set A and 4 mils (102 μm) for set B.

Blade Spacing Effects

In order to examine the effect of blade profile and blade thickness for as many seal designs as possible, seals of different pitch lengths were tested. As was expected, the

spacing of the blades was found to have a significant effect on the leakage through the seal. The results showed that the effect of cavity pitch was almost as significant as that of blade thickness and was considerably more significant than either the effect of cavity depth or blade profile. Similar results were obtained by Egli [15] in 1935 on seals with considerably larger clearances. In 1939, Hodkinson [16] explained this phenomenon and accounted for it by using a kinetic energy carry-over coefficient. While the current results are not surprising in light of these earlier references, it is worth noting that the carry-over effect remains significant even with the considerably tighter clearances of the current round of tests.

Of all the design factors examined, blade pitch was found to have an effect on seal leakage second only to that of blade thickness. Test results showed that the effect of cavity pitch was almost as significant (8% to 16% drop in leakage for one seal) as that of blade thickness and was considerably more consistently significant than either the effect of cavity depth or blade profile. Similar blade spacing results were obtained by Egli [43] on seals with considerably larger clearances. Hodkinson [47] explained this phenomenon and accounted for it by using a kinetic energy carry-over coefficient. While the current results are not surprising in light of these earlier references, it is worth noting that the carry-over effect remains significant even with the considerably tighter clearances of the current set of tests. Furthermore, the demonstration that a four-bladed seal with short blade pitch leaked almost exactly as much as a three-bladed seal with a longer pitch indicated that space limitations should not be the only concern when determining the number of blades in a given seal design.

The drop in leakage resulting from an increase in the pitch lengths of the pocket damper seals was less significant than that observed for the constant pitch labyrinth seal. This was primarily because fewer PDS cavities were affected by the changes in pitch. In the six PDS configurations tested, only the two inactive (or secondary) cavity lengths were changed; a change in the lengths of all the cavities would have had a more significant effect.

Cavity Depth Effects

The initial tests conducted to determine the effect of cavity depth showed that this design parameter had close to no impact on the leakage through the seal. A trend was observed that indicating that the leakage through the seal could be reduced slightly by making the cavities deeper, but the effect was close to inconsequential at the test supply pressures. Installing the cavity insert corresponded to an 80% reduction in cavity depth, but only led to increases in leakage rates of less than 1% for most supply pressures and less than 5% for the highest changes at the lowest supply pressures.

The second round of tests showed that cavity depth does have an effect on leakage, but that this effect is only apparent when the cavities are made very shallow. Reducing the cavity depth by 90% to 50 mils (1.27 mm) reduced leakage in both four-bladed and five-bladed seals. Reducing the cavity depth by 96% to 20 mils (0.508 mm) caused a drop in leakage for the four-bladed seal, but a small increase in leakage for the five-bladed seal. While this increase was close to negligible, it may indicate that a 20 mil (0.508 mm) cavity depth was shallower than a certain optimum value for the five-bladed seal in terms of leakage.

Supporting the idea of an optimum cavity depth are experimental results showing that smooth, or plain, seal seals generally leak more than labyrinth seals Figure 8.53 (taken from Childs [10], who also defined the plotted flow coefficient as described in the *Annular Gas Seal Comparisons* chapter of this dissertation). If the cavity depth is to be reduced until the cavity is completely filled, the seal would effectively become a smooth. This seems to indicate that there is a range of values of cavity depth (from zero to a small value) where the cavity depth would have a significant effect on the leakage, but that beyond that value the effect begins to attenuate. Furthermore, there is an optimum value of cavity depth that beyond which (increasing or decreasing) there will be a slight reduction in leakage.

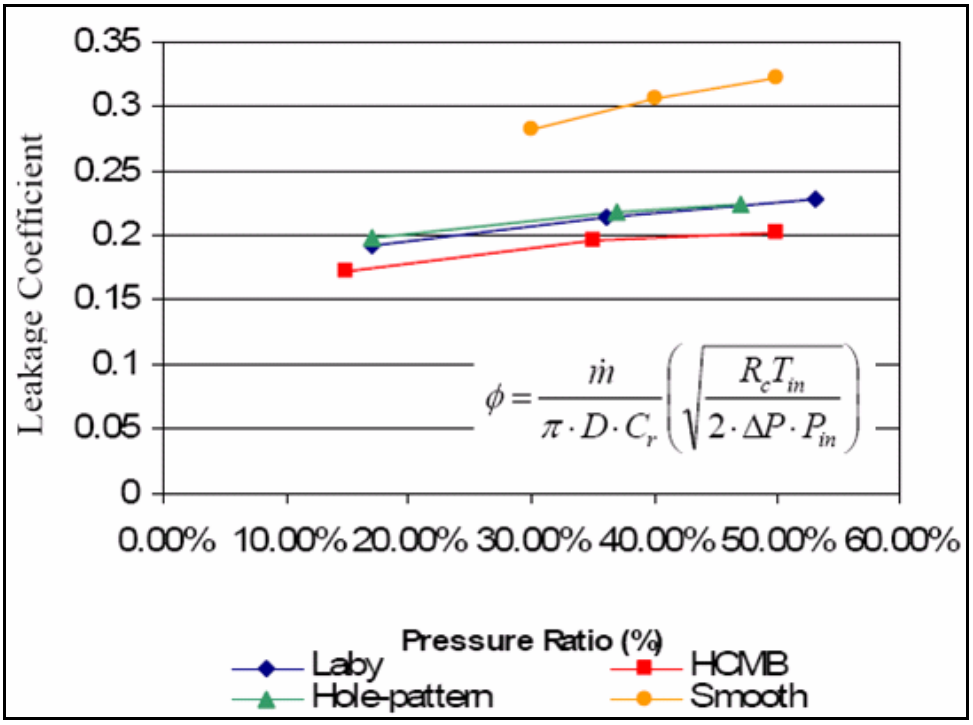

Figure 8.53 Comparison of leakage through smooth seals and labyrinth seals

Cavity Pressures

While not directly linked to the design parameters currently being investigated, the pressure drops across the seal blades were found to offer insight into the behavior of the flow through the seal. The St. Venant leakage model, as implemented in the pocket damper seal code (both conventional and fully-partitioned), has consistently predicted that the largest drop in pressure will occur across the last blade of the seal.

An explanation for the increased drop in pressure across the first blade lies in the fact that the effective clearance is smaller for the first blade than for the interior blades. The flow entering the first constriction of the seal approaches from a larger inlet flow area than the flow entering the remaining constrictions. The resulting smaller *vena contracta* acts like a tighter clearance as can be seen in Figure 8.54.

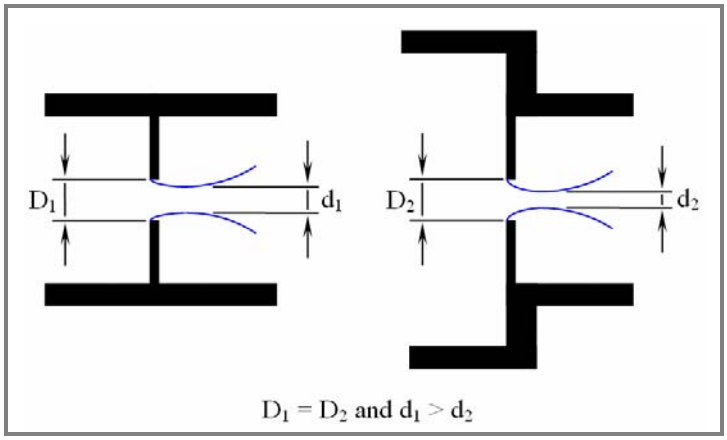

Figure 8.54 Reduced effective clearance for first seal blade

CHAPTER IX

EVALUATION OF LEAKAGE MODELS

Models for predicting the leakage through see-through labyrinth seals were presented in the *Leakage Model Descriptions* chapter of this dissertation. The experimental leakage data presented earlier, along with the leakage data obtained by Picardo [55] on labyrinth seals and by Gamal [40] and Ertas [41] on pocket damper seals are used in this chapter to evaluate these leakage models. Each equation was evaluated based on the accuracy with which it can predict:

- The rates of flow through the seals
- The distribution (or trend) of the static cavity pressures along the seals
- The effects of varying seal design parameters.

Modifications that were found to improve the prediction performance of some of the equations are also suggested. These new equations, which are either modified forms of the original equations or combinations of different aspects of the leakage models are referred to below as *Modified Leakage Equations*. A total of thirteen equations; eight found in the literature and five modified equations; are evaluated below.

In order to facilitate the evaluation, a comparison code was written to compare the leakage and pressure test data to the predictions of all the equations simultaneously. The leakage models were evaluated using the results of six high-pressure labyrinth seal cases, sixteen low-pressure labyrinth seal cases, and eight high-pressure pocket damper seal cases.

MODIFIED LEAKAGE MODELS

The suggested models are based on either combinations or modifications of the existing leakage equations described earlier. The first of these models uses the St. Venant Equation as a base model, but takes into account kinetic energy carryover by using a modified form of Hodkinson's kinetic energy coefficient. Rather than a binary

model for this coefficient (1 for the first blade and some other value for all the other blades), this model uses a progressively decreasing carryover coefficient in an attempt to simulate the increase in pressure drop across first few blades (this is explained in the *Chapter Discussion* section at the end of this chapter). This was an attempt to alter the pressure distribution and to make it more parabolic (and therefore to make it more closely match test data). This model is referred to in this dissertation as MOD 1.

$$\dot{m}_i = \mu_i \cdot \frac{P_i \cdot A_i}{\sqrt{\gamma \cdot R \cdot T_i}} \cdot \sqrt{\frac{2 \cdot \gamma^2}{\gamma - 1} \cdot \left[\left(\frac{P_{i+1}}{P_i} \right)^{2/\gamma} - \left(\frac{P_{i+1}}{P_i} \right)^{\gamma+1/\gamma} \right]} \qquad \textbf{(9.1)}$$

$$\mu_i = \sqrt{\frac{1}{1 - \left(\frac{i-1}{i} \right) \cdot \left(\frac{Cr_i / L_i}{(Cr_i / L_i) + 0.02} \right)}} \quad \text{where} \quad i = 1 \ldots n \qquad \textbf{(9.2)}$$

The second model also uses the St. Venant Equation as a base model, but accounts for kinetic energy carryover using Vermes' coefficient. The difference between this model and Vermes' Model (which used Martin's Equation) is that it uses an iterative, rather than a single-application, base equation, thereby simplifying programming and allowing direct calculation of intermediate pressure data. This model is referred to in this dissertation as MOD 2.

$$\dot{m}_i = \mu_i \cdot \frac{P_i \cdot A_i}{\sqrt{\gamma \cdot R \cdot T_i}} \cdot \sqrt{\frac{2 \cdot \gamma^2}{\gamma - 1} \cdot \left[\left(\frac{P_{i+1}}{P_i} \right)^{2/\gamma} - \left(\frac{P_{i+1}}{P_i} \right)^{\gamma+1/\gamma} \right]} \qquad \textbf{(9.3)}$$

$$\mu_i = \sqrt{\frac{1}{(1 - \alpha_i)}} \qquad \text{where} \qquad \alpha_i = \frac{8.52}{\frac{s_i - t_i}{Cr_i} + 7.23} \qquad \textbf{(9.4)}$$

Taking the preceding model one step further and combining the St. Venant Equation and Vermes' carryover coefficient with Chaplygin's flow coefficient produces an iterative model that takes into account all three model elements (base equation, carryover factor, and flow contraction factor). This change makes the model as complete as the model developed by Neumann or the model adapted by Scharrer. This model is referred to in this dissertation as MOD 3.

$$\dot{m}_i = \mu_i \cdot Cf_i \cdot \frac{P_i \cdot A_i}{\sqrt{\gamma \cdot R \cdot T_i}} \cdot \sqrt{\frac{2 \cdot \gamma^2}{\gamma - 1} \cdot \left[\left(\frac{P_{i+1}}{P_i} \right)^{2/\gamma} - \left(\frac{P_{i+1}}{P_i} \right)^{\gamma+1/\gamma} \right]} \qquad \textbf{(9.5)}$$

$$\mu_i = \sqrt{\frac{1}{(1-\alpha_i)}} \qquad \text{where} \qquad \alpha_i = \frac{8.52}{\frac{s_i - t_i}{Cr_i} + 7.23} \qquad \textbf{(9.6)}$$

$$Cf_i = \frac{\pi}{\pi + 2 - 5\beta_i + 2\beta_i^2} \qquad \text{where} \qquad \beta_i = \left(\frac{P_i}{P_{i+1}} \right)^{\gamma-1/\gamma} - 1 \qquad \textbf{(9.7)}$$

The fourth *Modified Leakage Model* eliminates Chaplygin's flow coefficient from Scharrer's model, leaving Vermes' carryover coefficient combined with Neumann's leakage equation. Comparing this and the previous model to the models found in the literature provides a way of examining the effectiveness of Chaplygin's coefficient (by omission in the case of this model and by inclusion in the case of the preceding model). This model is referred to in this dissertation as MOD 4.

$$\dot{m}_i = \mu_i \cdot A_i \cdot \sqrt{\frac{P_i^2 - P_{i+1}^2}{R \cdot T}} \qquad \textbf{(9.8)}$$

$$\mu_i = \sqrt{\frac{1}{(1-\alpha_i)}} \qquad \text{where} \qquad \alpha_i = \frac{8.52}{\frac{s_i - t_i}{Cr_i} + 7.23} \qquad \textbf{(9.9)}$$

Adding Chaplygin's flow coefficient to MOD 1, results in a model that is iterative, accounts for kinetic energy carryover (using Vermes' formula), accounts for flow contraction, and compensates for a parabolic pressure distribution. This model is referred to in this dissertation as MOD 5. The main elements of the five *Modified Leakage Models* are summarized in Table 9.1.

$$\dot{m}_i = \mu_i \cdot Cf_i \cdot \frac{P_i \cdot A_i}{\sqrt{\gamma \cdot R \cdot T_i}} \cdot \sqrt{\frac{2 \cdot \gamma^2}{\gamma - 1} \cdot \left[\left(\frac{P_{i+1}}{P_i} \right)^{2/\gamma} - \left(\frac{P_{i+1}}{P_i} \right)^{\gamma+1/\gamma} \right]} \tag{9.10}$$

$$\mu_i = \sqrt{\frac{1}{1 - \left(\frac{i-1}{i} \right) \cdot \left(\frac{Cr_i / L_i}{(Cr_i / L_i) + 0.02} \right)}} \quad \text{where} \quad i = 1 \ldots n \tag{9.11}$$

$$Cf_i = \frac{\pi}{\pi + 2 - 5\beta_i + 2\beta_i^2} \quad \text{where} \quad \beta_i = \left(\frac{P_i}{P_{i+1}} \right)^{\gamma-1/\gamma} - 1 \tag{9.12}$$

Table 9.1 Summary of suggested modified leakage models

Model	Fundemental Equation	K.E. Coefficient	Flow Coefficient
MOD 1	St. Venant	Modified Hodkinson	None
MOD 2	St. Venant	Vermes	None
MOD 3	St. Venant	Vermes	Chaplygin
MOD 4	Neumann	Vermes	None
MOD 5	St. Venant	Modified Hodkinson	Chaplygin

HIGH-PRESSURE LABYRINTH SEALS

Relevant geometric data and test conditions for Picardo's [55] labyrinth seals are listed in Table 9.2.

Table 9.3 summarizes the prediction errors (positive for over-prediction and negative for under-prediction) resulting from the use of each equation while the actual leakage predictions are shown in Figure 9.1 through Figure 9.6 (seal names refer to those used in Table 9.2). The highlighted cells in

Table 9.3 correspond to the four most accurate predictions (lowest errors) for each seal.

Table 9.2 Geometry and test conditions for Picardo's seals

Seal	Exit Pressure		Pressure Ratio	Radial Clearance		Flow-Rate	
-	(bar)	(psi)	-	(mm)	(mils)	(Kg/s)	(lb/s)
A1	11.2	163	0.16	0.2	7.87	0.450	0.990
A2	25.2	366	0.36	0.2	7.87	0.430	0.946
A3	36.4	528	0.52	0.2	7.87	0.405	0.891
B1	7.0	102	0.10	0.1	3.94	0.235	0.517
B2	21.7	315	0.31	0.1	3.94	0.230	0.506
B3	35.7	518	0.51	0.1	3.94	0.205	0.451

Inlet Pressure 70 bar (1016 psi) for all seals

The leakage model developed by Vermes and *Modified Leakage Models* 2 and 4 developed in this chapter predict the leakage through both of Picardo's seals (two different clearances) with reasonable accuracy. The model developed by Esser and Kazakia and MOD 1 each perform well for only one clearance. The three models that perform the best are all based on Vermes' kinetic energy carry-over coefficient. MOD 3, which also uses this coefficient, but also uses Chaplygin's flow coefficient, produces prediction errors of no less that 35% (under-prediction) for all six test cases.

Table 9.3 Prediction error summary for Picardo's seals

	Picardo's Labyrinth Seals					
Leakage Model	A1	A2	A3	B1	B2	B3
St. Venant	-15.7%	-15.3%	-25.5%	-19.3%	-19.5%	-17.6%
Martin	-16.8%	-16.2%	-26.0%	-20.5%	-20.4%	-18.2%
Hodkinson	44.1%	45.3%	28.2%	14.0%	14.2%	17.3%
Vermes	**-0.6%**	**0.2%**	**-11.6%**	**-12.7%**	**-12.5%**	**-10.1%**
Neumann	-11.8%	-13.7%	-24.9%	-29.5%	-32.2%	-31.7%
Zimmerman & Wolf	41.8%	42.3%	25.0%	13.7%	13.7%	16.3%
Esser & Kazakia	**0.7%**	**-0.4%**	**-12.8%**	-20.0%	-21.9%	-20.7%
Scharrer	-35.6%	-37.0%	-45.2%	-42.1%	-44.4%	-43.9%
Mod. 1	30.0%	30.1%	14.4%	**8.6%**	**8.0%**	**10.4%**
Mod. 2	**0.6%**	**1.1%**	**-11.1%**	**-11.3%**	**-11.5%**	**-9.5%**
Mod. 3	-36.7%	-37.4%	-45.2%	-43.7%	-45.0%	-44.2%
Mod. 4	**2.7%**	**1.6%**	**-11.1%**	**-8.3%**	**-10.5%**	**-9.1%**
Mod. 5	-19.2%	-19.4%	-29.5%	-29.4%	-32.9%	-31.9%

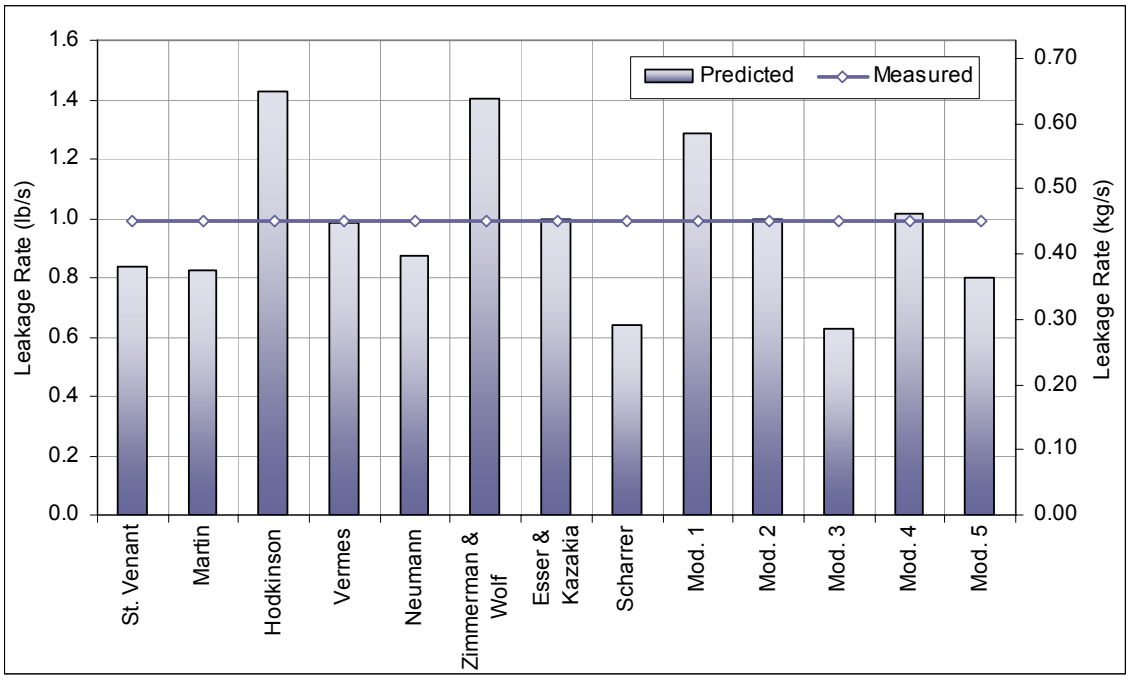

Figure 9.1 Leakage predictions for Picardo's seal A1

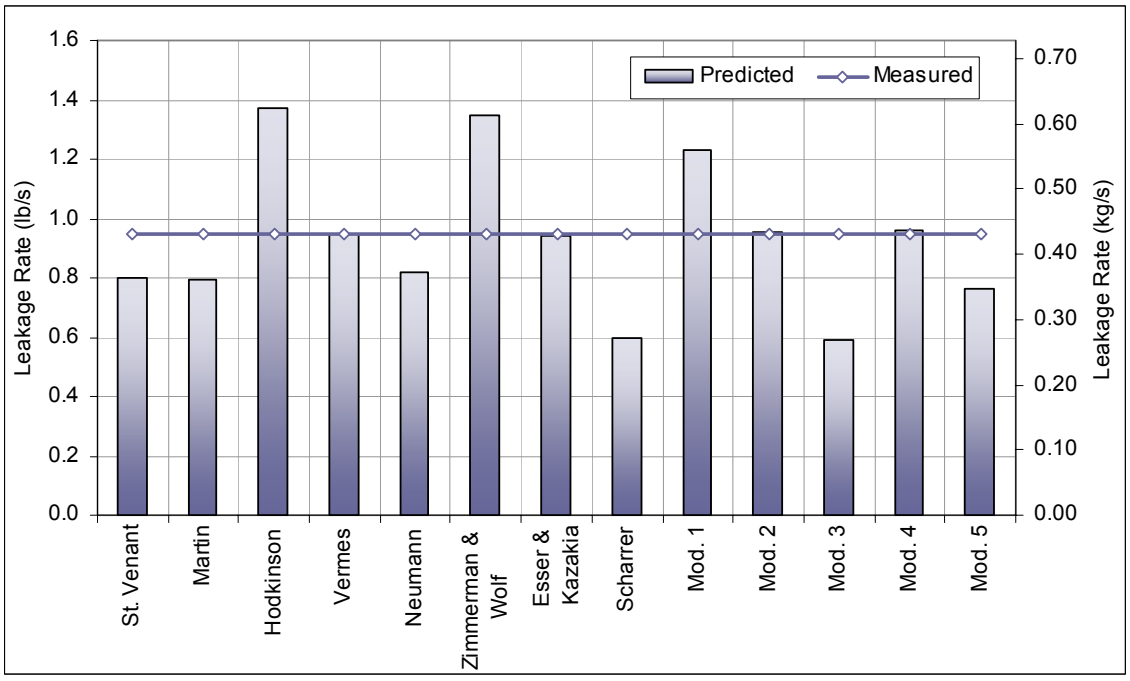

Figure 9.2 Leakage predictions for Picardo's seal A2

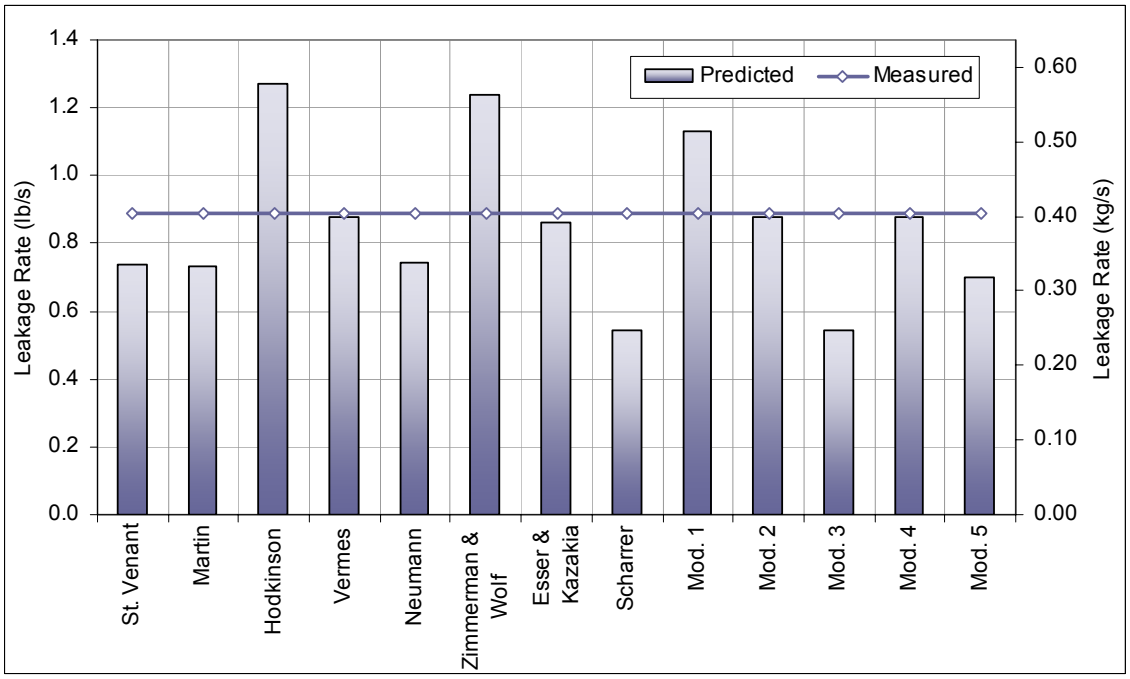

Figure 9.3 Leakage predictions for Picardo's seal A3

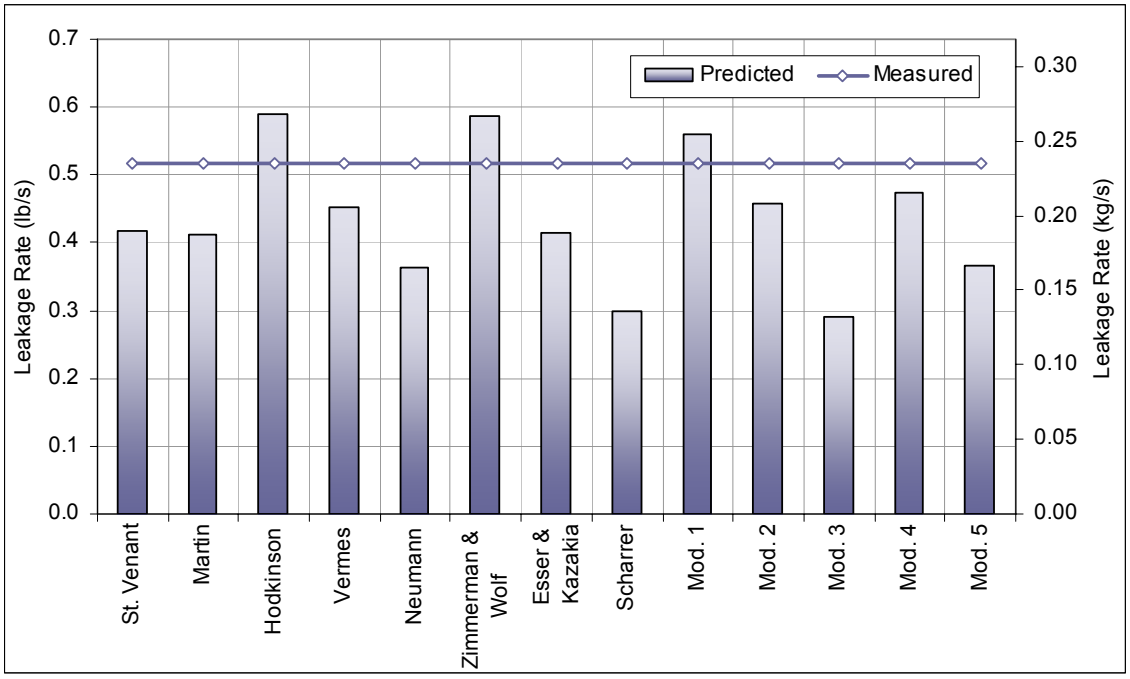

Figure 9.4 Leakage predictions for Picardo's seal B1

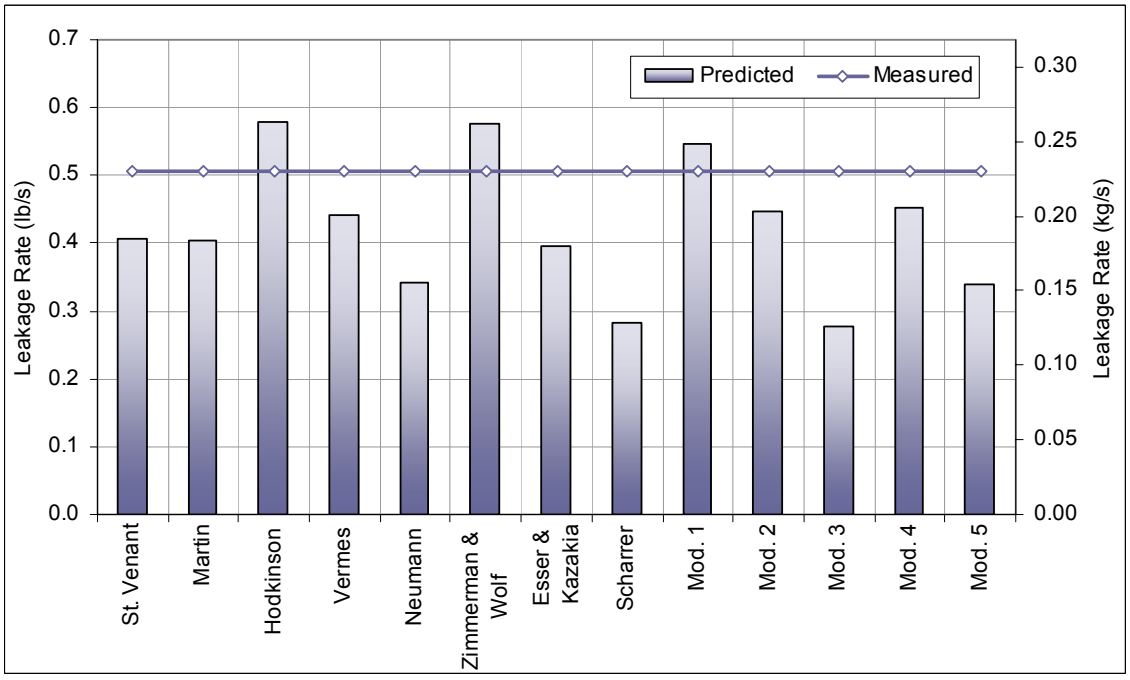

Figure 9.5 Leakage predictions for Picardo's seal B2

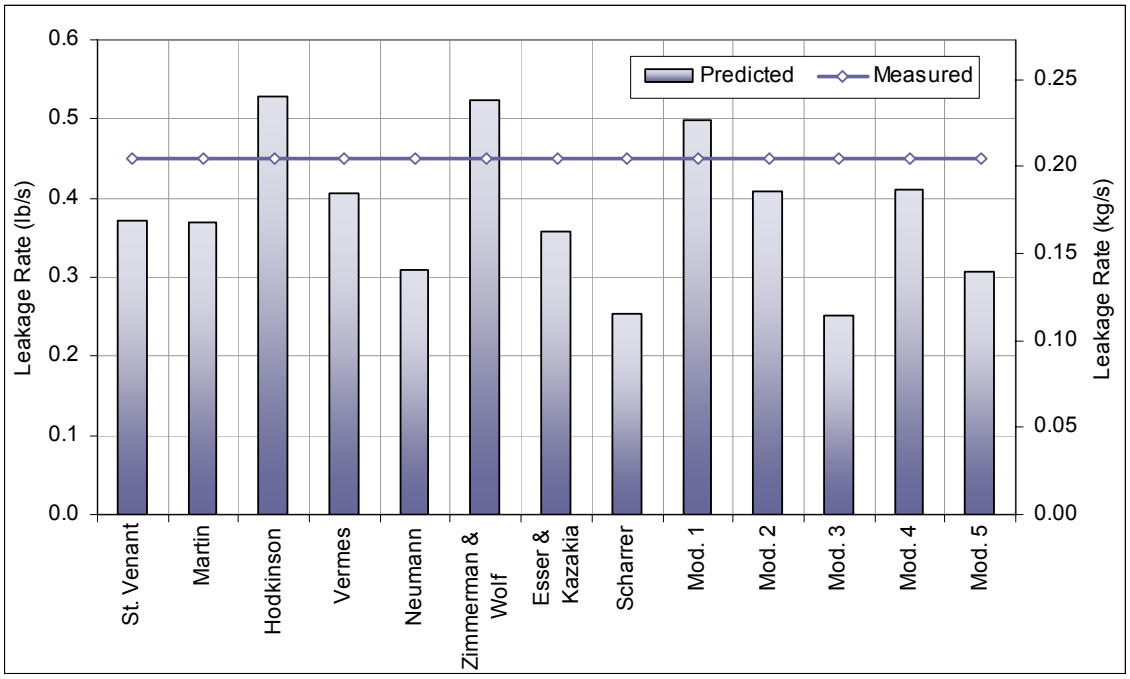

Figure 9.6 Leakage predictions for Picardo's seal B3

LOW-PRESSURE LABYRINTH SEALS

Since the low-pressure labyrinth seals were tested at a number of supply pressures, several runs of the model comparison code were required for each seal. As a demonstrative example, the leakage predictions and the measured rate of leakage through the four-bladed labyrinth seal of seal set B (long pitch) with a supply pressure of 100 psi (6.89 bar) and atmospheric back pressure are shown in Figure 9.7. For each seal, the evaluation of the leakage models is presented in the form of comparisons of each equation's prediction error for different supply pressures. Prediction errors for four different supply pressures and atmospheric back pressure are presented in Figure 9.8 for the six-bladed labyrinth seal of seal set B with long pitch (all seals discussed in this section have deep cavities and single-thickness blades). High prediction errors for all equations for the lowest pressure drop were observed for all the low-pressure comparisons. This pressure was eliminated from Figure 9.9 through Figure 9.11, which

show prediction errors for the six-bladed intermediate pitch, the four-bladed long pitch, and the four-bladed long pitch and double thickness labyrinth seals of set B.

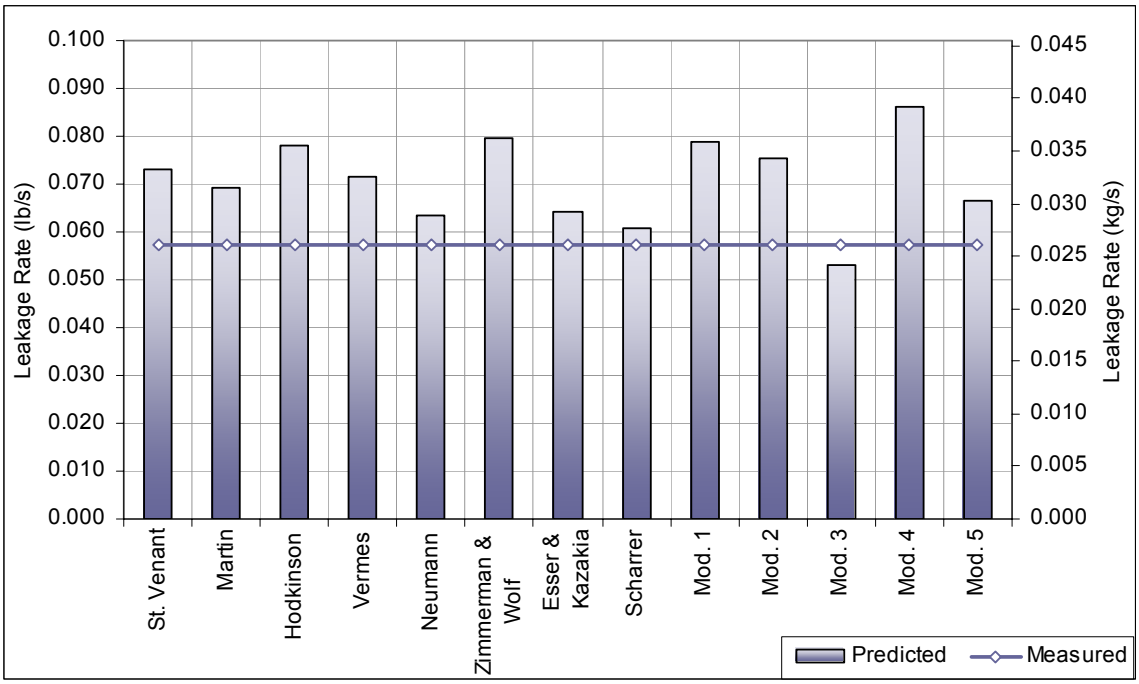

Figure 9.7 Leakage predictions for set B, 4 blades, long pitch, 100 psi (6.89 bar) P_{in}

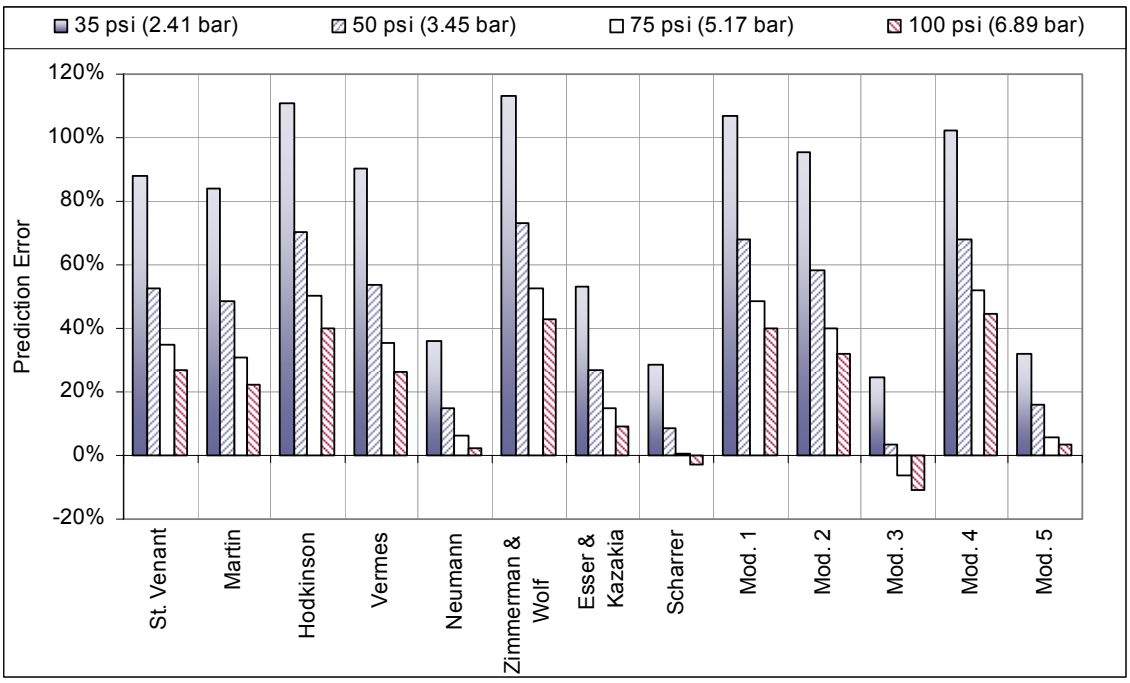

Figure 9.8 Prediction error for different supply pressures (set B, 6 blades, long pitch)

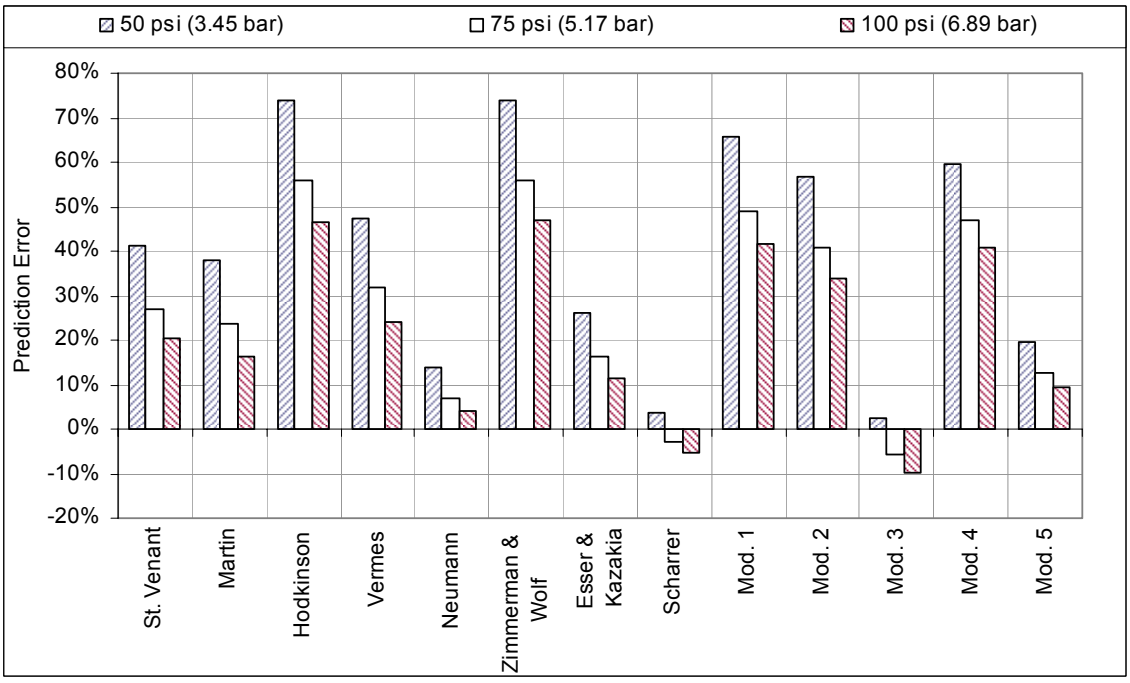

Figure 9.9 Prediction error (set B, 6 blades, intermediate pitch)

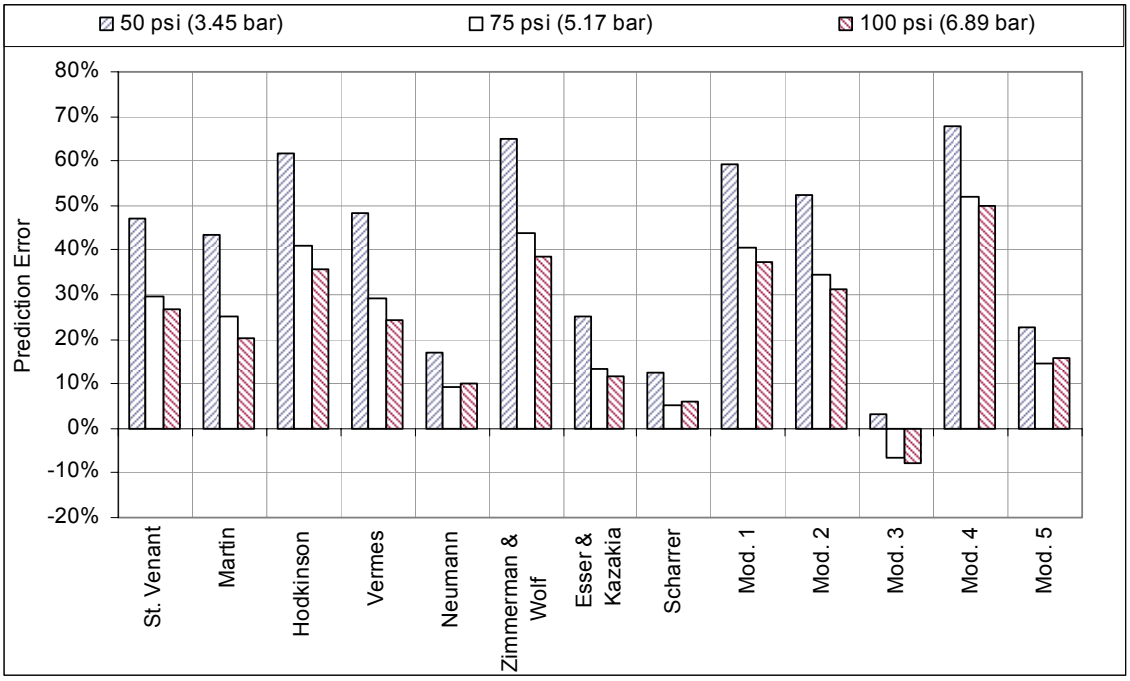

Figure 9.10 Prediction error (set B, 4 blades, long pitch)

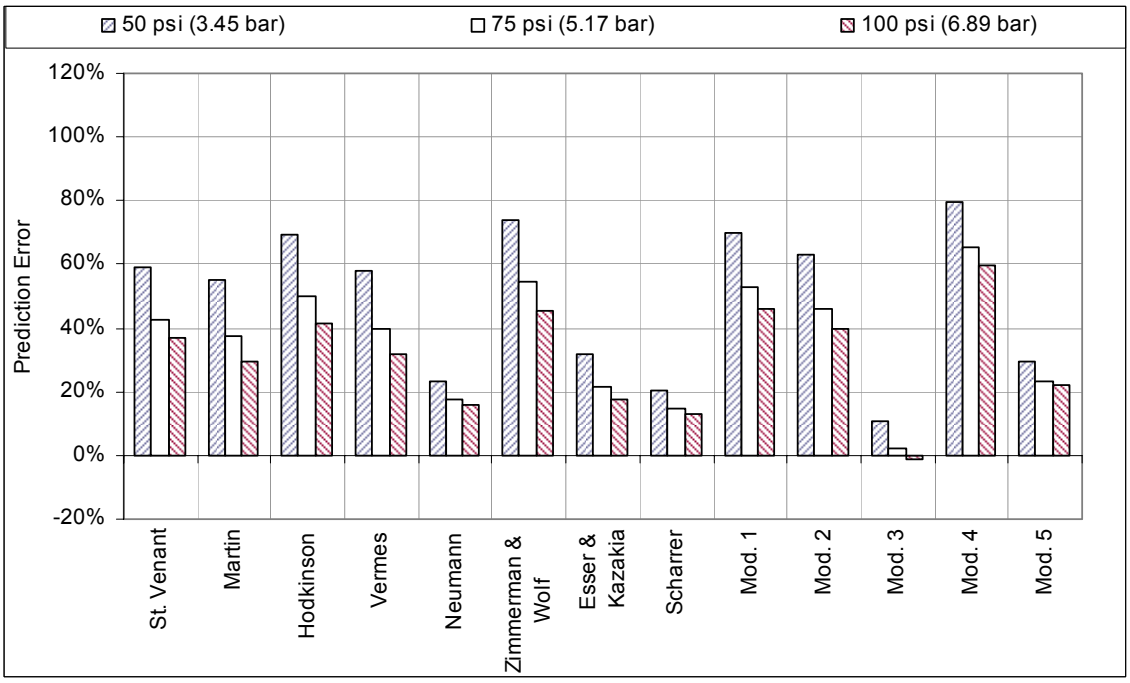

Figure 9.11 Prediction error (set B, 4 blades, long pitch, thick blades)

Neumann's Equation, Scharrer's Equation, and MOD 3 do the best job of predicting the leakage rates through these low-pressure seals. The three models that did the best job in the case of the high-pressure labyrinth seals all greatly over-predict the leakage through the lower-pressure seals. Esser and Kazakia's model can be seen as a compromise model that will limit prediction error to 20%-25%, but which will not perform as accurately as some of the other models in each individual case.

HIGH-PRESSURE POCKET DAMPER SEALS

The leakage models were also evaluated through comparisons to the high-pressure conventional pocket damper seal data presented by Gamal, Ertas, and Vance [52]. The test conditions and actual measured flow-rates through the eight seals used for the comparisons are summarized in Table 9.4. Leakage rate predictions for two of these seals are presented in Figure 9.12 and Figure 9.13. Prediction errors for the straight-through eight-bladed seal, the diverging eight-bladed seal, and the diverging six-bladed seal are shown in Figure 9.14, Figure 9.15, and Figure 9.16 respectively.

Table 9.4 Conventional high-pressure PDS test data

No. of Blades	Clearance Ratio	Pin (psi)	Pin (bar)	Pressure Ratio	ΔP (psi)	ΔP (bar)	Actual Flow (lb/s)	Actual Flow (Kg/s)
8	1 to 1	1046	72.09	0.56	911	62.78	0.7120	0.3236
8	1 to 1	1013	69.81	0.59	671	46.24	0.6882	0.3128
8	1 to 1	1030	70.99	0.52	491	33.84	0.6357	0.2890
8	1 to 1.5	1012	69.75	0.59	411	28.33	0.7341	0.3337
8	1 to 1.5	939	64.71	0.62	357	24.60	0.6592	0.2996
8	1 to 1.5	731	50.38	0.62	277	19.09	0.4938	0.2245
6	1 to 2	1000	68.92	0.60	400	27.57	0.8250	0.3750
6	1 to 2*	1000	68.92	0.60	400	27.57	0.9750	0.4432

** Beveled blade profile*

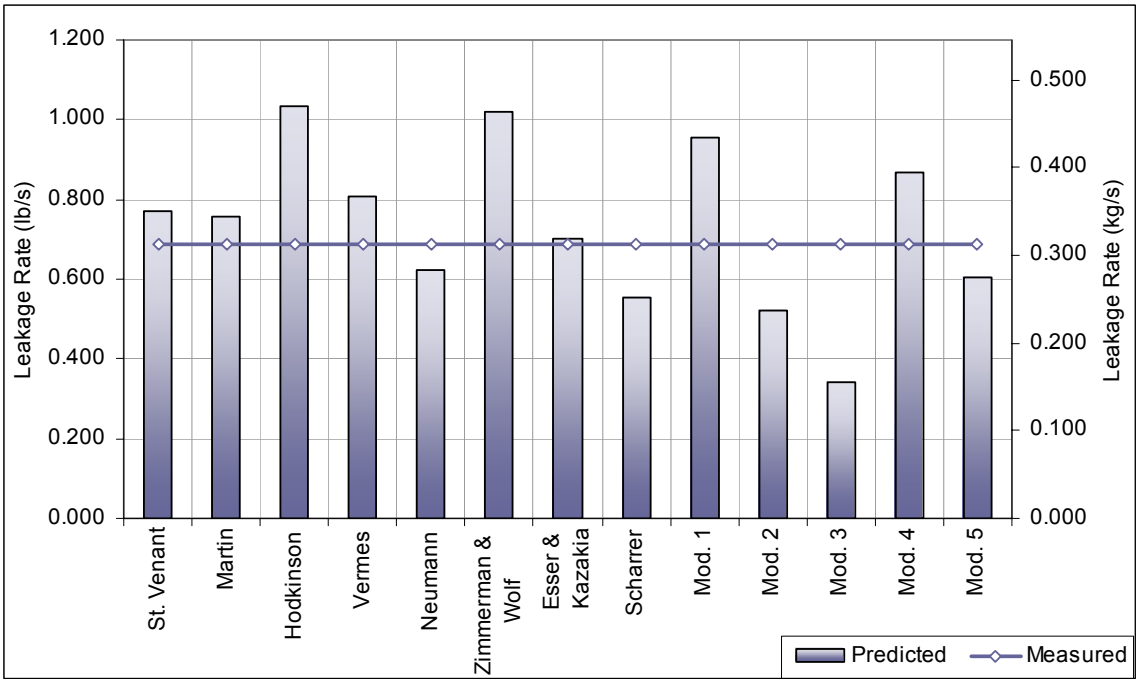

Figure 9.12 Leakage predictions for conventional 8-bladed PDS (1:1 CR, inter. ΔP)

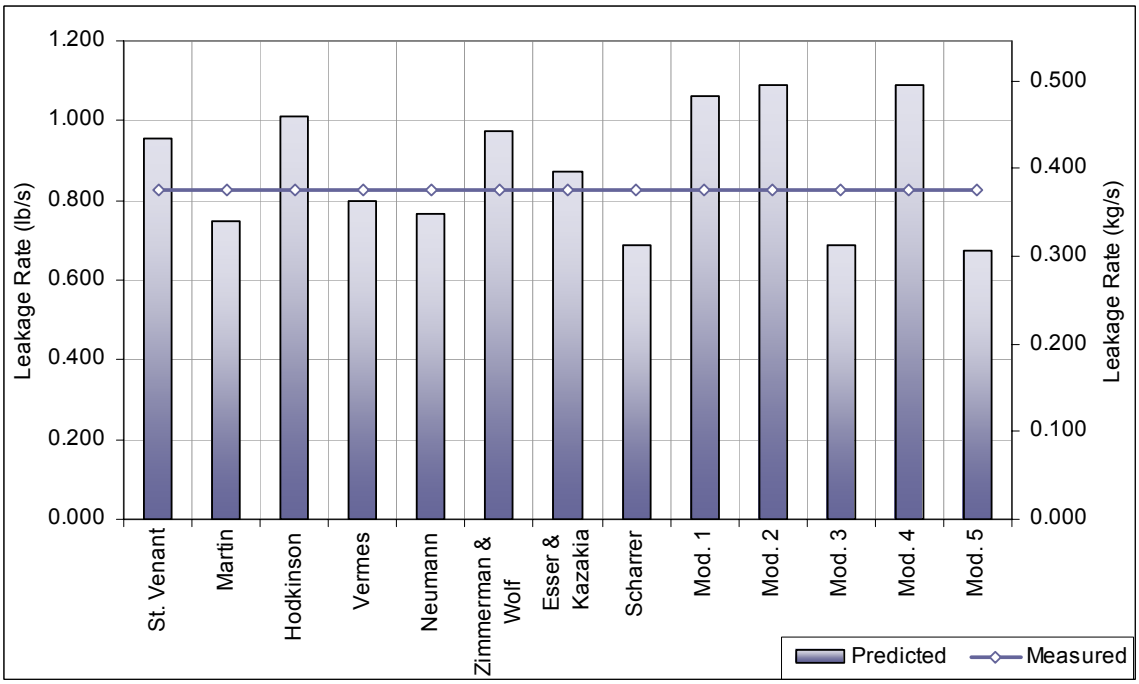

Figure 9.13 Leakage predictions for conv. 6-bladed PDS (1:2 CR, flat blade profile)

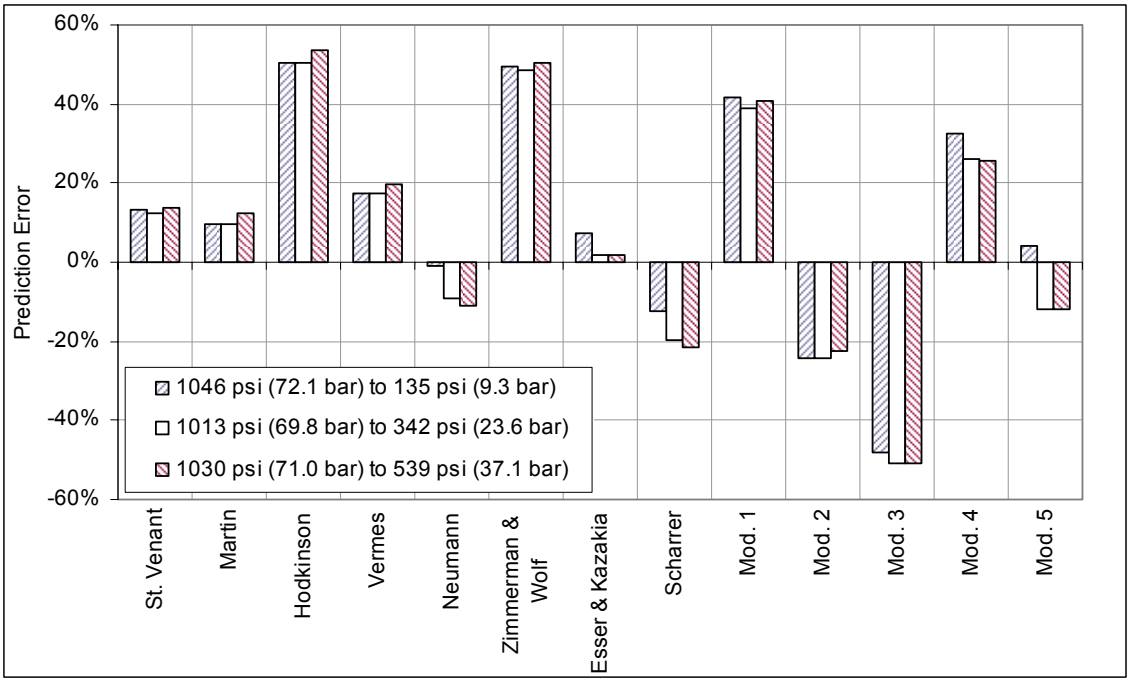

Figure 9.14 Prediction errors for conv. 8-bladed PDS (1:1 clearance ratio)

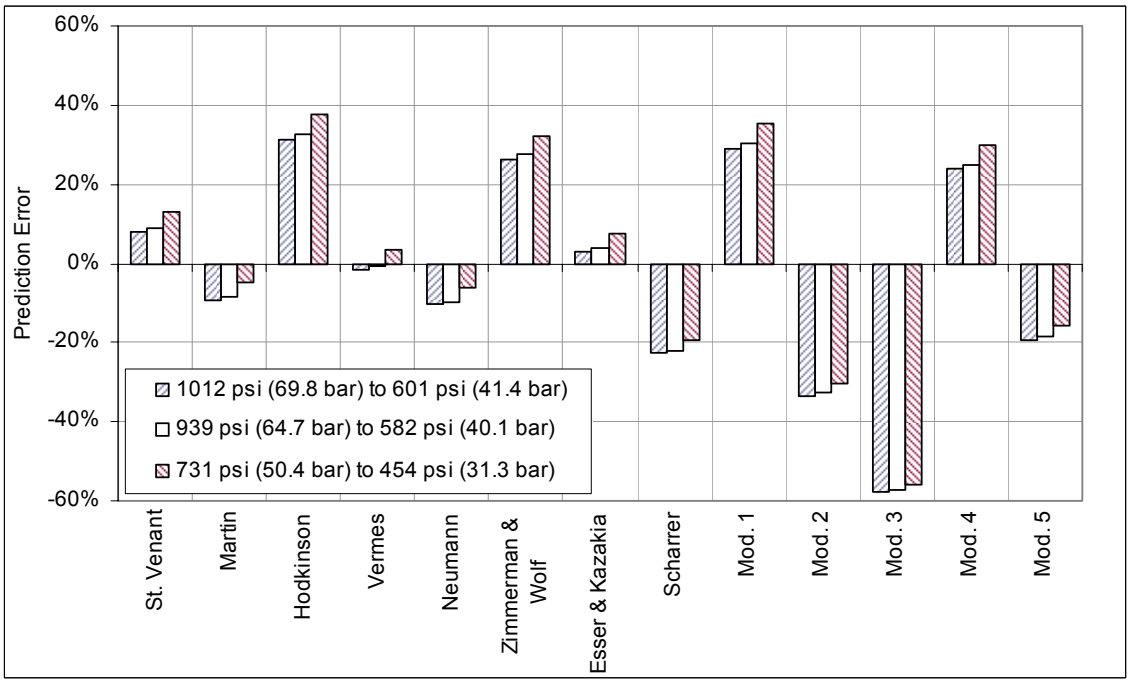

Figure 9.15 Prediction errors for conventional 8-bladed PDS (1:1.5 clearance ratio)

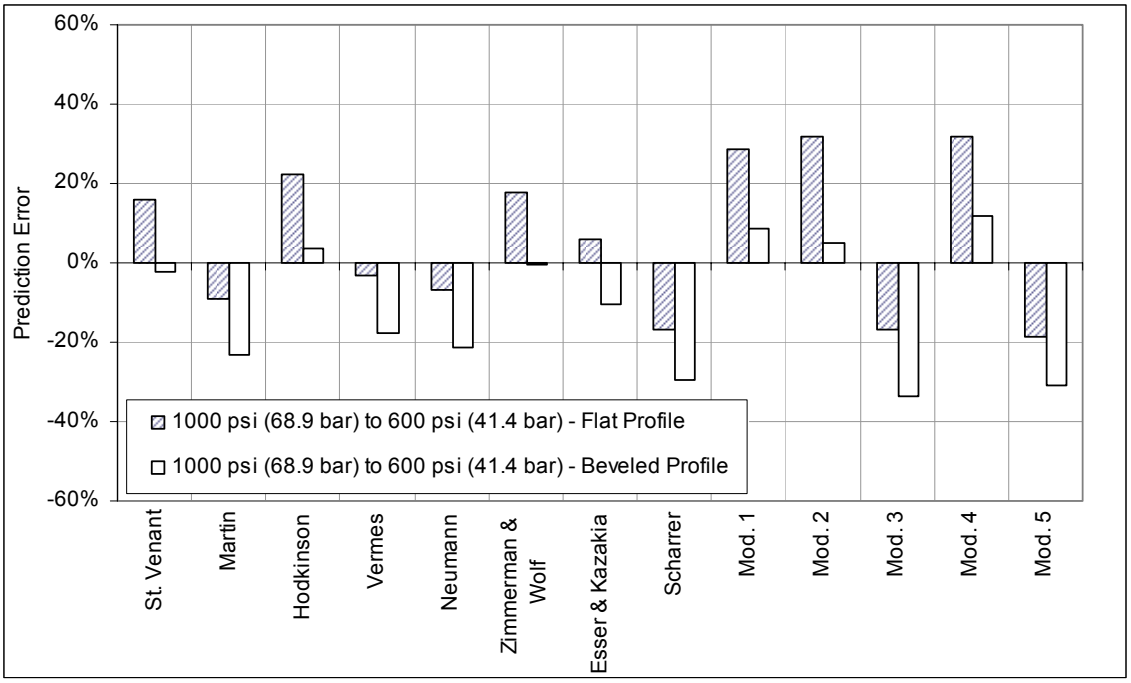

Figure 9.16 Prediction errors for conventional 6-bladed PDS (1:2 clearance ratio)

The St. Venant Equation, Martin's Equation, Vermes' Equation, Neumann's Equation, and Esser and Kazakia's Equation all predict the leakage through the seals with reasonable accuracy. All five of the *Modified Leakage Equations* do not perform particularly well.

CHAPTER DISCUSSION

Two preliminary observations can be made by a brief examination of the data. The first is that the two oldest equations, those of St. Venant and Martin, do not differ from each other considerably and it is the way in which each of them is applied that differentiates the two models. The main advantage of models like MOD 2 (which uses the St. Venant Equation) over Vermes' Model (which uses Martin's Equation) is that the latter involves a single-application method. For simple analysis, this is an advantage, but for step-by-step seal design, an iterative equation, such as the St. Venant Equation is considerably more useful. The second observation, which can be made by examining

the data from the high-pressure labyrinth seal tests, is that Chaplygin's formula is not the ideal form for the flow coefficient. The models that use this formula consistently under-predict the leakage rates through these seals. More involved observations are discussed in the following sub-sections.

Cavity Pressure Distributions

Each combination of basic leakage model and kinetic energy and flow coefficients affects the distribution of mean cavity pressures as well as the overall seal flow-rate. The effects on pressure distributions are discussed in this subsection with simulated results for Picardo's 1 mm (about 4 mils) clearance high-pressure labyrinth seal with a supply pressure of 1000 psi (68.9 bar). Figure 9.17 shows the pressure distribution predictions for this seal with a pressure ratio of 0.5. This figure includes pressure distributions indirectly obtained from single-application equations by using the calculated flow-rate and assuming a series of one-bladed seals to consecutively calculate each cavity pressure from inlet to exit. Figure 9.18 shows the pressure distributions predicted only by the iterative equations for the same seal with a pressure ratio of 0.8. Especially worth noting is that the pressure distributions of the St. Venant Equation, Martin's Equation, and Neumann's Equation are all monotonically increasing and it is only the flow coefficients which alter this distribution.

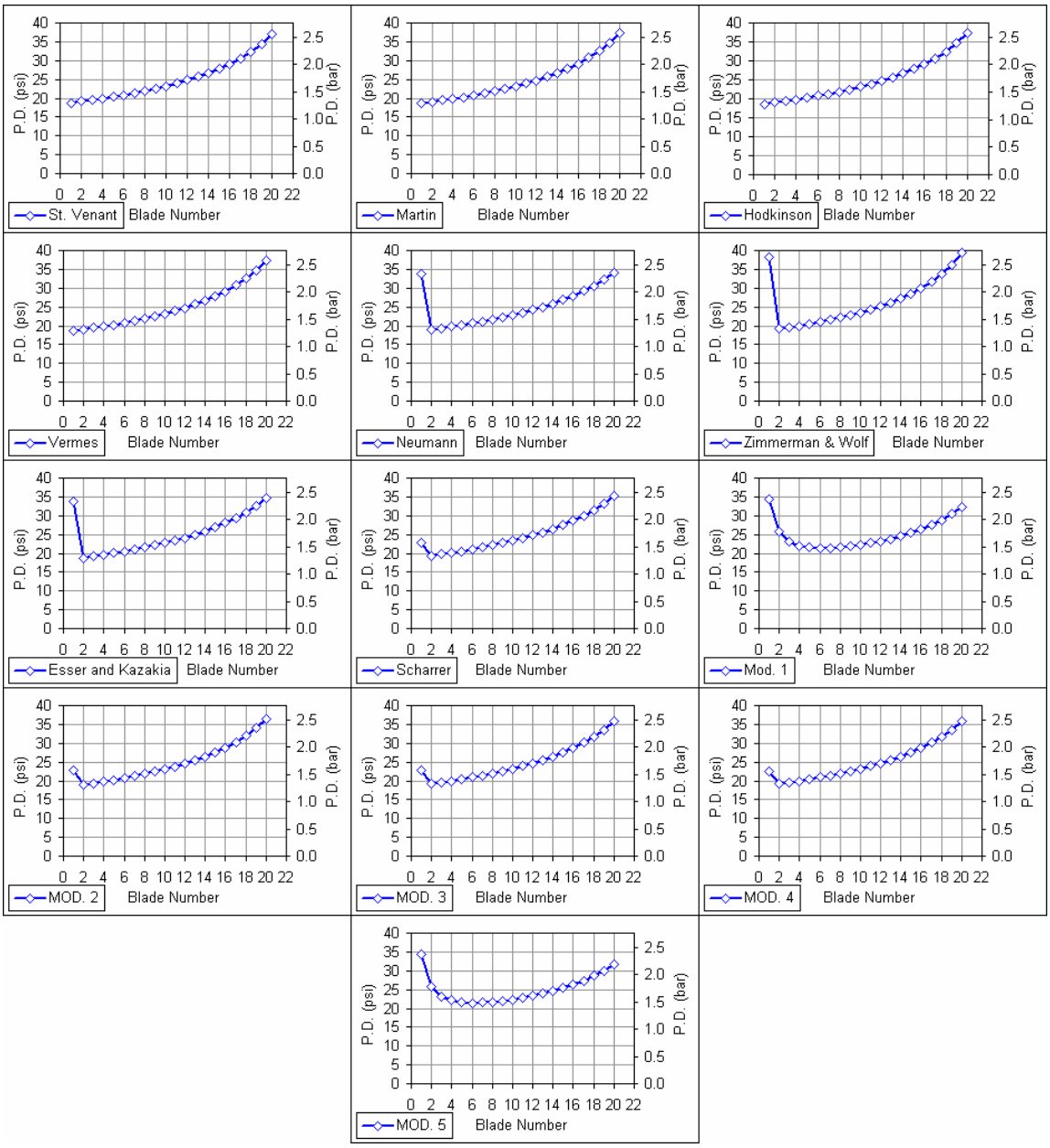

Figure 9.17 Pressure drop predictions for Picardo's seal with 0.5 pressure ratio

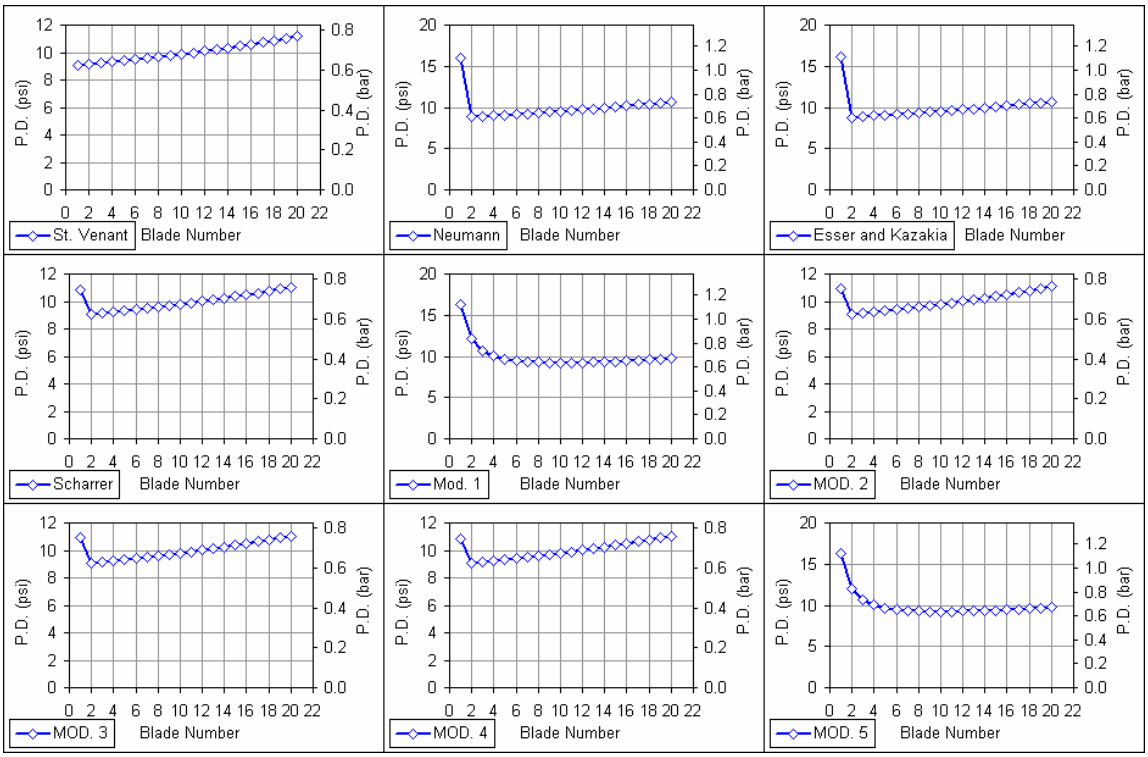

Figure 9.18 Pressure drop predictions for Picardo's seal with 0.8 pressure ratio

The kinetic energy carryover coefficients developed by Hodkinson, Vermes, and Neumann all have a large effect on the pressure drop across the first seal blade and a lesser effect on the drop across each of the other blades. This results in a downward *jump* in the pressure distribution, which is followed by the original monotonically increasing trend. This jump helps account for the experimentally observed high pressure drop across the first blade of a seal. The modified form of Hodkinson's coefficient that was developed for use with MOD 1 and MOD 5 gradually decreases for each blade along the length of a seal and so provides a smoother pressure distribution while still predicting high pressure drops across the first blade. This coefficient also predicts a flatter distribution across the interior blades and predicts lower drops across the last blades of the seal for higher pressure ratios (that is, for seal exit pressures that are closer to the seal inlet pressure). Both these predictions match experimental results obtained on low-pressure seals.

Thick Orifice Coefficients

Why all five *Modified Leakage Equations* perform poorly for the high-pressure pocket damper seals is not clear. This may be, to some extent, due to the fact that the increased thickness of the blades is not fully taken into account (this explanation also applies to the low-pressure labyrinth seals). It is not coincidental that the equations that under-predicted the leakage through Picardo's high-pressure labyrinths were the equations that most-accurately predicted the leakage through the low-pressure labyrinths. This is at least partially due to the increased thickness of the blades of the low-pressure seals. Some of the models discussed in this chapter do not take blade tip thickness into account at all. Others (models involving Vermes' carry-over coefficient) take tip thickness into account in a purely geometric sense (so far as it affects the blade thickness to spacing ratio). None of these models treat the blade thickness as a significant source of resistance to flow.

As was discussed in the *Literature Review* chapter of this dissertation, Bell and Bergelin [48] developed a set of flow coefficients for different shaped orifices. Their coefficient (C) for a thick sharp-edged centered orifice is given by Equation (9.13). For the single-thickness blades of the four-bladed low-pressure labyrinth seal of seal set B, the ratio Z is equal to 31.4, compared to 2.5 and 1.27 for Picardo's high-pressure seals. The values of C_c and the friction factor f_p are obtained as functions of Reynolds Number from graphs presented by Bell and Bergelin or can be calculated from equations they present.

$$\frac{1}{C^2} = \frac{1}{C_c^2} - \left[2 \cdot \sqrt{\frac{1}{C_c^2} - \frac{64}{\mathrm{Re}}} - 2 \right] \cdot F + 2 \cdot f_p \cdot Z \qquad \textbf{(9.13)}$$

$$F = \begin{cases} 0 & \text{for } Z < 1.15 \\ 1 - e^{-0.95 \cdot (Z - 1.15)} & \text{for } Z > 1.15 \end{cases} \quad \text{where} \quad Z = \frac{\text{Tip Thickness}}{\text{Radial Clearance}} \qquad \textbf{(9.14)}$$

Table 9.5 Thick orifice coefficient sample calculation

Seal	Z (-)	F (-)	Flow-Rate (Kg/s)	Cr (mm)	Re (-)	fp (-)	C (-)
High Pressure Labyrinth A (Larger Clearance)	1.271	0.108	0.405	0.2000	4050	0.010	0.665
High Pressure Labyrinth B (Smaller Clearance)	2.538	0.733	0.205	0.1000	1025	0.030	0.765
Low Pressure Labyrinth (4 Blades, Single Thickness)	31.250	1	0.026	0.1016	132	0.100	0.350

Calculations of the thick orifice coefficients (C in the table above) for three seals are shown in Table 9.5. The flow-rates for the seals in the order listed in the table were measured at inlet and exit pressures of 1016 and 528, 1016 and 518, and 100 and 15 psi (70 and 36.4, 70 and 35.7, and 6.89 and 1 bar) respectively. Although Equation (9.13) is intended for use in the transition range ($40<Re<4000$), this equation is used for all three seals for the purpose of this example. The calculated orifice coefficients show that while the flow coefficients for the high-pressure seals are within 15% of each other, the coefficient for the low-pressure seal (with considerably thicker blades) is about half this value.

Returning to the results of the leakage model evaluation for the high- and low-pressure labyrinth seals, the equations that most accurately predicted the leakage rates through the high-pressure seals over-predicted the leakage through the low-pressure seals by up to 50%. The calculation presented above supports the suggestion put forward earlier that the reason these equations failed to accurately predict the lower-pressure leakage data was because of the thickness of the low-pressure labyrinth seal blades.

Pitch Effects

While the leakage models presented do not satisfactorily account for blade thickness effects, they *are* designed to deal with blade spacing effects through the kinetic energy carryover coefficient. The St. Venant Equation and Martin's Equation are exceptions in this regard since they do not incorporate such a carryover coefficient. The remaining

equations do account for blade spacing and were found to predict its effects with surprising accuracy. Table 9.6 presents sample calculations of blade spacing effects for a six-bladed labyrinth seal of seal set B with single-thickness blades and deep cavities. This table shows the reduction in leakage resulting from going from intermediate spacing (0.25 in or 6.35 mm) to long spacing (0.5 in or 12.7 mm) between the blades for four pressure drops.

Table 9.6 Leakage model predictions of blade pitch effects

Model	Leakage reduction due to changing pitch from 1/4 to 1/2 in (6.35 to 12.7 mm)			
	100 psi (6.89 bar)	75 psi (5.17 bar)	50 psi (3.45 bar)	35 psi (2.41 bar)
St. Venant	-	-	-	-
Martin	-	-	-	-
Hodkinson	10.00%	10.00%	10.00%	10.00%
Vermes	3.24%	3.24%	3.24%	3.24%
Neumann	6.85%	6.90%	6.96%	7.01%
Zimmerman & Wolf	8.38%	8.31%	8.18%	8.01%
Esser & Kazakia	7.03%	7.03%	7.03%	7.03%
Scharrer	2.57%	2.59%	2.61%	2.63%
Mod. 1	6.53%	6.54%	6.45%	6.27%
Mod. 2	6.96%	6.96%	6.94%	6.84%
Mod. 3	6.76%	6.77%	6.77%	6.77%
Mod. 4	2.64%	2.64%	2.64%	2.64%
Mod. 5	7.20%	7.24%	7.31%	7.36%
Measured	**5.20%**	**6.06%**	**7.84%**	**7.53%**

Atmospheric back pressure for all cases

The highlighted values in Table 9.6 represent the measured drop in leakage resulting from the blade spacing increase for this seal. Neumann's Equation, MOD 1, MOD 2, and MOD 3 most accurately predict the measured reduction in leakage, especially for the higher supply pressures. Since the errors are more or less constant, they can be seen to be accurately predicting the experimentally determined trend showing that the effect of blade spacing is lessened with increasing pressure drop across the seal.

Model Performance

Vermes' equation, MOD 2 and MOD 4 seem to be the best equation to use for thin (close to knife-edged) blades. Combined with an empirically determined friction factor, they could also be used to accurately predict leakage through seals with thicker blades. Conversely, the equations that more closely matched the low-pressure data do not take into account thickness effects and as such, cannot be said to be accurate. These equations matched data measured using seals with an unaccounted-for feature and failed to match the data they were expected to accurately match. That being said, it is reasonable to assume that at higher pressures other factors come into play which have not been considered in this thesis and that there may be other reasons why these equations did not accurately predict high-pressure leakage data.

Vermes' Model, as he presented it, was based on Martin's single-application equation. MOD 2 and MOD 4 may therefore be of more use because of their reliance on the iterative St. Venant and Neumann's Equations respectively. Neither of these equations uses a flow-coefficient (MOD 4 is essentially Scharrer's Model without the flow coefficient), but empirically obtained discharge coefficients would increase their accuracy once they are determined for a given set of seals. The evaluations presented in this chapter do not eliminate the need for such correction factors, but they provide a means of selecting an equation that will most closely predict seal leakage if such factors are unavailable or before they are determined.

With respect to pressure distributions, equations based on Neumann's kinetic energy carry-over coefficient (those of Neumann and Esser and Kazakia) do a better job of matching experimentally determined trends than those based on Vermes' or Hodkinson's coefficient. The modified (decreasing with blade number) form of Hodkinson's coefficient not only matches the drop across the first blade, but also more closely matches the flat interior blade pressure drops. This coefficient, used in MOD 1 and MOD 5, is the only one that also predicts the parabolic rise in the pressure drop trend across the downstream blades at higher pressures and eliminates this rise at lower pressures. MOD 1 consistently over-predicted the measured leakage values through the

labyrinth seals (both low and high pressure) by about 40%. Combining this model with a flow coefficient to account for contraction (MOD 1 does not include a flow coefficient) would make it a useful model. MOD 4 does this using Chaplygin's formula, which has been shown to result in considerable under-prediction. Using a constant coefficient, such as the 0.716 value used by Esser and Kazakia, would virtually eliminate the 40% average over-prediction for most of the labyrinth seals, making MOD 1 as attractive a choice as Vermes' model, MOD 2 and MOD 4.

Reynolds Number Dependency

The above comparison and discussion of the various leakage models mentions that the differences in blade thickness is one possible reason for why different models provide the best predictions for different seals. A perhaps more significant reason, and one that applies regardless of geometric differences, is the dependence of the accuracy of the predictions on Reynolds Number defined by Equation (9.15).

$$\mathrm{Re} = \frac{2 \cdot Cr \cdot U}{\nu} \tag{9.16}$$

The leakage models examined in this dissertation do not feature Re-dependant coefficients whereas models like that of Sriti et al. [61] do take this dependency into consideration. Table 9.7 through Table 9.9 list the Reynolds numbers for the flow through high pressure labyrinth seals, low pressure labyrinth seals, and high pressure pocket damper seals for various test conditions and geometries.

Table 9.7 Re values for high pressure labyrinth seals

Inlet Pressure		Exit Pressure		Pressure	Radial Clearance		Re
bar	psi	bar	psi	Ratio	mm	mils	
70	1016	11.2	163	0.16	0.2	7.87	135,243
70	1016	25.2	366	0.36	0.2	7.87	129,232
70	1016	36.4	528	0.52	0.2	7.87	121,719
70	1016	7.0	102	0.10	0.1	3.94	70,565
70	1016	21.7	315	0.31	0.1	3.94	69,064
70	1016	35.7	518	0.51	0.1	3.94	61,557

Table 9.8 Re values for low pressure labyrinth seals

No. of	Inlet Pressure		Exit Pressure		Re
Blades	psi	bar	psi	bar	
4	30	2.0	15	1.0	1,565
4	35	2.4	15	1.0	2,160
4	40	2.7	15	1.0	2,739
4	45	3.1	15	1.0	3,233
4	50	3.4	15	1.0	3,816
4	55	3.8	15	1.0	4,322
4	60	4.1	15	1.0	4,815
4	75	5.1	15	1.0	6,482
4	100	6.9	15	1.0	8,851
6	30	2.0	15	1.0	1,196
6	35	2.4	15	1.0	1,717
6	40	2.7	15	1.0	2,226
6	45	3.1	15	1.0	2,656
6	50	3.4	15	1.0	3,129
6	55	3.8	15	1.0	3,622
6	60	4.1	15	1.0	4,027
6	75	5.1	15	1.0	5,306
6	100	6.9	15	1.0	7,509

Table 9.9 Re values for high pressure pocket damper seals

No. of Blades	Clearance Ratio	Pin (psi)	Pin (bar)	Pressure Ratio	ΔP (psi)	ΔP (bar)	Re
8	1 to 1	1046	72.09	0.56	911	62.78	97,328
8	1 to 1	1013	69.81	0.59	671	46.24	94,074
8	1 to 1	1030	70.99	0.52	491	33.84	86,898
8	1 to 1.5	1012	69.75	0.59	411	28.33	100,349
8	1 to 1.5	939	64.71	0.62	357	24.60	90,110
8	1 to 1.5	731	50.38	0.62	277	19.09	67,501
6	1 to 2	1000	68.92	0.60	400	27.57	112,775
6	1 to 2*	1000	68.92	0.60	400	27.57	133,279

** Beveled blade profile*

Figure 9.19 summarizes this information through a graphical comparison of the Reynolds Numbers corresponding to the leakage rates through six different seals. Re values are plotted for two low pressure labyrinth seals (with four and six blades), two high pressure labyrinth seals (with 1 mm and 2 mm or 3.9 and 7.9 mil radial clearances), and two high pressure pocket damper seals (straight-through and diverging clearance configurations).

Note that pressure ratio for the high pressure seals was approximately 0.5. This was also the approximate pressure ratio for the elevated back pressure tests for the low pressure seals. The Re values for the high pressure seals (both labyrinth and pocket damper) are between one and two orders of magnitude higher than those for the low pressure labyrinth seals.

This examination of Reynolds Numbers also explains the difference in model prediction accuracy for each of the high pressure labyrinth seals tested by Picardo. The average Re value for Picardo's Seal A (tighter clearance) was 128,000 for the three test conditions examined, while the average value for Seal B was 67,000. This difference in Re explains why Vermes' Equation, Esser and Kazakia's Equation, MOD 1, and MOD 4 predicted the leakage through Seal A with high accuracy (Figure 9.1), but under-predicted the leakage through Seal B (Figure 9.4).

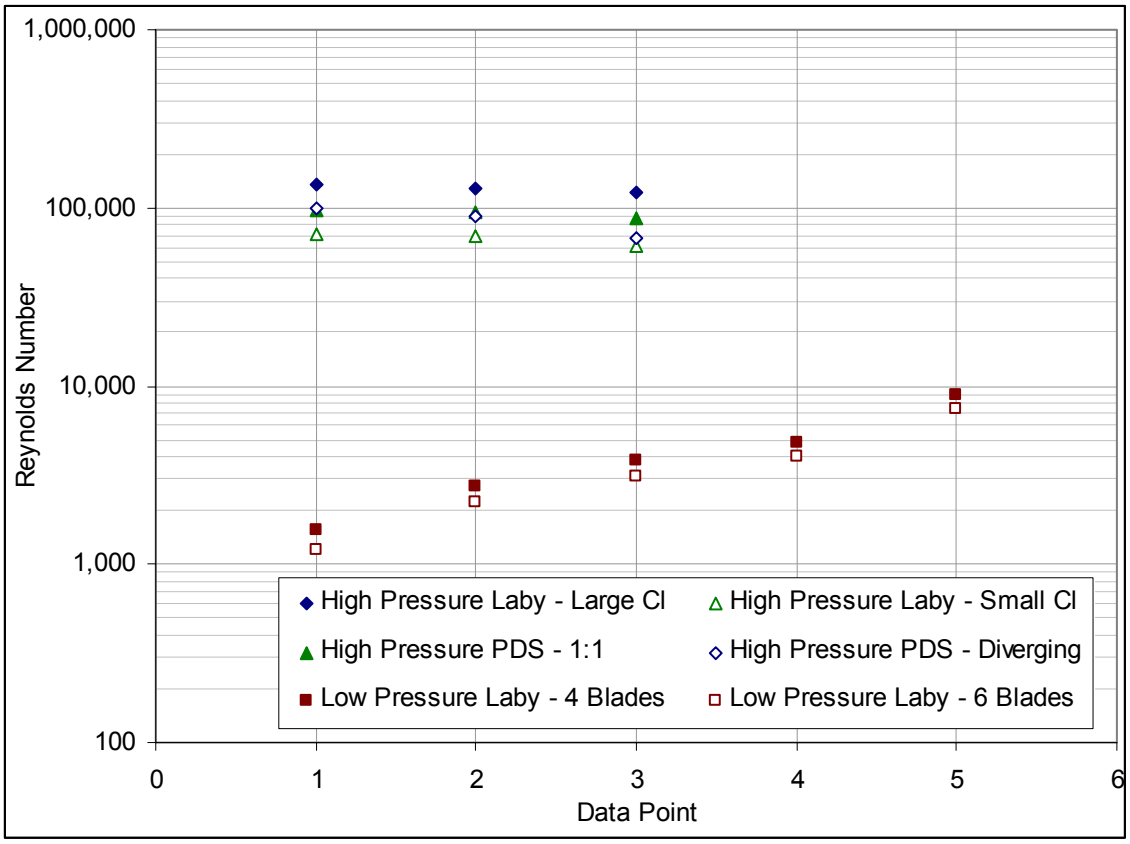

Figure 9.19 Range of Reynolds Numbers examined for different seals

CHAPTER X

ANNULAR GAS SEAL COMPARISONS

This chapter presents comparisons based on experimental data obtained from annular gas seals tested with supply pressures of up to 1000 psi (68.9 bar). The test data were obtained by Picardo and Childs [12] for labyrinth seals, Kerr [68] for smooth seals, Sprowl and Childs [69] for honeycomb seals, Childs and Wade [70] for hole-pattern seals, Ertas, Gamal, and Vance [71] for conventional pocket damper seals, and Ertas [41] for fully-partitioned pocket damper seals.

The magnitudes of the damping and stiffness for each seal are presented in terms of normalized coefficients defined by Equations (10.1) and (10.2) respectively (from Childs [72]). These equations result in normalized damping with units of seconds and normalized stiffness that is dimensionless (in the plots presented below, both normalized damping and stiffness values have been multiplied by 10^6).

$$C^* = \frac{C_{xx}}{\left(\frac{L \cdot D \cdot \Delta P}{C_r}\right)} \tag{10.1}$$

$$K^* = \frac{K_{xx}}{\left(\frac{L \cdot D \cdot \Delta P}{C_r}\right)} \tag{10.2}$$

Figure 10.1 indicates the degree to which these equations actually normalize damping results for pocket damper seals. The three lower curves in the figure represent the normalized damping of a straight-through (1:1 clearance ratio) conventional PDS for three pressure drops and an inlet pressure of approximately 1000 psi (68.9 bar). The proximity of the curves to each other over the range of test frequencies indicates that the equations used successfully normalize (in terms of pressure drop) the test data for these

seals. The two upper curves on the graph represent the normalized damping of a diverging (1:1.5 clearance ratio) conventional PDS for two pressure drops. In this case, the normalization also brings the curves closer together, somewhat eliminating the pressure drop effect, but does not work as well as for the straight-through seal. The test pressure conditions for the five seals used in generating this figure are summarized in Table 10.1.

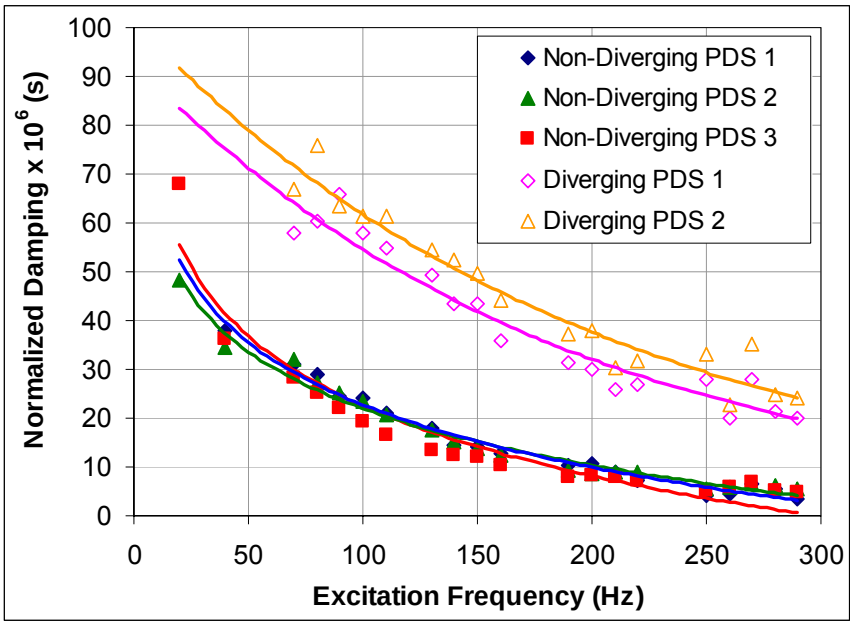

Figure 10.1 Example of PDS damping data normalization

Table 10.1 Test pressure conditions for 8-bladed pocket damper seals

Seal	Clearance Ratio	P_{in}		P_{out}		ΔP		Pressure Ratio
		(psi)	(bar)	(psi)	(bar)	(psi)	(bar)	
PDS 1	1:1 (Non-Diverging)	1000	68.9	510	35.1	490	33.8	0.51
PDS 2	1:1 (Non-Diverging)	1000	68.9	320	22.0	680	46.9	0.32
PDS 3	1:1 (Non-Diverging)	1000	68.9	100	6.9	900	62.0	0.10
PDS 4	1:1.5 (Diverging)	700	48.2	280	19.3	420	28.9	0.40
PDS 5	1:1.5 (Diverging)	700	48.2	428	29.5	272	18.7	0.61

DAMPING COMPARISON

Figure 10.2 shows the normalized damping for 6-, 8-, and 12-bladed conventional pocket damper seals and for a 6-bladed fully-partitioned PDS. In the case of the 8- and 12-bladed seals, data is shown for both straight-through and diverging configurations. As is customary for pocket damper seals and in accordance with PDS theory, the damping is highest at lower frequencies and drops off as the excitation frequency is increased.

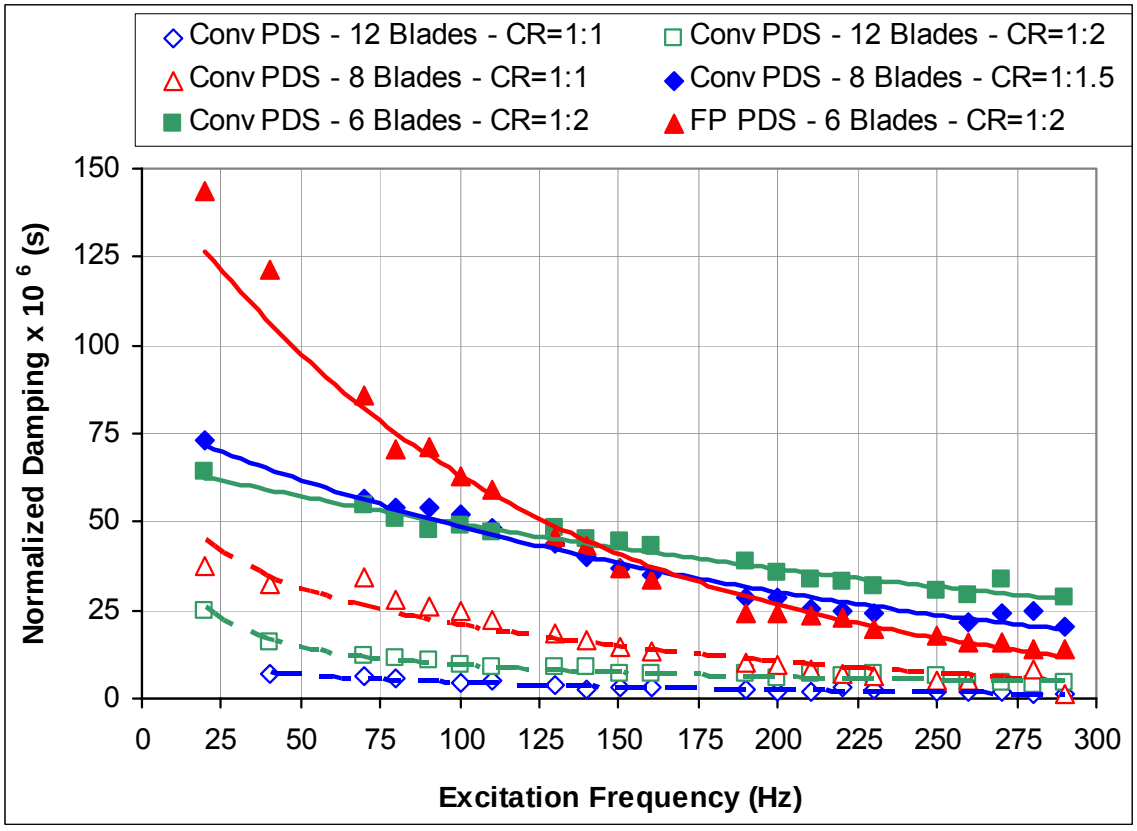

Figure 10.2 PDS normalized damping

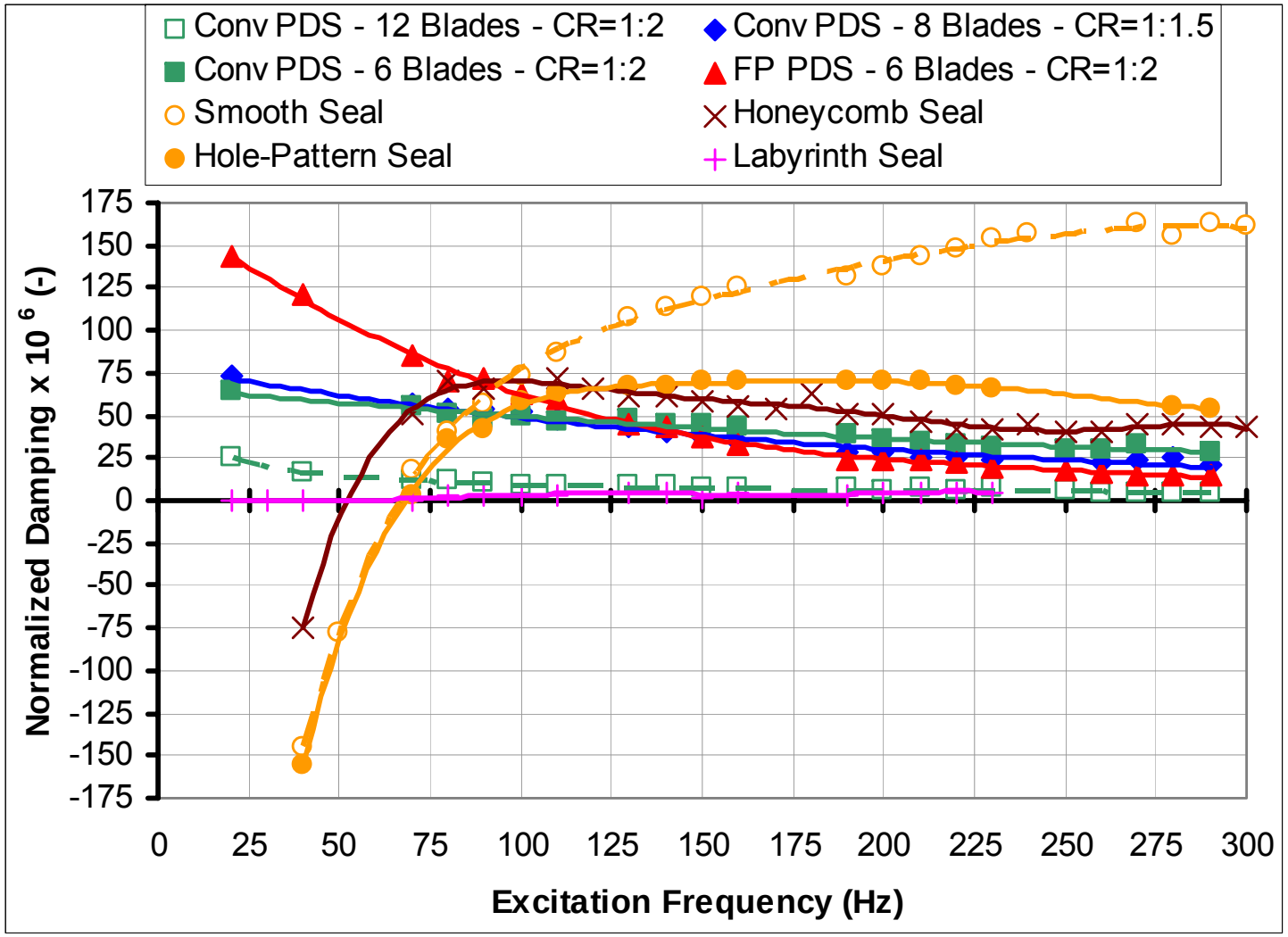

Figure 10.3 Normalized effective damping comparison

The normalized data for the diverging configurations of these seals are redrawn in Figure 10.3 along with effective damping data for smooth, labyrinth, hole-pattern, and honeycomb seals. This comparison is based on the assumption that the for a pocket damper seal, the direct damping is equivalent to the effective damping. This assumption is validated by static measurements by Gamal [40] and dynamic measurements by Ertas and Vance [73] of PDS cross-coupled stiffness coefficients. These measurements showed same-sign cross-coupled stiffness values, indicating that no destabilizing cross-coupling effects are present in pocket damper seals and that for a PDS the effective damping is practically identical to the direct damping. Especially worth noting is the high direct damping of the fully-partitioned pocket damper seal at low frequencies (up to 100 Hz).

STIFFNESS COMPARISON

Figure 10.4 shows the normalized stiffness for 6-, 8-, and 12-bladed conventional pocket damper seals and for a 6-bladed fully-partitioned PDS. In the case of the 8-bladed and 12-bladed seals, data is shown for both straight-through and diverging configurations. The normalized data for the diverging configurations of these seals are redrawn in Figure 10.5 along with normalized stiffness data for smooth, labyrinth, hole-pattern, and honeycomb seals.

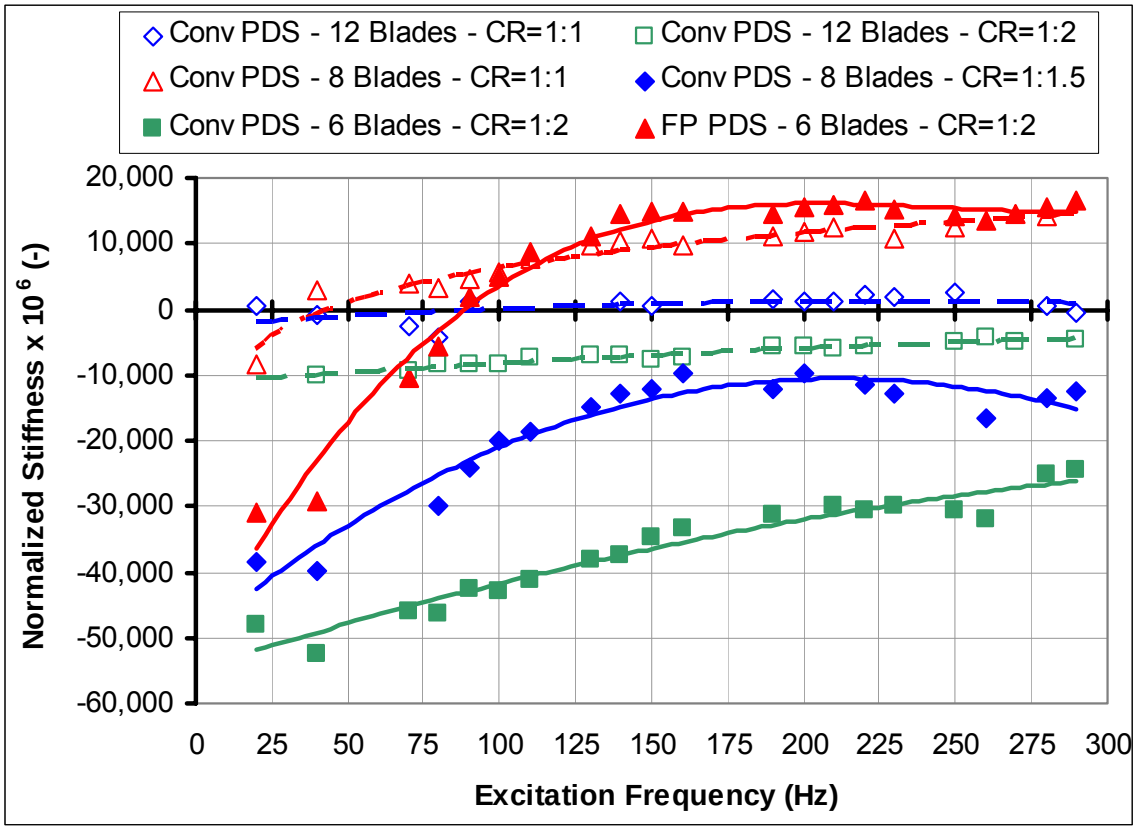

Figure 10.4 PDS normalized stiffness

Table 10.2 Pressure ratios for seals used in comparison plots

Seal Type and Configuration	Pressure Ratio
Labyrinth Seal	0.52
Honeycomb Seal	~ 0.5
Hole-Pattern Seal	~ 0.5
Smooth Seal	~ 0.5
Pocket Damper Seals	
12 Blades (Straight-Through)	0.179
12 Blades (Diverging)	0.214
8 Blades (Straight-Through)	0.516
8 Blades (Diverging)	0.531
6 Blades (Conventional Diverging)	0.498
6 Blades (Fully-Partitioned Diverging)	0.522

Note that the fully-partitioned seal, while providing higher damping, also has lower negative stiffness and has a zero stiffness cross-over frequency of 85 Hz. At the time this seal was tested, no tool for designing or analyzing fully-partitioned a PDS had been developed, and the test seal was designed using the optimization code used for maximizing the damping of conventional PDSs. Simulations with models since developed specifically for FP PDSs show that the pocket depth of the test seal was not optimum and that considerably more damping could have been obtained from the seal under the prescribed test conditions. The newer model also shows that the zero stiffness cross-over frequency could have been lowered with minor design modifications. It should also be noted, however, that the hole-pattern seal used for this comparison may not also have been of the optimum design. Shin et al. [74] showed that hole-pattern seal damping can be increased by varying the hole-depth in the axial direction. These measurements by Shin et al. showed an increase in effective damping by a factor of 1.6 and a 40% reduction in positive damping cross-over frequency as compared to a standard hole-pattern seal.

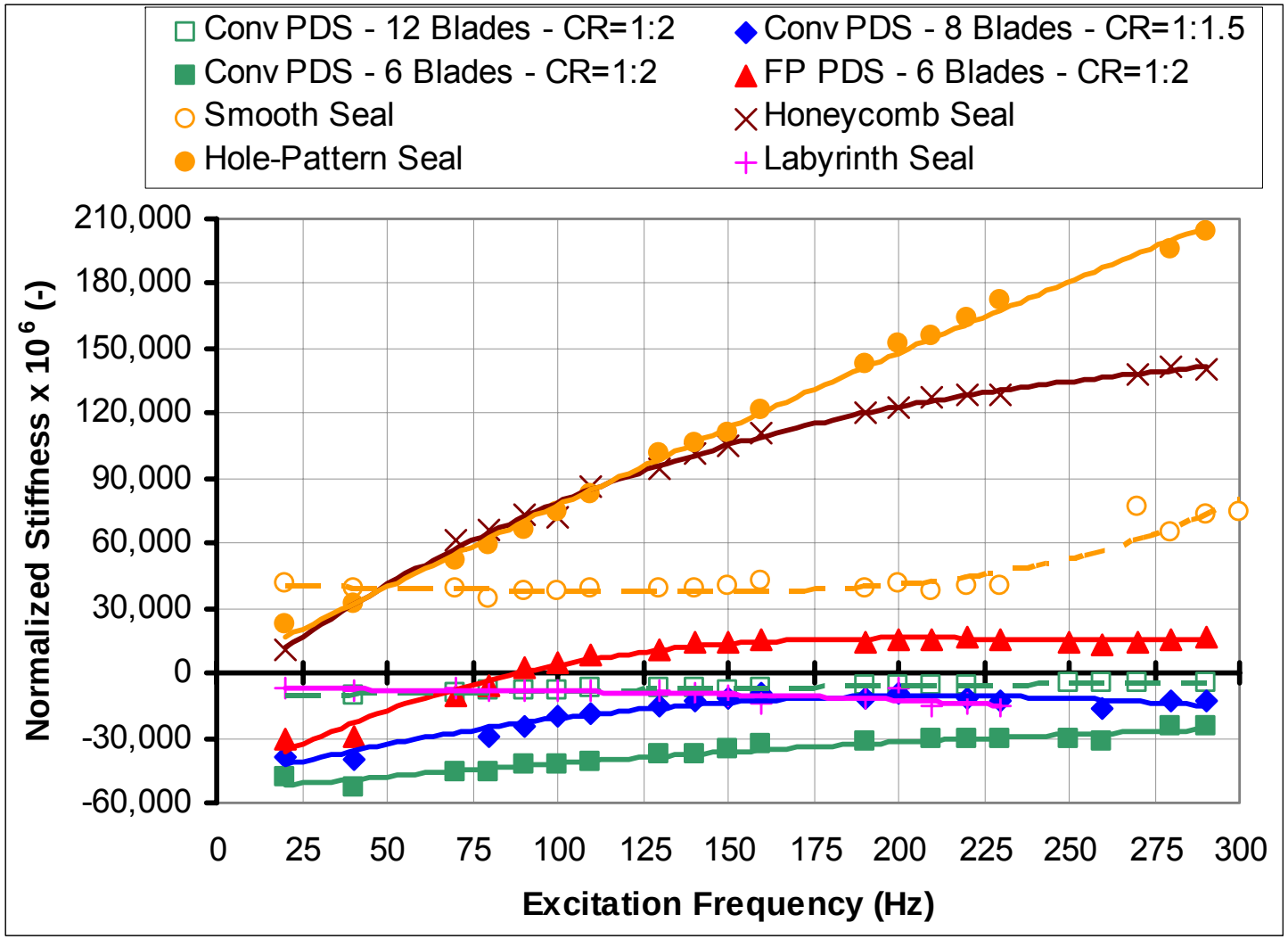

Figure 10.5 AGS normalized stiffness comparison

LEAKAGE COMPARISON

The mass flow-rates through the seals are presented in terms of dimensionless flow coefficients defined by Equation (10.3) (from Childs [72]). This equation differs from the flow coefficient equation more commonly found in the literature (Equation (10.4)) in that the pressure drop is taken into account in the non-dimensionalization (the more commonly used equation as defined by Yucel and Kazakia [75] employ a second P_{in} multiplier instead of the 2(ΔP) term).

Experimental leakage data from pocket damper seal tests was used to calculate dimensionless flow coefficient values for a straight-through (1:1 clearance) 8-bladed PDS. The calculated values were added to the plot obtained from Childs [72] for smooth, labyrinth, hole-pattern, and honeycomb seals (Figure 10.6). The pocket damper seals were tested with rotor speeds of 10,200, 15,200, and 20,200 RPM and slightly different leakage rates were obtained depending on the shaft rotational speed. The PDS results presented in the Figure 10.6 are those for a rotor speed of 10,200 RPM as this minimizes the effects of rotational speed on the comparison (see *Rotor Growth* subsection below).

$$\phi = \frac{\dot{m}}{\pi \cdot D \cdot Cr} \cdot \sqrt{\frac{R_c \cdot T_{in}}{2 \cdot \Delta P \cdot P_{in}}} \qquad \textbf{(10.3)}$$

$$\phi = \frac{\dot{m}}{\pi \cdot D \cdot Cr \cdot P_{in}} \cdot \sqrt{R_c \cdot T_{in}} \qquad \textbf{(10.4)}$$

Rotor Growth

The differences in leakage rates obtained for different rotor speeds were attributed in part (Gamal, Ertas, and Vance [52]) to centrifugal rotor growth, which reduced the clearances at higher speeds by up to 5%. Figure 10.7 shows the flow coefficients for the 8-bladed straight-through test PDS calculated using the initial clearances and Figure 10.8

shows the flow coefficients for the same seal using the effective clearances (compensated for rotor growth).

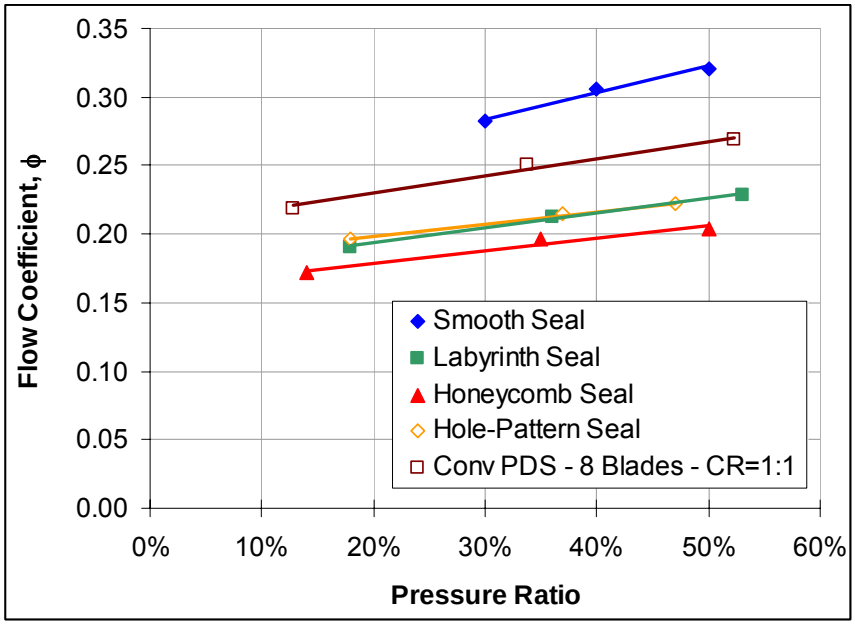

Figure 10.6 AGS leakage comparison

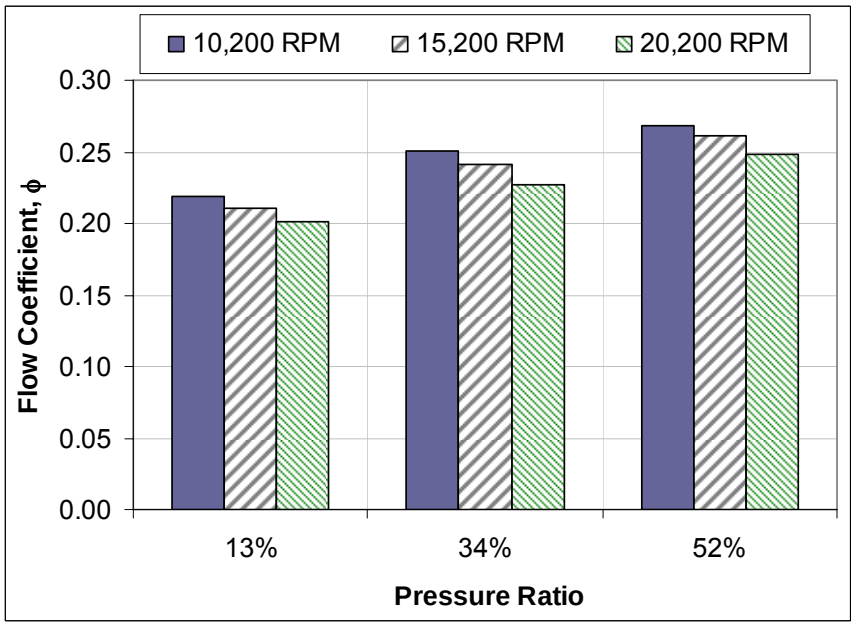

Figure 10.7 Conventional PDS leakage without shaft growth compensation

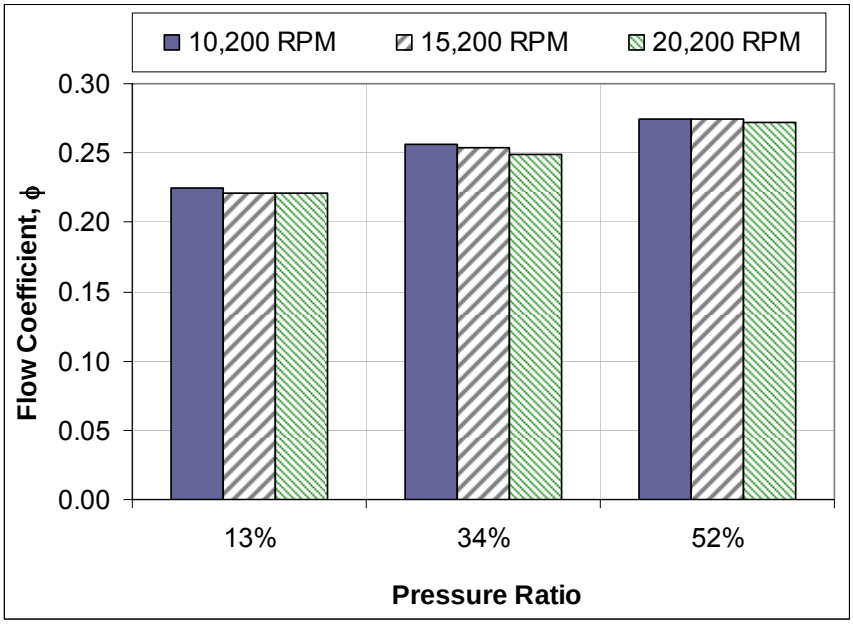

Figure 10.8 Conventional PDS leakage with shaft growth compensation

Labyrinth Leakage vs. PDS Leakage

In terms of leakage reduction, the PDS outperforms only the smooth seal and is outperformed by the labyrinth seal, hole-pattern seal, and honeycomb seal. This analysis compares seals with identical lengths, but it does not compare seals with the same number of blades in the case of the labyrinth seal and the PDS; the labyrinth seal tested had 20 blades while the pocket damper seal had 8 blades. PDS designs feature fewer blades than labyrinth seal designs for identical applications because of the need to maximize damping through enlarged cavity volume, it would not be accurate to conclude from Figure 10.6 that a PDS leaks more than a labyrinth seal. If two seals, a PDS and a labyrinth seal, with the same blade thickness and number of blades were to be compared, a PDS would have slightly lower leakage because of the effect of the partition walls discussed in Chapter VIII. Regardless of the partition walls and the thicker blades, however, the smaller number of blades and the diverging clearance of most PDS designs hinder their leakage reduction capability compared to that of labyrinth seals.

CHAPTER XI

FULLY-PARTITIONED POCKET DAMPER SEAL COMPARISONS

Comparisons of predictions of the fully-partitioned pocket damper seal model with test results are presented in this chapter. In addition, several observations on the effects of these seals that were made during the course of the research presented in this dissertation are presented. These observations include the design of pocket damper seals with orthotropic force coefficients and effects pocket depth on seal performance. A comparison of Ertas' [41] model to the current model is included, and interdependency of the cavity coefficients of a fully-partitioned seal on one another is discussed.

ROTORDYNAMIC MODEL EVALUATION

Figure 11.1 through Figure 11.4 show the damping and stiffness values predicted by the fully-partitioned pocket damper seal model alongside coefficient values measured by Ertas at supply pressures of 1000 psi (68.9 bar) for two different pressure ratios. In both cases, the direct damping is under-predicted by roughly a factor of two, but the dependency of the damping on frequency is predicted accurately. If the predicted damping values were multiplied by a constant value (approximately 2.25) at all frequencies the experimental values would be matched almost exactly, indicating that the trend, if not the values, are predicted correctly.

The model predicts stiffness values with reasonable accuracy, especially at frequencies above 100 Hz. In the case of the damping, the model errs on the safe side and under-predicts the damping at most frequencies. This is not true for the stiffness, however, since the model predicts a lower cross-over frequency than is shown by the test results. All four sets of data presented were measured at 10,200 rpm. A second predicted curve is included on each of the plots below to show the slightly improved accuracy of using the tighter effective clearances resulting from centrifugal rotor growth.

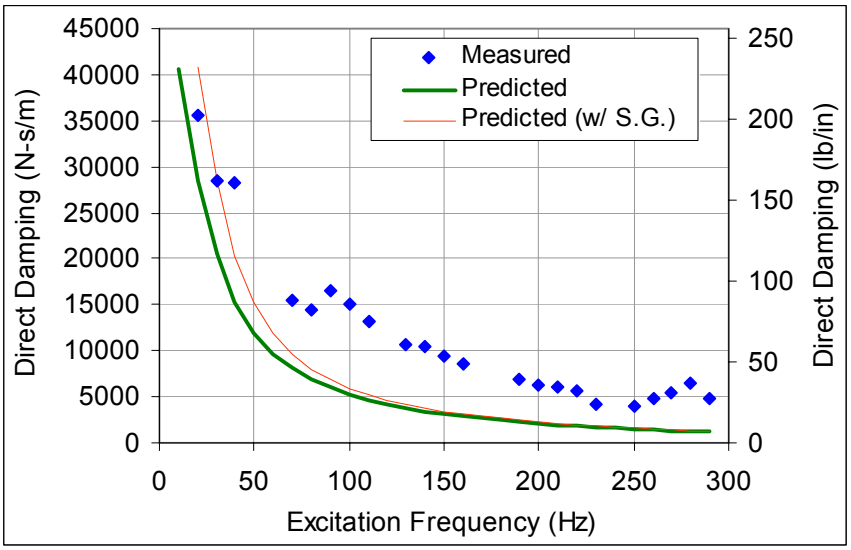

Figure 11.1 Comparisons to Ertas' PDS damping with 0.602 pressure ratio

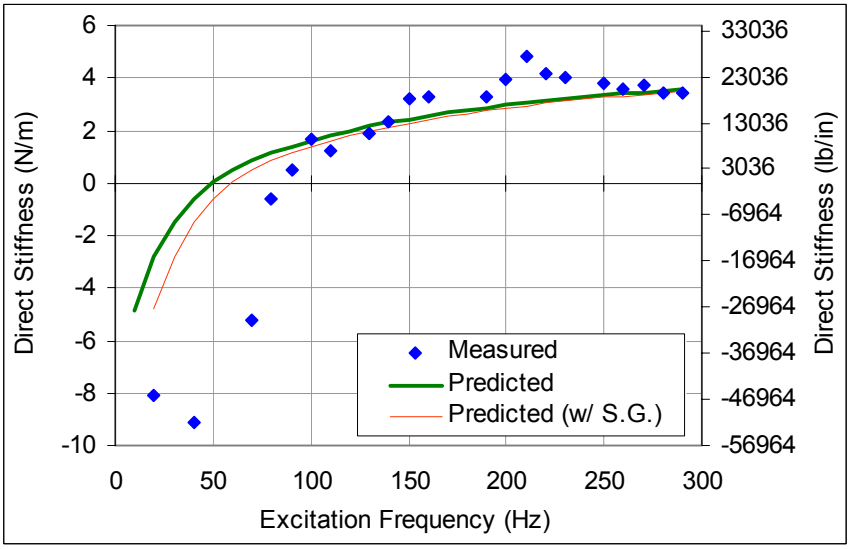

Figure 11.2 Comparisons to Ertas' PDS stiffness with 0.602 pressure ratio

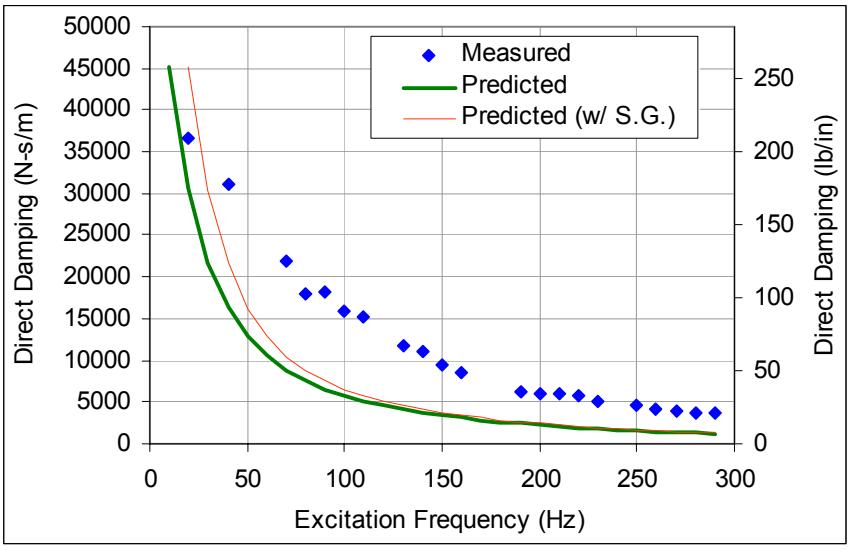

Figure 11.3 Comparisons to Ertas' PDS damping with 0.522 pressure ratio

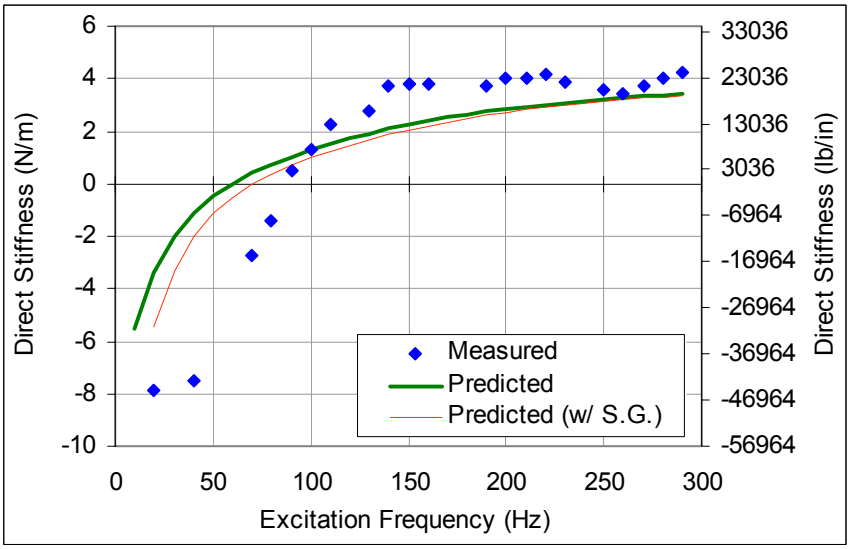

Figure 11.4 Comparisons to Ertas' PDS stiffness with 0.522 pressure ratio

POCKET DAMPER SEAL ASYMMETRY

The pocket damper seal model developed in this dissertation assumed a uniform geometry around the circumference of the seal. If, however, the size of the exit blade notches or the depths of the pockets are varied along the circumference (Figure 11.5),

the seal's stiffness and damping will differ based on the direction of excitation. In other words, the seal's rotordynamic coefficients will be orthotropic.

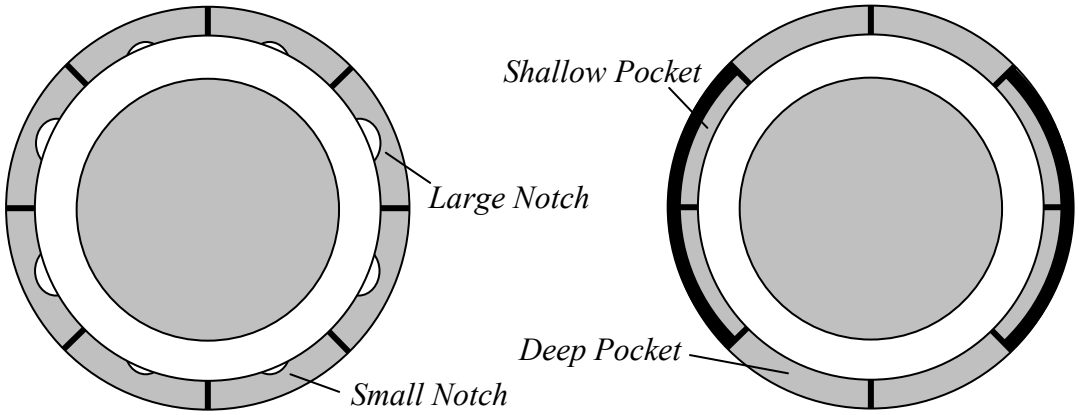

Figure 11.5 Asymmetric pocket damper seals

Figure 11.6 shows predictions for Ertas' six-bladed fully-partitioned pocket damper seal if four of the eight pockets are made shallower. For this case, the pockets along the x-direction have a pocket depth of 0.25 in (6.35 mm) and the pockets along the y-direction have the original depth of 0.56 in (14.22 mm), which creates a seal similar to the one shown in the right-hand diagram of Figure 11.5.

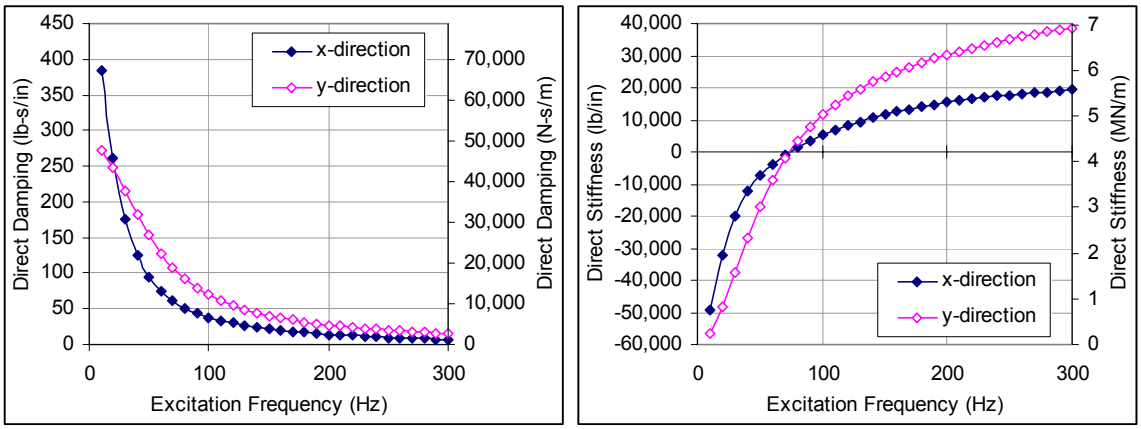

Figure 11.6 Damping and stiffness orthotropy (pocket depth asymmetry)

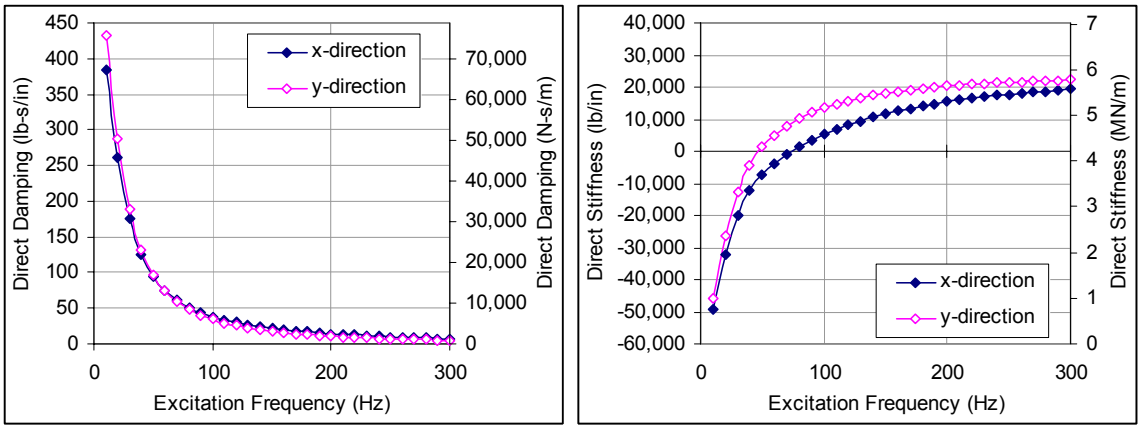

Figure 11.7 Damping and stiffness orthotropy (clearance ratio asymmetry)

Figure 11.7 shows predictions for the same seal with the original pocket depth, but with smaller exit-blade notches for the pockets in the y-direction. For this example, the effective exit clearance created by the original notches is 10 mils (0.20 mm) whereas the effective exit clearance for the y-direction notches is 7.5 mils (0.15 mm).

These two examples demonstrate that direct stiffness orthotropy, which is stabilizing, can be achieved using a pocket damper seal. Furthermore, Figure 11.7 shows that this orthotropy can be achieved with virtually no reduction in damping in either orthogonal direction. The utility of this observation may be limited because of the high damping provided by pocket damper seals; if the seal performs as it is intended to, stability is unlikely to be a problem. A much more significant achievement would be to determine a way to induce stiffness orthotropy in a labyrinth seal, which has low damping and for which the increased stability provided by stiffness orthotropy would be highly desirable.

CAVITY COEFFICIENT INTERDEPENDENCY

A major difference between fully-partitioned and conventional pocket damper seals arises from the coupled nature of the dynamic pressure equations of the fully-partitioned seals. Since the inlet and exit pressure for each cavity of a conventional pocket damper seal are constant (not modulated by rotor vibration), the stiffness and damping of each

cavity is independent of the stiffness and damping of all the other cavities. Only changes that alter the overall leakage through the seal (such as the clearance of one blade) will affect the coefficients in another cavity. For a fully-partitioned seal, however, changing the depth of a single cavity will alter the rotordynamic behavior of every other cavity in the seal. This interdependence means that minor changes to a single cavity can have significant effects on seal performance. The numerical example discussed below, which uses Ertas' six-bladed fully-partitioned seal as a starting point, demonstrates this interdependence. Assuming the seal has supply and exit pressures of 500 psi (34.46 bar) and 250 psi (17.23 bar) respectively and a uniform pocket depth of 0.15 in (3.81 mm) instead of the actual value of 0.56 in (14.22 mm) in the seal tested by Ertas, the resulting force coefficients are shown in Table 11.1.

Table 11.1 Variable pocket depth example - case 1

Cavity	Depth		Damping		Stiffness	
	(in)	(mm)	(lb-s/in)	(N-s/m)	(lb/in)	(MN/m)
1	0.15	3.81	22.5	3950	-641	-0.11
2	0.15	3.81	6.2	1088	2370	0.42
3	0.15	3.81	29.6	5196	2524	0.44
4	0.15	3.81	7.3	1282	3351	0.59
5	0.15	3.81	13.0	2282	-12609	-2.21
Overall	-	-	78.6	13798	-5005	-0.88

Table 11.2 Variable pocket depth example - case 2

Cavity	Depth		Damping		Stiffness	
	(in)	(mm)	(lb-s/in)	(N-s/m)	(lb/in)	(MN/m)
1	0.15	3.81	22.5	3950	-791	-0.14
2	0.15	3.81	6.2	1088	2322	0.41
3	0.15	3.81	29.2	5126	2128	0.37
4	0.15	3.81	7.1	1246	3239	0.57
5	0.05	1.27	10.2	1791	-13283	-2.33
Overall	-	-	75.2	13201	-6385	-1.12

Table 11.3 Variable pocket depth example - case 3

Cavity	Depth		Damping		Stiffness	
	(in)	(mm)	(lb-s/in)	(N-s/m)	(lb/in)	(MN/m)
1	0.15	3.81	22.5	3950	-489	-0.09
2	0.15	3.81	6.2	1095	2420	0.42
3	0.15	3.81	29.9	5249	2953	0.52
4	0.15	3.81	7.4	1299	3475	0.61
5	0.25	6.35	15.3	2686	-11707	-2.06
Overall	-	-	81.3	14279	-3348	-0.59

For this seal, almost two-thirds of the negative stiffness comes from the last cavity. Had this been a conventional seal, reducing the depth of the final cavity would have increased the stiffness (making it less negative) and would have reduced the direct damping of the final cavity alone. However, for this fully-partitioned seal, reducing the depth of the last cavity to 0.05 in (1.27 mm) had the opposite effect on stiffness, as shown in Table 11.2. Trying the opposite, and increasing the depth of the last cavity to 0.25 in (6.35 mm), not only makes the stiffness less negative, but also increases the damping (Table 11.3). Further increasing the depth to 0.5 in (12.7 mm) completely eliminates the negative stiffness and results in even higher damping (Table 11.4). It would be incorrect to assume that increasing pocket depth automatically implies an increase in damping and a reduction in negative stiffness. As shown in Table 11.5, increasing the depth of *all* the blades to 0.25 in (6.35 mm) results in significantly lower damping than that calculated for the initial design. Further increasing *all* the cavity depths to 0.5 in (12.7 mm) results in low positive stiffness, but also lowers the damping below that for any of the other designs (Table 11.6).

Table 11.4 Variable pocket depth example - case 4

Cavity	Depth		Damping		Stiffness	
	(in)	(mm)	(lb-s/in)	(N-s/m)	(lb/in)	(MN/m)
1	0.15	3.81	22.2	3897	-157	-0.03
2	0.15	3.81	6.2	1088	2530	0.44
3	0.15	3.81	29.7	5214	3997	0.70
4	0.15	3.81	7.4	1299	3790	0.67
5	0.50	12.70	19.1	3353	-8869	-1.56
Overall	-	-	84.6	14852	1291	0.23

Table 11.5 Variable pocket depth example - case 5

Cavity	Depth		Damping		Stiffness	
	(in)	(mm)	(lb-s/in)	(N-s/m)	(lb/in)	(MN/m)
1	0.25	6.35	16.5	2898	749	0.13
2	0.25	6.35	4.4	772	2759	0.48
3	0.25	6.35	19.1	3360	4315	0.76
4	0.25	6.35	4.7	817	3801	0.67
5	0.25	6.35	13.3	2327	-11678	-2.05
Overall	-	-	58.0	10175	-54	-0.0095

Table 11.6 Variable pocket depth example - case 6

Cavity	Depth		Damping		Stiffness	
	(in)	(mm)	(lb-s/in)	(N-s/m)	(lb/in)	(MN/m)
1	0.50	12.70	8.9	1562	695	0.12
2	0.50	12.70	2.0	353	2700	0.47
3	0.50	12.70	6.7	1182	3059	0.54
4	0.50	12.70	1.4	253	3520	0.62
5	0.50	12.70	15.7	2751	-9835	-1.73
Overall	-	-	34.8	6101	139	0.02

Changing pocket depths of single cavities (same depth for all pockets around one cavity) can significantly impact the performance of fully-partitioned pocket damper seals and can be used as an added design factor. While non-uniform pocket depths also influenced the coefficients of conventional seals, the effect is far more significant in the case of fully-partitioned configurations. This is at least in part due to the fact that changing the depth of one pocket in a conventional PDS changes only the coefficients of *that* pocket. However, changing the depth of one pocket in a fully-partitioned PDS changes the coefficients of *all* the pockets because of the coupled dynamic pressure equations.

FULLY-PARTITIONED PDS MODEL COMPARISON

The models developed in this thesis are identical to the one developed by Ertas for six-blades seals except for three factors; a more accurate modulated clearance area calculation is used, the model is not limited to seals with six blades, and the model is not limited to seals with four pockets. Several trial runs of both models were conducted and

the current code was found to predict between 10% and 20% higher damping than Ertas' model for seals of similar geometry to those he tested with similar pressure conditions. The difference between the two models was higher that 20% for low frequencies (up to 30 Hz). Since both models significantly under-predicted the measured damping, the higher predictions of the current model can be considered to be more accurate.

CHAPTER XII

CONCLUDING SUMMARY

The following points summarize the topics covered in this dissertation and the results that were presented. This dissertation discussed background work on the leakage characteristics and rotordynamic effects of pocket damper seals and see-through labyrinth seals, presented and evaluated theoretical models for labyrinth seal leakage and pocket damper seal force coefficients, and presented comparisons of these seals to other annular gas seals. Newly-obtained low-pressure results were used along with previously-published high-pressure labyrinth and pocket damper seal data to evaluate the models discussed. Also presented were comparisons of conventional and fully-partitioned pocket damper seal rotordynamic and leakage data to those of honeycomb, labyrinth, hole-pattern, and smooth annular seals.

TEST SUMMARY

Three categories of seal tests were discussed in this dissertation. High-pressure labyrinth seals were tested by Picardo at supply pressures of up to 1000 psi (69 bar). Two seals were tested; one with a 0.1 mm radial clearance and one with a 0.2 mm radial clearance. High-pressure pocket damper seals were tested by Gamal and by Ertas. Both straight-through (non-diverging) and diverging eight-bladed seal configurations and flat-tipped and beveled six-bladed seal configurations were tested at supply pressures of up to 1000 psi (69 bar). Both the high-pressure labyrinth seal and pocket damper seal leakage data presented correspond to pressure ratios (back pressure over supply pressure) of approximately 0.5. The third category involved low-pressure tests of labyrinth seals and pocket damper seals with different geometries. These seals were initially tested with atmospheric back pressure and supply pressures of up to 100 psi (6.9 bar). To provide data at more relevant pressure ratios, four of these seals were retested at supply pressures of 125 psi and 170 psi and pressure ratios ranging from 0.4 to 0.6.

EFFECTS OF SEAL DESIGN FACTORS

The effects of varying blade profile and blade thickness on the leakage through see-through labyrinth seals and pocket damper seals were examined. This was accomplished using a set of non-rotating tests on two-, three-, four-, five-, and six-bladed seals. The seals were tested both in the centered and off-center positions in order to examine the effect of eccentricity.

- Tests carried out to determine the effect of blade thickness showed that doubling the thickness of the blades reduced leakage rates by up to 20% for certain test configurations.
- Once the flat-tipped seals were tested, bevels were machined into the blades in order to examine the effect of blade profile. These tests produced more equivocal results; one set of tests showed that flat-tipped blades were more effective in limiting leakage, while tests on older hardware showed that downstream-beveled blades were more effective. Results indicated that both blade profile and blade thickness could be manipulated to reduce seal leakage, but that the influence of one of these parameters can, to some extent, negate the influence of the other (especially in cases with tighter clearances).
- Blade profile results, together with the results of the blade thickness tests, led to the conclusion that while both factors can be used to improve seal leakage performance, they can also work counter to each other in some cases, especially if the clearances are small.
- Tests showed that operating a seal eccentrically had the effect of increasing the leakage through the seal. This phenomenon was considerably more pronounced at lower supply pressures.
- Flow-rate measurements made during the first round of cavity depth tests showed virtually no change in leakage rates when the cavity depth was decreased from 0.5-in to 0.1-in (from 12.7 mm to 1.27 mm), while cavity pressure tests indicated a minor improvement in performance in the case of the deeper cavities. Installing the cavity

insert corresponded to an 80% reduction in cavity depth, but only led to increases in leakage rates of less than 1% for most supply pressures and less than 5% for the highest changes at the lowest supply pressures. The second round of tests showed that cavity depth did indeed have an effect on leakage, but that this effect was only apparent when the cavities are made very shallow. Reducing the cavity depth by 90% to 50 mils (1.97 mm) reduced leakage in both four-bladed and five-bladed labyrinth seals. Reducing the cavity depth by 96% to 20 mils (0.79 mm) caused a drop in leakage for the four-bladed seal, but a small increase in leakage for the five-bladed seal. While this increase was close to negligible, it may indicate that 20 mil (0.79 mm) cavity depth was shallower than the optimum value for the five-bladed seal in terms of leakage.

- Blade thickness was found to have a larger effect on labyrinth and pocket damper seal leakage than all the other design parameters except blade thickness. Test results showed that increasing cavity pitch reduced leakage by 8% (at high supply pressures) to 16% (at low supply pressures). This was considerably more significant than either the effect of cavity depth or blade profile. Similar results were obtained by Egli [43] in 1935 on seals with considerably larger clearances. In 1939, Hodkinson [47] explained this phenomenon and accounted for it by using a kinetic energy carry-over coefficient. Furthermore, a four-bladed seal with short blade pitch was demonstrated to leak almost exactly as much as a three-bladed seal with a longer pitch, indicating that blade spacing can, in some instances, be as important a factor as the number of blades when it comes to leakage reduction. This point is especially of value to users of pocket damper seals, which often have to increase blade spacing and reduce the number of blades to obtain desired rotordynamic force coefficients.
- The effect of partition walls was also examined by comparing conventional and fully-partitioned pocket damper seals. The latter were found to leak less and this trend was observed at all supply pressures.

CAVITY PRESSURE DISTRIBUTIONS

Cavity pressure measurements were also made for the low-pressure labyrinth and pocket damper seals. Test data was used to calculate pressure drops across both the blades and the cavities. The latter values are particularly important for pocket damper seal analysis since the rotordynamic coefficients of a single cavity are highly-dependent on the pressure drop across that cavity.

- The drop in pressure across the first *blade* of the seal was large relative to pressure drops across the interior blades of the seal. The fraction of the overall pressure that was dropped across the first blade is highest at low supply pressures and decreased at higher pressures. Conversely, the amount by which the pressure dropped across the last blade was greater than that dropped across the interior blades and increased with increasing supply pressure.
- The pressure drop was found to be initially highest across the first *cavity*, but as the supply pressure is increased, the pressure distribution became parabolic and eventually, the highest pressure drop was across the last blade. This means that for pocket damper seals with high pressure drops, it is desirable to increase the pitch of the last cavity at the expense of the other cavities (especially the interior cavities). For a constrained seal length, increasing the length of the final cavity requires a drop in the length of some of the other cavities. Since the pressure drop across the interior cavities is lower, the drop in damping cause by a reduction in their length would not outweigh the rise in damping caused by an increase in the length of the final cavity.
- The previous point also suggests a method of improving PDS leakage performance. Since the lengths of the interior cavities (and the first cavity for higher pressure drops) have a less significant effect on the rotordynamics of the seal, the lengths of these cavities can be reduced to make room for extra blades. It is important, however, that any reduction in blades not decrease the pitch to the point where blade spacing effects come into play and cause an increase in leakage.

LEAKAGE MODEL EVALUATION

Three base equations; the St. Venant Equation, Martin's Equation, and Neumann's Equation; were examined. These equations were combined with two flow contraction coefficients (a constant value for Esser and Kazakia and a geometry-dependent value for Chaplygin), which account for reduced effective clearance, at the vena contracta. The equations were also combined with four kinetic energy carryover coefficients (developed by Hodkinson, Neumann, Vermes, plus a modified form of Hodkinson's coefficient). In total, thirteen leakage equations were examined.

- The equations taken from the literature and the modified equations suggested were evaluated through comparisons to leakage and cavity pressure measurements made on low-pressure labyrinth seals and to previously published results for high-pressure labyrinth and pocket damper seals. Each equation was evaluated based on the accuracy with which it can predict the rates of flow through the seals, the distribution (or trend) of the static cavity pressures along the seals, and the effects of varying seal design parameters.
- Use of Chaplygin's flow coefficient was found to consistently result in significant under-predictions of the leakage through the seals. For several of the models evaluated, using Esser and Kazakia's constant value or using no flow coefficient at all resulted in more accurate predictions than Chaplygin's coefficient.
- The models based on the St. Venant Equation and on Neumann's Equation are iterative, and calculate cavity pressures consecutively, starting from the upstream end of the seal. Martin's Equation is a single-application model that uses the overall number of blades and the inlet and exit pressures to calculate the flow-rate through a seal. This equation does not explicitly calculate intermediate pressures, and so if cavity pressures are required, the equation must be applied (using the previously calculated flow-rate) to a series of one-bladed seals, thereby calculating each cavity pressure as the exit pressure of one of these one-bladed seals. The model developed by Zimmerman and Wolf is a two-step model which uses the St. Venant Equation for

the first blade and Martin's Equation for the remainder of this seal. This equation also does not directly provide intermediate cavity pressures.

- The kinetic energy carryover coefficients suggested by Hodkinson, Vermes, and Neumann, all predict a higher pressure drop across the first blade of the seal. This is followed by a sharp drop in leakage across the second blade and gradually increasing drops across the subsequent blades. The initial sharp drop was caused by all three coefficients using one value for the first blade and a constant value for the remaining blades. A modified form of Hodkinson's coefficient, which differs from blade to blade, was suggested in this dissertation. This was initially an attempt to smooth the pressure distribution and to show that there is a gradual reduction in pressure drop progressively across the first few blades. This coefficient was also found to more accurately predict the pressure drop distribution at the downstream end of the seal and to produce a flatter pressure drop distribution across the interior blades. For higher pressure drops, the distribution became parabolic, with the pressure across the final blades exceeding that across the initial blade. For lower pressure drops, the pressure drop distribution gradually decayed from the initial pressure drop across the first blade. Both these trends matched the low-pressure measurements, whereas the other three carry-over coefficients used showed a sharp reduction in pressure drop followed by a steady increase regardless of the pressure differential across the seal.
- Models based on Neumann's, Vermes', and the modified form of Hodkinson's carry-over coefficient all predicted the effect of changing blade spacing by within 7%. Hodkinson's original coefficient was found to be the least accurate in predicting this effect. The measured trend showing that the effect of blade thickness drops rapidly and then asymptotes to a lower value as the pressure ratio approaches 1 was predicted by the equations, and their accuracy remained almost constant as the inlet pressure was increased for a given back pressure.
- Unlike pitch effects, blade thickness effects were not accurately predicted by any of the evaluated models. Blade thickness is only taken into consideration by these models in geometric terms (in determining the flow coefficients) and not in terms of

a frictional resistance to flow. The equations that under-predicted the leakage rates through Picardo's high-pressure labyrinths were the same equations that most-accurately predicted the leakage through the low-pressure labyrinths. This is at least partially due to the increased thickness of the blades of the low-pressure seals and the leakage models that most accurately predicted the leakage rates through the high-pressure seals over-predicted the leakage through the low-pressure seals by up to 50%. Using a flow coefficient based on a coefficient of friction calculation (as suggested by Bell and Bergelin) showed that the equations that accurately predicted flow through Picardo's seals would result in reasonable predictions for the low pressure seals if frictional effects had been accounted for. The calculation method put forward by Bell and Bergelin adds a degree of complexity to the model because it would require incorporating the empirical variation of friction factor with Reynolds Number into the iterative model. It should also be noted that the calculated coefficient resulted in an under-prediction of the flow through the thicker blades. For this reason, this coefficient was not included in the models, but was simply calculated for both thin and thick blades to demonstrate the effect of blade thickness.

- Vermes' kinetic energy carryover coefficient was found to provide slightly better results than that of Neumann, but this improvement was not large. Use of the St. Venant Equation or of Neumann's Equation provided comparable results as long as the appropriate coefficients were used. Using a constant coefficient, such as the 0.716 value used by Esser and Kazakia, compensated for the over-prediction caused by using the modified form of Hodkinson's carryover coefficient. This resulted in an equation (MOD 1) that predicted leakage rates reasonably well, while also accurately predicting the distribution of pressure drops across the blades. Without such a coefficient, MOD 1 would not be as attractive a choice as Vermes' model, MOD 2 or MOD 4, which better predict flow-rates without flow coefficients, even if they do not accurately predict the pressure drop distributions.
- Examination of Reynolds Numbers explained the difference in model prediction accuracy for different seals. For example, the differences in Re values for the two

seals tested by Picardo explain why Vermes' Equation, Esser and Kazakia's Equation, MOD 1, and MOD 4 predicted the leakage through Seal A with high accuracy, but under-predicted the leakage through Seal B.

ANNULAR GAS SEAL COMPARISONS

Comparisons were made between previously-tested high-pressure labyrinth seals, pocket damper seals (both conventional and fully-partitioned), hole-pattern seals, honeycomb seals, and smooth annular seals. Normalized results were presented for effective damping, direct stiffness, and leakage for these seal types.

- For similar operating conditions, pocket damper seals have comparable damping to hole-pattern and honeycomb seals at excitation of approximately 70 Hz to 100 Hz. At lower frequencies the effective damping of pocket damper seals is higher than that for the other two seal types. For hole-pattern and honeycomb seals, the effective damping drops rapidly and becomes negative at low frequencies. For pocket damper seals, however, this damping decreases as the excitation frequency increases. The damping of the six-bladed fully-partitioned pocket damper seal that was analyzed was higher than that of the conventional pocket damper seals for the same pressure conditions.
- The negative stiffness values associated with conventional pocket damper seals can be a disadvantageous feature since they can reduce the first system eigenvalue and therefore drop the onset speed of instability. There is however, a cross-over frequency beyond which the stiffness becomes positive. For fully-partitioned pocket damper seals, this frequency can be lowered, and seals that do not exhibit any negative stiffness can be designed. For the conventional seals that were studied, cross-over frequencies did not fall within the 300 Hz test range, but a cross-over frequency of about 85 Hz was seen for the fully-partitioned seal. Furthermore, the magnitude of negative stiffness of a diverging, conventional PDS would be small compared to the rotor-bearing support stiffness for most applications (unless the

rotor is very softly supported or if the pressure drop across the seal is extremely high).

POCKET DAMPER SEAL ROTORDYNAMICS

The existing fully-partitioned pocket damper seal model, which had been developed for the specific case of a six-bladed seal, was expanded to accommodate seals with any number of blades and geometries. This model was implemented in the form of a design and analysis code that can be used to analyze leakage behavior and rotordynamic force coefficients of pocket damper seals. This code can be used to determine optimum blade clearances and pocket depths for a set of geometric constraints and operating conditions, examine the effect of primary to secondary pitch ratios and the number of pockets, and analyze the pressure-dependent and frequency-dependent behavior of a fully-partitioned seal.

- In addition to removing limitations on the number of blades, the model developed used a more accurate calculation of the modulation of the clearance area resulting from journal displacement. This resulted in a minor improvement of the damping prediction over the original six-bladed seal model.
- Asymmetric stiffness or pocket depth were shown, computationally, to result in stiffness and damping orthotropy in fully-partitioned pocket damper seals. Seals can be designed to have significant stiffness orthotropy (thereby improving rotordynamic stability) while minimizing damping (so that the seal has the maximum possible amount of damping in all directions).
- The coupled nature of the dynamic pressure equations for a fully-partitioned pocket damper seal resulted in cavity force coefficients that were interdependent. For a conventional seal, changing the geometry of one cavity (as long as the change is not a change in clearance, which would change the overall flow-rate through the seal) would not affect the other cavities in the seal. This is not true for fully-partitioned seals, in which changing one cavity (for example increasing its depth) would affect the damping and stiffness contributions of all the other cavities in the seal. This

interdependency meant that the optimum pocket depth of a fully-partitioned seal was found to be considerably smaller than that for a conventional seal. Another manifestation of the interdependency of the cavity coefficients on one another is that pitch ratio and clearance ratio effects are considerably more difficult to understand for a fully-partitioned PDS than for a conventional PDS.

- Fully-partitioned pocket damper seals were also found to differ from conventional pocket damper seals with respect to sensitivity to changes in clearance ratio. In the case of a uniform rub, which might eliminate the notches of a pocket damper seal, the damping of a conventional seal would drop much more drastically than that of a fully-partitioned seal, which produces significant damping even with a straight-through (non-diverging) configuration. Fully-partitioned seals, however, are more sensitive to changes to the downstream blades and cavities. For instance while a rub that results in a converging seal would be detrimental to both a conventional and a fully-partitioned seal's performance, a manufacturing error that results in a clearance convergence in the last cavity alone would have a much higher impact on a fully-partitioned seal. Conversely, increasing the notch size for the exit blade of a fully-partitioned seal would also have a much higher impact on a fully-partitioned seal (greatly increasing its damping) than on a conventional seal (only slightly increasing its damping).
- A fully-partitioned PDS can be designed to minimize, or completely eliminate, the negative stiffness usually associated with pocket damper seals. This means that the optimization process, which for conventional pocket damper seals was a matter of maximizing damping, becomes a search for a balance between high damping and low negative (or even positive) stiffness for a fully-partitioned seal.

OUTSTANDING POINTS

The following points arose during the course of the research described in this dissertation but were not addressed. Investigation of these points would require further experimental with variable-geometry equipment.

- A frictional flow resistance should be incorporated into the flow prediction models to account for flow across the thick blades that are a common feature of pocket damper seals and across the seal partition walls. An approach similar to that developed by Bell and Bergelin can be incorporated into the model.
- The accuracy of the model predictions has been shown to be sensitive to Reynolds number. This suggests that a model such as the one developed by Sriti et al., which incorporates Re-dependent flow coefficients, should be considered more closely.
- Since the flow contraction through the vena contracta reduces leakage and creates a smaller effective clearance, the effect of this on the clearance-dependent dynamic pressures (and therefore on force coefficients) should be examined.
- Both the current fully-partitioned model and the model developed by Ertas predict a much shallower depth at which damping is maximized than were predicted for conventional seals. These optimum depths would need to be verified experimentally.

NOMENCLATURE

A_i	Clearance area of the ith constriction [L^2]
A_s	Pocket sector area within seal blade boundary [L^2]
A_{r1}	Pocket sector area within centered rotor boundary [L^2]
A_{r2}	Pocket sector area within displaced rotor boundary [L^2]
ΔA	Change in pocket sector area within rotor boundary [L^2]
b_i	Base thickness of the ith blade [L]
C	Direct damping [(F·t)/L]
C^*	Normalized direct damping [t]
Cf	Flow contraction coefficient [-]
Cr_i	Radial clearance of the ith constriction [L]
d	Journal diameter [L]
f_P	Coefficient of friction [-]
h_i	Depth of the ith cavity [L]
K	Direct stiffness [F/L]
K^*	Normalized direct stiffness [-]
L_i	Length of the ith cavity [L]
$\dot{m}_i$	Mass flow-rate through the ith constriction [M/t]
n	Number of seal blades [-]
N	Number of seal pockets [-]
P_i	Pressure in the ith cavity [F/L^2]
P_{in}	Seal inlet pressure [F/L^2]
P_{out} *or* P_{exit}	Seal exit pressure [F/L^2]
PR	Ratio of seal inlet to exit pressures [-]
ΔP	Pressure drop across the seal [F/L^2]
r_s	Coordinate of seal blade boundary [L]
r_{r1}	Coordinate of centered rotor boundary [L]

r_{r2}	Coordinate of displaced rotor boundary [L]
R	Gas constant [(F·L)/(M·T)]
Re	Reynolds Number [-]
s_i	Distance between centers of two consecutive blades [L]
t	Time [t]
t_i	Blade tip thickness [L]
T_i	Temperature in the i^{th} cavity [T]
u_{cav}	Velocity of fluid in the i^{th} cavity [L/t]
u_i	Velocity of fluid passing through the i^{th} constriction [L/t]
V_i	Volume of the i^{th} cavity [L^3]
x	Journal displacement [L]
x, y	Displacement directions [-]
z	Height above reference line [L]
Z	Ratio of blade tip thickness to radial clearance [-]

Greek Symbols

δ	Static journal displacement [L]
φ	Dimensionless flow coefficient [-]
γ	Ratio of specific heat values [-]
μ_i	Kinetic energy carryover coefficient for the i^{th} constriction [-]
ρ_i	Density of fluid in the i^{th} cavity [M/L^3]
ω	Frequency of excitation [1/t]

Dimensions

F	Force
L	Length
M	Mass
t	Time
T	Temperature

REFERENCES

[1] Tiwari, R., Manikandan, S., and Dwivedy, S. K., 2005, "A Review of the Experimental Estimation of the Rotor Dynamic Parameters of Seals," Shock & Vibration Digest, **37**, (4), pp. 261-284

[2] Hendricks, R. C., Tam, L. T., and Muszynska, A., 2004 (July), "Turbomachine Sealing and Secondary Flows Part 2 - Review of Rotordynamics Issues in Inherently Unsteady Flow Systems With Small Clearances," NASA Report NASA/TM-2004-211991/PART2

[3] Martin, January 19, 1908 H. M., "Labyrinth Packings," Engineering, pp. 35-36

[4] Childs, D. W. and Vance, J. M., 1997, "Annular Gas Seals and Rotordynamics of Compressors and Turbines," Proceedings of 26th Turbomachinery Symposium, Texas A&M University, College Station, TX, pp. 201-220

[5] Alford, J. S., October 1965, "Protecting Turbomachinery from Self-Excited Rotor Whirl," ASME Journal of Engineering for Power, pp. 333-334

[6] Benckert, H., and Wachter, J., 1980, "Flow Induced Spring Coefficients of Labyrinth Seals for Applications in Rotordynamics," IMechE Proceedings of the 2nd International Conference on Vibrations in Rotating Machinery, Cambridge, England, pp. 53-63

[7] Childs, D. W. and Scharrer, J., 1986, "Experimental Rotordynamic Coefficient Results for Teeth-on-Rotor and Teeth-on-Stator Labyrinth Gas Seals," Journal of Engineering for Gas Turbines and Power, **108**, pp. 599-604

[8] Childs, D. W. and Scharrer, J., 1988, "Theory versus Experiment for the Rotordynamic Coefficient of Labyrinth Gas Seals: Part II – A Comparison to Experiment," Journal of Vibration, Acoustics, Stress and Reliability in Design, **110**, pp. 281-287

[9] Pelletti, J., 1990, "A Comparison of Experimental Results and Theoretical Predictions for the Rotordynamic Coefficients of Short (L/D = 1/6) Labyrinth Seals," MS thesis, Texas A&M University

[10] Wyssmann, H., Pham, T., and Jenny, R., 1984, "Prediction of Stiffness and Damping Coefficients for Centrifugal Compressor Labyrinth Seals," Journal of Engineering for Power, Paper No. 84-GT-86

[11] Wagner, N. G., Steff, K., 1996, "Dynamic Labyrinth Coefficients from a High-Pressure Full-Scale Test Rig Using Magnetic Bearings," Proceedings of the Conference on Rotordynamic Instability Problems in High-Performance Turbomachinery, NASA Conference Publication, no. 3344, pp. 95-111

[12] Picardo, A. and Childs, D. W., October 2005, "Rotordynamic Coefficients for a Tooth-on-Stator Labyrinth Seal at 70 Bar Supply Pressures: Measurements Versus Theory and Comparisons to a Hole-Pattern Stator Seal," ASME Journal of Engineering for Gas Turbines and Power, **127**, pp. 843-855

[13] Hirs G. G., 1973, "Bulk-Flow Theory for Turbulence in Lubricant Films," Journal of Lubrication Technology, Transactions of the ASME, **95** (2), pp. 137-146

[14] Iwatsubo, T., 1980, "Evaluation of Instability of Forces of Labyrinth Seals in Turbines or Compressors," Workshop on Rotordynamic Instability Problems in High-Performance Turbomachinery, Texas A&M University, NASA Conference Publication No. 2133, pp. 139-167

[15] Childs, D. W., 1993, *Turbomachinery Rotordynamics – Phenomena, Modeling, and Analysis*, John Wiley & Sons, New York

[16] Nelson, C., 1985, "Rotordynamic Coefficients for Compressible Flow in Tapered Annular Seals," ASME Journal of Tribology, **107**, pp. 318-325

[17] Childs, D. W. and Scharrer, J., 1986, "Iwatsubo-Based Solution for Labyrinth Seals: Comparison to Experimental Results," Journal of Engineering for Gas Turbines and Power, Transactions of the ASME, **108**, pp. 325-331

[18] Scharrer, J., 1988, "Theory Versus Experiment for the Rotordynamic Coefficient of Labyrinth Gas Seals: Part I – A Two Control Volume Model," Journal of Vibration, Acoustics, Stress and Reliability in Design, **110**, pp. 270-280

[19] Nordmann, R. and Weiser, H., 1988, "Rotordynamic Coefficients for Labyrinth

Seals Calculated by Means of a Finite Difference Technique," Workshop on Rotordynamic Instability Problems in High Performance Turbomachinery, Texas A&M University, pp. 161-175

[20] Rhode, D. L., Hensel, S. J., and Guidry, M. J., 1993 (July), "Three-Dimensional Computations of Rotordynamic Force Distributions in a Labyrinth Seal," Tribology Transactions, **36**, pp. 461-469

[21] Moore, J. J., 2003, "Three-Dimensional CFD Rotordynamic Analysis of Gas Labyrinth Seals," Journal of Vibration and Acoustics, **125** (4), pp. 427-433

[22] Kirk, G. R. and Guo, Z., 2006 (September), "Labyrinth Seal Forces for a High Speed Centrifugal Impeller Eye Seal", 7th IFToMM Conference on Rotor Dynamics, Vienna, Austria

[23] Murphy, B. T., and Vance, J. M., 1980, "Labyrinth Seal Effects on Whirl Instability," IMechE Proceedings, C306/80, pp. 369-373

[24] Lund, J. W., 1974, "Stability and Damped Critical Speeds of a Flexible Rotor in Fluid Film Bearings," ASME Journal of Engineering for Industry, **96**, pp. 509-517

[25] Vance, J. M., and Shultz, R. R., 1993, "New Damper Seal for Turbomachinery," Proceedings of the 14th Vibration and Noise Conference, ASME, Vibration of Rotating Systems, **60**, pp. 139-148

[26] Sundararajan, P., and Vance, J. M., 1995, "A Theoretical and Experimental Investigation of a Gas-Operated Bearing Damper for Turbomachinery - Part I & II: Experimental Results and Comparison with Theory," ASME Journal of Engineering for Gas Turbines and Power, **117**, pp. 742-756

[27] Shultz, R. R., 1996, "Analytical and Experimental Investigation of a Labyrinth Seal Test Rig and Damper Seals for Turbomachinery," M.S. thesis, Mechanical Engineering Department, Texas A&M University, College Station, TX

[28] Li, J., and Vance, J. M., 1995, "Effects of Clearance and Clearance Ratio on Two and Three Bladed TAMSEALs," Turbomachinery Research Consortium, TRCSeal-4-95, Turbomachinery Laboratory, College Station, TX

[29] Vance, J. M. and Li, J., October 1996, “Test Results of a New Damper Seal for Vibration Reduction in Turbomachinery,” ASME Transactions, Journal of Engineering for Gas Turbines and Power, **118**, pp. 843-846

[30] Richards, R. L., Vance, J. M., and Zeidan, F. Y., 1995, “Using a Damper Seal to Eliminate Subsynchronous Vibrations in Three Back to Back Compressors,” Proceedings of the 24th Turbomachinery Symposium, Texas A&M University, College Station, TX, pp. 59-71

[31] Ransom, R. L., Li, J., San Andres, L., and Vance, J. M., 1999, “Experimental Force Coefficients for a Two-Bladed Labyrinth Seal and a Four-Blade Pocket Damper Seal,” ASME Journal of Tribology, **121**, pp. 370-376

[32] Laos, H. E., 1999, “Rotordynamic Effects of Pocket Damper Seals,” Ph.D. dissertation, Mechanical Engineering Department, Texas A&M University, College Station, TX

[33] Li, J., Kushner, F. and De Choudhury, P., 2002, “Experimental Evaluation of Slotted Pocket Gas Damper Seals on a Rotating Test Rig,” Proceedings of ASME Turbo Expo, 47th International Gas Turbine & Aeroengine Technical Congress, Exposition & User Symposium, pp. 1125-1138

[34] Armstrong, J. and Perricone, F., 1996, “Turbine Instability Solution - Honeycomb Seals,” Proceedings of the 25th Turbomachinery Symposium, Texas A&M University, College Station, TX, pp. 47-56

[35] Vance, J. M., Sharma, A., and Jayakar, N., 2002, "Effect of Frequency and Design Parameters on Pocket Damper Seal Performance," Proceedings of Fluid Structure Interactions, New Orleans, LA, **23**, pp. 208–217

[36] Li, J., San Andres, L., Aguilar, R., and Vance, J. M., 2000 “Dynamic Force Coefficients of a Multiple-Blade, Multiple-Pocket Gas Damper Seal: Test Results and Analytical Validation,” ASME Journal of Tribology, **122** (1), pp. 317-322

[37] Sharma, A., 2001, “Experimental Determination of Dynamic Force Coefficients of a Pocket Damper Seal at Higher Frequencies,” M.S. thesis, Mechanical Engineering Department, Texas A&M University, College Station, TX

[38] Bhamidipati, L. N. K. S., 2003, "Rotordynamic Evaluation of Hybrid Damper Seals with Metal Mesh Elements," M.S. thesis, Mechanical Engineering Department, Texas A&M University, College Station, TX

[39] Kannan, B., 2003, "Development and Validation of an Analytical Model for the Notched Pocket Damper Seal," M.S. thesis, Mechanical Engineering Department, Texas A&M University, College Station, TX

[40] Gamal, A. M., 2003, "Analytical and Experimental Evaluation of the Leakage and Stiffness Characteristics of High Pressure Pocket Damper Seals," M.S. thesis, Mechanical Engineering Department, Texas A&M University, College Station, TX

[41] Ertas, B. H., 2005, "Rotordynamic Force Coefficients of Pocket Damper Seals," Ph.D. dissertation, Mechanical Engineering Department, Texas A&M University, College Station, TX

[42] Stodola, A., 1945, *Steam and Gas Turbines*, Translated by Loewenstein, L. C., vol. 1, Peter Smith, New York

[43] Egli, A., 1935, "The Leakage of Steam through Labyrinth Seals," Transactions of the ASME, **57**, pp. 115-122

[44] Spurk, J. H., 1997, *Fluid Mechanics*, Springer-Verlag, Berlin

[45] Friedrich, H., October 1933, "Untersuchungen ueber das Verhalten der Schaufelspaltdichtungen in Gegenlauf-Dampfturbinen," Mitteilungen aus den Forschungsanstalten GHH-Konzern, **2** (8), pp. 198-234

[46] Keller, C., 1937, "Flow Through Labyrinth Glands," Power Plant Engineering, **41** (4), pp. 243-245

[47] Hodkinson, B., 1939, "Estimation of the Leakage through a Labyrinth Gland," Proceedings of the Institution of Mechanical Engineers **141**, pp. 283–288

[48] Bell, K. J. and Bergelin, O. P., 1957 (April), "Flow Through Annular Orifices," ASME Transactions, **79** (3), pp. 593-601

[49] Zimmerman, H. and Wolff, K. H., 1987, "Comparison between Empirical and Numerical Labyrinth Flow Correlations," ASME 87-GT-86

[50] Wittig S., Schelling, U., Kim, S., and Jacobsen, K., 1987, "Numerical Predictions and Measurements of Discharge Coefficients in Labyrinth Seals," ASME 87-GT-188

[51] Morrison, G. L. and Rhode, G. L., 1992 (November), "Measured Effect of Step Axial Location on Labyrinth Seal Leakage," Journal of Propulsion and Power, **8** (6), pp. 1129-1130

[52] Gamal, A. M., Ertas, B. H., and Vance, J. M., 2006 (May), "High-Pressure Pocket Damper Seals: Leakage Rates and Cavity Pressures," Proceedings of the ASME IGTI Turbo Expo, Barcelona, Spain, GT2006-90585, pp. 1003-1012

[53] Vermes, G., 1961 (April), "A Fluid Mechanics Approach to the Labyrinth Seal Leakage Problem," ASME Transactions - Journal of Engineering for Power, **83** (2), pp. 161-169

[54] Whalen, J. K., Alvarez, E., and Palliser, L. P., 2004, "Thermoplastic Labyrinth Seals for Centrifugal Compressors," Proceedings of the 33rd Turbomachinery Symposium, Texas A&M University, College Station, TX, pp. 113-125

[55] Picardo, A. M., 2003, "High Pressure Testing of See-Through Labyrinth Seals," M.S. thesis, Mechanical Engineering Department, Texas A&M University, College Station, TX

[56] Vennard, J. K. and Street, R. L., 1982, *Elementary Fluid Mechanics*, John Wiley & Sons, New York

[57] Gurevich, M. I., 1965, Theory of Jets in an Ideal Fluid, Translated by Street, R. L. and Zagustin, K., Academic Press, New York

[58] Dereli, Y. and Eser, D., 2004, "Flow Calculations in Straight-Through Labyrinth Seals by Using Moody's Friction-Factor Model," Association for Scientific Research, Mathematical and Computational Applications, **9** (3), pp. 435-442

[59] Esser, D. and Kazakia, J. Y., 1995, "Air Flow in Cavities of Labyrinth Seals," International Journal of Engineering Science, **33** (15), pp. 2309-2326

[60] Kurohashi, M., Inoue, Y., Abe, T., and Fujikawa, T., 1980, "Spring and Damping Coefficients of the Labyrinth Seals," Vibrations in Rotating Machinery, pp. 215-

222

[61] Sriti, M, Agouzoul, M., Ouazar, D., and Micheau, P., 1997 (May), "Simulation Numerique D'Ecoulement Compressible dans les Joints Labyrinthe," Journal De Physique, III, **7** (5), pp. 1025-1037

[62] Benvenuti, E., Ruggeri, G., and Tomasini, E. P., 1979, "Analytical and Experimental Development of Labyrinth Seals for Process Centrifugal Compressors," AIChE Symposium Series, pp. 273-285

[63] Kearton, W. J. and Keh, T. H., 1952, "Leakage of Air through Labyrinth Glands of Staggered Type," Institution of Mechanical Engineers Proceedings, vol. 166 no. 2, pp. 180-188

[64] Vance, J. M., 1988, *Rotordynamics of Turbomachinery*, John Wiley & Sons, New York

[65] Childs, D. W. and Hale, K., 1994, "A Test Apparatus and Facility to Identify the Rotordynamic Coefficients of High-Speed Hydrostatic Bearings," ASME Journal of Tribology, **116**, pp. 337-344

[66] Marquette, O. R., Childs, D. W., and San Andrés, L., 1997, "Eccentricity Effects on the Rotordynamic Coefficients of Plain Annular Seals: Theory Versus Experiment," Transactions of the ASME, **119**, pp. 443-448

[67] Fasheh, J. I., 1972, "Review and Summary of Labyrinth Seal Theory and Design," TMR 2115-3351, Rocketdyne Report, Canoga Park, CA

[68] Kerr, B. G., 2005, "Experimental and Theoretical Rotordynamic Coefficients and Leakage of Straight Smooth Annular Gas Seals," M.S. thesis, Department of Mechanical Engineering, Texas A&M University, College Station, TX

[69] Sprowl, T. B. and Childs, D. W., 2004, "A Study of the Effects of Inlet Preswirl on the Dynamic Coefficients of a Straight-Bore Honeycomb Gas Damper Seal," Proceedings of the ASME Turbo Expo, **6**, pp. 619-629

[70] Childs, D. W. and Wade, J., 2004, "Rotordynamic-Coefficient and Leakage Characteristics for Hole-Pattern-Stator Annular Gas Seals - Measurements versus Predictions," ASME Journal of Tribology, **126** (2), pp. 326-333

[71] Ertas, B., Gamal, A., and Vance, J., 2006, "Rotordynamic Force Coefficients of Pocket Damper Seals," ASME Journal of Turbomachinery, **128**, pp. 725-737

[72] Childs, D. W., 2007, "Bearings + Gas Seals," MEEN 688 Course Presentation, Mechanical Engineering Department, Texas A&M University, College Station, TX

[73] Ertas, B. H. and Vance, J. M., 2007, "The Influence of Same-Sign Cross-Coupled Stiffness on Rotordynamics," ASME Journal of Vibration and Acoustics, **129** (1), pp. 24-31

[74] Shin, Y. S., Seifert, B., and Childs, D. W., 2006, "A Design to Improve the Effective Damping Characteristics of Hole-Pattern-Stator Annular Gas Seals," Proceedings of the ASME IGTI Turbo Expo, Barcelona, Spain, pp. 1271-1277

[75] Yucel, U. and Kazakia, J. Y., 2001 (January), "Analytical Prediction Techniques for Axisymetric Flow in Gas Labyrinth Seals", Technical Brief, Journal of Engineering for Gas Turbines and Power, **123**, pp. 255-257

APPENDIX

This appendix contains the detailed results of the leakage and cavity pressure tests referred to in the body of this report. The calibration and unit conversion information for the instrumentation used during the tests is also presented below.

SEAL DESCRIPTIONS

Detailed dimensioned drawings of the two-bladed air-buffer base unit (Figure A.1) and the spacer (Figure A.1) of seal set A are shown below.

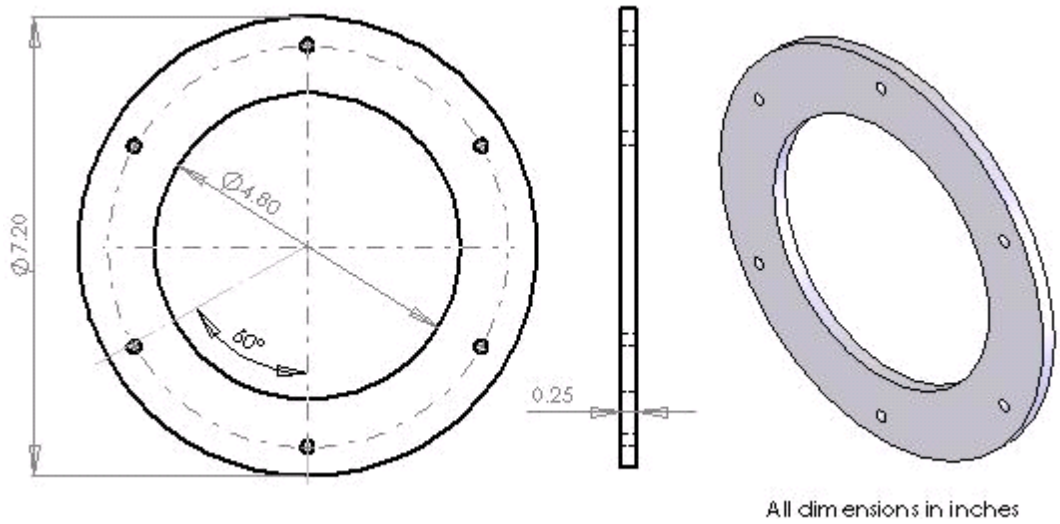

Figure A.1 Seal spacer (seal set A)

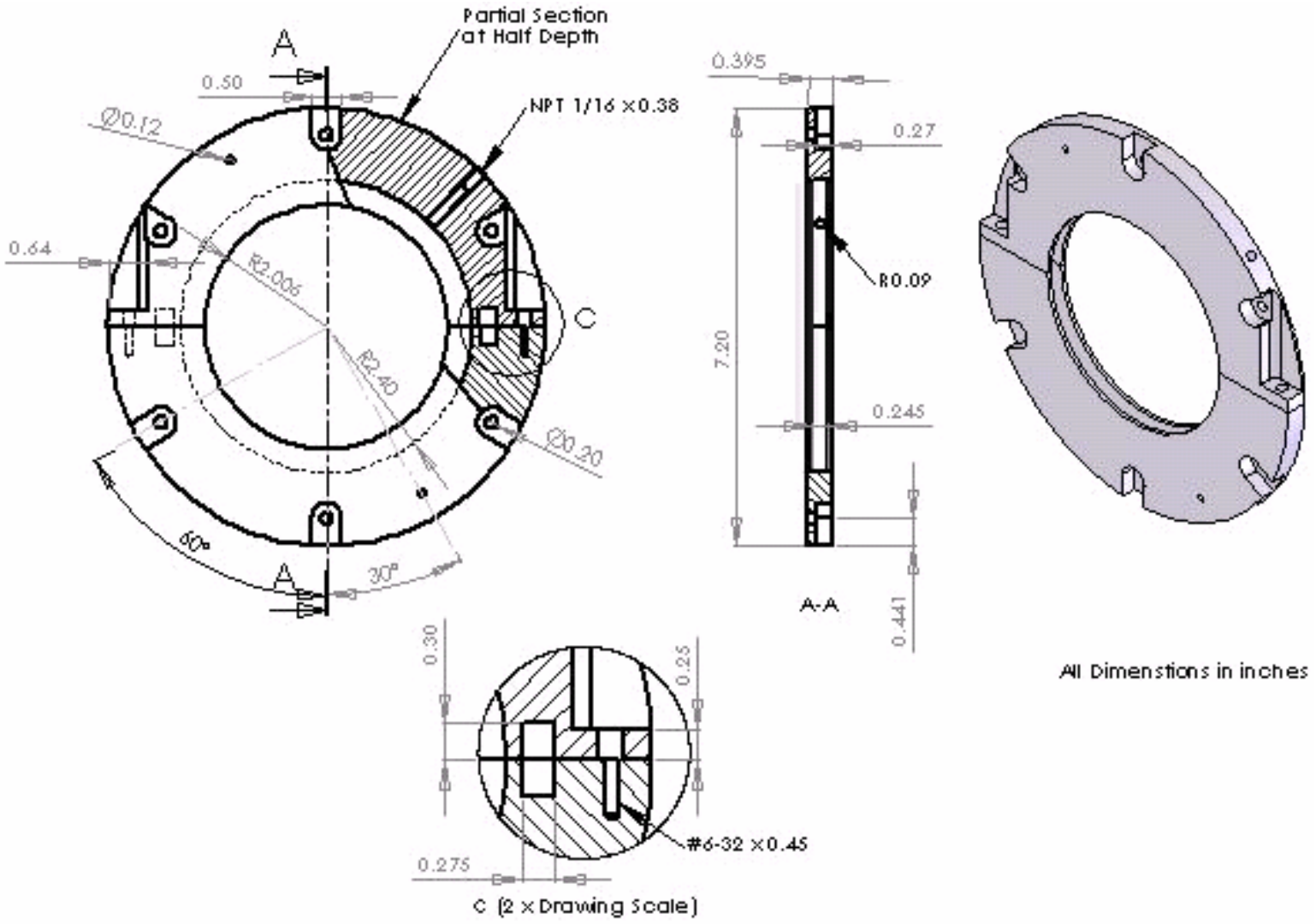

Figure A.2 Two-bladed air-buffer seal base unit (seal set A)

Table A.1 Labyrinth seal test matrix

Seal No.	No. of Blades	Pitch (in)	Pitch (mm)	Thickness (in)	Thickness (mm)	Profile	Depth (in)	Depth (mm)	Radial Clearance (mils)	Radial Clearance (μm)	Seal Length (in)	Seal Length (mm)	Seal Hardware
1	4	0.5	12.7	0.125	3.2	Flat	0.5	12.7	4	102	2.00	50.80	Set B
2	4	0.125	3.2	0.125	3.2	Flat	0.5	12.7	3	76	0.88	22.23	Set B
3	4	0.5	12.7	0.25	6.4	Flat	0.5	12.7	4	102	2.50	63.50	Set B
4	4	0.25	6.4	0.25	6.4	Flat	0.5	12.7	4	102	1.75	44.45	Set B
5	4	0.125	3.2	0.25	6.4	Flat	0.5	12.7	4	102	1.38	34.93	Set B
6	4	0.5	12.7	0.25	6.4	Dwn	0.5	12.7	4	102	2.50	63.50	Set B
7	4	0.125	3.2	0.25	6.4	Dwn	0.5	12.7	4	102	1.38	34.93	Set B
8	4	0.5	12.7	0.125	3.2	Flat	0.1	2.5	4	102	2.00	50.80	Set B
9	4	0.25	6.4	0.125	3.2	Flat	0.1	2.5	4	102	1.25	31.75	Set B
10	6	0.5	12.7	0.125	3.2	Flat	0.5	12.7	4	102	3.25	82.55	Set B
11	6	0.25	6.4	0.125	3.2	Flat	0.5	12.7	4	102	2.00	50.80	Set B
12	6	0.125	3.2	0.125	3.2	Flat	0.5	12.7	4	102	1.38	34.93	Set B
13	6	0.5	12.7	0.125	3.2	Flat	0.1	2.5	4	102	3.25	82.55	Set B
14	6	0.25	6.4	0.125	3.2	Flat	0.1	2.5	4	102	2.00	50.80	Set B
15	2	0.245	6.2	0.075	1.9	Flat	0.4	10.2	6	152	0.40	10.03	Set A
16	2	0.245	6.2	0.075	1.9	Up	0.4	10.2	6	152	0.40	10.03	Set A
17	2	0.245	6.2	0.075	1.9	Dwn	0.4	10.2	6	152	0.40	10.03	Set A
18	4	0.245	6.2	0.075	1.9	Flat	0.4	10.2	6	152	1.04	26.29	Set A
19	4	0.245	6.2	0.075	1.9	Up	0.4	10.2	6	152	1.04	26.29	Set A
20	4	0.245	6.2	0.075	1.9	Dwn	0.4	10.2	6	152	1.04	26.29	Set A
21	6	0.245	6.2	0.075	1.9	Flat	0.4	10.2	6	152	1.68	42.55	Set A
22	6	0.245	6.2	0.075	1.9	Up	0.4	10.2	6	152	1.68	42.55	Set A
23	6	0.245	6.2	0.075	1.9	Dwn	0.4	10.2	6	152	1.68	42.55	Set A

Down and *Up* refer to the side of the blade that is beveled (downstream or upstream)

DETAILED TEST RESULTS SEAL SET A

The leakage and static cavity pressure data for the three configurations of the six-bladed seal are shown in Table A.2. The test data for the four-bladed and two-bladed seals are shown in Table A.3 and Table A.4 respectively. In these tables, P_A represents the upstream pressure at the location of the flow meter, P_{IN} is the inlet pressure to the seal, and P_{OUT} is the seal's back pressure (atmospheric pressure for all test cases). P_{C3} and P_{C5} are the static pressures in the third and fifth cavities of the seal respectively. The volumetric flow-rate data is given in standard cubic feet per minute and the mass flow-rate in lb/s is calculated according to the following conversion equations:

$$\dot{V}_{ACFM} = 13.28 \cdot V$$

$$\dot{V}_{SCFM} = \dot{V}_{ACFM} \cdot \frac{P_A \cdot T_{ATM}}{P_{ATM} \cdot T_A}$$

$$\dot{m} = \dot{V}_{SCFM} \cdot \frac{\rho_{ATM}}{60}$$

The first equation calculates the volumetric flow-rate in actual cubic feet per minute from the voltage output of the Omega FLSC-9061 transmitter which conditions the signal coming from the flow meter. The second equation converts the volumetric flow-rate units to standard cubic feet per minute. The subscript A indicates the actual pressure or temperature at the flow meter while the subscript ATM indicates standard temperature and pressure conditions (70 ^{o}F and 14.7 Psi-a). The third equation, in which the density used is at standard temperature and pressure, calculates the mass flow-rate in lb/s.

Table A.2 Six-bladed seal (set A) leakage and cavity pressure test data

	P_A	P_{IN}	P_{OUT}	P_{C3}	P_{C5}	Flow-Rate (scfm)	Flow-Rate (lb/s)
Unbeveled	29.7	24	14.7	23.01	19.26	18.91	0.024
	39.7	29	14.7	27.72	22.29	26.72	0.033
	69.7	60	14.7	48.62	38.11	50.49	0.063
	69.7	59	14.7	49.25	39.1	50.74	0.063
	84.7	75	14.7	58.94	46.85	62.2	0.078
	104.7	92	14.7	71.28	56.96	77.64	0.097
	131.7	111	14.7	88	70.26	98.38	0.123
Beveled Downstream	29.7	23.7	14.7	20.87	16.47	15.91	0.02
	39.7	34.2	14.7	25.38	18.35	23.24	0.029
	71.7	66.4	14.7	44.63	28.96	45.27	0.057
	86.7	79.6	14.7	52.77	33.85	55.99	0.07
	107.7	99.23	14.7	65.41	42.41	70.24	0.088
	130.7	115.7	14.7	78.83	51.18	85.95	0.107
Beveled Upstream	29.7	23.7	14.7	24.45	17.46	17.33	0.022
	40.7	34.5	14.7	30.36	20.01	25.59	0.032
	68.7	58.7	14.7	48.37	30.1	45.8	0.057
	84.7	78.5	14.7	60.82	37.89	57.61	0.072
	106.7	97.09	14.7	75.99	47.16	73.05	0.091
	129.7	114.69	14.7	91.79	57.14	89.51	0.112

(All pressures in psi-a)

Table A.3 Four-bladed seal (set A) leakage and cavity pressure test data

	P_A	P_{IN}	P_{OUT}	P_{C3}	Flow-Rate (scfm)	Flow-Rate (lb/s)
Unbeveled	30.7	27	14.7	21.94	23.21	0.029
	39.7	31	14.7	25.73	31.45	0.039
	69.7	59	14.7	41.5	57.23	0.072
	87.7	75	14.7	52.2	72.72	0.091
	103.7	87	14.7	60.73	86.18	0.108
	129.7	107	14.7	75.32	108.02	0.135
Beveled Downstream	29.7	22.7	14.7	17.11	20.44	0.026
	40.7	31.7	14.7	21.2	30.88	0.039
	71.7	55.7	14.7	33.49	56.6	0.071
	86.7	64.7	14.7	37.4	68.68	0.086
	103.7	85.7	14.7	47.2	82.8	0.104
Beveled Upstream	29.7	22.7	14.7	17.42	21.54	0.027
	39.7	28.7	14.7	21.62	30.23	0.038
	71.7	57.7	14.7	38.3	57.64	0.072
	83.7	65.7	14.7	42.74	67.44	0.084
	103.7	83.7	14.7	53.06	83.93	0.105
	130.7	105.7	14.7	66.73	106.25	0.133

(All pressures in psi-a)

Table A.4 Two-bladed seal (set A) leakage and cavity pressure test data

	P_A	P_{IN}	P_{OUT}	Flow-Rate (SCFM)	Flow-Rate (lb/s)
Unbeveled	29.7	22	14.7	28.33	0.035
	39.7	28	14.7	39.62	0.05
	69.7	50	14.7	71.83	0.09
	81.7	60	14.7	84.5	0.106
	104.7	81	14.7	109.04	0.136
	129.7	100	14.7	135.43	0.169
	139.7	105	14.7	146	0.182
Beveled Downstream	29.7	19.7	14.7	26.24	0.033
	40.7	25.7	14.7	37.35	0.047
	70.7	52.7	14.7	66.48	0.083
	86.7	64.7	14.7	81.76	0.102
Beveled Upstream	31.7	20.7	14.7	28.2	0.035
	40.7	26.7	14.7	37.5	0.047
	69.7	49.7	14.7	66.29	0.083
	83.7	60.7	14.7	79.76	0.1
	104.7	78.7	14.7	100.53	0.126
	129.7	98.7	14.7	125.12	0.156
	139.7	105.7	14.7	134.89	0.169

(All pressures in psi-a)

DETAILED TEST RESULTS SEAL SET B

Table A.5 Labyrinth seal leakage rates for Set B

	P_{in}	psi-a	30	35	40	45	50	55	60	75	100
	Seal	bar-a	2.07	2.41	2.76	3.10	3.45	3.79	4.13	5.17	6.89
Leakage Rates	No. 1	lb/min	0.610	0.843	1.069	1.261	1.489	1.686	1.878	2.529	3.453
		Kg/min	0.277	0.383	0.486	0.573	0.677	0.766	0.854	1.149	1.569
	No. 2	lb/min	0.680	0.897	1.137	1.327	1.566	1.765	1.975	2.547	3.542
		Kg/min	0.309	0.408	0.517	0.603	0.712	0.802	0.898	1.158	1.610
	No. 3	lb/min	0.514	0.745	0.966	1.155	1.376	1.559	1.749	2.300	3.200
		Kg/min	0.234	0.339	0.439	0.525	0.625	0.708	0.795	1.046	1.454
	No. 4	lb/min	0.520	0.738	0.964	1.151	1.354	1.526	1.715	2.243	3.121
		Kg/min	0.236	0.336	0.438	0.523	0.616	0.693	0.779	1.019	1.418
	No. 5	lb/min	0.549	0.776	0.996	1.181	1.392	1.570	1.757	2.277	3.137
		Kg/min	0.250	0.353	0.453	0.537	0.633	0.714	0.799	1.035	1.426
	No. 6	lb/min	0.579	0.809	1.026	1.219	1.436	1.623	1.806	2.364	3.257
		Kg/min	0.263	0.368	0.467	0.554	0.653	0.738	0.821	1.075	1.480
	No. 7	lb/min	0.566	0.815	1.030	1.207	1.440	1.628	1.811	2.370	3.292
		Kg/min	0.257	0.370	0.468	0.549	0.655	0.740	0.823	1.077	1.497
	No. 9	lb/min	0.668	0.905	1.120	1.324	1.556	1.745	1.940	2.551	3.528
		Kg/min	0.304	0.412	0.509	0.602	0.707	0.793	0.882	1.160	1.604
	No. 8	lb/min	0.621	0.844	1.047	1.238	1.467	1.662	1.855	2.451	3.403
		Kg/min	0.282	0.384	0.476	0.563	0.667	0.756	0.843	1.114	1.547
	No. 10	lb/min	0.467	0.670	0.868	1.036	1.221	1.413	1.571	2.070	2.929
		Kg/min	0.212	0.305	0.395	0.471	0.555	0.642	0.714	0.941	1.331
	No. 11	lb/min	0.529	0.720	0.939	1.124	1.317	1.488	1.670	2.195	3.082
		Kg/min	0.241	0.327	0.427	0.511	0.598	0.676	0.759	0.998	1.401
	No. 12	lb/min	0.555	0.772	0.989	1.177	1.379	1.564	1.744	2.282	3.179
		Kg/min	0.252	0.351	0.449	0.535	0.627	0.711	0.793	1.037	1.445
	No. 13	lb/min	0.464	0.670	0.869	1.036	1.231	1.390	1.574	2.081	2.915
		Kg/min	0.211	0.304	0.395	0.471	0.559	0.632	0.715	0.946	1.325
	No. 14	lb/min	0.499	0.698	0.909	1.086	1.285	1.460	1.641	2.178	3.075
		Kg/min	0.227	0.317	0.413	0.493	0.584	0.664	0.746	0.990	1.398

Back pressure atmospheric for all seals

CALIBRATION DATA

The turbine flow-meter has a range of 0 to 130 actual cubic feet per minute. Over this range, the combined conversion factor for the flow-meter and the transmitter (which is essentially a signal conditioner) is 13.28 acfm/volt.

The conversion equation obtained from the calibration chart for the Kulite pressure transducer that was used to measure the static cavity pressures is shown below.

$$P = 9.945 \cdot V - 29.211$$

In this equation, the pressure read by the transducer in Psi-g is calculated in terms of the voltage output of the probe in millivolts.

VITA

Ahmed Mohamed Gamal Eldin was born in Giza (Egypt) and lived in Egypt until he and his family moved to Athens, Greece. He continued to travel with his family, living in Jeddah (Saudi Arabia), Louisville, Kentucky (USA), Brussels (Belgium), and Dubai (UAE), before receiving his high-school diploma from The International School of Choueifat in Sharjah (UAE). In 1994, Ahmed enrolled at The American University in Cairo where he majored in mechanical engineering and earned a *Bachelor of Science* in 1999, graduating *Magna Cum Laude*. In 2000, he returned to the United States and enrolled at Texas A&M University in College Station, Texas where he worked as a teaching assistant before joining the Turbomachinery Laboratory under the direction of Dr. John M. Vance. Ahmed's research has focused on the rotordynamic effects and leakage performance of annular gas seals. He received a *Master of Science* in 2003 and received a *Doctor of Philosophy* in 2007, both in mechanical engineering from Texas A&M University. Ahmed "Jimmy" Gamal can be contacted through Texas A&M University's Department of Mechanical Engineering at the following address:

Texas A&M University
Department of Mechanical Engineering
3123 TAMU
College Station, TX 77843-3123